

**SYNTHESIS OF CARBON NANOMATERIALS ON  
IMPREGNATED POWDERED ACTIVATED CARBON FOR  
REMOVAL OF ORGANIC COMPOUNDS FROM WATER**

**HAIYAM MOHAMMED ABDALRAHEEM ALAYAN**

**FACULTY OF ENGINEERING  
UNIVERSITY OF MALAYA  
KUALA LUMPUR**

**2018**

**SYNTHESIS OF CARBON NANOMATERIALS ON  
IMPREGNATED POWDERED ACTIVATED CARBON FOR  
REMOVAL OF ORGANIC COMPOUNDS FROM WATER**

**HAIYAM MOHAMMED ABDALRAHEEM ALAYAN**

**THESIS SUBMITTED IN FULFILMENT OF THE  
REQUIREMENTS FOR THE DEGREE OF DOCTOR OF  
PHILOSOPHY**

**FACULTY OF ENGINEERING  
UNIVERSITY OF MALAYA  
KUALA LUMPUR**

**2018**

UNIVERSITY OF MALAYA

**ORIGINAL LITERARY WORK DECLARATION**

Name of Candidate: **Haiyam Mohammed Alayan**

Matric No: **KHA14**

Name of Degree: **Doctor of Philosophy**

Title of Project Paper/Research Report/Dissertation/Thesis (“this Work”): **Synthesis of carbon nanomaterials on impregnated powdered activated carbon for removal of organic compounds from water**

Field of Study: **Advanced Materials & Technology**

I do solemnly and sincerely declare that:

- (1) I am the sole author/writer of this Work;
- (2) This Work is original;
- (3) Any use of any work in which copyright exists was done by way of fair dealing and for permitted purposes and any excerpt or extract from, or reference to or reproduction of any copyright work has been disclosed expressly and sufficiently and the title of the Work and its authorship have been acknowledged in this Work;
- (4) I do not have any actual knowledge nor do I ought reasonably to know that the making of this work constitutes an infringement of any copyright work;
- (5) I hereby assign all and every rights in the copyright to this Work to the University of Malaya (“UM”), who henceforth shall be owner of the copyright in this Work and that any reproduction or use in any form or by any means whatsoever is prohibited without the written consent of UM having been first had and obtained;
- (6) I am fully aware that if in the course of making this Work I have infringed any copyright whether intentionally or otherwise, I may be subject to legal action or any other action as may be determined by UM.

Candidate’s Signature

Date:

Subscribed and solemnly declared before,

Witness’s Signature

Date:

Name:

Designation:

**SYNTHESIS OF CARBON NANOMATERIALS ON IMPREGNATED  
POWDERED ACTIVATED CARBON FOR REMOVAL OF ORGANIC  
COMPOUNDS FROM WATER**

**ABSTRACT**

Carbon nanomaterials (CNMs) are known to be superior to many other existing materials in terms of their remarkable properties. Despite of their strong adsorption affinity, they are limited in practical water treatment application for their difficulties involved in dispersion and separation. Moreover, wastewater contamination by toxic organic compounds has become a world-wide environmental concern because of the undesirable effects of these contaminants. Therefore, this research has been undertaken to explore the potential of directly growing CNMs on microscale support such as the powder activated carbon (PAC) to develop a novel CNM hybrid adsorbent for the removal of bisphenol A (BPA) and methylene blue (MB) from water. In this regard, chemical vapor deposition reactor (CVD) was used to synthesize CNMs on nickel impregnated powdered activated carbon from the decomposition of methane and acetylene. The Design of experiment (DOE) based on the response surface methodology (RSM) with the central composite design (CCD) was used to optimize the reaction temperature, reaction time and gases flowrates to obtain the maximum adsorption along with the maximum possible yield for CNM. The results demonstrated that the optimum conditions were different depending on the characteristics of the carbon precursor and the adsorbate under investigation. The optimized growth conditions for methane decomposition were found at 933 °C, 20 min, and (H<sub>2</sub>/CH<sub>4</sub>) of 1.0. The produced CNM-PAC had multi-structures with groove-like features. Meanwhile, dense carbon nanotubes (CNTs) with tubular structures were dominant in the product obtained from the pyrolysis of acetylene at the optimum growth conditions of a reaction temperature of 550 °C, a

reaction time of 37.3 min, and a gas ratio ( $H_2/C_2H_2$ ) of 1.0. The physiochemical, and morphological properties of CNM-PAC samples at the optimal conditions were investigated using FESEM, TEM, EDX, BET, Raman spectroscopy, TGA, FTIR, and zeta potential. Adsorption studies for BPA and MB were carried out to evaluate the optimum removal conditions, kinetic, and isotherms. RSM-CCD experimental design was used to conduct the optimization studies and to determine the optimal conditions for the removal of BPA and MB by each selected adsorbent individually. The proposed models were optimized with respect to the operating pH, adsorbent mass and contact time as controlling parameters to correlate their effects on the removal efficiency of the pollutants and the adsorption capacity of the adsorbent. The optimization study showed that the maximum adsorption capacity for the removal of BPA and MB onto the CNM-PAC produced from methane was about 182 and 250 mg/g, respectively. The surface properties of CNT-PAC obtained from the pyrolysis of acetylene were modified by oxidative functionalization using two different methods: sonication with  $KMnO_4$ , and with  $KMnO_4/H_2SO_4$ , however, the best removal of MB was obtained with the as-prepared CNT-PAC sample. The adsorption behaviors showed that the adsorption kinetics and isotherms were in good agreement with the pseudo second-order equation and the Langmuir isotherm model, respectively with a maximum adsorption capacity of about 175 mg/g.

Keywords: carbon nanomaterials, chemical vapor deposition, bisphenol A, methylene blue, response surface methodology.

***SYNTHESIS OF CARBON NANOMATERIALS ON IMPREGNATED  
POWDERED ACTIVATED CARBON FOR REMOVAL OF ORGANIC  
COMPOUNDS FROM WATER***

**ABSTRAK**

Bahan nanomaterial karbon (CNMs) umumnya dipandang tinggi atau hebat berbanding daripada bahan-bahan lain dari segi sifat-sifat luar biasa yang dimilikinya. Walaupun mempunyai kadar penyerapan yang kuat, penggunaan CNMs dalam aplikasi rawatan air terutama bagi proses penyebaran dan pemisahan adalah terhad. Oleh itu, kajian ini telah dijalankan bagi meneroka potensi penghasilan CNM secara langsung terhadap sokongan berskala mikro seperti matriks karbon aktif untuk membangunkan penjerap hibrid berasaskan CNM yang baru, bagi proses penyingkiran bisphenol A (BPA) dan metilena biru (MB) daripada air. Dalam hal ini, reaktor pemendapan wap kimia (CVD) telah digunakan untuk menghasilkan CNMs daripada karbon aktif serbuk (PAC) melalui penguraian metana dan asetilena. Perisian Design of experiment (DOE) melalui metodologi response surface methodology (RSM) dengan central composite design (CCD) telah digunakan bagi melihat kesan tindak balas suhu, tindak balas masa dan kadar aliran gas pada prestasi penjerapan bersama-sama penghasilan maksimum CNM. Hasil kajian ini menunjukkan bahawa keadaan optimum untuk mendapatkan peratusan penyingkiran tertinggi dan juga penghasilan CNM tertinggi adalah berbeza bergantung kepada ciri-ciri karbon dan penyerap yang dikaji. Keadaan pertumbuhan optimum untuk penguraian metana didapati pada 933 °C, 20 min, dan (H<sub>2</sub> / CH<sub>4</sub>) sebanyak 1.0. CNM-PAC yang dihasilkan mempunyai pelbagai struktur dengan ciri-ciri seperti alur, dan serupa dengan keadaan permukaan sokongan PAC. Sementara itu, nanotub karbon (CNTs) yang padat dengan struktur-struktur tiub, telah mendominasi produk yang diperolehi hasil proses pirolisis daripada asetilena. Hasil tertinggi didapati pada keadaan pertumbuhan optimum pada suhu tindak balas 550 °C, masa tindak balas 37.3 minit, dan

nisbah gas ( $H_2 / C_2H_2$ ) sebanyak 1.0. Berdasarkan ujian pengoptimuman, sifat fisio-kimia, dan morfologi sampel CNM-PAC yang disediakan pada keadaan optimum telah disiasat menggunakan potensi spektrum FESEM, TEM, EDX, BET, Raman spektroskopi, TGA, dan FTIR. Kajian penyerapan untuk BPA dan MB telah dijalankan untuk menilai keadaan optimum bagi penyingkiran, kinetik dan juga isotherm. Design eksperimen RSM-CCD telah digunakan bagi kajian pengoptimuman dan juga untuk menentukan keadaan optimum bagi penyingkiran BPA dan MB oleh setiap penjerap yang terpilih. Model yang dicadangkan dioptimumkan berdasarkan pH operasi, jisim penjerap dan masa hubungan sebagai parameter kawalan untuk mengaitkan kesannya ke atas kecekapan penyingkiran bahan pencemar dan keupayaan penjerap penyerap. Kajian pengoptimuman menunjukkan bahawa kapasiti penyerapan maksimum untuk penyingkiran BPA dan MB ke atas CNM-PAC yang dihasilkan daripada metana adalah masing-masing sekitar 182 dan 250 mg/g. Sifat permukaan CNT-PAC yang diperoleh hasil daripada pirolisis asetilena yang telah diubahsuai oleh fungsian oksidatif menggunakan dua kaedah yang berbeza: proses sonication dengan  $KMnO_4$ , dan dengan  $KMnO_4 / H_2SO_4$ . Proses penyaringan telah dilakukan bagi penyingkiran MB daripada air menggunakan CNT-PAC yang telah disediakan dan sampel yang telah diubahsuai untuk memilih penyerap yang terbaik dengan kecekapan penyingkiran tertinggi. Dengan membandingkan keputusan yang diperolehi, penyingkiran terbaik oleh MB telah diperolehi dengan menggunakan sampel CNT-PAC. Data ekuilibrium telah dianalisis bagi sistem penyerap - penjerap yang menghasilkan kapasiti penjerapan maksimum sekitar 175 mg/g. Ciri-ciri penjerapan untuk semua jenis penjerap menunjukkan bahawa penjerapan kinetik dan isotherm mematuhi prinsip persamaan urutan pseudo kedua dan model Langmuir isotherm.

Keywords: carbon nanomaterials, chemical vapor deposition, bisphenol A, methylene blue, response surface methodology.

## ACKNOWLEDGEMENTS

In the name of Allah, the Most Gracious and the Most Merciful.

First and foremost, all the praises and deep gratitude towards almighty Allah who has given me the ability to pursue my studies at doctorate level.

I would like to extend my sincere appreciation to my main supervisor, Prof. Dr. Mohd Ali bin Hashim for his continued support and encouragement. I am grateful to Prof. Ali for allowing me to join the University of Malaya Centre for Ionic Liquids (UMCiL) group, and for his kindness and valuable advice during my academic endeavors despite his hectic schedule and growing responsibilities.

I would like to express my sincere gratitude to my co-supervisor Dr. Mohammed Abdulhakim AlSaadi for giving me the opportunity to work on this project as well as for his helpful supervision, generous support and persistent tolerance.

I would also extend my earnest gratitude to University of Malaya for making this study possible by providing funds and facilities. I owe gratitude to the support provided by all staff of the Department of Chemical Engineering during my research. Special thanks and warmest gratitude to my friends and colleagues who have given their time, know-how, technical assistance and kind consideration during my research.

Most importantly, none of this would have been possible without all sacrifices of my husband and my children. I am indebted to them for their diligent support with special care and love. Words cannot express my deepest and most heart-felt gratitude to my beloved mother and all my family members for their unwavering encouragement and prayers throughout my ups and downs. Last but definitely not least, I would like to dedicate this achievement to the memory of my beloved father who was constantly inspiring me to thrive for the betterment.



## TABLE OF CONTENTS

Abstract .....	iii
Abstrak .....	v
Acknowledgements .....	vii
Table of Contents .....	viii
List of Figures .....	xv
List of Tables .....	xix
List of Symbols and Abbreviations.....	xxiii
<b>CHAPTER 1: INTRODUCTION.....</b>	<b>1</b>
1.1 Overview .....	1
1.2 Problem statement .....	3
1.3 Research objectives .....	6
1.4 Research scope .....	7
1.5 Research methodology .....	7
1.6 Outline of the thesis.....	8
<b>CHAPTER 2: LITERATURE REVIEW.....</b>	<b>10</b>
2.1 Introduction .....	10
2.2 Carbon nanotubes .....	11
2.2.1 Structure of carbon nanotubes.....	11
2.2.2 Properties and uses of carbon nanotubes.....	13
2.2.2.1 Electrical properties .....	13
2.2.2.2 Mechanical properties .....	14
2.2.2.3 Thermal properties .....	15
2.2.2.4 Chemical properties .....	15

2.2.2.5	Adsorption properties .....	16
2.2.3	Multi-scale/ hybridized carbon structure.....	23
2.2.4	Powder Activated carbon catalyzing the synthesis of carbon nanotubes .	25
2.2.5	Synthesis of carbon nanotubes .....	26
2.2.5.1	Arc discharge .....	26
2.2.5.2	Laser ablation .....	27
2.2.5.3	Chemical vapor deposition (CVD).....	29
2.2.5.4	CVD support catalyst method .....	35
2.2.6	Mechanism of nanotube growth in CVD .....	37
2.2.7	Functionalization of carbon nanotubes .....	41
2.3	Organic pollutants .....	45
2.3.1	Bisphenol A.....	45
2.3.1.1	Structure and physicochemical properties of bisphenol A.....	45
2.3.1.2	Production and application.....	46
2.3.1.3	Exposure of BPA to the environment .....	47
2.3.1.4	Hazardous potential of BPA.....	49
2.3.1.5	Treatment methods.....	51
2.3.1.6	BPA removal by miscellaneous adsorbents .....	52
2.3.2	Organic dyes.....	60
2.3.2.1	Structure and physicochemical properties of methylene blue...	60
2.3.2.2	MB removal techniques .....	62
2.3.2.3	MB removal by miscellaneous adsorbents.....	64
2.4	Mechanism of adsorption on CNMs.....	69
2.4.1	Mechanism of adsorption of Bisphenol A onto CNMs.....	73
2.4.2	Mechanism of adsorption of methylene blue onto CNMs .....	76
2.5	Summary of literature review .....	78

<b>CHAPTER 3: METHODOLOGY</b> .....	<b>80</b>
3.1 Introduction .....	80
3.2 Materials .....	80
3.3 Instruments and measurements.....	82
3.3.1 Chemical vapor deposition reactor (CVD).....	82
3.3.2 Instruments and equipment for characterization .....	85
3.3.3 Additional instruments .....	85
3.4 Methods .....	86
3.4.1 Experimental Approach for carbon nanomaterials synthesis .....	86
3.4.1.1 Catalyst and support preparation.....	86
3.4.1.2 Growth of carbon nanomaterials on powdered activated carbon.....	87
3.4.1.3 Optimization of operating conditions for CNM-PAC growth ..	88
3.4.2 Design of experiment (DOE) for synthesis CNM-PAC.....	88
3.4.3 Functionalization of CNM-PAC for comparison .....	91
3.4.4 Adsorption studies.....	92
3.4.4.1 Batch adsorption experiments .....	92
3.4.4.2 Optimization of adsorption conditions.....	93
3.4.4.3 Kinetic studies .....	95
3.4.4.4 Adsorption isotherms .....	98
3.4.4.5 Screening and optimization of functionalized CNM-PAC .....	102
3.4.5 Characterization .....	103
3.4.6 General research plan flow chart.....	104
 <b>CHAPTER 4: SYNTHESIZING AND ADSORPTION STUDIES FOR CNM-PAC FROM METHANE DECOMPOSITION</b> .....	 <b>105</b>

4.1	Screening of CNM-PAC synthesis conditions .....	105
4.1.1	Design of Experiment (DOE) for Production of CNM-PAC from methane decomposition .....	105
4.1.2	Adsorption of BPA for DOE Screening.....	106
4.2	Statistical Analysis for the CNM-PAC growth .....	107
4.2.1	Analysis of variance (ANOVA) for the yield of CNM-PAC.....	107
4.2.2	Analysis of variance (ANOVA) for the removal of BPA onto CNM-PAC 110	
4.2.3	The interactive effects of selected parameters on the CNM-PAC growth and BPA adsorption .....	112
4.2.4	Summary of the optimization conditions for CNM-PAC synthesis from methane decomposition.....	116
4.3	Adsorption of bisphenol A (BPA).....	117
4.3.1	Design of experiment (DOE) for BPA adsorption .....	117
4.3.2	Analysis of variance (ANOVA).....	118
4.3.3	The interactive effects of selected parameters on BPA adsorption.....	123
4.3.4	Adsorption Kinetics.....	125
4.3.5	Adsorption isotherms .....	128
4.3.6	Mechanisms.....	132
4.3.7	Summary of the adsorption of BPA onto CNM-PAC.....	133
4.4	Adsorption of methylene blue (MB) .....	133
4.4.1	Design of experiment (DOE) for MB adsorption.....	133
4.4.2	Analysis of variance (ANOVA) .....	134
4.4.3	The interactive effects of selected parameters on MB adsorption .....	138
4.4.4	Adsorption kinetics .....	141
4.4.5	Adsorption isotherms .....	145

4.4.6	Mechanisms.....	148
4.4.7	Summary of the adsorption of MB onto CNM-PAC .....	148

**CHAPTER 5: CHARACTERIZATION OF CNM-PAC SYNTHESIZED FROM METHANE DECOMPOSITION..... 150**

5.1.1	Morphology and surface elemental analysis .....	150
5.1.2	Raman spectroscopy.....	154
5.1.3	Thermogravimetric analysis (TGA) .....	156
5.1.4	Surface chemistry analysis (FTIR) for BPA adsorption .....	158
5.1.5	Surface chemistry analysis (FTIR) for MB adsorption.....	159
5.1.6	BET Surface area .....	162
5.1.7	Point of zero of charge (PZC) .....	163
5.1.8	Zeta potential.....	164
5.1.9	Summary of characterization .....	166

**CHAPTER 6: SYNTHESIZING AND ADSORPTION STUDIES FOR CNM-PAC FROM ACETYLENE DECOMPOSITION..... 167**

6.1	Screening of CNM-PAC synthesis conditions .....	167
6.1.1	DOE for production of CNM-PAC from acetylene decomposition.....	167
6.1.2	Adsorption of MB for DOE Screening .....	168
6.2	Statistical Analysis for the CNM-PAC growth .....	169
6.2.1	Analysis of variance (ANOVA) for the yield of CNM-PAC.....	169
6.2.2	Analysis of variance (ANOVA) for the removal of MB onto CNM-PAC	
	171	
6.2.3	Effects of reaction temperature, reaction time and gas Ratio.....	174

6.2.4	Optimization of the selected parameters and study their interactive effects on the CNM-PAC growth .....	177
6.2.5	Summary of optimization the conditions of CNM-PAC synthesis from acetylene decomposition .....	181
6.3	Adsorption of Methylene blue (MB) .....	182
6.3.1	Primary screening.....	182
6.3.2	Design of experiment (DOE) for MB adsorption.....	184
6.3.3	Analysis of variance (ANOVA).....	185
6.3.4	The interactive effects of selected parameters on the adsorption of MB on O-CNT.....	188
6.3.5	Adsorption Kinetics.....	192
6.3.6	Adsorption isotherms .....	194
6.3.7	Mechanisms.....	197
6.3.8	Summary of the adsorption of MB onto O-CNT .....	199

**CHAPTER 7: CHARACTERIZATION OF CNM-PAC SYNTHESIZED FROM ACETYLENE DECOMPOSITION.....200**

7.1	FESEM and TEM analyses.....	200
7.2	Raman spectroscopy .....	202
7.3	Thermogravimetric analysis (TGA) .....	203
7.4	Surface chemistry analysis (FTIR).....	205
7.5	BET Surface area.....	206
7.6	Zeta potential .....	207
7.7	Summary of characterization.....	209

**CHAPTER 8: CONCLUSIONS AND RECOMMENDATIONS.....210**

8.1 Conclusion.....210

8.1.1 Synthesizing of carbon nanomaterials on powder activated substrate from methane decomposition.....210

8.1.2 Synthesizing of carbon nanomaterials on powder activated substrate from acetylene decomposition .....213

8.2 Recommendations .....215

**REFERENCES.....217**

**LIST OF PUBLICATIONS .....265**

University of Malaya

## LIST OF FIGURES

Figure 2.1: Graphite carbon $sp^2$ hybridization.....	12
Figure 2.2: Schematic models describing single-walled and multi-walled carbon nanotubes conceptually obtained from single graphene sheets (Mubarak, Sahu, et al., 2014).....	13
Figure 2.3: Schematic diagram of arc-discharge apparatus.....	27
Figure 2.4: Schematic drawings of a laser ablation.....	28
Figure 2.5: Schematic diagram of a CVD setup in its simplest form (Atchudan et al., 2015).....	31
Figure 2.6: Schematic diagram of thermal CVD apparatus.....	37
Figure 2.7: Widely-accepted growth mechanisms for CNTs: (a) tip-growth model, (b) base-growth model (Kumar & Ando, 2010).....	39
Figure 2.8: Strategies for chemical and physical functionalization of CNTs: a) covalent sidewall functionalization, b) covalent defect sidewall functionalization, c) non-covalent adsorption of surfactants, d) wrapping of polymers, and e) endohedral functionalization (Hussain & Mitra, 2011).....	42
Figure 2.9: BPA molecular structure (Pullket, 2015).....	45
Figure 2.10: Chemical production of BPA.....	46
Figure 2.11: Different adsorption sites on a homogeneous bundle of partially open-ended SWCNTs: (1) internal, (2) interstitial channel, (3) external groove site, and (4) external surface (Agnihotri et al., 2006).....	71
Figure 2.12: Schematic diagrams for adsorption of BPA on SWCNT. The letters I, II, III, and IV indicate the possible adsorption areas of surface, groove, interstitial spaces, and inner pores, respectively. SWCNT is presented as an example. BPA 1 is adsorbed on CNT with two benzene rings in the direction of tube axis. BPA 2 show the adsorption on the surface, whereas BPA 3 illustrate the wedging of this molecule in the groove area. The interstitial space is too small for the molecules to fit (Pan et al., 2008).....	75
Figure 2.13: Schematic illustration of the possible interaction between MWCNTs and methylene blue: (a) electrostatic attraction and (b) $\pi$ - $\pi$ stacking (Ai, Zhang, Liao, et al., 2011).....	76



Figure 3.1: Photograph of the in-situ CVD reactor.....	84
Figure 3.2: The experimental activities of this research. ....	86
Figure 3.3: First-order kinetic model illustration.....	96
Figure 3.4: Second-order kinetic model illustration. ....	97
Figure 3.5: Intraparticle diffusion kinetic model. ....	98
Figure 3.6: Langmuir isotherm model. ....	99
Figure 3.7: Freundlich isotherm model.....	101
Figure 3.8: Temkin isotherm model.....	102
Figure 3.9: Schematic diagram of the methodology adopted. ....	104
Figure 4.1: Predicted values vs. actual values CNM-PAC growth response.....	109
Figure 4.2: Predicted values vs. actual values BPA removal response. ....	112
Figure 4.3: Three-dimensional response surface representation for: CNM-PAC growth yield (Y), and BPA removal efficiency (RV %); (a, b) interaction with growth temperature and time, (c, d) interaction with growth temperature and gas ratio and (e, f) interaction with time and gas ratio.....	115
Figure 4.4: Predicted values vs. actual values for (a) BPA removal efficiency (RV1 %) and (b) adsorption capacity (Q1) on CNM-PAC.....	121
Figure 4.5: RSM plots of (a) BPA removal efficiency (RV1 %), and (b) adsorbent capacity (Q1) considering the effect of pH and dosage. ....	123
Figure 4.6: RSM plots of (a) BPA removal efficiency (RV1 %), and (b) adsorbent capacity (Q1) considering the effect of pH and contact time. ....	124
Figure 4.7: Pseudo-first order kinetic model for BPA adsorption. ....	127
Figure 4.8: Pseudo-second order kinetic model for BPA adsorption. ....	127
Figure 4.9: Intraparticle diffusion kinetic model for BPA adsorption.....	128
Figure 4.10: Langmuir isotherm model for BPA adsorption.....	129
Figure 4.11: Freundlich isotherm model for BPA adsorption. ....	130
Figure 4.12: Temkin isotherm model for BPA adsorption. ....	130

Figure 4.13: Predicted values versus actual values for (a) removal response and (b) adsorption capacity response. ....	137
Figure 4.14: RSM plots of MB removal efficiency and adsorbent capacity considering the effect of (a) pH and dose, (b) pH and contact time and (c) dose and contact time. ....	139
Figure 4.15: RSM plots of the adsorption capacity considering the effect of (a) pH and dose, (b) pH and contact time and (c) dose and contact time. ....	140
Figure 4.16: Fittings of different kinetics models for MB adsorption on the synthesized CNM-PAC; (a) Pseudo-first order, (b) Pseudo-second order and (c) Intraparticle diffusion at optimum conditions. ....	144
Figure 4.17: The isotherm plots for MB adsorption on CNM-PAC following (a) Langmuir, (b) Freundlich, and (c) Temkin model. ....	146
Figure 5.1: (a) FESEM and (b) TEM images for Ni-PAC before growth reaction. ....	151
Figure 5.2: (a) FESEM and (b) TEM images of CNM-PAC obtained at optimal conditions. ....	152
Figure 5.3: EDX analyses for (a) PAC, (b) Ni-PAC and (c) CNM-PAC synthesized at optimal conditions. ....	154
Figure 5.4: Raman spectra of Ni-PAC and CNM-PAC. ....	155
Figure 5.5: TGA curves for PAC, Ni-PAC and CNM-PAC. ....	157
Figure 5.6: FTIR spectra of BPA, CNM-PAC before, and after BPA adsorption. ....	159
Figure 5.7: FTIR spectrums for free MB and CNM-PAC before and after adsorption. ....	161
Figure 5.8: Determination of the point of zero charge of the CNM-PAC by the pH drift analysis. ....	164
Figure 6.1: Predicted vs. actual values for CNM-PAC yield ( $Y_{C_2H_2}$ %). ....	171
Figure 6.2: Predicted values vs. actual values MB removal response. ....	173
Figure 6.3: Response surface plots for the effects of reaction temperature and reaction time on CNM-PAC ( $Y_{C_2H_2}$ ); at fixed gas ratio 1.0 (a) and 4.0 (b), effects of deposition temperature and gas ratio at fixed reaction time 20 (c) and 60 min (d), and effects reaction time and gas ratio at fixed growth temperature 550°C (e) and 750°C (f). ....	176

Figure 6.4: Three-dimensional response surface representation for: MB removal efficiency ( $R_{V_{C_2H_2}}$ %) on CNM-PAC; (a) interaction with growth temperature and time, (b) interaction with growth temperature and gas ratio and (c) interaction with time and gas ratio. ....	180
Figure 6.5: Primary screening study for all adsorbents. ....	182
Figure 6.6: Effect of contact time on the removal efficiency of MB for all adsorbents. ....	184
Figure 6.7: Predicted values vs. actual data for MB adsorption on O-CNT adsorbent (a) removal (%) and (b) adsorbent capacity (mg /g).....	187
Figure 6.8: Surface response representation of the interaction of removal efficiency of MB onto O-CNTs with (a) pH and dose, (b) pH and contact time and (c) dose and contact time.....	190
Figure 6.9: Surface response representation of the interaction of adsorption capacity of MB onto O-CNTs with (a) pH and dose, (b) pH and contact time and (c) dose and contact time.....	191
Figure 6.10: Fittings of different kinetics models for MB adsorption on O-CNT; (a) Pseudo-first order, (b) Pseudo-second order and (c) Intraparticle diffusion at optimum conditions. ....	193
Figure 6.11: The isotherm plots for MB adsorption on CNM-PAC; (a) Langmuir, (b) Freundlich, and (c) Temkin model. ....	195
Figure 7.1: FESEM and TEM images of O-CNT. ....	201
Figure 7.2: FESEM image of CNT, CNF, CS and helix cum produced at 750 °C. ....	201
Figure 7.3: Raman spectrum of O-CNT and KS-CNT. ....	203
Figure 7.4: TGA curves for O-CNTs, O-CNTs-MB, and KS-CNTs.....	204
Figure 7.5: FTIR spectrum for O-CNTs, MB and O -CNTs-MB.....	206
Figure 7.6: Determination of the point of zero charge of the O-CNTs by the pH drift. ....	208

## LIST OF TABLES

Table 2.1: Carbon nanotubes as organic compounds adsorbent. ....	18
Table 2.2: Comparison of arc-discharge, laser ablation and CVD methods.....	32
Table 2.3: Summary of synthesis of CNTs using CVD techniques.....	34
Table 2.4: Physicochemical properties of bisphenol A. ....	45
Table 2.5: Available quality standards for BPA in the aquatic matrices. ....	48
Table 2.6: Concentrations of BPA in aquatic environment in different countries.....	48
Table 2.7: Effects of low-dose of BPA exposure in animals. ....	50
Table 2.8: Characteristics of some of different adsorbents used for BPA removal.....	54
Table 2.9: Properties and structure of methylene blue.....	62
Table 2.10: Advantages and disadvantages of dyes removal methods (Robinson et al., 2001). ....	63
Table 2.11: Reported results of batch adsorption studies on the removal of MB from water by different adsorbents. ....	66
Table 3.1: List of reagents, chemicals and gases utilized in this research. ....	81
Table 3.2: General properties and chemical structure of bisphenol A.....	81
Table 3.3: General properties and chemical structure of methylene blue.....	82
Table 3.4: Technical specifications of CVD utilized in this research.....	83
Table 3.5: Independent variables and their coded and actual levels in the CCD for CNM-PAC synthesis from CH <sub>4</sub> decomposition. ....	90
Table 3.6: Independent variables and their coded and actual levels in the CCD for CNM-PAC synthesis from C <sub>2</sub> H <sub>2</sub> decomposition.....	90
Table 3.7: Experimental CCD data for the synthesis parameters of CNM-PAC using CH <sub>4</sub> decomposition. ....	90
Table 3.8: Experimental CCD data for the synthesis parameters of CNM-PAC using C <sub>2</sub> H <sub>2</sub> decomposition. ....	91
Table 3.9: List of design of experiments runs for BPA adsorption using CNM-PAC obtained from CH <sub>4</sub> decomposition. ....	94

Table 3.10: List of design of experiments runs for MB adsorption using CNM-PAC obtained from CH <sub>4</sub> decomposition.....	94
Table 3.11: List of design of experiments runs for MB adsorption. ....	103
Table 4.1: Experimental CCD data for synthesis parameters from CH <sub>4</sub> decomposition. ....	106
Table 4.2: ANOVA results for the yield of CNM-PAC growth. ....	108
Table 4.3: List of the actual and predicted values of the CNM-PAC yield. ....	109
Table 4.4: ANOVA results for BPA removal % for CNM-PAC growth optimization	111
Table 4.5: List of the actual and predicted values of the BPA removal efficiency. ....	111
Table 4.6: Constraints for optimization of production conditions for CNM-PAC for BPA removal.....	116
Table 4.7: Solutions for the optimum conditions suggested by DOE software for CNM-PAC growth.....	116
Table 4.8: Summary of CCD for parameters of BPA adsorption on CNM-PAC.....	117
Table 4.9: CCD of experimental parameters for BPA removal by CNM-PAC.....	118
Table 4.10: ANOVA results for BPA Removal % (RV1) by CNM-PAC.....	119
Table 4.11: ANOVA results for BPA adsorption capacity (Q1) on CNM-PAC. ....	120
Table 4.12: List of the actual and predicted values for BPA removal (RV1) and adsorption capacity responses (Q1). ....	120
Table 4.13: Constraints for optimization process based on CCD for BPA adsorption.	122
Table 4.14: Potential optimization conditions based on CCD for BPA removal. ....	122
Table 4.15: Linearized equations of studied kinetic models for BPA adsorption on CNM-PAC.....	126
Table 4.16: Linearized equations of studied isotherm models for BPA adsorption on CNM-PAC. ....	131
Table 4.17: Previously reported maximum adsorption capacities of various adsorbents for Bisphenol A removal. ....	131
Table 4.18: Summary of CCD for MB adsorption variables on CNM-PAC.....	134

Table 4.19: CCD of experimental variables for MB removal by CNM-PAC. ....	134
Table 4.20: ANOVA results for MB Removal % (RV2) by CNM-PAC. ....	136
Table 4.21: ANOVA results for MB adsorption capacity (Q2) by CNM-PAC.....	136
Table 4.22: List of the actual and predicted values for MB removal (RV2) and adsorption capacity responses (Q2). ....	137
Table 4.23: Constraints for optimization process based on CCD for MB adsorption. .	141
Table 4.24: Potential optimization conditions based on CCD for MB removal. ....	141
Table 4.25: Linearized equations of studied kinetic models for MB adsorption on CNM-PAC.....	143
Table 4.26: Linearized equations of studied isotherm models for MB adsorption on CNM-PAC.....	147
Table 4.27: Comparison between the maximum adsorption capacity ( $q_m$ ) of CNM-PAC and other reported adsorbents for MB removal. ....	147
Table 5.1: Some of the predicted functional groups on the surface of synthesized CNM-PAC before and after adsorption of organic pollutants.....	162
Table 5.2: Summary of BET results for PAC, Ni-PAC and CNM-PAC.....	163
Table 5.3: Zeta potential results for PAC and the different carbon structures produced .....	166
Table 6.1: Experimental CCD data for the synthesis parameters from $C_2H_2$ decomposition. ....	168
Table 6.2: ANOVA results for the yield of CNM-PAC growth from $C_2H_2$ decomposition. ....	169
Table 6.3: List of the actual and predicted values of the CNM-PAC yield from $C_2H_2$ decomposition. ....	170
Table 6.4: ANOVA results for MB removal % for CNM-PAC growth optimization..	172
Table 6.5: List of the actual and predicted values of the MB removal efficiency. ....	173
Table 6.6: Optimization constraints for CNM-PAC production.....	178
Table 6.7: The optimum conditions suggested by DOE for CNM-PAC growth.....	178

Table 6.8: CCD of experimental parameters for MB removal by O-CNT. ....	185
Table 6.9: ANOVA results for MB Removal % (RV3) by O-CNT. ....	186
Table 6.10: ANOVA results for the adsorption capacity of O-CNT (Q3).....	186
Table 6.11: Constraints for optimization process based on CCD for MB adsorption. .	188
Table 6.12: Potential optimization conditions based on CCD for MB removal onto O- CNT. ....	188
Table 6.13: Experimental values of constants of adsorption kinetics models. ....	192
Table 6.14: Linearized equations of studied isotherm models for MB adsorption on O- CNT. ....	196
Table 6.15: Comparison between the maximum adsorption capacity ( $q_m$ ) of O-CNT and other reported adsorbents for MB removal. ....	196
Table 7.1: Summary of BET results for PAC, Ni-PAC, O-CNTs, and KS-CNTs. ....	207
Table 7.2: Zeta potential results for PAC and the different carbon structures produced. .....	208

## LIST OF SYMBOLS AND ABBREVIATIONS

<b>Abbreviation</b>	<b>Definition</b>
AC	: Activated carbon
ANOVA	: Analysis of variance
BPA	: Bisphenol A
BET	: Brunauer-Emmett- Teller
$C_0$	: Initial adsorbate concentration
$C_t$	: Concentration at any time t in liquid phase
$C_e$	: Equilibrium concentration in liquid phase
CCD	: Central composite design
CV	: Coefficient of variation
CVD	: Chemical vapor deposition
CCVD	: Catalytic chemical vapor deposition
CNM	: Carbon nanomaterial
CNF	: Carbon nanofiber
CNT	: Carbon nanotube
CNM-PAC	: Carbon nanomaterial grown on powdered activated carbon
CNT-PAC	: Carbon nanotube grown on powdered activated carbon
CNP	: Carbon nano-particle
$CH_4$	: Methane
$C_2H_2$	: Acetylene
DOE	: Design of experiment
DWNT	: Double-walled carbon nanotube
EDX	: Energy-dispersive X-ray spectrometer
EDC	: Endocrine disrupter compound
FTIR	: Fourier transform infrared spectroscopy



<b>Abbreviation</b>	<b>Definition</b>
FESEM	: Field emission scanning electron microscopy
ID	: Intraparticle diffusion
K-CNT	: Potassium permanganate functionalized CNT
KS-CNT	: Potassium permanganate and sulfuric acid functionalized CNT
$K_d$	: Intraparticle diffusion constant
$K_f$	: Freundlich constant
$K_L$	: Langmuir constant
$K_T$	: Temkin constant
$K_1$	: Pseudo first order rate constant
$K_2$	: Pseudo second order rate constant
MWCNT	: Multi-walled carbon nanotube
MB	: Methylene blue
Ni-PAC	: Nickel doped powder activated carbon
$1/n$	: Intensity factor in Freundlich isotherm
O-CNT	: CNT on powder activated carbon at optimal growth conditions
PAC	: Powder activated carbon
PZC	: Point of zero charge
pKa	: The acid dissociation constant of a solution
$q_e$	: Equilibrium adsorption capacity
$q_{e,cal}$	: Calculated equilibrium adsorption capacity
$q_{e,exp}$	: Experimental equilibrium adsorption capacity
$q_m$	: Maximum adsorption capacity
$q_t$	: Adsorption capacity at any time t by the adsorbent

<b>Abbreviation</b>	<b>Definition</b>
RSM	: Response surface methodology
$R^2$	: Correlation coefficient
$R_L$	: Separation factor
RV	: Removal efficiency
SWCNT	: Single-walled carbon nanotube
S.D.	: Standard deviation
TEM	: Transmission electron microscopy
TGA	: Thermo-gravimetric analyzer
UV-vis	: Ultraviolet visible
VLS	: Vapor–liquid–solid model
VSS	: Vapor–solid–solid model
$\chi^2$	: Chi-square
Y	: Predicted responses

## CHAPTER 1: INTRODUCTION

### 1.1 Overview

Nanotechnology has been identified as utmost promising technology that opened new horizons of extreme engineering on the nanometer scale to create and utilize materials, devices and systems with new properties and functions. Nanotechnology encompasses the potential utilization of the of novel nanomaterials unique properties in many fields, e.g., energy (Hussein, 2015; Liu, Jin, & Ding, 2016), medicine (Mishra, 2016) , electrical industries (Contreras, Rodriguez, & Taha-Tijerina, 2017), food industry (Chellaram et al., 2014) and pollution treatment (Adeleye et al., 2016; Bashir & Chisti, 2014; De La Cueva Bueno et al., 2017). Not to mention, the global momentum of nanotechnology is dramatically participating in addressing, resolving and improving potential remediation prospects and provide remarkable advances in diminishing the adverse impact of the environmental pollutants (Shunin et al., 2018). The exceptional merits of nanomaterials such as thermal, electrical, mechanical, optical structural and morphological properties promoted their features for many applications where they can be functioned as nano-sensors, nanomembranes, nanorods, nanowires, disinfectant and nano-adsorbents (Murty et al., 2013). A variety of efficient materials have been developed in wastewater treatment including activated carbon, metal oxides, clay, silica and modified composites. However, nano-adsorbents with their high specific surface area, short intraparticle diffusion distance and tunable surface chemistry offer many possibilities for novel applications in water treatment (Sadegh, Shahryari-ghoshekandi, & Kazemi, 2014). Nano-adsorbent can be produced by chemical vapor deposition (CVD), sol-gel, chemical solution deposition (CSD), photocatalytic deposition (PD), deposition-precipitation (DP), ultrasonic irradiation, thermal and hydrothermal processes, *etc.* (Khajeh, Laurent, & Dastafkan, 2013).

Regarding to the conspicuous physiochemical properties of carbon nanomaterials (CNMs) and the lack of efficiency and selectivity of conventional adsorbents, carbon CNMs such as single walled carbon nanotubes (SWCNTs), multiwalled carbon nanotubes (MWCNTs), and graphene have been in the spotlight of scientific and industrial community as a promising alternative to traditional adsorbents, from the environmental and technological perspectives. The emergence of carbon nanostructures including carbon nanotubes (CNTs), carbon nano-particles (CNPs) and carbon nanosheets have enlightened the opportunities of their exploitation as appealing alternative sorpents for different pollutants in water (O'connell, 2012). Carbon nanotubes (CNTs), since their discovery by Wiles and Abrahamson (Wiles & Abrahamson, 1978) and re-discovery by Iijima in 1991 (Iijima, 1991), have been highlighted as outstanding materials due to their exceptional characteristics such as large surface area, well defined cylindrical hollow structure, as well as their unique electrical, mechanical, optical, physical and chemical properties (Khan, Kausar, & Ullah, 2016). Accordingly, CNTs have shown remarkable potential as competent adsorbents and suitable candidates for removal of a wide range of organic and inorganic contaminants from large volumes of wastewater due to their highly porous structure, large specific surface area, light mass density and strong interaction with the pollutants (Kim & Choi, 2017). However, some shortcomings hinder the application of CNTs and lower their ability to remove certain compounds, such as agglomeration, their poor dispersion in aqueous media and the successful recovery from the aqueous phase are troublesome and pose a significant challenge (Liu et al., 2013). Therefore, there is an exigent demand for extensive investigations to fabricate new hybrids materials to manipulate special properties of the nanomaterials seeking for versatile, effective utilization of CNMs for highly selective removal of pollutants (Kyzas & Matis, 2015; Santhosh et al., 2016).

The recent uncontrolled discharge of hazardous substances is leading to the development of a wide array of wastewater treatment techniques to meet the stringent environmental rules and regulations. Thus, there is great concern for improving efficient, sustainable and low-cost technologies to screen and adequately treat toxic environmental pollutants (Mohmood et al., 2013). Adsorption has been considered as one of the most effective techniques to wide range of contaminants from aqueous solution by virtue of low energy cost, ease of operation and environmental friendliness (Kyzas & Matis, 2015).

## **1.2 Problem statement**

CNMs have strong interactions with emerged contaminants due to their high aspect ratio, fibrous mesoporous structure, and large specific surface area. They have shown great potential as competent adsorbents for removal wide range of pollutants (Abkenar, Malek, & Mazaheri, 2015; Ren et al., 2011; Yu et al., 2013). Despite their strong adsorption affinity, the successful recovery of dispersed CNMs from aqueous phase, the sharp decrease in the surface area due to agglomeration and poor dispersion pose a significant challenge and hinder their practical application in water treatment (Al-Hamadani et al., 2015). Quite similarly to graphene and most of CNMs, CNTs suffer from bundling phenomena because of  $\pi$ - $\pi$  adhesion and van der Waals interactions between tubes which is generally responsible for the agglomeration tendency. Accordingly, the ineffective dispersion and recovery of nanostructures are considered serious limitations of CNT and all isolated nanomaterials which will restrain their application in any adsorption process. Not to mention, the most promising method for non-biodegradable organic pollutants is “adsorption” due to its simple process design, low cost, its ability to remove multiple components simultaneously, easy mode of operation without producing a large amount of toxic sludge and can be coupled with other mechanisms (Gupta, Ali, et al., 2012). Nevertheless, the utilization of inappropriate adsorbents will deprive the achievement of such extraordinary advantages. Therefore, it is necessary to emphasis on

developing innovative adsorbents that can overcome the current drawbacks and maximize the above characteristics. (Ravi & Vadukumpully, 2016; Smith & Rodrigues, 2015b).

Possible approaches was suggested to address these limitations include centrifugation and attachment of magnetic iron nanoparticles (Fan et al., 2012; Tang & Lo, 2013). However, both options will reduce significantly the cost-effectiveness and add complexity to the adsorption process. In view of the notable advances in nanotechnology and the imperative demand to develop innovative adsorbents for environmental remediation, this study enlightens an auspicious class of hybrid solid by directly growing carbon nanostructures on micro-scaled carbon support (Ansari; Laurila, Sainio, & Caro, 2017; Mleczko & Lolli, 2013). It is believed that the combination of nanocarbon material with non-carbon support structures would lead to deterioration of the overall compound properties and chemical stability because of the discontinuities in transport and in chemical properties (Meshot et al., 2017; Rajbhandari et al., 2013). Therefore, fabricating hybridized carbon materials with good performance has motivated the growing research interest towards production of potential alternatives to the conventional adsorbents (Liu, Sun, & Huang, 2010).

Recently, the introduction of powder activated carbon (PAC) as analogues of non-carbon supports was found worthy to be exploited especially in producing new type of CNM and such unique incorporation is expected to be an excellent adsorbent. Activated carbon (AC) acts as a stable carbon matrix, and the appearance of CNMs on carbon substrates not only provides additional active sites but also shifts the pore size distribution and reduces the effect of pore blocking on microporous channels (Sing, 2014). Furthermore, using AC substrate for growing CNM prevents their agglomeration due to the porous structure of the substrate. Carbon has fascinating physical and chemical characteristics and the area of nanocarbon-carbon hybrids has become encouraging in a wide variety of electronic and electrochemical applications (Ampelli, Perathoner, &

Centi, 2014; Zhao et al., 2012), however, their potential use as catalyst support to prepare these hybrids has not yet been fully investigated (Titirici et al., 2015). Still there are not many examples of utilizing this concept in water treatment and purification. Among the studied systems (Diring et al., 2010; Song et al., 2016; Yu, Goh, et al., 2014), activated carbon appeared to be very promising candidate for the growth of CNMs, moreover, the impact of the Ni/powder activated carbon (Ni-PAC) substrate on producing CNMs with multi-scale-porous structure was not explored in detail especially in monitoring their adsorptive performance for the removal of organic contaminants from aqueous solution.

The growing number of contaminants entering water supplies due to human activity is an important environmental problem worldwide, especially for those toxic and nonbiodegradable contaminants that raise public health concerns (Speltini et al., 2016; Yu, Zhao, et al., 2014b). During recent decades, research scientists and governmental authorities have become increasingly concerned about the exposure of humans and wildlife to a class of chemicals known as endocrine disruptor compounds (EDCs). These substances have the potential to interfere with the hormonal system, producing adverse developmental and reproductive effects even at very low levels. Among the EDCs, bisphenol A (BPA) is found to be acutely toxic to the living organisms between 1000-10,000  $\mu\text{g/L}$  for both fresh water and marine species (Kabir, Rahman, & Rahman, 2015; Locatelli et al., 2016). Another example of organic based industrial pollutants is methylene blue (MB) dye which is an issue of critical importance in various industries, such as textile, paper, plastic, leather, food, cosmetic, etc. MB is a cationic dye which is known to be very stable, difficult to biodegraded and widely disposed into water bodies. The improper disposal of MB significantly causes serious problems to the photosynthetic activity in aquatic life as well as the danger effects on human body. MB is toxic if inhaled or ingested, it can cause irritation, allergy difficulties in breathing, vomiting, diarrhea and nausea (Ezzeddine et al., 2016). BPA and MB are persistent organic pollutants that are

stable toward biological and chemical treatments, which can not only cause esthetic problems, but also exhibit high biotoxicity and potential mutagenic and carcinogenic effects. Therefore, it is important to treat and control the discharge of these hazardous substances to protect and preserve the natural water systems (Bhatnagar & Anastopoulos, 2017; Fu et al., 2015).

Finally, this research is an attempt to reduce the cost of isolation, and enhance the adsorbent capacity through synthesizing new type of hybrid carbon nanomaterials (CNMs) on powder activated carbon (PAC) substrate to end up with multi-structure materials from nano to micro scale. The prepared hybrid material is chemically homogeneous as it consists basically of carbon but poses a heterogeneous structure of multiscale scale particles at different shapes. The hybrid structures were evaluated for removal of a model organic contaminants; bisphenol A (BPA) and methylene blue (MB) from water. Furthermore, as compared with previous studies which concern only about high yields, the present investigation optimized the growth conditions of CNMs in conjunction with the pollutant removal efficiency. This distinctive procedure allows preparing the best material structure with the highest possible adsorption capacity.

### **1.3 Research objectives**

The objectives of this research are:

- 1- To synthesize a new type of multi-scale carbon nanomaterials onto powder activated carbon substrate from methane and acetylene pyrolysis using chemical vapor deposition reactor.

- 2- To determine the optimum growth conditions of CNMs such as (reaction temperature, reaction time and feed stock gas ratio) to produce the maximum yield together with the maximum removal efficiency of bisphenol A and methylene blue by using Design of Experiment (DOE), and to identify the physical and chemical changes on the carbon surface after CNMs growth at the optimal conditions.



3- To determine and optimize the effects of pH, adsorbent dose and contact time on the adsorption performance of organic pollutants by predicting adequate mathematical model. The kinetics and isotherm parameters of different adsorbate-adsorbent systems under study were also investigated.

4- To compare the adsorption performance of the functionalized and as-prepared carbon nanomaterials.

#### **1.4 Research scope**

The main motivation to conduct this research is to introduce hybrid CNM structures with improved capabilities for the removal of model organic contaminants. The synergistic effect of hybrid materials could offer remarkable adsorptive performance respect to those from the concomitant individual components. This research is an attempt to benefit from physicochemical properties of CNMs and PAC in developing new adsorbents to be utilized in multipurpose platforms specifically water treatment. Therefore, these easy prepared hybrid structures could open a new opportunity for developing a qualified adsorbent in remediation of contaminated water.

#### **1.5 Research methodology**

This research is constructed from the following stages:

- 1- Synthesizing CNMs on the surface of PAC.
- 2- Optimizing the growth parameters to obtain high yield of the CNMs along with maximum removal percentage for BPA and MB.
- 3- Characterization of CNMs produced at the optimal growth conditions using FESEM, TEM, EDX, Raman, TGA, FTIR, BET surface area and zeta potential.
- 4- Utilizing the synthesized CNMs as adsorbents for BPA and MB removal from water.

5- Modifying the produced CNMs with potassium permanganate ( $\text{KMnO}_4$  and  $\text{H}_2\text{SO}_4$ ) and compare their adsorption performance with the as-obtained CNMs.

6- Applying an estimated regression model using response surface methodology (RSM) to optimize the experimental conditions for growth process and removal of organic pollutants from water.

7- Investigating the adsorption kinetics and isotherm models along with their perspective parameters.

## **1.6 Outline of the thesis**

This research is constructed from eight chapters as follows:

Chapter 1 (Introduction) is an introductory chapter includes a brief background about CNMs including CNTs and carbon-based nano-adsorbents along with problems encountered during their application in adsorption system. The aims and objectives of the research work were mentioned followed by the methodology and finally, the scope of the study.

Chapter 2 (Literature Review) presents a review of the relevant scientific literature on CNMs and hierarchical carbon nanostructures. It focuses on their fabrication and functionalization methods. This chapter also demonstrates the history of different types of CNMs, as well as the most common processes applied to remove BPA and MB dye from water.

Chapter 3 (Materials and Methods) discusses the detailed research methodology including CNMs synthesis, characterization and modification as well as the methods of batch adsorption work and response surface methodology (RSM) studies. All materials, equipment and analytical instruments involved in this research are described in this chapter as well.

Chapter 4 (Results and Discussion) comprises the obtained research results and discussion from RSM method to synthesize and optimize the growth of CNM-PAC

hybrid from methane decomposition in conjunction with ANOVA analysis for each adsorption system.

Chapter 5 (Results and Discussion) provides the results and discussion gained from the surface characterization of the synthesized CNM-PAC from the decomposition of methane which is requisite to understand the adsorption mechanisms.

Chapter 6 and Chapter 7 (Results and Discussion) present results and discussion found from the optimization of the growth of CNM-PAC using acetylene, RSM, ANOVA and regression models of the adsorbate-adsorbent system together with full characterization of the prepared material at the optimal growth conditions.

Chapter 8 (conclusion) summarizes the overall findings of this study and the last section of this chapter includes some recommendations for future work.

## CHAPTER 2: LITERATURE REVIEW

### 2.1 Introduction

In view of the importance of water quality and emerging nanotechnology momentum, attempts have been made to present the opportunities for leapfrogging scenarios in the development and alteration of various aspects of water treatment by adsorption using nanomaterials. In this regard, nanomaterials/nano-adsorbents were suggested as efficient cost-effective and practical solution for potential removal of various pollutants using their unrivaled features (Kunduru et al., 2017). The unique properties of carbonaceous nanomaterials most commonly cited as a potential adsorbent for water and wastewater are size, shape, and surface area; molecular interactions and sorption properties (Weiss et al., 2012).

The search for new supports that will impart stability to the metallic nanoparticles has led to a new type of hybrid material that consists of metallic nanoparticles attached to the surface of carbon structures (Guerra & Herrero, 2010; Karousis et al., 2016). In many cases, the combination of two materials can create properties superior to those of either building constituents. One growing area of interest is the fabrication of multi-scale hybrid carbon structures that have been developed by growing carbon nanomaterials (CNMs) on high surface area substrates having open, interconnected porosity. CNMs grown onto porous substrates have been mostly limited to oxide or metallic foams. However, the unique physical and chemical properties of activated carbon such as large specific surface area, pore size control, large pore volume, and tuning of the hydrophobicity boosted their utilization to catalyze the growth of carbon nanostructures. The obtained nano-hybrids with their rigorous control of the pore size enabled the adsorption of even large pollutants (Libbrecht et al., 2017). In the view of the outstanding advances in nanotechnology and the urgent need to develop new approaches for environmental remediation, this study

demonstrates the potential of using multi-scale carbon structures as robust, reusable solids suitable for removal of aqueous pollutants from wastewater.

## **2.2 Carbon nanotubes**

Carbonaceous nanomaterials are the most-studied emerging nanomaterials in recent years. They can be classified as nano-diamonds, fullerene, carbon onions, graphene, multiwalled carbon nanotubes (MWNTs), and single-walled carbon nanotubes (SWNTs). Carbon nanotubes (CNTs), a new form of the carbon family, is considered as a revolution in nanotechnology development have lately drawn significant attention because of their physical, chemical, mechanical, electrical, and optical properties (Mallakpour & Khadem, 2016). Carbon nanotube represents the simplest chemical composition, however, shows the most extreme diversity among nanomaterials in structures and structure-property relations (Saha, Jiang, & Martí, 2014).

### **2.2.1 Structure of carbon nanotubes**

Carbon nanotubes are novel nanomaterials consisting of one or more graphite sheets wrapped around itself into a seamless cylinder of nanoscale radius of less than 100 nanometer (nm) and a length up to 20 cm with both ends usually "capped" with half of a fullerene-like molecule. Bonding in the hexagonal graphite sheet of carbon atoms is essentially in a  $sp^2$  hybridization state (De Volder et al., 2013). The hexagonal lattice structure is stacked on top of one another to form a 3D crystal which is kept together by the relatively weak van der Waals forces between these layers. The  $1s$  and  $2p$  orbitals can produce  $\sigma$  bonds and the third  $p$  orbital builds a  $\pi$  bond with an identical  $p$  orbital on another carbon atom. In graphite, three  $\sigma$  bonds are formed in-plane with an  $\pi$  bond out-of-plane (Kang et al., 2016). However, the circular curvature of CNTs will cause  $\sigma$ - $\pi$  rehybridization in which the three bonds are partly out of the plane; the  $\pi$  orbital is more

delocalized outside the tube, thus makes CNTs mechanically stronger and chemically more active than graphite (Figure 2.1) (Nessim, 2010).

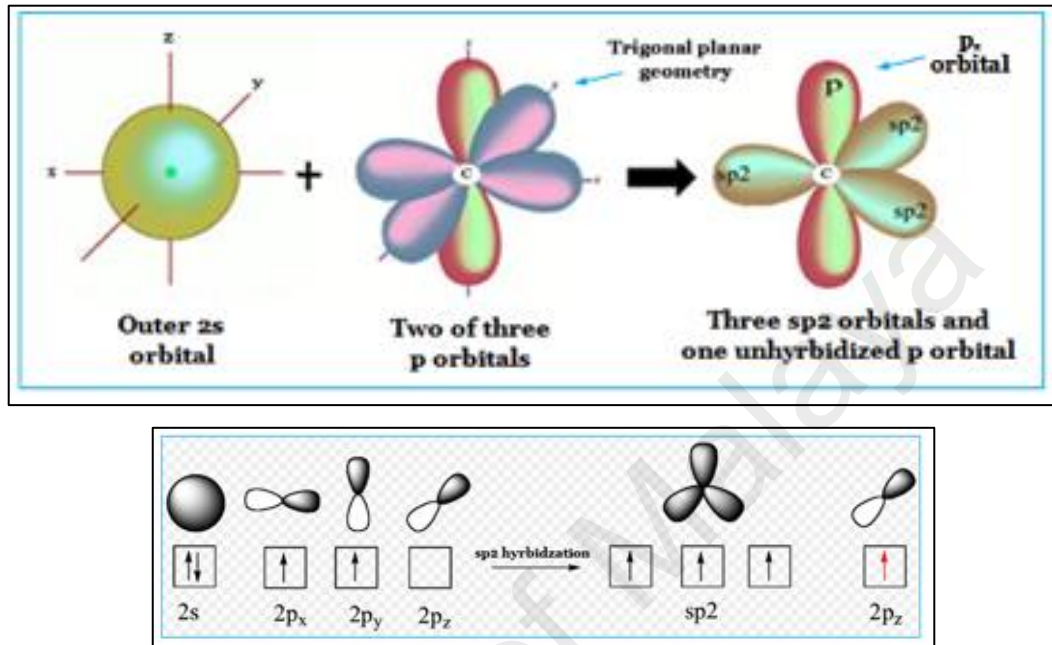


**Figure 2.1: Graphite carbon  $sp^2$  hybridization.**

There are two major classes of carbon nanotubes: single-walled and multi-walled tubes based on the number of graphite layers. As shown in Figure 2.2, a single graphitic sheet rolled-up would give one circumferential layer is described as a single-walled carbon nanotube, while several sheets that are possible to roll-up around a concentric axis would give a multi-walled nanotube. Diameter less than 2 nm is usually found for SWNTs and MWNTs have much wider but are usually less than 100 nm in diameter (Allaadini, Aminayi, & Tasirin, 2015). CNTs are extremely hydrophobic and the physical structure of CNTs is further complicated by the large van der Waals forces and  $\pi$ -stacking which tend nanotubes to form bundles or ropes and, thus inhibit their dispersion in water (Li, Liu, et al., 2015).

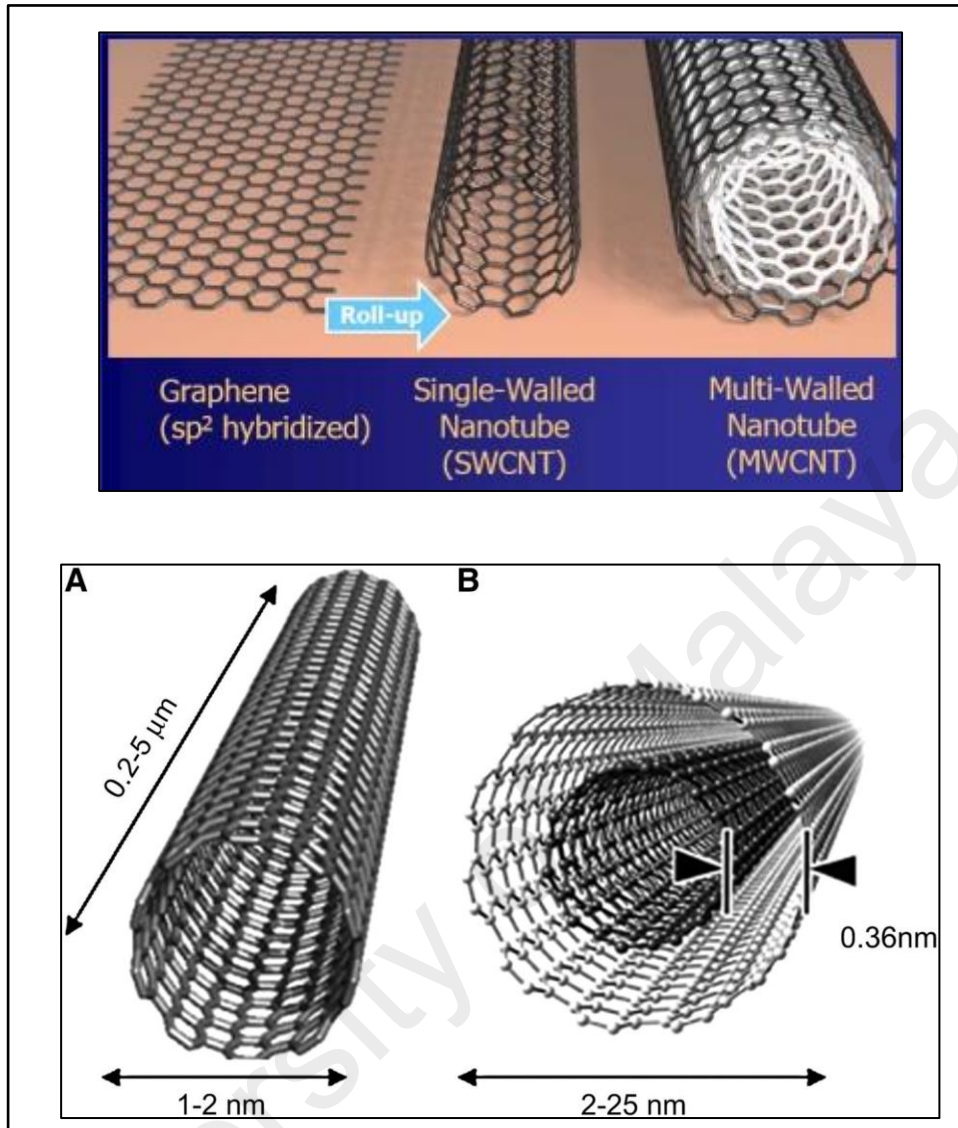


**Figure 2.2: Schematic models describing single-walled and multi-walled carbon nanotubes conceptually obtained from single graphene sheets (Mubarak, Sahu, et al., 2014).**

## 2.2.2 Properties and uses of carbon nanotubes

### 2.2.2.1 Electrical properties

Electrical properties is one of the most significant features of CNTs because of their unique one dimensional nano-structures, electrons can be conducted in nanotubes without being scattered (Meunier et al., 2016). The CNTs are very polarizable and allowed to conduct due to the electrons in the  $\pi$ - system. The absence of scattering of the electrons during conduction and remaining coherent in a straight line is known as ballistic transport.

This mechanism for electron transport allows the nanotube to conduct without dissipating energy. Another interesting electronic aspect of CNTs is that they can be metallic or semiconducting depending on their diameter and chirality. The band gap of semiconducting tubes has been seen to be inversely proportional to the diameter of the tube, as they start resembling graphite, which is a zero band-gap material (semi-metal) (Helal, 2015). There has been much interest in utilizing carbon nanotubes in electronic devices such as transistors, electrodes in electrochemical reactions and sensors due to their high electrical conductivity and relative inertness. Furthermore, they are potential candidates to produce electronic appliances that will consume less energy and produce less heat too (Rao, Gopalakrishnan, & Maitra, 2015; Soma, Radhakrishnan, & Sarat Chandra Babu, 2017).

#### **2.2.2.2 Mechanical properties**

CNTs exhibit extraordinary mechanical properties; they are remarkable strong, robust and have very high Young's modulus. They are as stiff as diamond, with tensile strength  $\sim 200$  GPa. Under all mechanical stresses, they have a nondestructive failure mechanism such as buckling or flattening (Liang, Han, & Xin, 2013). They are five times stronger than stainless steel, although, they are very light weight relative to it. These exceptional mechanical properties of CNTs make their application in composite materials is very promising. Thus, they can enhance the stiffness of a polymer, add multifunctionality (such as electrical conductivity) to polymer based composite systems. Efforts are made to obtain tougher ceramics by fabricating the CNT containing ceramic-composites (Ahmad, Yazdani, & Zhu, 2015). Also, under electric stimulation, nanotubes can mechanically deflect and this opens applications such as actuators or cantilevers. Nanotubes has also been suggested to be used as anode for lithium ion batteries, membrane material for batteries and fuel cells, and chemical filters (Park, Vosguerichian, & Bao, 2013).



### 2.2.2.3 Thermal properties

The intrinsic characteristic of the strong  $sp^2$  lattice dominates the thermal transport in CNTs, rather than by phonon scattering on boundaries, producing very high thermal conductivity (K) values. Single walled carbon nanotubes (SWCNTs) are expected show remarkably high thermal conductivity and converge to graphene at high temperature. Inter-shell coupling in MWCNTs result in a low-temperature specific heat that matches that of three-dimensional graphite (Balandin, 2011). Pop et al. (2006), measured a thermal conductivity of almost  $3500 \text{ Wm}^{-1} \text{ K}^{-1}$  at room temperature for a 2.6 mm long SWCNT with a diameter of 1.7 nm (Pop et al., 2006), similarly, Kim et al. measured a thermal conductivity above  $3000 \text{ Wm}^{-1} \text{ K}^{-1}$  at room temperature for multi-wall CNTs (Kim et al., 2001). Thermal management and dissipation have become a very significant issue and these high values for thermal conductivity of CNTs will contribute another useful property for electrical applications such as future microprocessors (Balandin, 2011; Sun, Meany, & Wang, 2014).

### 2.2.2.4 Chemical properties

As-produced carbon nanotubes are insoluble in organic solvents and aqueous solutions which has imposed great limitations to the use of CNTs (Cheng et al., 2010). Although, sonication of the CNTs can enhance their dispersion in some solvents, but the precipitation immediately occurs when this process is interrupted. On the other hand, it has been demonstrated that CNT can interact with different classes of compounds (Smith & Rodrigues, 2015a; Yu, Zhao, et al., 2014a). CNT can be considered as electron donors (alkali metals) and can act as guest–host compounds with electron acceptors (e.g., iodine, halogens, bromine,  $\text{FeCl}_3$ ,  $\text{HNO}_3$ ). The guest species can be introduced within the graphene shells of MCWNTs or inside the bundles of SWNTs in the open inter-tubular spaces. In addition, CNT can be more soluble by their chemical integration into inorganic, organic, and biological systems. Not to mention, the formation of CNT supramolecular

complexes has led to the remarkable fabrication of nano-devices (Hanelt et al., 2012; Pochorovski et al., 2015).

#### **2.2.2.5 Adsorption properties**

Compared to the large dimensions of traditional sorbents, low sorptive efficiency and limited active sites surface area, the nano-adsorbents and carbon-based nanomaterials offer a substantial advancement with their good adsorption kinetics as demonstrated by their high specific surface area, tunable pore size and surface chemistry (Sadegh et al., 2017). Nano-adsorbents are broadly classified into metallic nanoparticles (NPs) and carbonaceous nanomaterials (CNMs). Among the nanoscale metal oxides, the magnetic nanoparticles have drawn a considerable concern as a more cost efficient, effective adsorbent for water treatment. Not to mention among carbon-based nanomaterials, the adsorption-related applications of CNTs have received considerable attention to solve environmental pollution problems (Ghaedi et al., 2013; Ravi & Vadukumpully, 2016). CNTs have been proposed as substitutes for activated carbon as they display outstanding competency for gas and liquid phases, such as organic vapors, heavy metal ions and inorganic pollutants due to the availability of binding sites, the strong solute–sorbent interactions and their high specific surface areas stand comparison with those of activated carbons (ACs) (Luo et al., 2013). CNTs hold interesting positions in carbon-based adsorptive materials as they provide chemically inert surfaces for physical adsorption and the adsorbed molecules can deal directly with various well-defined adsorption sites (Apul & Karanfil, 2015). CNTs have been evaluated for the sorption of 1,2-dichlorobenzene (DCB) and it was reported that they can be used with a maximum sorption capacity of 30.8 mg/g (Peng et al., 2003). Novel sorbents consisting of cerium oxide supported on carbon nanotubes (CeO<sub>2</sub>-CNT) were effective sorbents for As (V) (Peng, Luan, Ding, et al., 2005). Moreover, both SWCNTs and MWCNTs have been investigated for their ability to remove trihalomethanes and ethylbenzene from aqueous solution (Bina et al.,

2011; Lu, Chung, & Chang, 2006). CNTs have exhibited remarkable adsorption ability and high removal efficiency for many organic pollutants (Table 2.1), including organic dyes (e.g., Cationic, reactive, azoic, basic and acid dyes etc.) (Bazrafshan et al., 2015; Gupta et al., 2013). Pharmaceuticals (e.g., Cephalexin, tetracycline, olaquinox, carbamazepine, etc.) (Jafari & Aghamiri, 2011; Ji et al., 2010; Zhang, Xu, et al., 2011), pesticides (Yu, Zhao, et al., 2014c), phenolic compounds (Abdel-Ghani, El-Chaghaby, & Helal, 2015; Cai et al., 2003; Sheng et al., 2010; Yang et al., 2008) and other toxic compounds (Apul & Karanfil, 2015).

University of Malaya

**Table 2.1: Carbon nanotubes as organic compounds adsorbent.**

Organic pollutant type	Examples	CNM modification	Adsorption isotherm	Remarks	Reference
Phenolic compounds; benzene derivatives and other toxic organics	Pentachlorophenol (PCP)	MWCNTs Oxidized by H <sub>2</sub> O <sub>2</sub> , HNO <sub>3</sub> and KMnO <sub>4</sub>	Langmuir, Freundlich and Fritz–Schlunder	Lower PCP adsorption by CNTs by increasing the oxygen functional groups (carboxylic, phenolic and lactonic).	(Abdel Salam & Burk, 2008)
	2,4,6 trichlorophenol (TCP)	Modified with HNO <sub>3</sub>	Polanyi–Manes	The increased hydrophilic carboxylic groups and surface area increased the adsorption capacity for TCP.	(Chen, Shan, et al., 2009)
	Benzene, toluene, ethylbenzene and <i>p</i> -xylene (BTEX)	Sodium hypochlorite (NaOCl) oxidation	Langmuir and Freundlich	Oxidation increased the purity, carbon containing defects, carboxylic groups and surface charge negativity which enhanced the BTEX adsorption.	(Su, Lu, & Hu, 2010)

**Table 2.1 (continued)**

<b>Phenolic compounds; benzene derivatives and other toxic organics</b>	Bisphenol A (BPA)	MWCNT-COOH	Langmuir and Freundlich	The reduced uptake at pH is 9–11 is because of the increased repulsion forces and a reduction of $\pi$ - $\pi$ interaction between bisphenolate anions and the sorbent.	(Bohdziewicz & Kamińska, 2013)
	Bisphenol A (BPA)	Untreated SWCNTs	————	Controlled by $\pi$ - $\pi$ electron donor–acceptor mechanism.	(Pan et al., 2008)
	Bisphenol A (BPA)	MWNTs-COOH	Langmuir	$\pi$ - $\pi$ interaction between bisphenolate anions and the sorbent.	(Bohdziewicz & Kamińska, 2013)
<b>Organic Dyes</b>	Methylene blue (MB)	MWCNTs oxidized by HNO <sub>3</sub>	Langmuir	MB removal by $\pi$ - $\pi$ electron donor acceptor interaction and electrostatic attraction.	(Li, Du, et al., 2013)
	Methylene blue (MB)	MWCNTs loaded with magnetite	Langmuir	The electrostatic attraction and $\pi$ - $\pi$ stacking interactions between (M-CNTSs) and (MB) was responsible for the high adsorption capacity.	(Ai, Zhang, Liao, et al., 2011)

**Table 2.1 (continued)**

Organic Dyes	Methylene blue (MB)	Untreated cylindrical graphene-carbon nanotube (G-CNT) hybrid	Freundlich	The electrostatic attraction between the negatively charged G-CNT hybrid and the MB.	(Ai & Jiang, 2012b)
	Methylene blue, (MB) and methyl orange, (MO)	Alkali-activated MWCNTs	Freundlich	multiple adsorption interaction mechanisms (hydrogen bonding, $\pi$ - $\pi$ electron-donor-acceptor interactions, electrostatic interactions, mesopore filling).	(Ma et al., 2012)
	Reactive red M-2BE (RRM)	Untreated MWCNTs	Liu	The controlling step is the electrostatic attraction of the negatively charged dyes to the positively surface charged MWCNT adsorbent at pH 2.	(Machado et al., 2011b)
	Direct Yellow 86 (DY86) Direct Red 224 (DR224)	Untreated MWCNTs	Freundlich	The affinity between DY86 and CNTs was less than that between DR224 and CNTs (physio-process).	(Kuo, Wu, & Wu, 2008)

**Table 2.1 (continued)**

Pharmaceuticals	Tetracycline (TC)	Untreated MWCNTs	Langmuir	The adsorption mechanism is probably the non-electrostatic $\pi$ - $\pi$ dispersion interaction and hydrophobic interaction.	(Zhang, Song, et al., 2011)
	Ibuprofen (IBU)	CNTs Oxidized with HNO <sub>3</sub> , (O-CNTs)	Polanyi-Manes Model	Less adsorption capacity for O-CNTs than that of pristine CNTs.	(Cho, Huang, & Schwab, 2011)
	Ciprofloxacin (CPI)	Graphitized MWCNTs, (MG), carboxylized (MC), and hydroxylized (MH).	Freundlich and Dubinin-Ashtakhov (DA).	Higher sorption on MH than MC attributed to the $\pi$ - $\pi$ electron donor-acceptor interactions.	(Li, Zhang, et al., 2014)
	Ofloxacin (OFL)	Graphitized MWCNTs, (MG), carboxylized (MC), and hydroxylized (MH).	Freundlich	Several mechanisms including electrostatic interactions, cationic exchange, and hydrogen bond enhanced the sorption of OFL.	(Peng et al., 2012)
	Sulfamethoxazole (SMX)	Graphitized (MG), carboxylized (MC), and hydroxylized (MH).	Dubinin-Ashtakhov	The adsorption sequence: MH > MG > MC due to $\pi$ - $\pi$ electron donor-acceptor interactions at low pHs	(Zhang, Pan, et al., 2010)

**Table 2.1 (continued)**

<b>Pesticides</b>	Atrazine	Untreated MWCNTs	Polanyi–Manes	reversible adsorption of atrazine at external surface of CNTs.	(Yan et al., 2008)
	Diuron and dichlobenil	Untreated MWCNTs	Polanyi–Manes	The hydrogen bonding was the main adsorption mechanism and the removal was reduced by increasing the oxygen containing groups.	(Chen et al., 2011)
	Diuron, fluridone and norflurazon	Purified SWCNTs by mixture of H <sub>2</sub> SO <sub>4</sub> and HNO <sub>3</sub>	Freundlich and Dubinin Ashtakhov (DA)	Hydrogen bonding and hydrophobic interactions controlled the adsorption mechanism.	(Sun et al., 2012)



### 2.2.3 Multi-scale/ hybridized carbon structure

Activated carbon, carbon fibers, aerogels, and nanostructures of carbon are well-suited as carbon-based adsorbents. Nanostructures of carbon such as carbon nanotubes (CNTs), graphene, and bucky-balls, have recently gained significant interest (Qu, Alvarez, & Li, 2013; Ren et al., 2011; Tan et al., 2012). Among them, CNTs in the isolated powder form have been reportedly exhibited high adsorption performance, but successful recovery of nanostructures create a significant challenge and calls for additional separation steps (Ma et al., 2012; Yao et al., 2010). Their poor dispersion in the aqueous media because of the hydrophobicity of the graphitic surface is the main drawback of CNTs that significantly hinders their application. Although, the strong intermolecular van der Waals interactions between tubes create loose bundles/aggregates that contain grooves and interstitial spaces which are recognized as high adsorption energy sites for organic species, it was suggested that the effective surface area of CNTs was reduced due to those aggregates (Fernandes et al., 2015). This is a critical limitation of stand-alone CNT and all isolated nanomaterials in general, since their dispersion in water can relate to uneconomical material loss and pose toxicity risks to the aquatic environment, not to mention, the significant reduction in the cost-effectiveness will be if the material cannot be reused and recovered easily (Zhu et al., 2009). Centrifugation and attachment of magnetic iron nanoparticles are suggested proposed approaches to address this limitation, and both options add cost and complexity to the adsorption process (Tang et al., 2014; Tang & Lo, 2013).

The hierarchical carbon structure in synthetic multi-component systems using tubes, foams, and particles fibers maximize the interfacial and contribute more numerous micro- and mesoporous structures. Multiscale support systems have attracted considerable attention in many fields ranging from energy storage to catalysis, sensing, and medical treatments due to their unlimited possible combinations of distinct properties (Wang,

Pandit, et al., 2017). Those effective applications indicated the great potential of CNT based hybrid nanomaterials as novel functional agents to improve material's performance. There is an ever-increasing demand for increasing the interfacial area by grouping multiple functionalities into the minimum space, while maintaining the other properties as needed. This is achieved by integrating the small attached individual components on a larger support and the connecting channels and other auxiliary space will still be needed for integration. Therefore, the ultimate objective will come from the overall surface area available in a given volume to support components (Schütt et al., 2017).

Carbon nanomaterials have been grown on many flat surfaces and simple geometries (Cong et al., 2012; Kumar & Ando, 2010). CNMs grown onto porous substrates have been mostly limited to metallic or oxide supports (Awadallah et al., 2016). Attaching multi-walled carbon nanotubes (MWCNTs) onto the substrate surface is one method for creating enhanced hierarchical interfaces (Avilés, de Jesús Kú-Herrera, & Oliva-Avilés, 2017; Tang et al., 2011). The success in this approach is substantially depend on the possibility of strongly attaching CNTs inside the pores of porous substrate. However, the growth of the nanotubes is directly related to substrate shape and composition (Ashraf et al., 2016). This process facilitates the growth of a dense and strongly attached CNT even inside the pores of the larger porous substrate. Thus, the surface-interaction related applications can be enhanced by the availability of the entire surface of the attached nanotubes, including those inside the deeper pores. This strong hierarchical structure offers a bimodal pore distribution combining the microporous characteristics of nanoscale carbon elements with mesoporous structures to produce superior properties with respect to those of the individual building blocks. These structures that can be engineered at both micro and nanoscales has proven to be promising in many applications ranging from thermal management, composite toughening, bio-sensing, to the catalytic grown of

dendritic structures such as CNTs/CNFs (Mukhopadhyay & Karumuri, 2010; Tang et al., 2010).

#### **2.2.4 Powder Activated carbon catalyzing the synthesis of carbon nanotubes**

Activated carbon (AC) has been explored extensively among the different carbon materials due to its attractive properties: the chemical inertness, the high surface area with controllable porosity, rapid adsorption capability, the graphitic character flexibility which is related to heat and electronic conductivity, the low cost of production, and tunable hydrophobicity or -philicity degree induced by the surface chemistry (Li & Zhao, 2013). The porous network of AC has relatively broad pore-size distributions and an abundant presence of micropores (pore size < 2 nm) which greatly influences its adsorption affinity. Thus utilizing activated carbon support will provide the dual purpose as the porous substrate to embed the catalyst and an effective adsorbent as well. (Chuenchom, Kraehnert, & Smarsly, 2012).

Remarkably, it is also found that porous carbon black could motivate CNM and/or CNT formation due to its advantage of density, more growth sites, high surface areas, and less nanoparticle aggregation during the reduction process, leading to good particle dispersion and high yield of the grown carbon nanostructures (Han et al., 2014; Lin et al., 2016). Accordingly, the adsorption performance is boosted due to the excellent characteristics of the large surface area of the CNTs along with abundant porous structure. Therefore, the dual advantage of the formation of CNTs on activated carbon surface to form the new multifunctional structure with unique physical, chemical and electronic properties attracts much attention in the potential applications of environmental remediation (Ravi & Vadukumpully, 2016; Sivakumar et al., 2011; Zhou et al., 2014a).

## 2.2.5 Synthesis of carbon nanotubes

Different techniques can be used to produce various types of carbon nanotubes and other types of carbon nanostructure materials. This section demonstrates different methods for synthesizing nanotube and their status are briefly described. Arc discharge, laser ablation and chemical vapor deposition (CVD) are the most well-known techniques being used. However, economically convenient large-scale production and purification methods still should be exploited.

### 2.2.5.1 Arc discharge

In the early stage, the carbon nanotubes were being produced by the carbon arc discharge. Sumio Iijima accidentally observed the structures of the CNTs for the first time during using the arc-discharge method for the production of fullerene soot (Iijima, 1991). The carbon arc easily generates the high temperatures needed to vaporize carbon atoms into a plasma ( $> 3000^{\circ}\text{C}$ ). The stability of the plasma, inert gas pressure, the current density, and cooling of chamber and electrodes influence the yield of CNTs. To produce nanotubes, this method encloses two carbon electrodes put in the next nearness to each other ( $\sim 1$  mm). The electrodes are put in environment of an inert gas like argon or helium, and then the electrodes pass a big current (Chen, 2015). The nanotubes created from the deposition of the vaporized carbon liberated from the first electrode into pillar-like tubes onto the opposite electrode. The electric arc vaporizes a hollow graphite anode associated with a mixture of a transition metal (such as Ni, Fe or Co) and graphite powder. The operative conditions involve  $2000\text{-}3000^{\circ}\text{C}$ , 100 amps, 20 volts and the inert gas flow is introduced at 50-600 Torr. The Nanotubes created using this method are usually short tubes with diameters ranging from 0.6 to 1.4 nm for single walled and 10 nm diameter multi walled nanotubes. This method is relatively easy to implement, and will produce yields of 30%. The nanotubes produced contain more impurities compared to other

methods, and the consistency of the shape, wall, and lengths of the tubes are somewhat random (Aqel et al., 2012).

Figure 2.4 shows a schematic diagram of arc-discharge apparatus for the synthesis of carbon nanotubes. This apparatus should be connected to a vacuum line along with a diffusion pump, and to a helium supply. The two electrodes are usually made of high purity graphite rods. Typically, the anode is a long rod around 6 mm in diameter and the shorter rod cathode approximately 9 mm in diameter. Effective cooling of the cathode has been shown to be crucial factor in producing good quality nanotubes (Arora & Sharma, 2016).

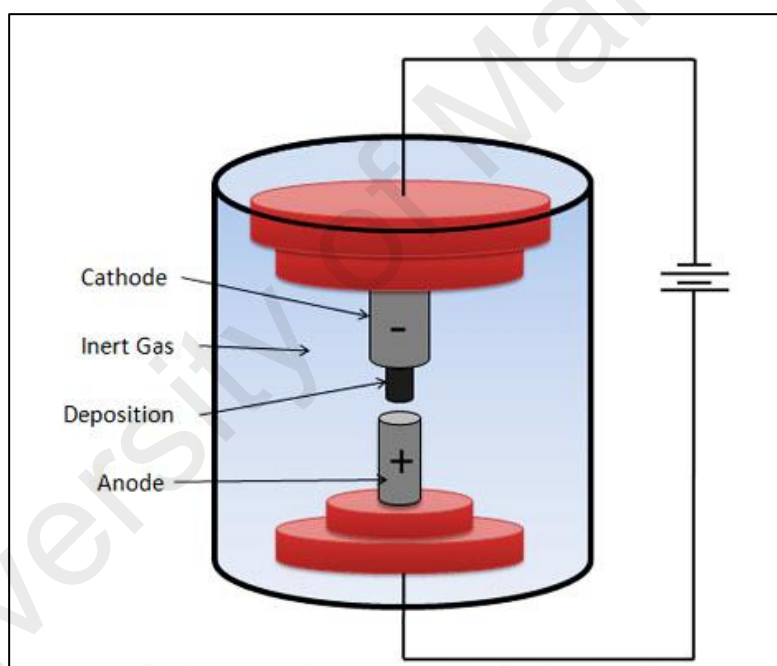


**Figure 2.3: Schematic diagram of arc-discharge apparatus.**

### 2.2.5.2 Laser ablation

Pulsed laser vaporization, or laser ablation technique, is an efficient route for fabricating bundles of SWNTs with a narrow distribution. Similar to the carbon Arc-discharge method, this method vaporizes the carbon and later deposits it onto a substrate (Szabó et al., 2010). In laser ablation, a target consisting of graphite mixed with a small amount of transition metal particles as catalyst is placed at the end of a quartz tube

enclosed in a furnace. A laser beam is used to ablate the carbon atoms from the carbon target. Quick condensation of the small vaporized carbon species produce larger clusters, possibly including fullerenes (Bystrzejewski et al., 2008). The target is exposed to an argon ion laser beam, which vaporizes graphite and nucleates carbon nanotubes in the shockwave just in front of the target. The reaction temperature has been found to affect the yield and quality of these products. Argon flow through the reactor heated to about 1200 °C by the furnace carries the vapor and nucleated nanotubes, which continue to grow (Mubarak, Abdullah, et al., 2014). The nanotubes are deposited on the cooler quartz tube downstream from the furnace. MWCNTs are produced by using a pure graphite target, but SWCNT are synthesized from graphite target mixed with equal amounts of Co and Ni (Figure 2.4). The laser ablation produces condensates which is contaminated with carbon nanotubes and carbon nanoparticles. Higher yield of SWNTs with better properties are produced by the laser vaporization than SWNTs produced by arc-discharge. Purer nanotubes are obtained by laser ablation (up to about 90 % purity) than those obtained by the arc discharge. The laser technique is not economically recommended because the produced amount of CNTs per day is not as high as arc discharge method, laser powers required are high process and involves high-purity graphite rods (Manzano-Ramírez et al., 2013).

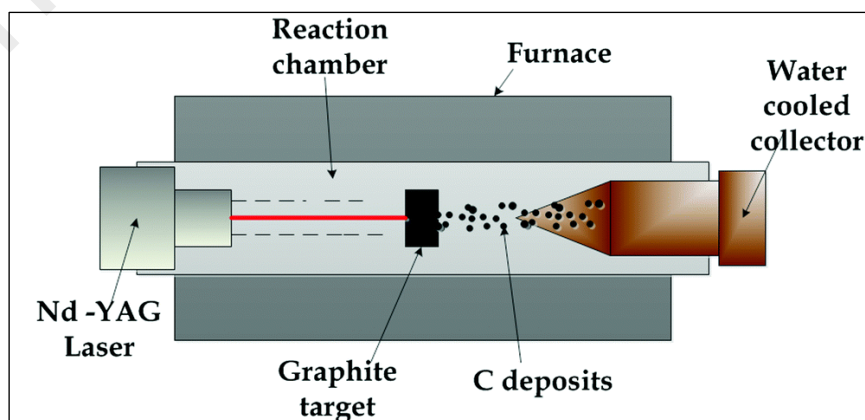


**Figure 2.4: Schematic drawings of a laser ablation.**

### 2.2.5.3 Chemical vapor deposition (CVD)

Chemical vapor deposition (CVD) has emerged as one of the most promising tool for economically producing large quantities of CNTs of various thicknesses and on various substrates. CVD route is very different from the electric arc discharge and laser vaporization (Varshney, 2014). Arc discharge and laser vaporization can be considered as high temperature ( $>3000$  K) and short time reaction ( $\mu\text{s}$ - $\text{ms}$ ) methods, whereas CVD is a medium temperature (700-1473K) and long-time reaction (typically minutes to hours) approach. The arc discharge and laser vaporization drawback is mainly attributed with that the CNTs are produced as standalone on their own; thus, CNTs do not grow on a patterned or conventional substrate (Qian, 2001). From 1998 onward, rapid and notable progress has been undertaken in the development of CVD to classify it as a highly controlled technology to produce CNTs. Today, it is possible to fabricate high quality MWNTs and SWNTs directly onto substrates or in bulk as a raw material. CVD is a versatile technique suitable for the manufacturing of coatings, powders, fibers, monolithic components, corrosion applications as well as large variety of compounds including carbides, nitrides, oxides, and many others (Shah & Tali, 2016c). A major advantage of CVD is that the CNTs can be used directly without further purification unless the catalyst particle is required to be removed. In this process, thermal decomposition of the hydrocarbon precursor over a heated metal catalyst, diffusion of carbon, nucleation and growth of carbon nanotubes. (Kumar & Ando, 2010).

In 1890, French scientists observed the formation of carbon filaments during experiments involving the passage of cyanogens over red-hot porcelain (Schultzenberger & Schultzenberger, 1890). By mid-twentieth century, CVD was a well-known method for synthesizing carbon microfibers using thermal decomposition of hydrocarbons in the presence of metal catalysts. In 1952, Radushkevich and Lukyanovich reported electron micrographs obviously exhibiting tubular carbon filaments of 50–100 nm diameter

obtained from thermal decomposition of carbon monoxide in the presence of iron catalyst at 600 °C (Khalaj, Monajjemi, & Diudea, 2016). In 1953, Davis et al. published detailed electron micrographs and XRD spectra of carbon nanofibers grown from the reaction of CO and Fe<sub>2</sub>O<sub>4</sub> at 450 °C in blast furnace brick works (Davis, Slawson, & Rigby, 1953). In the 1970s extensive works were carried out independently by Baker and Endo to synthesize and understand carbon fibers (Baker et al., 1972) and tubular nanofibers (Cheng et al., 2004; Ci et al., 2000; Kim et al., 2006; Lee et al., 2002). But, there were no indications that it could also be used for the synthesis of carbon nanotubes until Yacamán et al., (1993) reported this method the first time for the production of nanotubes (José-Yacamán et al., 1993).

The simplest form of CVD apparatus is shown in Figure 2.5. Several studies have proposed different possibilities based on the reaction conditions and post deposition product analyses, which are often contradicting (Nessim et al., 2009). Therefore, no single mechanism for CNT growth is well established till date. Nevertheless, the most widely-accepted mechanism that can be is based on the catalytic decomposition of carbon precursor gases on catalysts, in the form of thin films or as deposited nanoparticles. The growth temperature typically varies between 700 °C and 900 °C as high temperature is necessary for the catalysis to occur. Hydrocarbon vapor first decomposes into carbon and hydrogen species after contacting the “hot” metal nanoparticles; and hydrogen flies away. As carbon gets dissolved into the metal, the carbon precipitates out after the carbon-solubility limit is reached in the metal and crystallizes in the form of a stable cylindrical network (Gromov et al., 2016).



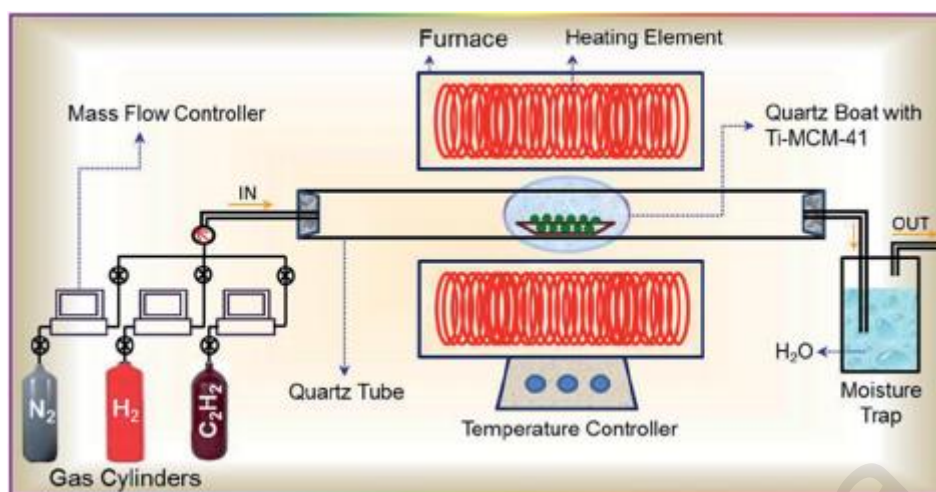


**Figure 2.5: Schematic diagram of a CVD setup in its simplest form (Atchudan et al., 2015).**

These are the basic principles of the CVD process. In the past decade, the carbon nanotubes synthesis have been developed with different techniques of CVD, such as plasma enhanced CVD (PECVD) (Meyyappan et al., 2003), thermal chemical CVD (Lee & Park, 2000), and catalytic pyrolysis of hydrocarbon (Cheng et al., 1998). CVD is a simple and economic technique for producing CNTs at low temperature and ambient pressure, as compared to arc-discharge and laser-ablation approaches. It provides CNTs with high yield and purity, offers utilizing plenty of hydrocarbons in any state, enables the growth of CNT in a variety of forms on various substrates such as powder, coiled, entangled or aligned, and thin or thick films nanotubes (Prasek et al., 2011). Based on the summarized comparison in Table 2.2, CVD process is highly selective, very simple, easily reproducible and can be classified as the most promising low cost scaled technique for producing large quantities of carbon nanotubes.

Usually transition metals (Fe, Ni, Co) or alloys catalysts are required in CVD based syntheses of CNTs (Lee et al., 2010). The main role of the catalyst in the CVD process is to decompose the carbon source via either heat (thermal CVD) or plasma irradiation (plasma-enhanced CVD, PECVD) which will nucleate to form CNTs. The rate of carbon decomposition, yield, and quality of products in CNT synthesis are considerably determined by the choice of catalyst.

**Table 2.2: Comparison of arc-discharge, laser ablation and CVD methods.**

Method	Temperature (°C)	Nanotube graphitization	Nanotube yield	Nanotube selectivity	Relative nanotube quantity
Arc discharge	3000-4000	high	< 30%	low	low
Laser ablation	~ 3000	high	~ 70%	low	low
CVD	500-1100	middle	40-80%	high	high

The choice of catalyst is probably the most important variable in synthesizing CNT, defining the yield, selectivity, rate of carbon decomposition and quality of products. Kathyayaini et al. (2008), reported that the decomposition of acetylene shows significant higher activity with cobalt than iron under similar reaction conditions (Kathyayaini et al., 2008). Most of research to date has investigated supported catalyst systems, where the metal-substrate interactions play a significant role in determining the morphology of the prepared catalyst and, thus, on the resulting mechanism for CNTs growth (Kudo, 2016).

Concerning the carbon source, methane (Palizdar et al., 2011), ethane (Tomie et al., 2010), ethylene (Narkiewicz et al., 2010), acetylene (He et al., 2011), xylene (Shirazi et al., 2011), their mixture (Li et al., 2010), isobutene (Santangelo et al., 2010) or ethanol (Yong, Fang, & Zhi-Hua, 2011) are the most preferred hydrocarbons in CVD. The efficiency of CNTs growth, in the case of gaseous carbon source strongly depends on the concentration of the gas phase and the reactivity of intermediates produced as a result of hydrocarbon decomposition. Thus, it can be predicted that in order to initiate CNT growth more efficiently, these intermediates should be produced in the gas phase to have the potential of physisorption or chemisorption on the catalyst surface (Shukla et al., 2010).

Lyu et al. (2003), simultaneously synthesized SWNTs and double-walled carbon nanotubes (DWNTs) by catalytic decomposition of CH<sub>4</sub> over Fe–Mo/Al<sub>2</sub>O<sub>3</sub> catalyst.

High-resolution transmission electron microscopy observation showed that produced carbon materials consist of about 70% SWNTs and about 30% DWNTs. The diameters of SWNTs are in the range of 0.8–1.5 nm while the outer and inner diameters of DWNTs are in the range of 1.75–3.1 and 0.95–2.3 nm, respectively. Raman analysis indicates that the synthesized SWNTs and DWNTs have high-quality graphite structure (Lyu et al., 2003).

Kim et al. (2005), described the synthesizing of unusual multi-walled carbon nanotubes in a large quantity through a catalytic chemical vapor deposition method (CCVD) using a floating reactant and subsequent thermal treatment up to 2600 °C. Main characteristics of these nanotubes are (1) relatively wide distribution of diameters ranging from 20 to 70 nm, (2) high purity, (3) highly straight and crystalline layers, (4) very low interlayer spacing (0.3385 nm) and low intensity ratio value ( $I_D/I_G = 0.0717$ ) (Kim et al., 2005).

Flahaut et al. (2005), investigated the effect of catalyst preparation conditions on the synthesis of carbon nanotubes (CNTs) by CCVD. The combustion route was used to prepare catalysts by using either citric acid or urea as fuel. They found that in the case of citric acid, the milder combustion conditions obtained can either increase the CNTs yield with fewer walls or can limit the carbon nanofibers formation, depending on the catalyst composition. (Flahaut, Laurent, & Peigney, 2005). Table 2.3 shows the summary of some CVD processes conditions and the resulting product. It is specified that the different parameters have acting on the resulting product with different manner. The combination of three major parameters namely temperature, carbon source and catalyst is the most effective factor in the identification of the obtained carbon nanomaterial.

**Table 2.3: Summary of synthesis of CNTs using CVD techniques.**

Catalyst - substrate	Carbon Source	Reaction Condition		Product Quality	Reference
		Temperature °C	Flow rate ml/min		
Fe-Mo - Al <sub>2</sub> O <sub>3</sub>	C <sub>2</sub> H <sub>2</sub>	950 - 1200	C <sub>2</sub> H <sub>2</sub> : 20 Ar : 300	SWNTs 70% DWNTs 30%	(Ruoff, Qian, & Liu, 2003)
Co/Fe - zeolite	C <sub>2</sub> H <sub>2</sub>	900	C <sub>2</sub> H <sub>2</sub> : 10 Ar : 250	DWNTs > 80% Do ~ 3 - 6 nm	(Hiraoka et al., 2003)
Fe(CO) <sub>5</sub>	CH <sub>4</sub>	1050	CH <sub>4</sub> : 125 N <sub>2</sub> : 1000	MWCNTs: 15 - 420 nm	(Kuo et al., 2005)
Fe - Al <sub>2</sub> O <sub>3</sub>	C <sub>2</sub> H <sub>6</sub>	660	C <sub>2</sub> H <sub>6</sub> : 60 H <sub>2</sub> : 60	MWCNTs : 30 nm	(Louis et al., 2005)
Fe <sub>3</sub> O <sub>4</sub> - Si	toluene/ ferrocene	800-850	Ar : 1000	MWCNTs: 2-25 nm	(Pinault et al., 2005)
Co - Kaolin Co - ceramic	C <sub>2</sub> H <sub>2</sub>	750	C <sub>2</sub> H <sub>2</sub> : 50 N <sub>2</sub> : 200	CNTs: 30-40 nm Carbon nano sphere (CNS) : d= 50-500 nm	(Xu et al., 2005)
Fe - CaO	CO <sub>2</sub>	790	CO <sub>2</sub> : 750 H <sub>2</sub> : 1500	MWCNTs: 50 nm	(Xu & Huang, 2007)
Fe/Mo, Fe/Ru-Al <sub>2</sub> O <sub>3</sub> / SiO <sub>2</sub>	CH <sub>4</sub>	900	CH <sub>4</sub> ~ 6000	SWNTs : (~ 42 wt%)	(Cassell et al., 1999)
Co, Fe, Cu - SiO <sub>2</sub> , zeolite, clay	C <sub>2</sub> H <sub>2</sub>	700	C <sub>2</sub> H <sub>2</sub> : ~ 8 N <sub>2</sub> : ~75	MWNTs: (71-76%) SWNTs: (low yield)	(Fonseca et al., 1998)
Co/Mo, Co/V, Co/Fe -SiO <sub>2</sub> , Zeolite	C <sub>2</sub> H <sub>2</sub>	497- 697	C <sub>2</sub> H <sub>2</sub> N <sub>2</sub> : 15-25 ~300	MWNTs 68% 8-40 nm	(Kukovecz et al., 2000)
Mo - Quartz	CO	1200	CO : ~1200	SWNTs: 1-5 nm	(Dai et al., 1996)
Co/Mo - SiO <sub>2</sub>	CO	700	CO : ~100	MWNTs (4%) and SWNTs (88%)	(Alvarez et al., 2001)
Co, Ni, Fe - MgO	H <sub>2</sub> - CH <sub>4</sub>	1000	H <sub>2</sub> : ~300 CH <sub>4</sub> : ~75	SWNTs : (70-80 %)	(Colomer et al., 2000)
Mg <sub>0.9</sub> Co <sub>0.1</sub> O	H <sub>2</sub> /CH <sub>4</sub>	1000	CH <sub>4</sub> : ~ 250	SWNTs (64 %)/ DWNTs (> 80 %) 0.5 – 5 nm	(Flahaut et al., 2005)

**Table 2.3 (continued)**

Fe/Mo - Quartz	CH <sub>4</sub>	875	CH <sub>4</sub> : Ar (1:1 ratio)	DWNTs (in high yields)	(Endo et al., 2005)
Fe - Al <sub>2</sub> O <sub>3</sub>	CH <sub>4</sub>	900	—	DWNTs :1- 6 nm	(Cumings, Mickelson, & Zettl, 2003)
Al/ Fe/ Mo - Si	C <sub>2</sub> H <sub>2</sub>	1000	C <sub>2</sub> H <sub>2</sub> : ~ 50 -250	SWNTs : ~ 1.3 nm	(Lacerda et al., 2004)
Single or multi - Fe, Co, Ni - Al <sub>2</sub> O <sub>3</sub> , SiO <sub>2</sub>	C <sub>2</sub> H <sub>4</sub>	1080	C <sub>2</sub> H <sub>4</sub> : ~30 N <sub>2</sub> : ~80	Bundles of isolated SWNTs : 0.2 – 0.7 nm	(Cheng et al., 2004)
Al/ Fe/ Mo - Si	C <sub>2</sub> H <sub>2</sub>	1000	C <sub>2</sub> H <sub>2</sub> : ~ 50 -250	SWNTs : ~ 1.3 nm	(Lacerda et al., 2004)
M(C <sub>5</sub> H <sub>5</sub> ) <sub>2</sub> (M=Fe,Co,Ni), Fe(CO) <sub>5</sub>	C <sub>2</sub> H <sub>2</sub>	1100	Ar : ~975 H <sub>2</sub> : ~25 C <sub>2</sub> H <sub>2</sub> : ~50	SWNTs : ~1 nm	(Satishkumar et al., 1998; Satishkumar et al., 2000)
Fe/Mo - SiO <sub>2</sub> , Si	CH <sub>4</sub>	900	CH <sub>4</sub> : ~1500 H <sub>2</sub> : ~125	SWNTs	(Franklin et al., 2001)

#### 2.2.5.4 CVD support catalyst method

The structure and chemical state of the substrate are more significant than that of the metal and the same catalyst has different impact on different support materials. Commonly used substrates in CVD are graphite (Baker et al., 1972), quartz (Andrews et al., 1999; Kumar & Ando, 2003), silicon (Kumar et al., 2004), silicon carbide (Ding et al., 2003; Murakami et al., 2004), silica (Mattevi et al., 2008), alumina (Cheung et al., 2002), alumina-silicate (zeolite) (Kumar & Ando, 2005; Willems et al., 2000), CaCO<sub>3</sub> (Couteau et al., 2003), magnesium oxide (Ago et al., 2004). Investigation of the catalyst–substrate interaction with utmost attention should be undertaken for an efficient CNMs growth. Thus, the catalytic behavior of the metal would be terminated because of the metal–substrate reaction and chemical bond formation. It is confirmed that the morphology of CNMs grown on porous supports using CVD is strongly affected by the

porosity, the structure, and chemical composition of the support as well as the concentration of the metal and morphology of the metal catalyst (Doustan & Pasha, 2016; Prieto et al., 2014). Veziri et al. (2009), studied the effect of Ni metallic catalysts supported on three different porous substrates (microporous alumino-phosphate molecular sieves, activated carbon, and macroporous polymeric beads) on the structural morphology of CNTs. The group observed that the Ni catalyst is sensitive to metal-support interactions producing coiled, fibrous and belt-like structures (Veziri et al., 2009).

High yields of CNTs with a narrow diameter distribution have significantly resulted from zeolite supports with catalysts in their nanopores (Kumar & Ando, 2005). Alumina supports offers good metal dispersion and thus a high density of catalytic sites and unwanted defective MWCNTs or graphite particles due to the strong metal-support interaction. Accordingly, they are considered a better catalyst substrate than silica supports (Nagaraju et al., 2002). Such interactions significantly minimize the aggregation of the metal species and prevent them from forming large clusters (Ago et al., 2004).

One of the methods of supporting catalyst on the substrate is incipient wetness impregnation. For example,  $\text{Fe}(\text{NO}_3)_3 \cdot 9\text{H}_2\text{O}$  is impregnated on alumina powder by dissolving the salt in a solvent such as deionized water, then the substrate powder was added to the same solvent. The two mixtures mixed together then dried and grinded (Delzeit et al., 2002). The substrate is placed in a ceramic boat and positioned in the center of the CVD furnace after it is washed with distilled water and diluted hydrofluoric acid solution to remove all contaminants, as shown in Figure 2.6. After the injection of the hydrocarbon source along with the catalyst into the chamber of the furnace tube, very thin film of transition metal catalyst is deposited over the substrate catalyst. The organic catalyst will decompose during the injection of the catalyst-hydrocarbon precursor mixture into fine cluster catalyst and deposit over the substrate (Yan et al., 2015). Xu et al. (2005), utilized the two different substrates, kaolin plate and ceramic plate in chemical

vapor deposition to investigate the importance of substrates. The decomposition of  $C_2H_2$  was carried out at  $750\text{ }^\circ\text{C}$  in nitrogen atmosphere. Two different types of carbon nanostructures were produced, carbon nanotubes and carbon spheres (Xu et al., 2005).

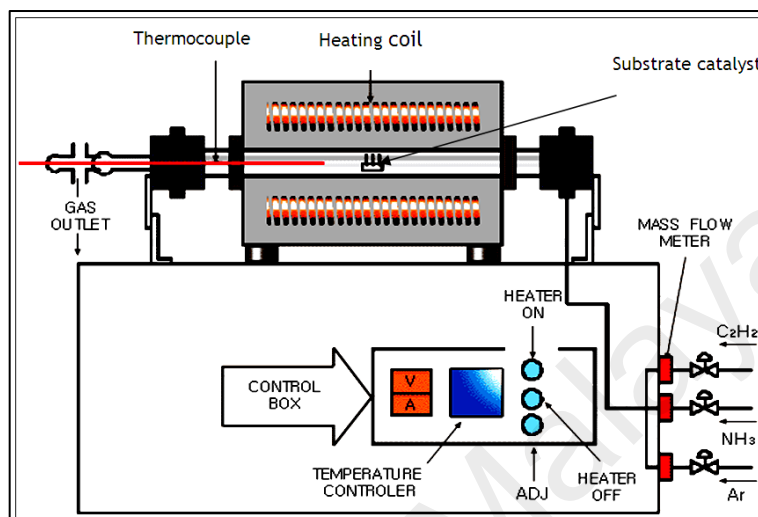


**Figure 2.6: Schematic diagram of thermal CVD apparatus.**

Chen et al. (2009), attempted to prepare carbon nanomaterials on activated carbon (AC) directly avoiding impregnation with metal catalyst. AC prepared from biomass already contains iron that can be considered as a “natural catalyst” and can catalyze the formation of CNFs (Chen, Timpe, et al., 2009b). Veziri et al. (2008), synthesized CNTs on pellets of activated carbon using Ni as a catalyst. They found that the reaction temperature has strong effect on nanotube growth leading to an optimal value of  $750^\circ\text{C}$ , while the growth rate was continuously suppressed for a reaction duration longer than 5 min, the nanotube size distribution was broadened, and the formation of amorphous carbon was favored (Veziri et al., 2008).

### 2.2.6 Mechanism of nanotube growth in CVD

Enormous investigations were published describing how to grow CNMs by varying the carbon sources, processing gases, the catalyst materials, etc. after Iijima 1991 paper. However, most of papers did not include significant insights on their growth mechanisms.

As of today, publications more likely presented respectable discussion which reviewed different aspects of the current understanding of the CNTs growth mechanism using CVD (Acomb, Wu, & Williams, 2015; Jourdain & Bichara, 2013b).

Growth mechanism of CNTs in CVD process is not completely understood, different models exist but some of them cannot unambiguously explain the mechanism. The vapor–solid–solid (VSS) model is the most accepted growth model which derives from the vapor–liquid–solid (VLS) model originally suggested by Wagner and Ellis for growth of silicon whiskers (Wagner & Ellis, 1964). In CVD process, the growth of nanotube on catalyst particles is similar to a conventional gas–solid interaction method such as the deposition of thin film on substrates. Using the VSS model, the excess carbon from the decomposition of the hydrocarbon precursor gases precipitates on the catalyst surface, adsorption of species onto the catalyst surface followed by diffusion into the catalyst. Finally, the surface reactions lead to film growth and nanotube nucleation at the edges of the catalyst (Kudo et al., 2014). Figure 2.7 shows two main models for growth of CNTs on a substrate. **Tip-growth**; the nanotube lifts the catalyst from the substrate because of the weak interaction of the catalyst–substrate, and during the growth the catalyst particles are pushed upwards, the precursor is supplied through the upper region of the catalyst while carbon atoms are diffused downwards as the nanotube nucleates and grows below the catalyst. CNT will grow continuously as long as the concentration gradient exists in the metal, and the metal’s top is open to receive fresh carbon from the decomposition of carbon precursor. Once the metal is overall covered with excess carbon, the CNT growth is ceased due to catalyst deactivation (Romero Rodríguez, 2017). **Base-growth**, base growth model proposed by Sinnott et al., in the same manner of tip growth model, with the assistance of catalyst particles, the pyrolyzed hydrocarbon products are first adsorbed on the particle surface and the carbon atoms are liberated (Seah, Chai, & Mohamed, 2014). When the catalyst surface was supersaturated, these liberated carbon atoms diffuse



into a catalyst and precipitate on the upper surface to form cylindrical-shaped graphite sheets. In this model, the interaction force between the catalyst particles and the substrate surface is sufficiently strong, and CNT precipitation fails to push the metal particle up. Thus, CNT grows up with the catalyst particle rooted on its base. The nanotube growth will cease if the carbon supply is insufficient or the particle surface is contaminated. Moreover, some research groups claim that during the growth, a combination of both growth models might be enhanced due to the presence of more than one catalyst dot (Saha et al., 2014).

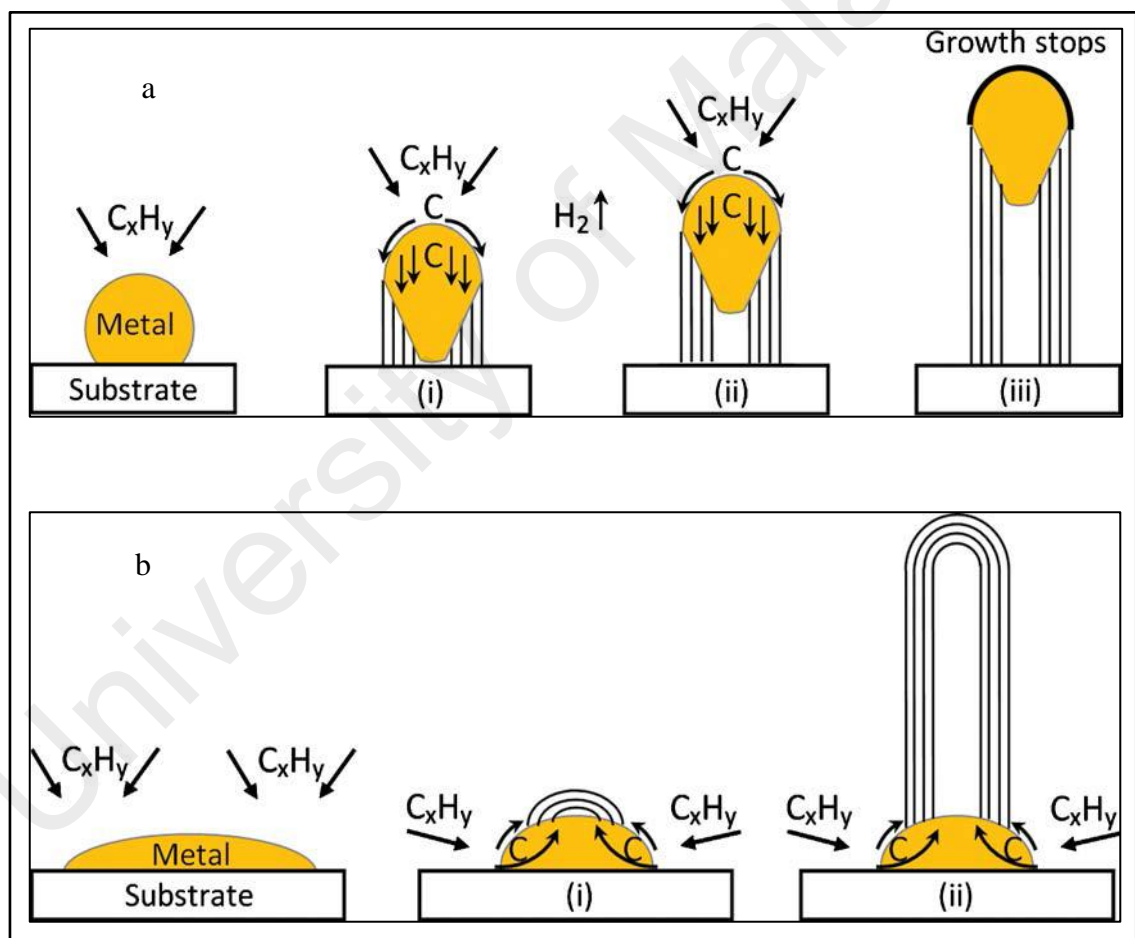


**Figure 2.7: Widely-accepted growth mechanisms for CNTs: (a) tip-growth model, (b) base-growth model (Kumar & Ando, 2010).**

Baker et al., (1972) suggested in the model of the growth of carbon fibers that the carbon liberated from acetylene decomposition at 600°C diffuses through the nickel cluster due to a thermal gradient of the exothermic decomposition. Thus precipitated carbon on the rear side of the cluster and forms the fiber (Baker et al., 1972). The observed activation energies for the filament growth were in accordance with those for diffusion of carbon through the corresponding metal such as Co, Fe, Cr, etc. (Wirth et al., 2012). Whether the growth follows the tip or base growth model, is explained by a weaker or stronger metal-support interaction respectively (Jourdain & Bichara, 2013a).

Oberlin et al., (1976) modified the Baker model. They proposed that the fiber formation is enhanced by a catalytic process through the surface diffusion of carbon atoms around the catalyst, rather than by bulk diffusion of carbon through the catalytic cluster. This model suggests the diffusion of carbon atoms only occurs on the outer surface of the metal cluster and the cluster acts as a seed for the fiber nucleation (Oberlin, Endo, & Koyama, 1976).

Raty et al., (2005) investigated the early stages of SWCNT formation on iron nanoparticles. Their study showed that the growth occurs from the root on Fe catalyst after the formation of a curved  $sp^2$  cap bonded carbon sheet by rapid diffusion of carbon atoms on the curved metal surface. They proposed that the floating of the formed graphene on the curved surface was attributed to the weak adhesion between the cap and iron while the border atoms of the cap remain adhered to the metal. Since more carbon atoms join the border, the cap is pushed up and thus constituting a cylindrical wall. Furthermore, they did not observe at the nanoscale any tendency of carbon atoms to penetrate inside the catalyst (Raty, Gygi, & Galli, 2005).

### 2.2.7 Functionalization of carbon nanotubes

The academia and industry research has been focusing on CNT modification as there are issues regarding their solubility, hydrophobicity of their stable graphitic structure, aggregation, and difficult manipulation that has imposed a significant limitation on their potential applications (Karousis et al., 2016). Functionalization of CNTs is directly affected by their chemical composition, particle size, and surface nature. Consequently, functionalization of CNTs has gained lots of attention as an attempt to remove CNTs impurities and to introduce different functional groups, which subsequently enhance CNTs solubility, graphitic networks and improving their process ability (Hu et al., 2010). CNTs can be modified through the addition of functional groups on its surface by the formation chemical bonds between the modifier and CNTs surface or physical adsorption of the modifying species to the surface of CNTs (Hayyan et al., 2015). CNTs exhibit chemistry differs from other regular carbon materials because of their unique small diameter, and structural properties. Accordingly, they shown a great affinity to interact with different compounds and to be integrated into organic, inorganic and biological systems (Amara et al., 2015). The main approaches for the modification of CNTs are shown in Figure 2.8 and can be grouped into three categories: (a) the covalent attachment of chemical groups via chemical reactions with the  $\pi$ -conjugated skeleton of CNT; (b) the noncovalent adsorption or wrapping of various functional molecules; and (c) the endohedral filling of their inner empty cavity (Karousis, Tagmatarchis, & Tasis, 2010). Chen et al., (1998) reported the saturation of 2% of the carbon atoms in SWCNTs with C-Cl due to the addition of chlorine (Cl) to the sidewalls SWCNTs via reaction with soluble dichlorocarbene, which resulted in significant changes in the electronic structure (Chen et al., 1998). Mickelson et al., (1998) reported fluorination of SWCNTs with  $F_2$  gas flow at temperatures of 250-600 °C for 5 hrs. The authors demonstrated that this type of modification offers a starting point for a numerous side-wall chemical

functionalization (Mickelson et al., 1998). Fluorination is one of the methods enabling an efficient simultaneous functionalization and purification of carbon nanotubes (Adamska & Narkiewicz, 2017). Strong inorganic acids such as sulfuric acid nitric acid and their mixtures are the most common conventional materials used for functionalization are High volatile organic solvents, oxidizing and reducing agents such as  $\text{KMnO}_4$ ,  $\text{H}_2\text{O}_2$ ,  $\text{NaClO}$ ,  $\text{KOH}$  and  $\text{NaOH}$  have been widely used in this respect.

The acid treatment produces carboxylic and hydroxylic groups ( $\text{COOH}$ ,  $\text{OH}$ ,  $\text{C}=\text{O}$  and  $\text{SO}_3\text{H}$ ) on the external surface of the CNTs. Basically, this technique involves refluxing of CNTs in boiling acids including nitric acids, sulfuric acid, or a mixture of both (Kumar, Jiang, & Tseng, 2015). Utilizing such harsh conditions of extensive ultrasonic modification lead to the opening of the tube caps as well as the etching along the walls and defects formation associated with the release of carbon dioxide. The final products are fragments of nanotube with 100 to 300 nm lengths with decorated ends and sidewalls by a high density of different oxygen containing groups mostly carboxyl groups (Majewska, 2015; Santangelo et al., 2012).

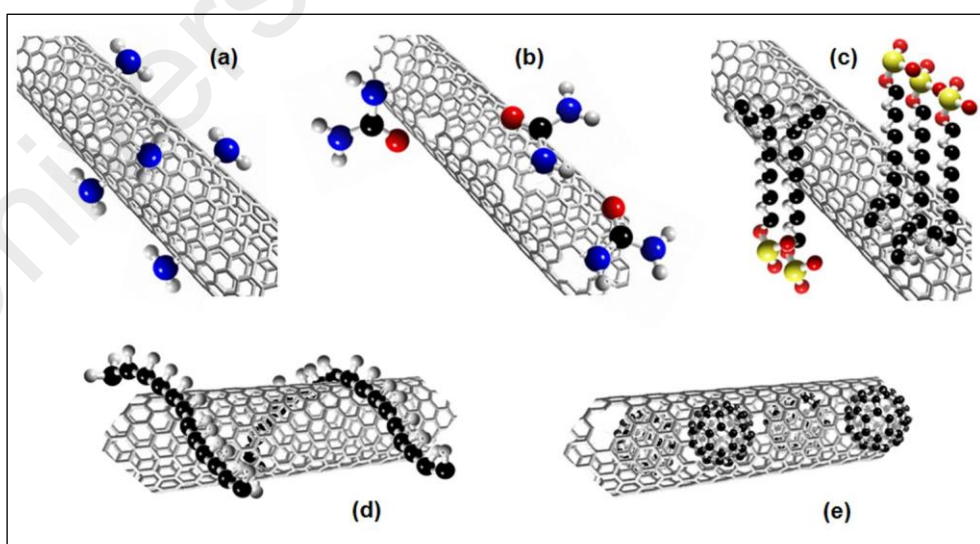


**Figure 2.8: Strategies for chemical and physical functionalization of CNTs: a) covalent sidewall functionalization, b) covalent defect sidewall functionalization, c) non-covalent adsorption of surfactants, d) wrapping of polymers, and e) endohedral functionalization (Hussain & Mitra, 2011).**

Oxidized MWCNTs were used for the adsorption of lead, copper and cadmium ions (Mubarak, Sahu, et al., 2014; Peng, Luan, Di, et al., 2005) and trihalomethanes (Lu, Chung, & Chang, 2005) from aqueous solutions. These studies concluded that oxidized CNTs show higher adsorption affinity for the target pollutants compared with other adsorbents such as activated carbon. Li et al., (2007) oxidized CNTs with H<sub>2</sub>O<sub>2</sub> and KMnO<sub>4</sub> for 3 h at 80 °C, however, nitric acid was refluxed with the suspension for 1 h at 140 °C. with and HNO<sub>3</sub>. They reported that Cadmium (II) adsorption removal for the three kinds of oxidized CNTs was increased due to the added functional groups compared with the as-grown CNTs. Analysis demonstrated that the KMnO<sub>4</sub> oxidized CNTs hosted manganese residuals, and these accordingly contributed to cadmium sorption to a yet-undefined extent (Li et al., 2007).

The adsorption process of phenol was studied by Luz-Asunción et al., (2015) using carbon nanomaterials (CNMs). The adsorption was achieved with as received SWCNTs, MWCNTs and after oxidation treatment, also graphene oxide and reduced graphene oxide were used. Hydrogen peroxide was used to modify CNTs under microwave irradiation and the graphene oxide reduction was achieved by using ascorbic acid. The authors reported that phenol removal occurs by  $\pi$ - $\pi$  interactions and hydrogen bonding and not by electrostatic interactions. Their results demonstrated that the surface area of CNMs has promoted the adsorption of phenol and the removal efficiency was reduced due to the presence of oxygenated groups (de la Luz-Asunción et al., 2015). CNTs modified with hydrophilic groups have shown an improvement in their dispersion in aqueous media which is another direct consequence of surface modification. Rosenzweig et al., (2013) demonstrated that CNTs had higher adsorption capacity for copper after modification with acid (COOH) and (OH) moieties. They reported that the aggregation state of CNTs could be limited due to the formation of new accessible sites (Rosenzweig et al., 2013).

An additional important aspect to consider is that the increasing of oxygen-containing functional groups could be a double-edged sword. Thus, the adsorption efficiency of CNMs might be adversely affected by surface functionalization. Wu et al., (2012) thoroughly explored the adsorption affinity of oxidized MWCNT for organic compounds in water. They found that the significant decreased uptake of the oxidized MWCNT was attributed to the competition of water molecules; meanwhile, the adsorption affinity of organic chemicals were not changed because the adsorption interactions including the hydrophobic effect and  $\pi$ - $\pi$  forces remained constant (Apul & Karanfil, 2015; Wu et al., 2012). Many studies demonstrated with particular attention the magnetite modified multi-walled carbon nanotubes (M-MWCNTs) because they can be easily removed from aqueous solution by magnetic separation. Magnetic CNTs (M-CNTs) hybrids have showed excellent adsorption properties for dye removal (Yu et al., 2012).

Although, the ease of processing is the goal of functionalization at the same time, their adsorption properties with organic chemicals can be significantly altered. On one hand increasing the hydrophilicity of CNTs via functionalization will increase their wettability and make them suitable for the adsorption of relatively low molecular weight and polar compounds (Piao, Liu, & Li, 2012). On the other hand, the functional groups may increase the diffusional resistance as revealed from the kinetic studies of modified CNTs demonstrated which will accordingly, reduce the accessibility and uptake of CNT surfaces towards organic chemical (Gupta & Saleh, 2013; Mulzer et al., 2016).

## 2.3 Organic pollutants

### 2.3.1 Bisphenol A

#### 2.3.1.1 Structure and physicochemical properties of bisphenol A

Bisphenol A (BPA) is the common name for 2,2-Bis (4-hydroxyphenyl) propane, an organic compound with two phenol moieties. It is a building block for several important polymers and polymer additives (Huang et al., 2012). Figure 2.9 shows the tetrahedral molecular structure of BPA. The molecular structure has surface area of 4.32 nm<sup>2</sup> and volume of 0.70 nm<sup>3</sup>. The maximum distance between the hydroxide groups is 0.94 to 1.119 nm, height 0.53 nm and the benzene ring width of 0.325 to 0.43 nm. Table 2.4 summarizes the physicochemical properties of BPA (Pullket, 2015).

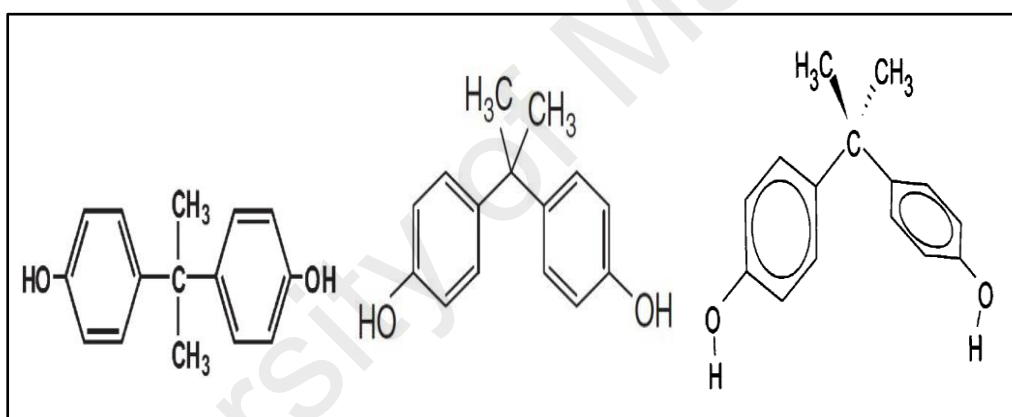


Figure 2.9: BPA molecular structure (Pullket, 2015).

Table 2.4: Physicochemical properties of bisphenol A.

Properties		References
Case Number	80-05-7	(Haynes, 2014)
Formula	C <sub>15</sub> H <sub>16</sub> O <sub>2</sub>	(Haynes, 2014)
IUPAC name	4,4'-(propane-2,2-diyl) diphenol	(Haynes, 2014)
Molecular Weight	228.287g/mol	(Haynes, 2014)
Density	1.195 g/cm <sup>3</sup>	(Staples et al., 2000)
Melting point (0C)	153 °C	(Haynes, 2014)
Boiling point	220 °C	(Haynes, 2014)
Aqueous solubility	120-300 mg/L	(Verschuere, 1983)

**Table 2.4 (continued)**

Henry's Constant (25°C)	1x 10 <sup>-10</sup>	(Staples et al., 2000)
Vapor pressure	5.3 x 10 <sup>-6</sup> Pa	(Cousins et al., 2002)
Vapor pressure @ 170 0C	0.2 mm Hg	(Verschueren, 1983)
log <i>K</i> <sub>ow</sub>	2.20 - 3.82	(Staples et al., 2000)
	3.40	(Cousins et al., 2002)
Log <i>K</i> <sub>oc</sub>	314	(Staples et al., 2000)
p <i>K</i> <sub>a</sub>	9.59 and 10.2	(Staples et al., 2000)

### 2.3.1.2 Production and application

BPA was first synthesized by A. P. Dianin in 1891 and later in the 1930s it was investigated during the exploration for synthetic estrogens for pharmaceutical applications (Varandas, 2014). At that time, it was examined for its estrogenic properties but rejected when Diethylstilbestrol (DES) was found to have better potential for pharmaceutical use. Nevertheless, since the early 1950s until now, the majority of the BPA produced is at most used as a monomer for polycarbonate and epoxy resins (Suhrhoff & Scholz-Böttcher, 2016). BPA is synthesized from acetone and phenol with a by-product of water as described in Figure 2.10.

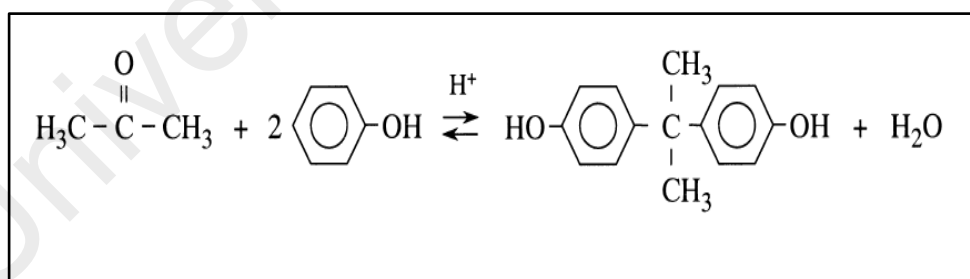


**Figure 2.10: Chemical production of BPA.**

BPA is also used in the manufacturing of phenol resins, polyesters, polyacrylates, coatings, intermediates in flame retardants, and packaging and has been widely used in the manufacture of shampoo, sunscreen lotions, bar soaps, nail polish, and face lotions/cleanser, besides in producing dental sealants and bonding agents. BPA is, definitely one of the highest volume chemicals produced worldwide, > 8 billion pounds



each year and > 100 tones released into the atmosphere by annual production (Chen et al., 2016).

### **2.3.1.3 Exposure of BPA to the environment**

The spread of BPA contamination in the environment comes from humans and its manufacturing process. Thus, its exposure had seen in the surface fresh water, landfill leachate, wastewater, air, and dust particles. About 100 tons BPA released into the atmosphere each year from worldwide production (Makinwa & Uadia, 2015). The leachates of BPA from household effluent and industrial effluent passed through the other environment phases. The leaching of BPA monomer results from the hydrolysis of the ester bond linking BPA molecules in polycarbonate and resins which are found in the plastic food containers and bottles when it contacts with water at room temperature. The rate of BPA leaching increases with temperature rises, and it depends on the pH of the aqueous media. Furthermore, the leaching rate from old, worn-out products is notably enhanced compared with new products which can reach to more than 1000-fold. When the leachate reaches the aquatic environment even after dilution can be at levels that could have an adverse health effect on humans (Eggen, Moeder, & Arukwe, 2010). BPA is a challenging problem because it has a high solubility in water, reproductive toxicity, and teratogenicity. Also, it affects the ecosystem even at levels as low as 0.1 ppb. In recent years, BPA detected in surface water, industrial wastewater, groundwater, and even in drinking water due to the increased production of BPA. BPA has started to become an urgent priority not only in the drinking water industry but also in food and wastewater sludge (Pignotti et al., 2017). Table 2.5 and Table 2.6 shows the available environmental quality standards for BPA and the major studies reported in the literature about BPA in aquatic matrices respectively. Studies also have indicated that human water bodies such as serum, urine, amniotic fluid, and placental tissue have confirmed the presence of BPA (Lee et al., 2017).

**Table 2.5: Available quality standards for BPA in the aquatic matrices.**

Description	Value (mg/m <sup>3</sup> )	Reference
Surface water-proposed water quality objective (Canada)	5	(Careghini et al., 2015)
Drinking water-standard (Canada)	1800	(MOE, 1997)
Water-regional screening level, tap water (USA)	77	(Haseman et al., 1986)

**Table 2.6: Concentrations of BPA in aquatic environment in different countries.**

Location	Comments	BPA levels mg/m <sup>3</sup>	Reference
Singapore	Surface coastal water	< 0.002 – 2.47 Mean 0.40	(Basheer, Lee, & Tan, 2004)
China	Estuarine and marine water from Jiaozhou Bay	0.0015 – 0.262	(Fu, Li, & Gao, 2007)
India, Indonesia, Singapore, Malaysia, Thailand, Cambodia, and Philippines 1	Green mussel (1994–1999)	1–13.7	(Isobe et al., 2007)
R Portugal	River and coastal waters	0.07–4.0 Mean 1.0	(Azevedo et al., 2001)
Germany	Elbe River and some of its tributaries	0.017 – 0.776 Mean 0.105	(Heemken et al., 2001)
Japan	Estuarine and marine waters from Okinawa, and Ishigaki Islands	< 0.005 – 0.08 Mean 0.02	(Kawahata et al., 2004)
Spain	Lobregat River basin	< 0.09 – 2.97 Mean 0.44	(Céspedes et al., 2005)
Mexico City, Mexico	Surface water (dams)	< 0.0005 – 0.007 (52 %)	(Félix–Cañedo, Durán–Álvarez, & Jiménez–Cisneros, 2013)
Brazil	Rivers crossing Sao Luis island	< 0.46	(Melo & Brito, 2014)

**Table 2.6 (continued)**

UK	–	0.006 – 0.068	(Luo et al., 2014)
Greece	–	0.055 – 0.152	(Luo et al., 2014)
Korea	–	0.0075 – 0.334	(Luo et al., 2014)
Switzerland	Glatt River	0.009 – 0.076	(Voutsas et al., 2006)
Italy	Tiber River	< 0.03 – 0.14 Mean 0.07	(Patrolecco et al., 2006)
South Korea	Han River	0.0069 – 0.059	(Yoon et al., 2010)
Switzerland	Glatt River	0.009 – 0.076	(Voutsas et al., 2006)
Canada	–	Mean 0.0021 Maximum 0.087	(Luo et al., 2014)

#### 2.3.1.4 Hazardous potential of BPA

Since 1930, BPA has been suspected to be hazardous to human due to the estrogenic activity, and has recently been identified as an endocrine disrupter compound (EDCs). EDCs are a structurally different class of emerging contaminants that have been detected in aquatic bodies (Bhatnagar & Anastopoulos, 2017). EDCs unfavorably affect human health and ecosystems by disrupting development, growth, and reproduction, because they can mimic natural hormones in the endocrine systems (Anwer, Chaurasia, & Khan, 2016; Huang & Weber, 2005). EDCs include (a) natural compounds including steroid hormones naturally produced by humans and animals and (b) anthropogenic compounds namely, synthetic hormones or industrial and agricultural chemicals (pesticides, bisphenol A, phthalates plasticizers, etc.). Phenolic compounds contain an important class of endocrine disruptors; many matching the structural features of natural estrogens thus, motivating the estrogenic toxicity via binding to estrogen receptors (Griffith, 2013). Even

though BPA having lower estrogenic activity than of 17 $\beta$ -Estradiol, the recent researches show that BPA still can stimulate some cellular responses and induce various endocrine-related pathways. Accordingly, it has harm impact on the environment and cause a potential health risk to humans even at low levels (Rubin, 2011). Table 2.7 shows the impact of low levels of BPA exposure on animals. BPA can cause disorders of the immunological system, development of tumors in the breast and prostate, neurological problems, anomalies in reproduction and development, even infertility.

**Table 2.7: Effects of low-dose of BPA exposure in animals.**

<b>Dose (<math>\mu\text{g}/\text{kg}/\text{d}</math>)</b>	<b>Effects (measured in studies of animals)</b>	<b>Reference</b>
0.025	"Permanent changes to genital tract"	(Markey et al., 2005)
0.025	"Changes in breast tissue that predispose cells to hormones and carcinogens"	(Muñoz-de-Toro et al., 2005)
1	"Long-term adverse reproductive and	(Newbold, Jefferson, &
2	"Increased prostate weight 30% "	(Nagel et al., 1997)
2	"Lower body weight, increase of anogenital, distance in both genders, signs	(Honma et al., 2002)
2.4	"Decline in testicular testosterone"	(Akingbemi et al., 2004)
2.5	"Breast cells predisposed to cancer"	(Murray et al., 2007)
10	"Prostate cells more sensitive to hormones and cancer"	(Ho et al., 2006)
10	"Decreased maternal behaviors"	(Palanza et al., 2002)
30	"Reversed the normal sex differences in brain structure and behavior"	(Kubo et al., 2003)
50	"Adverse neurological effects occur in non-human primates"	(Leranth et al., 2008)
50	"Disrupts ovarian development"	(Adewale et al., 2009)

Also, different human diseases such as recurrent miscarriage, ovarian dysfunction, and endometrial hyperplasia associated with the levels of bisphenol A in human's blood. Therefore, these adverse impacts have raised concerns since reproductive toxicity could result from the prolonged exposure to environmentally relevant concentrations of BPA (Peretz et al., 2014). The Canadian government was the first country to classify BPA as a dangerous substance. In this context, selling, importing, and advertising of baby bottles that contained BPA is prohibited. In response to American Chemistry Council request, the European Commission and Food and Drug Administration (FDA) in 2012 forbidden the use of BPA in polycarbonate infant feeding bottles, sippy cups, and restricted the use of BPA based resins in coatings for infant formula packaging. In this context, selling, importing and advertising of baby bottles that contained BPA is prohibited (Park et al., 2015; Qin et al., 2015; Usman & Ahmad, 2016). Kumar reported that the overall priority for BPA was second place out of 100 chemicals as endocrine-disrupting chemicals, pharmaceuticals, personal care products. BPA was third place for the occurrence, was 35 for ecological effect, was 29 for the health effect, and out of the EDC; BPA was the second highest priority of concern when compare to the surface/source water (Kumar & Xagorarakis, 2010).

#### **2.3.1.5 Treatment methods**

The recent studies demonstrated that the pharmaceuticals, personal care products (PPCPs), and endocrine-disrupting have the ability to pass the traditional water treatment processes (Ebele, Abdallah, & Harrad, 2017). Due to the environmental risk of BPA, several methods have been developed to remove BPA from wastewater such as biological treatment (Burke, Duennbier, & Massmann, 2012; Guerra et al., 2015), Coagulation, flocculation, and sedimentation (Stackelberg et al., 2007), nanofiltration (Zielińska et al., 2016), reverse osmosis (Yüksel, Kabay, & Yüksel, 2013), advanced oxidation processes (Sharma, Mishra, & Kumar, 2015; Zhang & Li, 2014), ozone (Umar et al., 2013; Von

Sonntag & Von Gunten, 2012) and membrane bioreactors (Chen, Huang, & Lee, 2008; Yang et al., 2013) and adsorption (Bhatnagar & Anastopoulos, 2017; Fu et al., 2015; Gupta, Mittal, & Gajbe, 2005). However, due to the high chemical stability of BPA, these treatments did not achieve complete removal from the aqueous phase. Owing to its high effectiveness, simple design, low cost, low energy requirements and less production of harmful byproducts, adsorption technique has proved to more efficient and advantageous over other reported physio-chemical methods (Feng et al., 2012; Jung et al., 2015). The effective adsorption process could be achieved by an adsorbent with a superior adsorption capacity for the target adsorbate. Thus, the most important adsorbent features for any application are capacity, cost, selectivity, kinetics, regenerability, and compatibility (Dehghani et al., 2016).

#### **2.3.1.6 BPA removal by miscellaneous adsorbents**

Various adsorbents have been reported for BPA elimination from water, for example, Kuo (2009), utilized as-grown and modified CNTs to remove BPA from aqueous solution. The surface of CNTs was modified by applying microwave irradiation along with  $\text{SOCl}_2/\text{NH}_4\text{OH}$ . The author suggested that the modification method was effective as established by the larger specific surface area of the modified CNTs than that of as-grown CNTs. The maximum adsorption capacity of as-grown and modified CNTs was 60.98 and 69.93 mg/g, respectively. The kinetic studies showed that the adsorption of BPA onto CNTs associated by intraparticle diffusion (Kuo, 2009).

Zhou et al., (2012) evaluated the behavior of BPA removal from aqueous solutions onto some bio-sorbents such as sawdust, peat, bagasse, and rice husk. The author reported that peat showed great adsorption potential as a natural sorbent material, compared with the other investigated materials. The study demonstrated that the modified peat surface with hexadecyltrimethylammonium bromide (HTAB) exhibited high sorption affinity for BPA of 1.71 mg/g. The study indicated that the hydrophobic interaction between the

grafted HTAB groups and phenyl groups is the most removal force influencing the adsorption process. Furthermore, the BPA removal was preferred in the binary solute system of BPA and phenol, and the adsorption of BPA was promoted with the increase in ionic strength and the sorbent dose in a neutral solution (Zhou, Lu, & Lu, 2012).

Koduru et al., (2016) studied the removal of BPA from aqueous solutions using crystalline hybrid adsorbents fabricated of a goethite/activated carbon (GPAC). The study reported the adsorption capacity of BPA was increased with an increasing in the iron oxide concentration in GPAC. They demonstrated that the removal of BPA on GPAC was well fitted with the pseudo-second-order kinetics and Freundlich isotherm. They found that the maximum adsorption capacity of BPA on GPAC was 62.5 mg/g (Koduru et al., 2016).

Table 2.8 summarizes the characteristic of various adsorbents that have been used as adsorbents for the removal of BPA from aqueous solution such as clays (Park et al., 2014; Rathnayake et al., 2016; Zheng et al., 2013), zeolites (Dong et al., 2010; Wang et al., 2016), chitosan (Dehghani et al., 2016; Kimura et al., 2012), carbon and graphene based adsorbents (Bele, Samanidou, & Deliyanni, 2016; Gong et al., 2016; Libbrecht et al., 2015; Liu et al., 2009; Tang et al., 2016; Wang, Qin, et al., 2015; Xu, Wang, & Zhu, 2012), imprinted polymers (Liu, Zhong, et al., 2016; Pichon & Chapuis-Hugon, 2008; Wolska & Bryjak, 2014), composite materials (Abkenar et al., 2015; Cui et al., 2016; Guo et al., 2011; Li, Gondal, & Yamani, 2014), agricultural wastes (Chang et al., 2012; Soni & Padmaja, 2014; Wirasnita et al., 2014), and nanomaterials (Dehghani et al., 2015; Farmany et al., 2016; Samadi et al., 2016; Tripathi et al., 2014; Zhou, Wang, et al., 2016)

**Table 2.8: Characteristics of some of different adsorbents used for BPA removal.**

<b>Adsorbent</b>	<b>Surface area (m<sup>2</sup>/g)</b>	<b>Initial adsorbate concentration, solid/liquid</b>	<b>pH, time/min</b>	<b>Isotherm models</b>	<b>Kinetic models</b>	<b>Maximum adsorption Capacity (mg/g)</b>	<b>Reference</b>
<b>Nanomaterials</b>							
MWCNTs	NA	2-50 mg/L, 0.5 g/L	9, 60	Freundlich - Langmuir	Pseudo-second-order	71.0	(Dehghani et al., 2015)
SWCNTs	NA	2-50 mg/L, 0.5 g/L	9, 60	Langmuir	Pseudo-second-order	111.11	(Dehghani et al., 2015)
SWCNTs	78.2	10 mg/L, 0.125 g/L	6, 30	Langmuir	Pseudo-second-order-intraparticle diffusion	59.17	(Kuo, 2009)
Graphene	327	10 mg/L, 10 mg/100mL	6, 30	Langmuir	Pseudo-second-order	182.8	(Xu et al., 2012)
Antimony nanoparticle/ MWCNTs	110	20,60, 100 mg/L; 100,200, 400 mg/L	7, 60	Langmuir	Pseudo-first-order	Removal : 93%	(Samadi et al., 2016)



**Table 2.8 (continued)**

Fe <sub>3</sub> O <sub>4</sub> -polyaniline core-shell nanomaterials	NA	1-20 mg/L, 20 mg/25 mL	7, 300	Freundlich	Pseudo-second-order	23.09	(Zhou, Wang, et al., 2016)
Reduced graphene oxide/magnetic nanoparticles(rGr-MNP)	NA	20 mg/L, 10 mg/50 mL	6, 120	Langmuir	Pseudo-second-order	125	(Zhang et al., 2014)
<b>Clay</b>							
Pure Ca montmorillonite (Ca-MT)	75.725	NA	7.0,240	Langmuir	Pseudo-second-order	151.52	(Zheng et al., 2013)
Montmorillonite (organoclays)	NA	5 - 500 mg/L, (0.2-0.3 g)/40 mL	7.0, 60	Langmuir	Pseudo-second-order	256.41	(Park et al., 2014)
Palygorskite (MT)	104.4	0.01-10 mg/L, 3.0 g/25 mL	>10-12, 100	Langmuir	NA	77.3	(Berhane et al., 2016)

**Table 2.8 (continued)**

<b>Zeolites</b>							
Hydrophobic zeolite	504.5	10-90 mg/L, 0.5 g/L	7, 140	Redlich– Peterson	Pseudo-second-order	111.11	(Tsai, Hsu, et al., 2006)
Cetyltrimethyl ammonium bromide -zeolite	9.78	50 mg/L, 1 g/L	10,210	Freundlich	Pseudo-second-order	237.85	(Wang et al., 2016)
Hexadecyltrimethyl ammonium (HDTMA-Zeolite)	91.5	100 mg/L 0.05 g/250 mL	5, 60	NA	NA	114.9	(Dong et al., 2010)
<b>Chitosan</b>							
Laboratory synthesized chitosan	5.0	0.5 mg/L 0.06g/L	5,75	Langmuir	Pseudo-second-order	27.02	(Dehghani et al., 2016)
Chitosan/fly-ash-composite	NA	100 mg/L	7, 180	Langmuir	Pseudo-second-order	31.92	(Suzuki et al., 2010)
<b>Carbon based adsorbents</b>							
Commercial activated carbon (F20)	996	60 mg/L, 10 mg/100 mL	7, NA	NA	Pseudo-second-order	317.67	(Liu et al., 2009)

**Table 2.8 (continued)**

Commercial carbon (W20) modified thermal treatment	1760	60 mg/L, 10 mg/100 mL	7, NA	NA	Pseudo-second-order	430.33	(Liu et al., 2009)
Commercial carbon (F20) modified with nitric acid	900	60 mg/L, 10 mg/100 mL	7, NA	NA	Pseudo-second-order	115.37	(Liu et al., 2009)
Commercial carbon (F20) modified thermal treatment	1000	60 mg/L, 10 mg/100 mL	7, NA	NA	Pseudo-second-order	223.48	(Liu et al., 2009)
Mesoporous carbon (soft - templated)	476	5-70 mg/L, 10 mg/100 mL	NA, 60	Freundlich	Pseudo-second-order	156	(Libbrecht et al., 2015)
<b>Graphene</b>							
Graphene	327	2-50 mg/L, 10 mg/100 mL	6, 300	Langmuir	Pseudo-second-order	181.81	(Xu et al., 2012)

**Table 2.8 (continued)**

Graphene oxide	20.93	10-500 mg/L, 0.05 g/ 20 mL	3, 60	Langmuir	Pseudo- second-order	17.27	(Xu et al., 2012)
<b>Imprinted polymer</b>							
Molecularly imprinted polymer	NA	20 mg/L, 5mg/6 mL	NA	Freundlich	Pseudo-second -order	40.31	(Zhao, Fu, & Zhang, 2016)
Bisphenol A imprinted microbeads	NA	10-150 mg/L, 10mg/10 mL	4, NA	Freundlich	Pseudo-second -order	82.4	(Bayramo glu et al., 2016)
Self-assembled porous microspheres-fibers	193.27	50 mg/L	6,40	Langmuir	Pseudo-second -order	327.84	(Cui et al., 2016)
Non-imprinted microbeads	NA	10-150 mg/L, 10 mg/ 10 mL	4, NA	Freundlich	Pseudo-second -order	62.9	(Bayramo glu et al., 2016)

**Table 2.8 (continued)**

<b>Composite materials</b>							
Self-assembled porous microspheres fibers	193.27	50 mg/L	6,40	Langmuir	Pseudo-second-order	327.84	(Cui et al., 2016)
Magnetic non-template imprinted polymers based on kaolinite/Fe <sub>3</sub> O <sub>4</sub>	142.9	20-400 mg/L, 0.01 g/10.0 mL	7, 360	Langmuir	Pseudo-second order	112.4	(Guo et al., 2011)
Hydrophobic magnetic montmorillonite	NA	0-200mg/L, 50mg/50mL	7,5	Langmuir	Pseudo-second-order	59.17	(Salehinia et al., 2016)
<b>Agriculture waste</b>							
Activated carbon from rice straw agricultural waste	1, 304.8	7-55 mg/L, 10 mg/100 mL	2.35-11, 90	Langmuir	Pseudo-second-order	181.81	(Chang et al., 2012)
Palm shell based activated carbon	143.15	NA, 10-100 mg/25 mL	7, 8 hr	Langmuir	Pseudo-second-order	62.5	(Soni & Padmaja, 2014)
Activated carbon derived from oil palm empty fruit bunch	86.62	20-100 mg/L, 1.0 g/L	2-9, 18	Langmuir	Pseudo-second-order	41.98	(Wirasnita et al., 2014)

### **2.3.2 Organic dyes**

Today, widespread applications and many processing units such as, textiles, cosmetics, paper, printing and pharmaceutical discharge large amounts of wastewaters that contain variety of synthetic dyes that imposes an objectional threat to the environment (Gupta et al., 2013). Till date, more than 100,000 commercial dyes are known with an annual production of  $>7 \times 10^5$  tons /year (Shindy, 2017). The total dye consumption in textile industry worldwide is more than 10,000 tons/year and approximately 100 tons/year of dyes are discharged into waste streams. The textile industry plays a major role in the economy of Asian and other countries. Wastewater effluents in the textile industry contain several kinds of synthetic dyestuff that are esthetically and environmentally unacceptable. Currently, several different types of dye are used in industries, including basic, acid, direct, reactive and dispersive dyes. The intricate chemical structure of dyes contributes in their resistance to light, oxidation, conventional biological and physical oxidation treatments and boost their non-biodegradability nature (Subramani & Thinakaran, 2017). The improper discharge of toxic dyes into open water cause prevalent ecological risks by reducing the oxygen and sunlight penetration and consequently affecting the photosynthesis activity in aquatic planktons. Methylene blue (basic blue 9) is one of the most commonly used thiazine (cationic) dyes. It is known to be water-soluble and its cationic features originating from the positively charged sulfur or nitrogen centers, This group of dyes is considered as toxic colorants and can cause harmful effects, therefore, the targeted removal of such compounds has attracted a growing amount of attention (Ai, Zhang, & Chen, 2011).

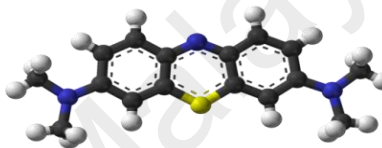
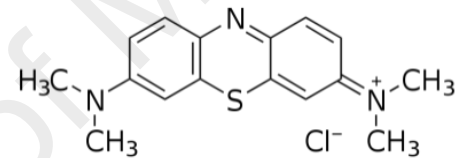
#### **2.3.2.1 Structure and physicochemical properties of methylene blue**

Methylene blue (MB) is an important cationic dye and widely used for dyeing cotton, wood and silk (Zare, Gupta, et al., 2015). It is water soluble, carries positive charge, highly visible and produce colored cations in solution. MB is a heterocyclic aromatic

chemical compound whose molecular formula is  $C_{16}H_{18}N_3SCl$ . It is not inflammable and is not an explosion hazard, the properties and structure of methylene blue are listed in Table 2.9. One hydrated methylene blue molecule has three water molecules. At room temperature it is solid, odorless, and dark green. Its choice in this work was guided by its high solubility in water and its strong adsorption onto solids (Karima, Mossab, & A-Hassen, 2010). It is intensely used as a model compound for removing organic contaminants and colored bodies from aqueous solution. It is also used as an indicator in oxidation-reduction reactions, a stain in bacteriology, also finds applications as antidotes for cyanide poisonings, antiseptics for fire burns and used in the treatment of methemoglobinemia at therapeutic doses. The excited state of MB which is generated by light can stimulate oxygen to yield oxidizing radicals which in turn can assist the cross-linking of amino acid residues in proteins in biological systems (Gurr, 2012).

Dyes are commonly known as carcinogenic and mutagenic substances and has various harmful effects on human health (Abdel-Shafy & Mansour, 2016). Acute exposure to methylene blue may cause severe health problems to mankind including dysfunction of brain, nervous system, kidney, liver and reproductive system (Gui et al., 2014). MB may cause skin photosensitization on and gives a bluish color. On inhalation, it can give rise to difficult breathing and inadvertent ingestion through the mouth produces a burning sensation and may cause nausea, diarrhea, vomiting, and gastritis. Accidental large doses produce severe headache, chest pain, profuse sweating, mental confusion. Consequently, environmental concerns have focused on finding proper treatment techniques to control this toxic dye in the industrial effluents prior to its discharge into receiving aquatic matrices (Abou-Gamra & Ahmed, 2016).

**Table 2.9: Properties and structure of methylene blue.**

<b>Dye name</b>	Methylene Blue
<b>IUPAC name</b>	3,7-bis (Dimethylamino)-phenothiazin-5-ium chloride
<b>Molecular formula</b>	$C_{16}H_{18}N_3SCl$
<b>Molar mass</b>	319.85 g/mol
<b>Melting point</b>	100-110 °C (with decomposition)
<b>Boiling point</b>	The lowest known value is 100°C (Decompose)
<b>3D Conformer</b>	  The 2D structure shows a phenothiazine ring system with a sulfur atom at the bottom, a nitrogen atom at the top, and a positive charge on the nitrogen atom. Two dimethylamino groups are attached to the ring system, one on the left and one on the right. The left group is shown as H <sub>3</sub> C-N-CH <sub>3</sub> and the right group is shown as N <sup>+</sup> (CH <sub>3</sub> ) <sub>2</sub> -CH <sub>3</sub> with a Cl <sup>-</sup> counterion.

### 2.3.2.2 MB removal techniques

The removal of dyes from waste effluent is considered an environmental challenge because even a small quantity of dye in water can be toxic and highly visible, therefore, there is an utmost need for versatile and effective process that can efficiently remove these dyes to protect and preserve the natural water systems (Swati, 2017). Several treatment methods have been reported for methylene blue removal such as biological treatment (Gupta, Nayak, & Agarwal, 2015), advanced chemical oxidation (Gupta, Jain, et al., 2012; Gupta et al., 2011; Saleh & Gupta, 2012), coagulation/ flocculation (Moghaddam, Moghaddam, & Arami, 2010; Szyguła et al., 2009), electrochemical treatment (Duman et al., 2016) and photodegradation (Gupta et al., 2011). Nevertheless, these methods suffer from many restrictions. Table 2.10 shows the advantages and disadvantages of different dye removal methods. Among all of these methods, adsorption



is proved to be the most effective, simple and economic process due to its ability to purify and capture the dye molecule without subsequent disturbing water quality or generating toxic secondary pollutants (Seow & Lim, 2016).

**Table 2.10: Advantages and disadvantages of dyes removal methods (Robinson et al., 2001).**

Methods	Advantageous	Disadvantageous
<b>Chemical treatments</b>		
Oxidative	Simplicity of application	Process ( $H_2O_2$ ) agent needs to activate by some means
$H_2O_2$ +Fe(II) salts (Fentons reagent)	Fentons reagent is a suitable chemical means	Sludge generation
Ozonation	Ozone can be applied in its gaseous state and does not increase the volume of wastewater and sludge	Short half-life (20 min)
Photochemical	No sludge is produced and foul odors are greatly reduced	Formation of by-products
Sodium hypochlorite (NaOCl)	Initiates and accelerates azo-bond cleavage	Release of aromatic amines
Electrochemical destruction	No consumption of chemicals and no sludge build up	Relatively high flow rates cause a direct decrease in dye removal
<b>Biological treatments</b>		
Decolorization by white-rot fungi	White-rot fungi can degrade dyes using enzymes	Enzyme production has also been shown to be unreliable Under aerobic
Other microbial cultures (Mixed bacterial)	Decolorized in 24–30 h	conditions azo dyes are not readily metabolized
Adsorption by living/dead microbial biomass	Certain dyes have a particular affinity for binding with microbial species	Not effective for all dyes

**Table 2.10 (continued)**

Anaerobic textile-dye bioremediation systems	Allows azo and other water- soluble dyes to be decolorized	Anaerobic breakdown yields methane and hydrogen sulfide
<b>Physical treatments</b>		
Adsorption by activated carbon	Good removal of wide variety of dyes	Expensive
Membrane filtration	Removes all dye types	Concentrated sludge production, membrane fouling
Ion exchange Regeneration	No adsorbent loss	Not effective for all dyes
Irradiation	Effective oxidation at lab scale	Requires a lot of dissolved O <sub>2</sub>
Electro kinetic coagulation	Economically feasible	High sludge production

### 2.3.2.3 MB removal by miscellaneous adsorbents

Many studies have been reported for MB removal on different adsorbents from water for example, fly ash (Keleşoğlu et al., 2012), chitin (Dotto et al., 2015) , low cost adsorbents (Hameed, 2009; Rafatullah et al., 2010), lignin (Kushwaha, Gupta, & Chattopadhyaya, 2014), barley straw (Oei et al., 2009), nanocomposites (Gupta & Nayak, 2012; Wang et al., 2011; Yao et al., 2012) sawdust (Garg et al., 2004), wheat bran (Hamdaoui & Chiha, 2007), Kaolinite (Zhang, Ping, et al., 2013), zeolite (Li, Zhong, et al., 2015), polymer (Ge et al., 2012), carbon fibers (Cherifi, Fatiha, & Salah, 2013), carbon nanotubes graphene oxide (Bradder et al., 2010; Ramesha et al., 2011) and most of all, activated carbon (Altıntig et al., 2017a; Li, Du, et al., 2013; Yang & Qiu, 2010) . Annadurai et al. (1996), used a natural biopolymer, chitin, to adsorb methylene blue. The obtained results showed high adsorption efficiency which was increased by increasing

the temperature, pH and adsorbent dose (Annadurai & Krishnan, 1996). In like manner, McKay and co-workers explored the removal of two basic dyestuffs, methylene blue and safranin from aqueous solutions by adsorption on low cost adsorbents such as hair, cotton waste, teak wood bark, rice husk and coal. Their investigation reported the monolayer saturation capacities for methylene blue were 914, 312, 277, 158 and 250 mg/g for bark, rice husk, cotton waste, hair and coal, respectively (McKay, Porter, & Prasad, 1999).

Garg et al. (2004), investigated the potential use of Indian rosewood sawdust which was pretreated with formaldehyde and sulfuric acid for the removal of methylene blue from simulated wastewater. The group examined the effect of different system conditions, including adsorbent dosage, initial dye concentration, pH and contact time. It was found that the percentage of MB removal was increased by increasing the adsorbent amount. The maximum MB was sequestered within 30 min at the optimum pH of 7.0. The group demonstrated the adsorption of methylene blue on rosewood sawdust followed was well fitted with a first order rate equation (Garg et al., 2004).

Gong et al. (2009), examined the adsorption efficiency of the magnetic multiwalled carbon nanotube nanocomposite for cationic dyes; methylene blue (MB), neutral red (NR) and brilliant cresyl blue (BCB), from aqueous solution. The results showed the cationic dyes adsorption was increased with pH due to the electrostatic attractions. Their study suggested that the kinetic data were well described by a pseudo second-order model and the maximum adsorption capacity values of the magnetic nanocomposites for MB, NR and BCB were 15.74 mg/g, 20.33 mg /g and 23.55 mg /g, respectively (Gong et al., 2009). Table 2.11 displays the results of previous adsorption studies on the removal of MB from water by different adsorbents.

**Table 2.11: Reported results of batch adsorption studies on the removal of MB from water by different adsorbents.**

Type of adsorbent	Adsorbate, adsorbent	pH	Contact time (min)	Maximum Adsorption capacity (mg/g)	Adsorption Isotherm	Kinetic model	Reference
<b>Carbon nanotubes</b>							
MWCNT (untreated)	20mg/L, 20 mg	6	120	59.7	Langmuir, Freundlich	Pseudo-second-order	(Wang et al., 2012)
MWCNTs (acid washed)	5–40 mg/L, 15mg/50mL	7	90	64.7	Langmuir	Pseudo-second-order	(Yao et al., 2010)
Oxidizes MWCNTs (HNO <sub>3</sub> )	300 mg/L, NA	9	75	54.54	Langmuir	NA	(Rodriguez et al., 2010)
Fe <sub>3</sub> O <sub>4</sub> – MWCNTs (HNO <sub>3</sub> )	10–30 mg/L, 20 mg/50mL	7	120	48.06	Langmuir	Pseudo-second-order	(Ai, Zhang, Liao, et al., 2011)
MWCNTs/ $\gamma$ -Fe <sub>2</sub> O <sub>3</sub>	20 mg/L, 50mg/50mL	6	240	42.3	Freundlich	NA	(Qu et al., 2008)
Alkali-activated MWCNTs	200-270 mg/L, 30 mg/ 40mL	7	180	399	Langmuir	Pseudo-second-order	(Ma et al., 2012; Zare, Gupta, et al., 2015)
MWCNTs	40–120 mg/L, 25mg/50mL	6	200	176.02	Langmuir	Pseudo-second-order	(Li, Du, et al., 2013)

**Table 2.11 (continued)**

<b>Graphene</b>							
Gr (untreated)	60 mg/L, 0.02–0.17g/100 mL	10	250	153.85	Langmuir	Pseudo-second- order	(Liu, Li, et al., 2012)
GO (untreated)	188-1000 mg/L,1.5g/L	6	60	714	Freundlich	NA	(Yang et al., 2011)
r-GO	10–50 mg/L, NA	10	60	17.3	Langmuir	Pseudo-second- order	(Ramesha et al., 2011)
Graphene-CNT	10-30 mg/L, 20 mg/50 mL	10	180	81.97	Freundlich	Pseudo-second- order	(Ai & Jiang, 2012b)
<b>Carbon materials made from solid wastes and coal-based sorbents</b>							
Activated sludge biomass	100mg/L, 10mg/90 mL	7	60	256.41	Freundlich- Langmuir	Pseudo-second order	(Gulnaz et al., 2004)
Straw activated carbon	600g/l, 2g/L	7.2	35	472.1	Langmuir	Pseudo-second- order, intraparticle	(Kannan & Sundaram, 2001)
Commercial AC	100 mg/L, 10 g/L	7	35	890.0	Langmuir	Pseudo-first-order	(Hameed, Din, & Ahmad, 2007)

**Table 2.11 (continued)**

Clay							
Attapulgite-COOH	200 mg/L, 0.025 g/25 mL	5	60	208.33	Langmuir	Pseudo-second-order	(Zhang, Wang, & Wang, 2015)
Modified Ball clay (MBC)	100 mg/L, 0.2 g/250 mL	12	200	100	Redlich–Peterson, Freundlich	Pseudo-second-order	(Auta & Hameed, 2012b)
Montmorillonite	600 mg/L, 0.1 g/50 mL	11	60	280	Langmuir	Pseudo-second-order	(Almeida et al., 2009)

## 2.4 Mechanism of adsorption on CNMs

Understanding the molecular interactions, partitioning and sorption, properties dominating the carbon nanomaterials is a joint effort between experimentalists and theorists that have enhanced elucidating the sorption mechanisms and improved optimization of sorbent properties. Adsorption is a surface phenomenon which involves retaining atoms, molecules, or ions of a given substance in the available active sites of a certain surface (Ghasemian & Palizban, 2016). It takes place because of the unbalance interactions or forces. Thus, the porous adsorbent tends to accumulate a layer of adsorbate to satisfy the residual surface forces. Adsorption of an adsorbate by adsorbents should be described in two aspects: adsorption capacity and affinity. Adsorption capacity is governed by the potential space of a sorbent available for adsorption of a given adsorbate, while adsorption affinity is dependent on the strength of attractive forces between adsorbate and adsorbent (Das et al., 2017; Yang & Xing, 2010). Molecules and atoms can attach themselves onto the surfaces in two ways, via; physisorption and chemisorption.

In physisorption, there is a weak Van der Waal's attraction of the adsorbate to the surface (Thines et al., 2017). During the process of physisorption, no breakage of the covalent structure of the adsorbate takes place, so the physisorbed molecule retains its identity. However, in chemisorption, the interaction is much stronger than physisorption and the adsorbate sticks to the solid by the formation of a chemical bond with the surface (Gao et al., 2017). Different possible interactions including **hydrophobic effect**,  **$\pi$ - $\pi$  bonds**,  **$\pi$ - $\pi$  electron-donor-acceptor (EDA) interaction**, **hydrogen bonds**, and **electrostatic interactions** have been proposed and are responsible for the adsorption of organic chemicals on CNMs surface. These interactions, their strengths, and contribution to the overall sorption are dependent on the properties of both organic chemicals and the

CNMs. In addition, properties of the compound of interest or reorganization after adsorption, alteration of adsorbent structure has been reported (Zhang et al., 2016).

Among CNMs, CNTs are considered very strong adsorbents for hydrophobic organic compounds. There are four possible sites (Figure 2.11) in CNT bundles for the adsorption of different pollutants. 1) the curved outside surface of individual nanotubes bundles; 2) grooves formed at the contact between adjacent tubes on the outside of the bundle; 3) internal sites within an interior pore of an individual tube (accessible only if the caps are removed and the open ends are unblocked); and 4) inside an interstitial channel formed at the contact of three or more tubes in the bundle interior (Pignatello, Mitch, & Xu, 2017; Sigmund et al., 2016). The access of molecules to the pores of the internal tube is either through the open ends of CNTs, or the tube walls defects. A particular molecule can be excluded alone for size considerations of some of these sites. A consensus is that the close-ended CNTs adsorb the molecules on the grooves, on the outer surface sites, and on large-diameter stacking-defect induced interstitial channels (ICs). For as-produced CNTs, both ends are generally closed, thus the adsorption starts in the grooves between adjacent tubes on the perimeter of the bundles and the largest accessible interstitial channels which are easily accessed for both adsorption and rapid desorption (Zhao, Liu, et al., 2016).

Because of the strong hydrophobic nature and high surface area of carbon nanotubes, have significant affinity to organic chemicals, especially to nonpolar organic compounds, such as naphthalene (Gotovac et al., 2007). CNTs have an exceptionally high aspect ratio which is also important factor that provides a special confinement effect with specific adsorption sites. This leads to completely different physical behavior compared with most conventional sorbents. As a result, the sorption capacity is higher than would be predicted based on surface area measurement (Wu et al., 2016).



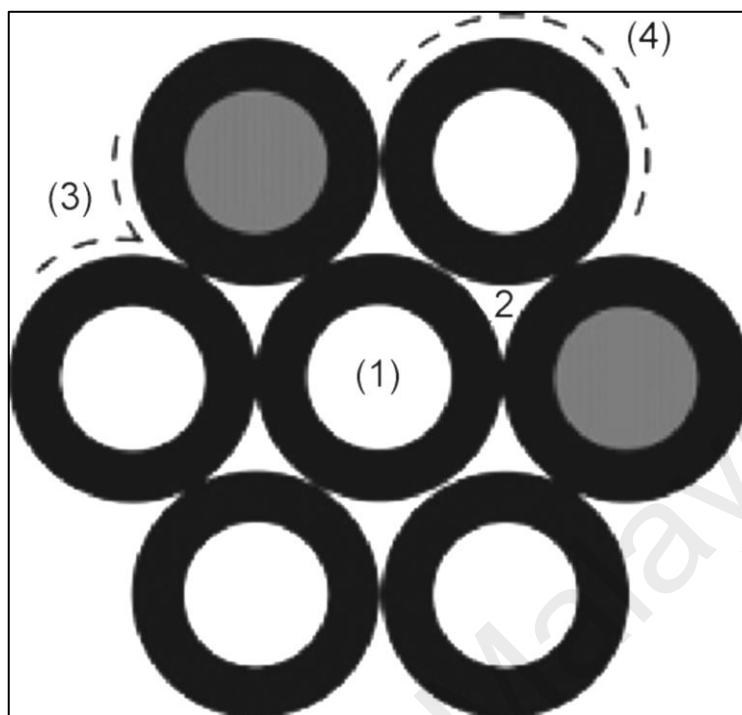


**Figure 2.11: Different adsorption sites on a homogeneous bundle of partially open-ended SWCNTs: (1) internal, (2) interstitial channel, (3) external groove site, and (4) external surface (Agnihotri et al., 2006).**

Multiple mechanisms have been proposed to control the adsorption of organic compounds by CNMs. The addressing and quantification of the relative importance of these individual contributions are a challenging task, which reveals this current CNMs adsorption area has yet to be treated and need of further investigation. However, some previous studies indicated that adsorption is more controlled by certain parameters than others. According to Yang investigation, the hydrophobic driving forces play important roles in the adsorption capacity of organic compounds to CNTs; however they cannot completely explain adsorption (Yang, Zhu, & Xing, 2006). Electrostatic interactions,  $\pi$ - $\pi$  interactions and hydrogen bonding also influence adsorption interactions considerably. The hydrophobic forces that are either associated with the protonation state of ionizable compounds or with the polarity and size of the molecule are the predominant repulsive

force that repels organic contaminants from water onto the CNMs surface. The molecular size has direct impact on adsorption because the steric hindrances overcome the hydrophobic affinity. Chen et al. (2007), finding confirmed that the molecular sieving effect prevent bulky 1,2,4,5-tetrachlorobenzene molecules from accessing the innermost surfaces (Chen, Duan, & Zhu, 2007). Pan et al. (2008), reported that the groove regions of CNTs are easily wedged because of the rotating structure of bisphenol A unlike rigid 17 $\alpha$ -ethinyl estradiol molecules (Pan & Xing, 2008).

Additionally, several of the studies indicated that the adsorption improvement of the organic compounds to carbon nanotubes might be due to the important implication of the electronic polarizability of the aromatic rings on the surface of carbon nanotubes (Zhao et al., 2003). The graphitic surfaces of CNTs have regions with rich and poor  $\pi$  electrons, the interaction of  $\pi$  electrons influence adsorption. Thus, the  $\pi$  electron-rich CNT surface allows  $\pi$ - $\pi$  interactions with organic molecules with benzene rings or C=C bonds, such as polar aromatic compounds and poly-aromatic hydrocarbons (PAHs) (Ersan et al., 2017a). Lin and Ren et al. (2011), stated that the non-aromatics have relatively lower sorption affinity than aromatic compounds toward CNTs (Lin & Xing, 2008; Ren et al., 2011). Furthermore, hydrogen bond with the graphitic surface of CNTs could also be formed by organic compounds which have functional groups such as -COOH, -OH, and -NH<sub>2</sub>. These groups can act as hydrogen-bonding donors and form hydrogen bonds with graphite sheets of CNMs, where the benzene rings of graphite sheets of CNMs act as the hydrogen-bonding acceptors (Tričković et al., 2016). However, the insignificant effects of hydrogen-bonding interaction on adsorption of solutes without hydrogen-bonding donor ability could be attributed to that the stronger hydrogen-bonding interaction between functional groups of CNMs and water molecules than that would be with the organic solutes, which results in the competitive sorption of water with organic solutes.

Not to mention, the surface chemistry of CNTs is greatly influence their adsorption behavior. It is worth to mention that the greater adsorption affinity of ionized species than the unionized species was basically ascribed for the electrostatic attractions of opposite charges between ionized compounds and CNT surfaces (Sotelo et al., 2012). The electrostatic interaction is directly related to the nature of charge of both CNMs and organic chemicals. Hence, electrostatic repulsion will occur between the dissociated anions of the phenolic chemicals and the CNMs which can be negatively charged as pH increased (Engel & Chefetz, 2016).

#### **2.4.1 Mechanism of adsorption of Bisphenol A onto CNMs**

Bisphenol A has a unique butterfly chemical structure and could wedge into the heterogeneous surface sorption sites of CNMs. Thus, three types of adsorption sites are available for adsorption on CNM; aggregates or bundles, groove area, and interstitial pores (Ersan et al., 2017b). Zhao et al. (2002), reported that adsorption energy and charge transfer of several small molecules in groove and interstitial sites of the bundles are much higher than those on the surface area, because of the increased number of CNMs interacting points with sorbate molecules (Zhao et al., 2002). The BPA molecule has two benzene rings attached through a single bond to a carbon atom which facilitate its rotation form various angles. BPA molecule could wedge into the groove region because of its “butterfly” structure (BPA 3 in Figure 2.12). The two benzene rings in BPA molecule could be adsorbed on CNT surface area parallel with the tube axis, around the circumference, or in diagonal direction. If both benzene rings of BPA attach on CNTs in the direction of tube axis, they must stay in a same flat plane (BPA 1). The flat configuration; according to the calculation by Efremenko is unlikely the main mode of adsorption (Efremenko & Sheintuch, 2006). However, BPA could be adsorbed with two benzene rings around the circumference of CNTs (BPA 2 in Figure 2.12) depending on

the tube diameter. But, for the CNTs with larger diameter, a higher steric energy must be spent for the change of molecular conformation of BPA to provide a wider angle between the two benzene rings of BPA. In this case, BPA would have only one benzene ring adsorbed on CNMs as this conformational change is less favorable (Yang et al., 2008; Yang & Xing, 2010).

The adsorption of chemicals containing benzene rings on CNMs has been shown to be dominated by the  $\pi$ - $\pi$  bond interaction force. The phenol group is a charge donor, and CNMs could be either donor or acceptor. Thus, the  $\pi$ - $\pi$  bond formed between BPA and CNMs is a donor-acceptor system (Li, Jiang, et al., 2013). Kwon (2015), reported the use of graphene as an adsorbent for the removal of BPA from aqueous solutions. Reduced graphene oxide (rGO) was prepared via both a thermal exfoliation method (T-rGO) and a chemical reduction method using hydrazine (H-rGO). The author demonstrated that T-rGO exhibited at least 2.5 times larger adsorption selectivity toward BPA versus phenol compared to H-rGO. The study proposed that T-rGO contains higher concentrations of hydroxyl groups and other oxygen functional groups and both hydrogen bonds and  $\pi$ - $\pi$  interactions may be responsible for the selective adsorption of T-rGO toward BPA (Kwon & Lee, 2015).

Bayramoglu et al. (2016), prepared BPA-imprinted polymer in the beaded form via precipitation polymerization. The molecular imprinted (MIP) microbeads were used under different experimental conditions for selective binding of BPA from aqueous solutions. The MIP microbeads showed a maximum binding affinity for removal of BPA at pH 4. The author reported that the adsorption of BPA on the MIP microbeads was attributed to the  $\pi$ - $\pi$  interaction between the phenyl groups of BPA and the phenyl group in the polymer, in addition to the hydrogen-bonding between the hydroxyl groups of the polymer chains and BPA molecules (Bayramoglu et al., 2016).

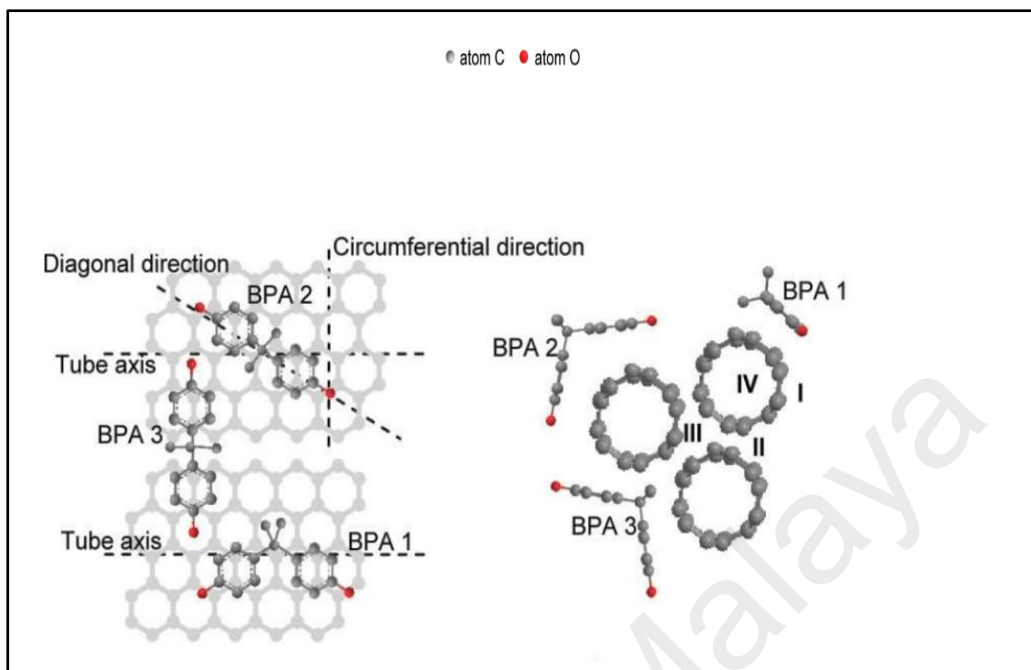


**Figure 2.12: Schematic diagrams for adsorption of BPA on SWCNT. The letters I, II, III, and IV indicate the possible adsorption areas of surface, groove, interstitial spaces, and inner pores, respectively. SWCNT is presented as an example. BPA 1 is adsorbed on CNT with two benzene rings in the direction of tube axis. BPA 2 show the adsorption on the surface, whereas BPA 3 illustrate the wedging of this molecule in the groove area. The interstitial space is too small for the molecules to fit (Pan et al., 2008).**

Koduru et al. (2016), have been prepared goethite iron oxide particles impregnated activated carbon composite (GPAC) to remove BPA in the presence of natural organic matter (NOM). Their results indicated that the electro-chemical interaction between the iron oxides along with the active sites of PAC and the molecular interactions between NOM and BPA have enhanced BPA adsorption on GPAC (Koduru et al., 2016).

Li et al. (2015), investigated the adsorption of three organic chemicals including bisphenol A (BPA), ciprofloxacin (CIP), and 2-chlorophenol (2-CP) on carbon nanofibers (CNFs) was investigated. In this study it was assumed that the molecular size of the pollutants, micro/mesoporous structure of CNFs,  $\pi$  electron and hydrophobic interaction

play important roles on the high adsorption capacity exhibited by CNFs (Li, Chen, et al., 2015).

#### 2.4.2 Mechanism of adsorption of methylene blue onto CNMs

CNMs as adsorbents are suitable candidate for the pre-concentration and removal of pollutants from large volumes of wastewater. The intensive results indicated that the main adsorption mechanism of cationic and anionic dyes to CNMs is attributed to the  $\pi - \pi$  electron donor acceptor interaction between the electron acceptors (aromatic molecules) and the electron donors of carbon nanomaterials (the highly polarizable graphene sheets) in addition to the strong surface complexation between ions and functional groups (Figure 2.13) (Liu et al., 2014; Manilo, Lebovka, & Barany, 2016).

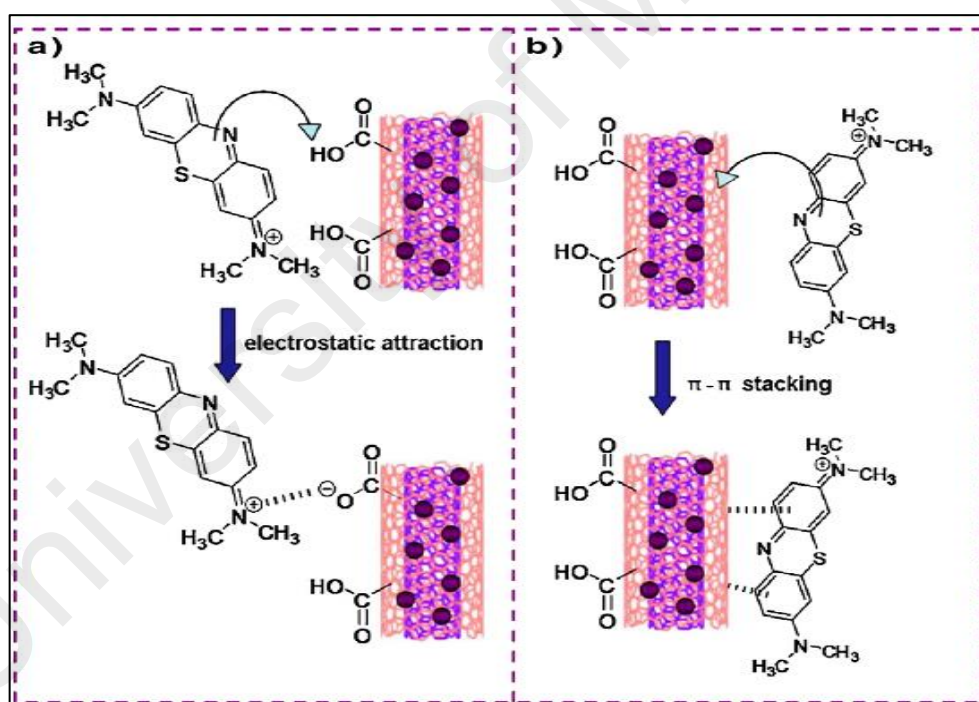


**Figure 2.13: Schematic illustration of the possible interaction between MWCNTs and methylene blue: (a) electrostatic attraction and (b)  $\pi$ - $\pi$  stacking (Ai, Zhang, Liao, et al., 2011).**

The removal of MB from aqueous solution using MWNTs and CNF as adsorbents was studied by Rodriguez et al. (2010). They reported that of the adsorption capacity CNF was higher than for MWCNT and the untreated MWCNT exhibited high affinity for MB than treated MWCNT-HCl. Their findings proposed that the high adsorption was attributed to the very strong van der Waals forces and hydrophobic interactions between the carbon nanomaterial and the dye. Furthermore, they demonstrated that the low affinity of treated CNT was because of the existence of ionic repulsion between the MWCNT modified and the dye, both with positive charges in water (Rodriguez et al., 2010).

Li et al. (2013), reported the adsorption performance of three acid treated carbonaceous materials, activated carbon, graphene oxide, and multi-walled carbon nanotubes for the removal of methylene blue dye from aqueous solution. They found that the adsorption capacity follows an order of GO > CNTs > AC. They demonstrated that the high removal of MB onto GO and CNTs might be attributed to  $\pi$ - $\pi$  electron donor acceptor interactions with graphene surfaces. MB has C-C double bonds and contains electrons which can easily interact with the electrons of benzene rings on GO and CNT surfaces through  $\pi$ - $\pi$  electron coupling. Their study demonstrated the role of the electrostatic attraction between the positively charged dye ions (MB<sup>+</sup>) and the negatively charged adsorbents (Li, Du, et al., 2013).

In the study investigated by Ai et al. (2011), the FTIR analysis suggested the efficient removal of MB from aqueous solution with the synthesized magnetite-loaded multi-walled carbon nanotubes (M-MWCNTs) was mostly attributed to the electrostatic attraction and  $\pi$ - $\pi$  stacking interactions between MWCNTs and MB (Ai, Zhang, Liao, et al., 2011).

The adsorption of methylene blue onto calcined titanate nanotubes (CTNTs) was studied by Xiong et al. (2010). They reported that the adsorption mechanism was mainly

associated with electrostatic attraction and the corresponding maximum adsorption capacity was of 133.33 mg/g. They observed that in the whole pH range (2.5-11), the surface of CTNTs possessed a dominant negative charge. Thus, cationic MB molecules were easily adsorbed onto negatively charged sites of CTNTs by charge attraction (Xiong et al., 2010).

Self-assembled cylindrical graphene-carbon nanotube (G-CNT) hybrid showed good removal efficiency of 97% at the initial MB concentration of 10 mg/L with a maximum adsorption capacity of 81.97 mg/g. The group demonstrated that the lower observed performance for the removal of methylene blue (MB) at lower pH value could be ascribed to the protons competition with the MB for the available adsorption sites on the G-CNT hybrid surface. However, the study proposed that when the pH value increases to a certain extent, the surface of the G-CNT hybrid may get negatively charged that would lead to the increase in the adsorption capacity due to the electrostatic attraction between the negatively charged G-CNT hybrid and the MB cation (Ai & Jiang, 2012b).

Alkali-activated multiwalled carbon (CNT-A) was utilized as an adsorbent material for removal of cationic and anionic dyes in aqueous solutions. Experimental results indicated that CNTs-A have excellent adsorption capacity for methylene blue (399 mg/g) and methyl orange (149 mg/g). Their investigation proposed that the multiple adsorption interaction mechanisms ( $\pi$ - $\pi$  electron-donor-acceptor interactions, electrostatic interactions, hydrogen bonding, mesopore filling) have to some extent their role in the remarkable adsorption capacity of dye onto CNTs-A (Ma et al., 2012).

## **2.5 Summary of literature review**

A detailed and updated overview was presented in this chapter covering the historical background, structure, properties, production methods of carbon nanomaterials and their potential use in wastewater treatment.



Although a good number of researches have been conducted regarding fabrication of CNMs, however some shortcomings lower their ability to remove certain compounds and their successful recovery from the aqueous phase pose a significant challenge. So, it would be our major focus to reduce the cost of isolation, and enhance the adsorbent capacity through synthesizing new type of hybrid carbon nanomaterials on nickel powder activated carbon substrate to end up with multi-structure carbon materials, optimize their growth conditions, characterize their surface morphological features and carry out subsequent adsorption studies for the removal of bisphenol A and methylene blue dye from aqueous solution.

University of Malaysia

## CHAPTER 3: METHODOLOGY

### 3.1 Introduction

This chapter describes the method, approaches and empirical techniques applied to accomplish the objective of the research. This chapter comprises from three sections. The first section covers the list of chemicals and reagents along with physiochemical properties of the organic pollutants; (BPA and MB), whereas the second section provides the description of the structure and operational characteristics of instruments used including the drawing of the experimental setup, and description of the characterization systems are presented in section two also. The third section includes experimental approach for synthesizing the adsorbent by using DOE, model development using ANOVA analysis, optimization process, batch adsorption studies, kinetics and isotherm investigations. In addition, the section describes the experimental uptakes of the pollutants by batch sorption studies and analyzes the adsorption equilibrium process in terms of kinetics and isotherm features of the adsorbent-adsorbate system. The last section presents a schematic flow chart displaying the main experimental activities conducted to implement the project.

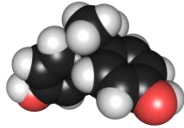
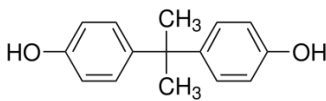
### 3.2 Materials

The list of reagents and chemicals used to conduct in this research as well as their corresponding suppliers, purity grade and applications are listed in the Table 3.1. Table 3.2 and Table 3.3 display the general properties of bisphenol A and methylene blue respectively. The Material Safety Data Sheet (MSDS) of all materials used in this research were considered and understood before starting the experimental activities.

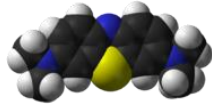
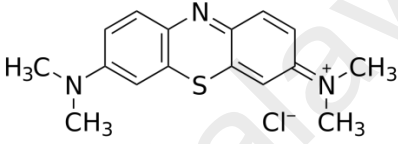
**Table 3.1: List of reagents, chemicals and gases utilized in this research.**

Material	Supplier	Purity grade	Application
powder activated carbon (PAC) – palm shell based	Sigma Aldrich	≥ 98.0 %	Used as growth substrate
Ni (NO <sub>3</sub> ) <sub>2</sub> ·6H <sub>2</sub> O	Sigma Aldrich	≥ 98.0 %	Source of nickel (Ni <sup>+2</sup> ) ions catalyst
Bisphenol A (BPA)	Merck	≥ 98.0 %	Used as adsorbate
Methylene blue (MB)	Sigma Aldrich	≥ 90.0 %	Used as adsorbate
sodium hydroxide	Sigma Aldrich	98-99 %	Used to adjust pH
hydrochloric acid	Sigma Aldrich	36.6-38 %	Used to adjust pH
Sulfuric acid	Sigma Aldrich	95-97 %	Used to functionalize CNMs
Potassium permanganate	Sigma Aldrich		Used to functionalize CNMs
Methane	AGS, Malaysia	99.99 %	Used for production CNMs
Acetylene	AGS, Malaysia	99.99 %	Used for production of CNMs
Purified hydrogen	AGS, Malaysia	99.99 %	Used for reduction and production of CNMs
Purified nitrogen	AGS, Malaysia	99.99 %	Used for purging and calcination

**Table 3.2: General properties and chemical structure of bisphenol A.**

Characteristics	Values
Molecular formula	C <sub>15</sub> H <sub>16</sub> O <sub>2</sub>
Molecular weight (g/mol)	228.29
Chemical class	<a href="#">diphenylmethane</a> derivatives
λ <sub>max</sub> nm	277
Space filling model	
Chemical structure	

**Table 3.3: General properties and chemical structure of methylene blue.**

Characteristics	Values
Molecular formula	C <sub>16</sub> H <sub>18</sub> ClN <sub>3</sub> S
Molecular weight (g/mol)	319.8
Chemical class	Cationic dye
$\lambda_{\max}$ nm	665
Space filling model	
Chemical structure	

### 3.3 Instruments and measurements

This section is divided into three main sub-categories; a lab-scale horizontal reactor, instruments for CNMs characterization and accessories and consumables.

#### 3.3.1 Chemical vapor deposition reactor (CVD)

The growth of CNMs process using chemical vapor deposition method was carried out in situ OTF-1200-80mm Dual Zone Tube Furnace. The tubular reactor consists of furnace equipped with one 50 mm diameter fused quartz tube for immediate use (OD: 80 mm; ID: 72 mm; Length: 1000 mm). Split two-zone tube furnace which can achieve faster heating up to 1200 °C and create a different thermal gradient by setting different temperature of each zone via two segments programmable temperature controllers. The furnace includes one 40" L fused quartz tube with vacuum flanges, valves and equipped with mechanical vacuum pump and three channel gas flowing system. Piping system for inlet and outlet of gases produced during the reaction were fixed in the entrance and exit of the quartz tube. The inlet flange has three circular openings to be connected to the feed pipes. Inlet pipes were connected to the hydrocarbon source line (CH<sub>4</sub> or C<sub>2</sub>H<sub>2</sub>), hydrogen

(H<sub>2</sub>) and the inert gas (N<sub>2</sub>). The outlet flange has one opening to be connected to the flue gasses. Table 3.4 and Figure 3.1 illustrate the CVD system utilized in this research and its technical specification, respectively.

**Table 3.4: Technical specifications of CVD utilized in this research.**

<b>Item</b>	<b>Parameter</b>
<b>Power</b>	4KW
<b>Voltage</b>	AC 220-240V Single Phase, 50/60 Hz
<b>Max. Temperature</b>	1200 °C
<b>Max. Heating Rate</b>	≤ 20 °C /min
<b>Suggested Normal Heating</b>	Rate ≤10 °C /min
<b>Tube Size and Materials</b>	OD: 80 mm; ID: 72mm; Length: 1000 mm, 4"(100 mm) Quartz tube
<b>Heating Zone Length</b>	Each Zone Length:6" (150mm)
<b>Temperature Controllers</b>	PID automatic control via SCR (Silicon Controlled Rectifier) power control, 30 steps programmable
<b>Temperature Accuracy</b>	±1 °C
<b>Heating Elements</b>	Fe-Cr-Al Alloy doped by Mo
<b>Weight</b>	40 Kg

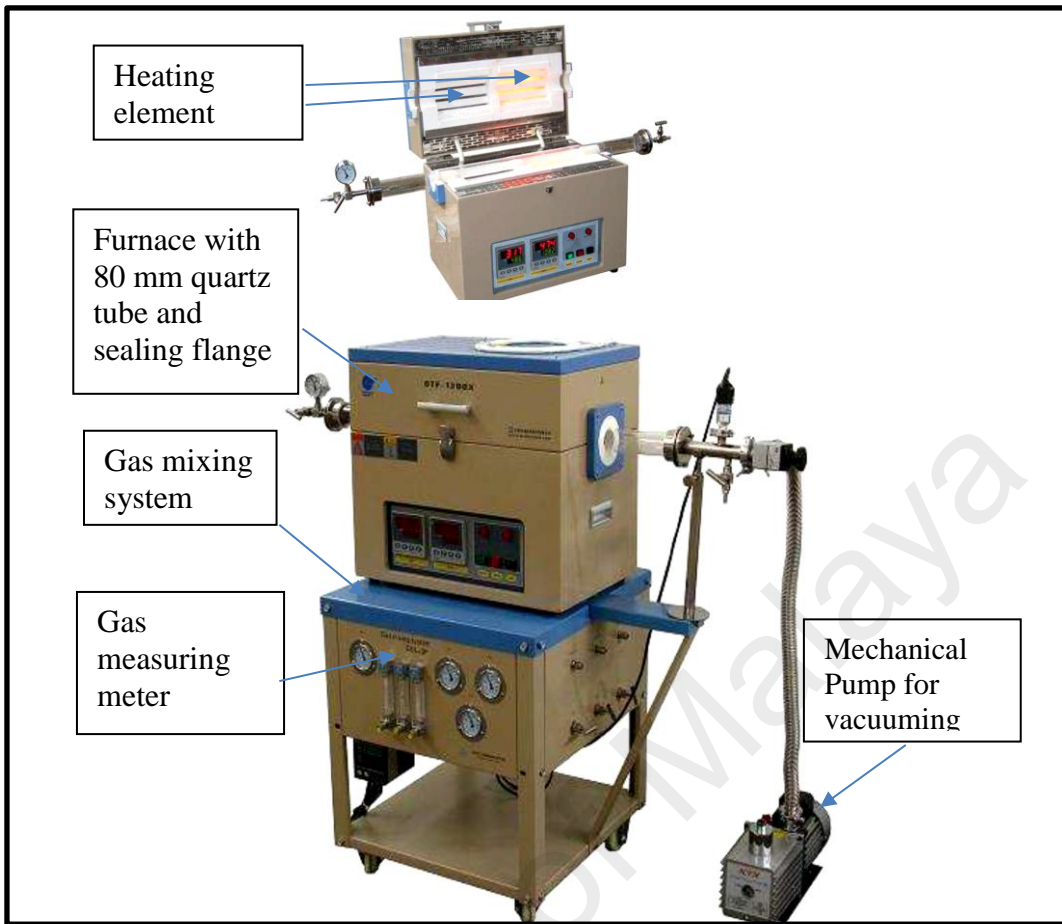


Figure 3.1: Photograph of the in-situ CVD reactor.

### 3.3.2 Instruments and equipment for characterization

Field-emission scanning electron microscope (**FE-SEM**) equipped with an energy-dispersive X-ray spectrometer (**EDX**) (Quanta FEG 450, EDX-OXFORD) was used to obtain high resolution images of the nano-sized structure to study the CNM-PAC morphology and the surface elements. Other morphological features were observed using a transmission electron microscope (**TEM**). Thermogravimetric analysis (**TGA**) was obtained using Thermal Analyzer (STA-6000, PerkinElmer®) in an oxygen environment and heating rate of 10 °C/min. Surface area analysis was performed using Gas Sorption System (micromeritics ASAP2020, TRISTAR II 3020, USA) following Brunauer-Emmett-Teller (**BET**) method. The prepared CNM-PAC was also characterized by **Raman spectroscopy** (Renishaw System 2000 Raman Spectrometer). The CNM-PAC surface chemistry before and after organic pollutant adsorption was investigated using Fourier transform infrared (**FTIR**) spectroscopy (PerkinElmer® FTIR spectrometer), by grinding the sample with KBr to form pellets and the wavenumbers range was 500–4000 cm<sup>-1</sup>. **UV-Visible absorption spectroscopy** (PerkinElmer® spectrophotometer) was used in adsorption experiments and water analysis. The prepared samples were conducted for **zeta potential** using a Zetasizer (Malvern, UK). Water suspensions were prepared at a concentration of 0.01g/100 ml and left for 1 h sonication before the measurement. All pH measurements were carried out using pH/Ion Benchtop meter (Mettler Toledo Seven Compact).

### 3.3.3 Additional instruments

- 1- Vacuum oven (Mettler VO500)
- 2- Digital balance (Mettler Toledo AG204)
- 3- Ultrasonic bath (JAC, Korea, model JAC 2010P)
- 4- Orbital laboratory shaker

- 5- Table – Top low speed Centrifuge (CNC-104 L550, China)
- 6- Vacuum pump station (model DAA-P601-LD, Germany)
- 7- Membrane 0.45  $\mu\text{m}$  (Sartorius stedim biotech GmbH 37070, Germany)

### 3.4 Methods

The experimental steps followed to carry out the objectives of this study are demonstrated in Figure 3.2.

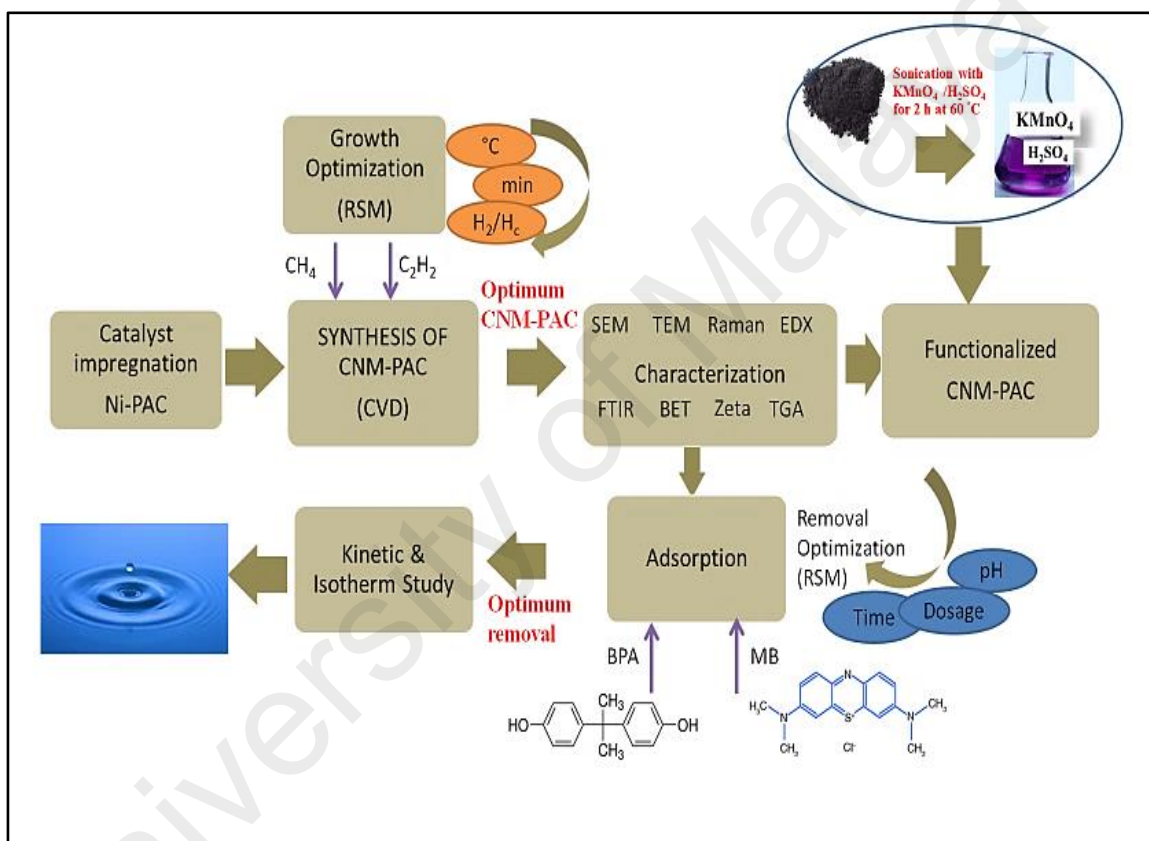


**Figure 3.2: The experimental activities of this research.**

#### 3.4.1 Experimental Approach for carbon nanomaterials synthesis

##### 3.4.1.1 Catalyst and support preparation

PAC (2 g) was dried overnight at 120 °C and mixed with Ni (NO<sub>3</sub>)<sub>2</sub>·6H<sub>2</sub>O (5 mL; 1 wt %) and acetone. The mixture was sonicated for 1 h at 60 °C/40 kHz. Ni-doped PAC (Ni-PAC) dispersion was dried at 100 °C and then grounded thoroughly. For the



preparation of metal catalyst nanoparticles, a two-stage thermal treatment was performed: calcination at 350 °C for 2 h followed by temperature programmed reduction (TPR) with H<sub>2</sub> gas at 600 °C for 1 h in N<sub>2</sub> atmosphere (200 mL/min) within the CVD tubular furnace. The final impregnated substrate (Ni-PAC) was then used for CNM-PAC production (Onundi et al., 2011).

#### 3.4.1.2 Growth of carbon nanomaterials on powdered activated carbon

In total, 200 mg of the thermally treated Ni-PAC was placed in a ceramic alumina boats and shuffled into the CVD reaction tube in the tubular quartz reactor. The temperature programmed deposition (TPD) was set at 750 °C–1000 °C with ramping rate of 10° C/min. To initiate the growth, we allowed a flow of H<sub>2</sub> was mixed with CH<sub>4</sub> at a ratio of ranging from 1 to 4 to pass through a heated reactor from 20–60 min. After the CNMs grew, the reactor was cooled down by using N<sub>2</sub> flow (200 mL/min), and the deposited CNMs were then collected from a ceramic boat. Thus, the overall CNMs growth via CVD could proceed through carbonaceous precursors feedstock decomposition on a Ni–PAC surface to generate small carbon fragments which were subsequently diffused on the Ni catalysts surface to grow a graphitic tubular structure around the particles. Finally, CNM-PAC growth was terminated when the catalytic activity of Ni particles stopped. The deposited carbon nanomaterials produced in the reactor were collected from the ceramic boat and the growth yield was calculated using Equation (3.1):

$$\text{Yield \%} = \frac{m_{after}^{catal} - m_{blank}^{catal}}{m_{blank}^{catal}} \times 100 \quad (3.1)$$

where  $m_{after}^{catal}$  is the total mass of the product after reaction, and  $m_{blank}^{catal}$  is the weight of the PAC substrate treated similarly as in growth reaction conditions but without

introduced any type of carbon sources. This experiment was necessary to determine the loss of weight in catalyst-substrate hybrid prior to CNM growth.

#### **3.4.1.3 Optimization of operating conditions for CNM-PAC growth**

The adsorption capacity of an adsorbent is the most significant property which is highly contingent by the working variables. For preparing an efficient adsorbent, the removal efficiency is a major concern along with its yield for economic feasibility of the whole process. Accordingly, the growth parameters of CNM on powdered activated carbon (CNM-PAC) were optimized to obtain active surface with maximum removal percentage. Nevertheless, for evaluating the effect of process variables on the quality of the final-product, an acceptable experimental design is imperative (Angulakshmi, Sivakumar, & Karthikeyan, 2012). Several researchers have used response surface methodology (RSM) which is a compilation of statistical techniques for reduced number of experimental runs to assess the impact and the interactions of multiple parameters and developing regression models. RSM comprises three stages; process experimental design outline at different operating condition, response surface analyses using the obtained regression model and process optimization. The central composite design (CCD) is well appropriate in the case of standard RSM technique which is commonly used for process optimization (Ronix et al., 2017).

#### **3.4.2 Design of experiment (DOE) for synthesis CNM-PAC**

A design of experiment (DOE) with a central composite design (CCD) was utilized to optimize the synthesis parameters including growth temperature (A), growth time (B) and hydrogen to hydrocarbon source flow rate ratio ( $H_2/CH_4$ ) or ( $H_2/C_2H_2$ ) (C). Full factorial CCD for the three numerical variables, consisting of 8 factorial points (coded as -1 and +1), 6 axial  $\alpha$  points (coded as -1.682 and +1.682) and 6 replicates at the

center points (coded as 0,0) were employed. In this study the optimum conditions for CNM-PAC growth was determined by setting the percentage of growth yield (Y) and pollutant removal efficiency (RV %) as responding model. Production conditions was varied according the data generated by DOE in order to obtain the optimum growth conditions to produce the maximum yield of CNM-PAC associated with the highest removal efficiency of the investigated pollutant. Each response was employed to generate an empirical model that correlates the responses to the growth parameters using the proposed regression model represented by Equations (3.2) and (3.3) (Tan, Ahmad, & Hameed, 2008):

$$x_i = \frac{X_i - X_i^x}{\Delta X_i} \quad (3.2)$$

Where  $x_i$  is the coded value of the  $i^{\text{th}}$  independent variable,  $X_i$  is the natural value of the  $i^{\text{th}}$  independent variable,  $X_i^x$  denotes the natural value of the  $i^{\text{th}}$  independent variable at the center point, and  $\Delta X_i$  is the value of step change.

$$Y = b_0 + \sum_i^n b_i x_i + \left( \sum_{i=1}^n b_{ii} x_i \right)^2 + \sum_{i=1}^{n-1} \sum_{j=i+1}^n b_{ij} x_i x_j \quad (3.3)$$

where Y is the predicted response,  $b_0$  the constant coefficient,  $b_i$  the linear coefficients,  $b_{ij}$  the interaction coefficients,  $b_{ii}$  the quadratic coefficients and  $x_i$ ,  $x_j$  are the coded values of the CNM-PAC synthesis variables. Table 3.5 and Table 3.6, present the coded and actual levels of process parameters for CH<sub>4</sub> and C<sub>2</sub>H<sub>2</sub> decomposition, respectively. Also, Table 3.7 and Table 3.8 shows the complete design matrix of the required experiments for CH<sub>4</sub> and C<sub>2</sub>H<sub>2</sub>, respectively.

**Table 3.5: Independent variables and their coded and actual levels in the CCD for CNM-PAC synthesis from CH<sub>4</sub> decomposition.**

Variable name	Factor	Range	
		Low (-1)	High (+1)
Temperature, °C	A	750	1000
Growth Time, min	B	20	60
H <sub>2</sub> /CH <sub>4</sub> flow rate	C	1	4

**Table 3.6: Independent variables and their coded and actual levels in the CCD for CNM-PAC synthesis from C<sub>2</sub>H<sub>2</sub> decomposition.**

Variable name	Factor	Range	
		Low (-1)	High (+1)
Temperature, °C	A	550	750
Growth Time, min	B	20	60
H <sub>2</sub> /C <sub>2</sub> H <sub>2</sub> flow rate	C	1	4

**Table 3.7: Experimental CCD data for the synthesis parameters of CNM-PAC using CH<sub>4</sub> decomposition.**

Run	Variables		
	A Temperature, °C	B Time, min	C Gas Ratio
1	850	40	2.5
2	950	20	4.0
3	750	60	4.0
4	850	20	2.5
5	1000	20	1.0
6	750	20	4.0
7	750	60	1.0
8	950	60	4.0
9	750	40	2.5
10	950	20	1.0
11	850	40	4.0
12	950	60	1.0
13	850	60	2.5
14	750	20	1.0

**Table 3.8: Experimental CCD data for the synthesis parameters of CNM-PAC using C<sub>2</sub>H<sub>2</sub> decomposition.**

Run	Variables		
	A Temperature, °C	B Time, min	C Gas Ratio
1	650	40	2.5
2	550	20	1.0
3	550	60	4.0
4	750	60	1.0
5	650	20	1.0
6	550	20	4.0
7	750	20	4.0
8	750	20	1.0
9	650	60	1.0
10	750	60	4.0
11	550	60	1.0

### 3.4.3 Functionalization of CNM-PAC for comparison

The synthesized CNM-PAC at the optimal growth conditions (O-CNTs) was dried overnight at 100 °C to eliminate any water on carbon surface. A 1M solution of KMnO<sub>4</sub> was prepared at 70 °C for ease of solvation. CNM-PAC was oxidized by the following procedures: (1) 200 mg of CNM-PAC was mixed with 7 ml of the previous permanganate solution inside a 20-ml glass vial; (2) the mixture was subjected to ultrasound waves using an ultrasonic bath at 70 °C for 3 h; (3) CNM-PAC was collected by a filtration process under vacuum using filter paper with a pore size of 0.45 µm; (4) the CNM-PAC was washed several times with 0.01M HCl and distilled water until a clear, transparent and neutral product was obtained; and (5) the collected cake was dried for 3 h at 100 °C and dubbed K-CNTs.

In a procedure similar to the previous chemical treatment of the CNM-PAC, in a 20-ml glass vial, 7 mL of the prepared KMnO<sub>4</sub> solution was mixed with 200 mg of CNM-PAC and 3 mL of 0.5 M H<sub>2</sub>SO<sub>4</sub>. The vial was sealed and subjected to ultrasound waves in ultrasonic water bath at 70 °C for 3h. After that, the suspension was filtered under

vacuum using 0.45  $\mu\text{m}$  pore size filter paper. The collected CNM-PAC was then washed several times with distilled water and 0.01 M HCl to eliminate oxidant traces until neutral solution of  $\text{pH} = 7$  was obtained. The oxidized CNM-PAC was put in closed crucible and dried at 100  $^{\circ}\text{C}$  for 3 h and referred as KS-CNTs.

#### **3.4.4 Adsorption studies**

Batch adsorption tests were carried out to investigate the adsorption affinity of CNM-PAC for removal of bisphenol A (BPA) and methylene blue (MB) from water. The adsorption processes for each pollutant subjected to three studies: batch experiments, optimization, kinetic and isotherm. The concentration of BPA and MB were determined using a UV-visible spectrophotometer at 277 and 665 nm, respectively.

##### **3.4.4.1 Batch adsorption experiments**

Adsorption studies were undertaken using Erlenmeyer flasks (250 ml) with glass stoppers. The freshly prepared stock solutions of adsorbate (BPA and MB) were prepared by dissolving requisite amount of the adsorbate in a 1000 ml volumetric flask followed by addition of deionized water to the mark. Batch adsorption experiments were conducted on the CNM-PAC produced from the DOE growth experimental runs. A fixed dosage of each adsorbent (10 mg) into 50 mL of the pollutant (50 mg/L) at  $\text{pH} = 6.0$  was shaken for 120 min at a constant agitation speed (180 rpm) at room temperature. A known volume of the solution was at the end of the adsorption time removed and centrifuged at 4000 rpm for 10 min. The sorbate concentration in the supernatant was measured by UV-vis spectrophotometer by monitoring the maximum absorbance wavelength and the removal efficiency percentage of was determined according to Equation (3.4), accordingly. The obtained CNM-PAC was fully characterized and optimization study was conducted to optimize the adsorption parameters of organic pollutant removal using the synthesized

CNMs-PAC at the selected optimum conditions of growth. The percent removal of adsorbate was calculated as follows:

$$\mathbf{Removal} (\%) = \frac{(C_o - C_t)}{C_o} \times 100 \quad (3.4)$$

whereas the amount of adsorbate adsorbed at equilibrium contact time,  $q_e$  (mg/g) was calculated according to Equation 3.5:

$$\mathbf{q}_e = \frac{(C_o - C_e)V}{w} \quad (3.5)$$

where,  $C_o$ ,  $C_t$  and  $C_e$  (mg/L) are the liquid-phase concentrations of adsorbate at initial concentration, at time  $t$  (min) and equilibrium time respectively,  $V$  is the volume of the solution (L) and  $w$  is the mass of adsorbent used (g).

#### **3.4.4.2 Optimization of adsorption conditions**

Experimental design methodology (DOE, version 7.0) was adopted in the optimization of pollutant removal by the synthesized CNM-PAC. The removal efficiency was mathematically described as the function of adsorption parameters and were modeled using RSM-CCD). The optimum conditions for BPA and MB adsorption by setting a range of the adsorption parameters including, pH (2-11), dose (5-20 mg) and contact time (10-120 min). The removal efficiency (RV, %) and adsorption capacity (mg/g) were set as model responding. The investigated parameters were denoted as  $X_1$  for the pH,  $X_2$  for the dosage (mg), and  $X_3$  for contact time (min). List of design of the experimental runs for BPA and MB adsorption is presented in Table 3.9 and Table 3.10, respectively.

**Table 3.9: List of design of experiments runs for BPA adsorption using CNM-PAC obtained from CH<sub>4</sub> decomposition.**

Run	Variables		
	X <sub>1</sub> pH	X <sub>2</sub> Adsorbent dose, (mg)	X <sub>3</sub> Contact time, (min)
1	2	20.0	10
2	3	5.0	120
3	7	10.0	65
4	11	20.0	120
5	7	12.5	20
6	7	10.0	40
7	2	20.0	120
8	3	5.0	10
9	11	5.0	120
10	6	12.5	40
11	7	12.5	40
12	5	15.0	65
13	7	15.0	20
14	11	20.0	10
15	10	15.0	20

**Table 3.10: List of design of experiments runs for MB adsorption using CNM-PAC obtained from CH<sub>4</sub> decomposition.**

Run	Variables		
	X <sub>1</sub> pH	X <sub>2</sub> Adsorbent dose, (mg)	X <sub>3</sub> Contact time, (min)
1	6	10	70
2	7	10	120
3	7	10	40
4	2	5	10
5	11	15	20
6	6	15	70
7	3	20	40
8	11	15	120
9	3	15	120
10	7	10	70
11	11	5	120
12	3	5	120
13	7	15	70
14	3	10	70
15	11	5	20



### 3.4.4.3 Kinetic studies

The removal of adsorbates from aqueous media by the adsorbent is a time dependent process. However, the properties of the adsorption process will totally depend on physiochemical features of the adsorbate, adsorbent and the operating variables. The assessment of kinetics parameters was similar to that of batch equilibrium experiments. The kinetics experiments were conducted at the optimum conditions determined by DOE. The initial BPA and MB concentration was 50 mg/L. The applicability of the studied kinetic models was examined at contact time of (5, 10, 20, 25, 30, 40, 50, 60, 70, 80, 100, 110, 120, 130, 140, 150, 160, 170 min, and 24 h). The rate of sorption was determined by employing three kinetic models on the experimental data, pseudo first order, pseudo second order and intraparticle diffusion.

#### (a) *Pseudo first order*

This model is defined as Lagergren and Svenska, (Lagergren, 1898) has been widely used to predict sorption rate which is primarily based on the adsorption capacity ( $q$ ) (Lagergren, 1898). The linearized form of Lagergren equation can be described as follow:

$$\ln(q_e - q_t) = \ln q_e - k_1 t \quad (3.6)$$

where  $q_e$  and  $q_t$  (mg/g) are the amounts of adsorbate adsorbed at equilibrium and at time  $t$  (min) respectively, and  $k_1$  (L/min.) is the adsorption rate constant. The plot of  $\ln(q_e - q_t)$  versus  $t$  (Figure 3.3) gives the slope of  $k_1$ , and intercept of  $\ln q_e$ . This equation is commonly does not fit well with all range of contact time, but it is generally relevant for the initial stage of the adsorption sorption process (Wong et al., 2004).

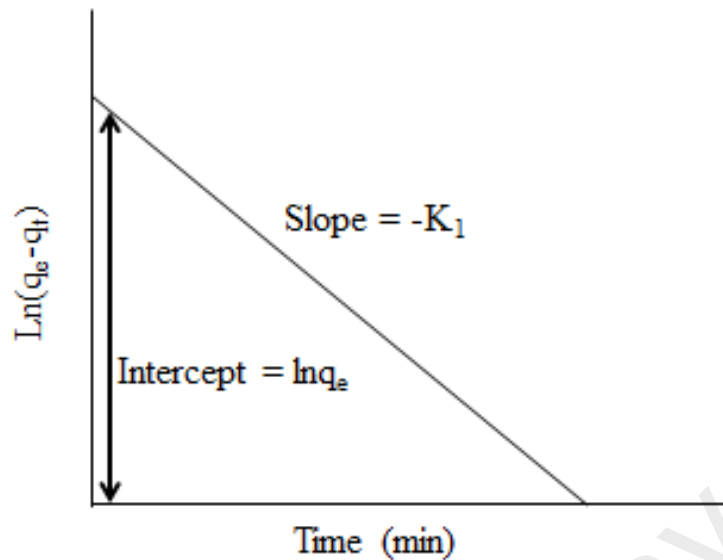


**Figure 3.3: First-order kinetic model illustration.**

**(b) Pseudo second order**

The pseudo second order equation which was developed by Ho and McKay (1999), predicts the sorption performance over the whole range of the adsorption system. This model provides the best correlation of the obtained data and assumes that the chemical adsorption mechanism can be considered as the rate controlling step (Ho & McKay, 1999). The chemical adsorption commonly involves valence forces through sharing or exchange of electrons between adsorbent and adsorbate (Taty-Costodes et al., 2003). The linearized form is presented as follows:

$$\frac{t}{q_t} = \frac{1}{k_2 q_e^2} + \frac{t}{q_e} \quad (3.7)$$

where,  $q_e$  (mg/g) and  $k_2$  (g/mg min) are the amount of adsorbate adsorbed at equilibrium and the rate constant of second order adsorption, respectively. The constants of the model can be evaluated from the linear plot of  $t/q_t$  versus  $t$  (Figure 3.4), where values of  $k_2$  and  $q_e$  were determined from the slope and the intercept of the plot, respectively.

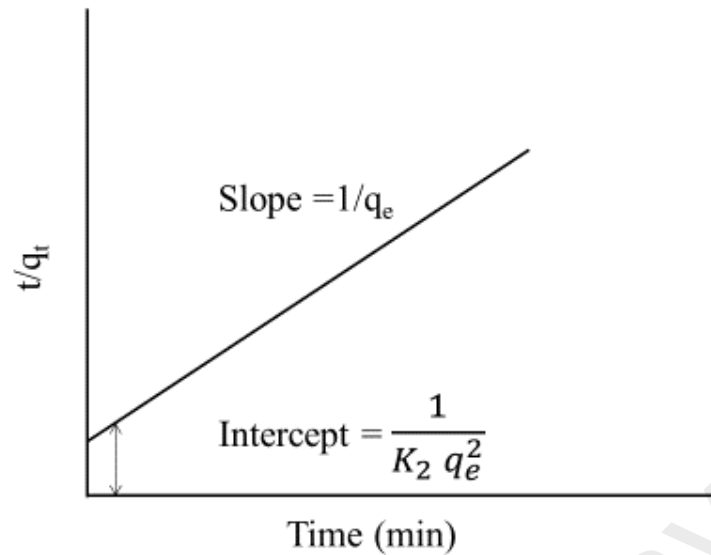


**Figure 3.4: Second-order kinetic model illustration.**

(c) *Intraparticle diffusion*

intraparticle diffusion model (ID) is defined as Weber and Morris equation (1962), which suggests that the adsorbate uptake is almost proportionally varying with the square root of time as presented in Equation (3.8) (Weber & Morris, 1963):

$$q_t = K_d t^{0.5} + C \quad (3.8)$$

where,  $q_t$  (mg/g) is the amount of pollutant adsorbed at time  $t$ ,  $K_d$  (mg/g. min<sup>0.5</sup>) is the intraparticle diffusion rate constant and  $C$  represents the initial value of  $q_t$  at  $t = 0$  and it give an estimation for the effect of the of boundary layer thickness. The values of  $K_d$  and  $C$  can be determined from the slope and intercept of the plot of  $q_t$  against  $t^{0.5}$  (Figure 3.5). Intraparticle diffusion model is commonly used for most of the sorption processes to test the role of diffusion as the rate controlling step. Thus, the intraparticle diffusion is considered as the unique rate controlling step if the linear plot of  $q_t$  versus  $t^{0.5}$  passes through the origin, otherwise, the sorption process governed by other mechanism such as film diffusion along with intraparticle diffusion (Abdel-Ghani, Rawash, & El-Chaghaby, 2016).

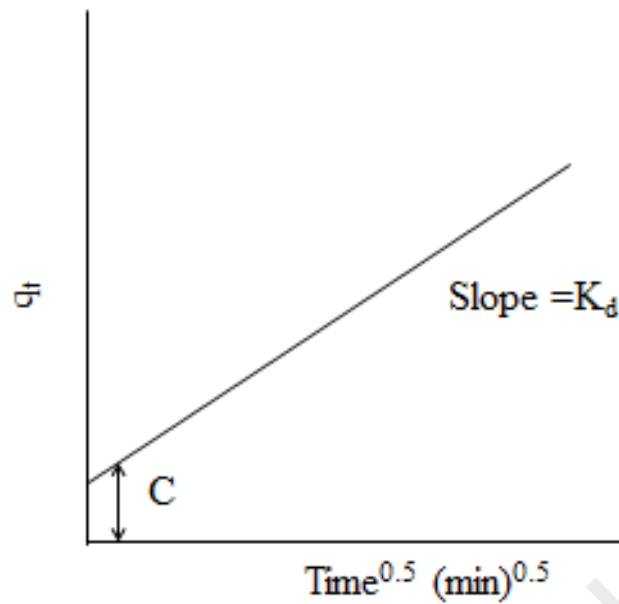


**Figure 3.5: Intraparticle diffusion kinetic model.**

#### 3.4.4.4 Adsorption isotherms

Adsorption isotherms describe the equilibrium relationships between the amount of solute adsorbed sorbent and the residual portion left in the solution at constant temperature. To designate the adsorption process, the experimental data was fitted with different isotherm models (e.g. Langmuir, Frenudlich and Temkin). The varied porous structures of the adsorbent and the unlike sorbate-sorbent interactions produce different shapes of the adsorption isotherms. Under predefined and optimized adsorption conditions, the adsorption isotherms parameters were evaluated to estimate the suitability of our adsorbent for the adsorption of BPA and MB. Thus, various initial concentration of the pollutants prepared (5, 10, 20, 30, 40, 50, 60, 70, 80, and 90 mg/L) to determine the equilibrium concentration at the equilibrium conditions. The correlation coefficient ( $R^2$ ) was evaluated to demonstrate the best isotherm mode to designate the adsorption process.

(a) **Langmuir**

Known as the ideal localized monolayer model which was established essentially for adsorption of gases onto solid adsorbent (Langmuir, 1918). The underlying assumptions of this isotherm are:

- 1- Adsorption is taking place on certain sites of the sorbate.
- 2- One molecule only or ion of the sorbate can be adsorbed by each site.
- 3- All sorption sites have the same sorption energy.

The linearized form of Langmuir model is given by Equation 3.9:

$$\frac{C_e}{q_e} = \frac{1}{q_m} C_e + \frac{1}{K_L q_m} \quad (3.9)$$

where  $C_e$  (mg/L) is the adsorbate equilibrium concentration,  $q_e$  (mg/g) is the amount of adsorbate adsorbed per unit mass of adsorbent.  $K_L$  (L/mg) and  $q_m$ , (mg/g) are Langmuir constant related to rate of adsorption and maximum adsorption capacity, respectively.

The values of  $K_L$  and  $q_m$  can be calculated by plotting  $C_e/q_e$  versus  $C_e$  (Figure 3.6).

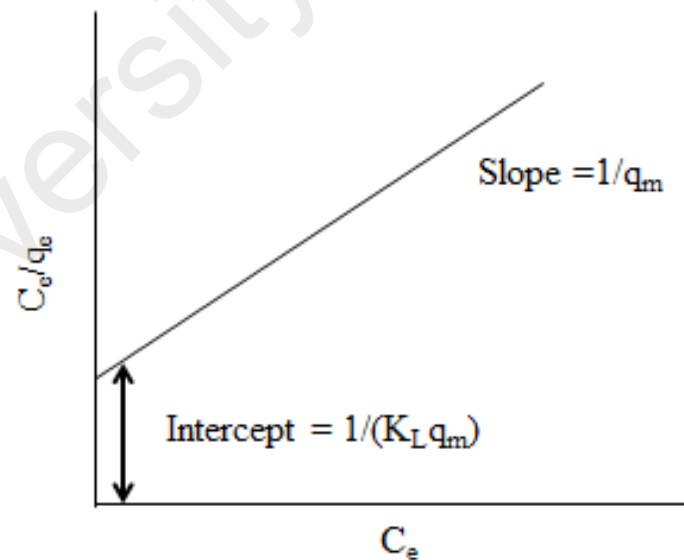


**Figure 3.6: Langmuir isotherm model.**

The separation factor which is the essential characteristic of the Langmuir isotherm is defined by Weber (1974) (Weber & Chakravorti, 1974) as:

$$R_L = \frac{1}{1 + K_L C_i} \quad (3.10)$$

where,  $K_L$  (L/mg) is the Langmuir constant and  $C_i$  is the adsorbate initial concentration (mg/L). The parameter  $R_L$  which indicates the nature of the adsorption process: unfavorable ( $R_L > 1$ ), linear ( $R_L = 1$ ), favorable ( $0 < R_L < 1$ ) or irreversible ( $R_L = 0$ ) (Crini, 2008).

(b) **Freundlich**

Freundlich isotherm describes adsorption process which occurs onto heterogeneous adsorbent surface encompasses sites of wide-ranging affinities. It is implied that after the sorbate engaged to the stronger binding sites, the binding site force decreases with the cumulative degree of the site occupation. Unlike Langmuir isotherm, this model describes reversible adsorption system and not limited to the formation of monolayer (Freundlich, 1906; Nazal et al., 2016). The linearized form of Freundlich isotherm is given by Equation (3.11):

$$\ln q_e = \ln K_f + \frac{1}{n} \ln C_e \quad (3.11)$$

Where, the amount of adsorbate adsorbed onto adsorbent for a unit equilibrium concentration is presented by the distribution coefficient,  $K_f$  (L/mg) and  $1/n$  gives an indication of the heterogeneity of the adsorbent surface and its adsorption intensity, thus, as the heterogeneity increases as the value of  $1/n$  gets closer to zero (Foo & Hameed, 2010). The plot of  $\ln q_e$  versus  $\log C_e$  displayed in Figure 3.7 gives a straight line with slope of  $1/n$  and intercept of  $\ln K_f$ .

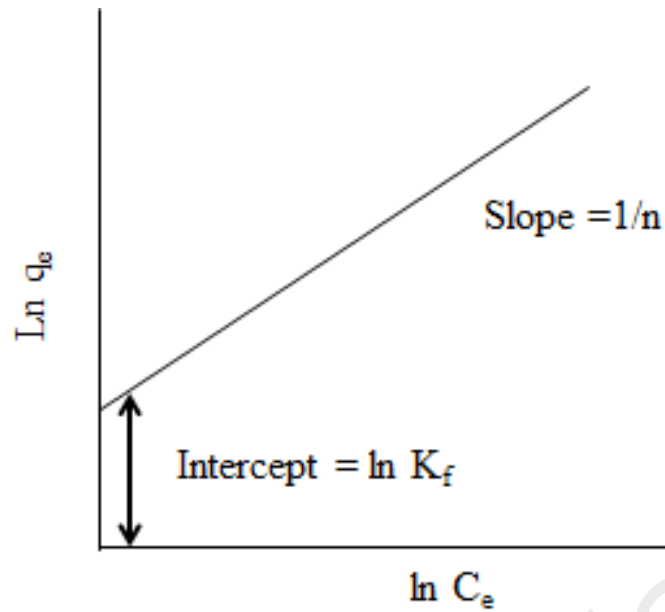


**Figure 3.7: Freundlich isotherm model.**

(c) *Temkin*

Temkin isotherm assumes that the linear decrease in the heat of adsorption of all adsorbate molecules in the layer is mainly attributed to the adsorbent-adsorbate interaction and the adsorption is described by atypical distribution of binding energies (Temkin & Pyzhev, 1940). The Temkin model has generally expressed as the linearized form in Equation (3.12):

$$q_e = B_1 \ln K_T + B_1 \ln C_e \quad (3.12)$$

A linear line of  $q_e$  versus  $C_e$  (Figure 3.8) yields the Temkin isotherm constants;  $B_1$  as the slope and  $B_1 (\ln K_T)$  as the intercept. Where,  $B_1 = RT/b$ , R is the gas constant (8.314 J/mol K), K the absolute room temperature in kelvin, b represents the heat of adsorption (J/mol) and  $K_T$  is the Temkin binding constant (L/g).

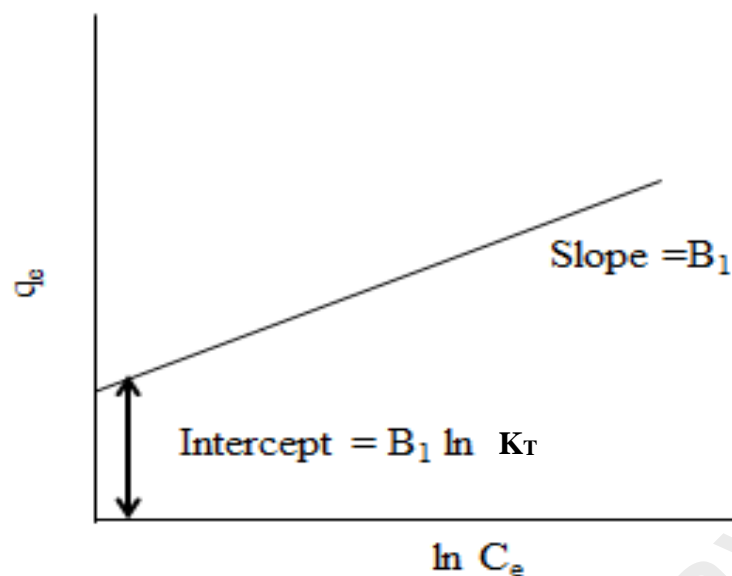


**Figure 3.8: Temkin isotherm model.**

#### 3.4.4.5 Screening and optimization of functionalized CNM-PAC

Initial adsorption screening was conducted to compare the removal efficiency of all produced adsorbents (O-CNTs, K-CNTs, and KS-CNTs). A fixed dosage of each adsorbent (10 mg) was shaken for 30 min at room temperature into 50 ml of a MB stock solution of 50 mg/L at a constant agitation speed of 180 rpm. The screening study was carried out at pH 3 and pH 11. The adsorbent with the highest removal percentage was chosen for further optimization studies of MB removal from aqueous solution.

The adsorption batch experiments were performed to investigate the performance of the adsorbent proposed by the screening study using CCD-RSM to optimize the conditions of MB removal. For adsorption optimization study, the investigated parameters were denoted as  $X_1$  for the pH (3-11),  $X_2$  for the adsorbent dosage (5-20 mg) and  $X_3$  for the contact time (10-140 min). The initial concentration and agitation speed were fixed to 50 mg/L and 180 rpm, respectively. The optimum conditions for MB adsorption was determined by two responding parameters; the removal percentage (RV %) and the adsorption capacity (Q mg/g). The proposed design experiments for MB



removal for the selected adsorbent are listed in Table 3.11. The adsorption kinetics and isotherms were conducted by employing the optimum conditions resulted from the DOE.

**Table 3.11: List of design of experiments runs for MB adsorption.**

Run	Variables		
	X <sub>1</sub> pH	X <sub>2</sub> Adsorbent dose, (mg)	X <sub>3</sub> Contact time, (min)
1	7	15	140
2	8	20	90
3	11	15	10
4	9	20	90
5	11	20	140
6	5	15	90
7	10	20	60
8	8	15	40
9	11	10	20
10	10	20	60
11	11	10	60
12	11	20	135
13	11	20	60
14	3	5	140

### 3.4.5 Characterization

Based on the optimization study, the selected samples were characterized to identify their morphology, surface area, surface charge and surface functional groups. FESEM was used to observe the morphology of the concerned adsorbents. High resolution TEM was utilized to obtain valuable information about the nanomaterials structure, presence of amorphous material, defects and quality. The surface area for the examined samples were determined based on BET using the fully Automated Gaz Sorption System. Raman shift was obtained for the optimal synthesized CNM-PAC samples and their thermal stability was analyzed using thermogravimetric analysis (TGA). FTIR was used to study the functional group of the as prepared CNM-PAC before and after adsorption process.

zeta potential was evaluated by using Zetasizer to determine the surface charge of the examined samples.

### 3.4.6 General research plan flow chart

The overall experimental activities carried out in this study are illustrated by following flow chart represented by Figure 3.9.

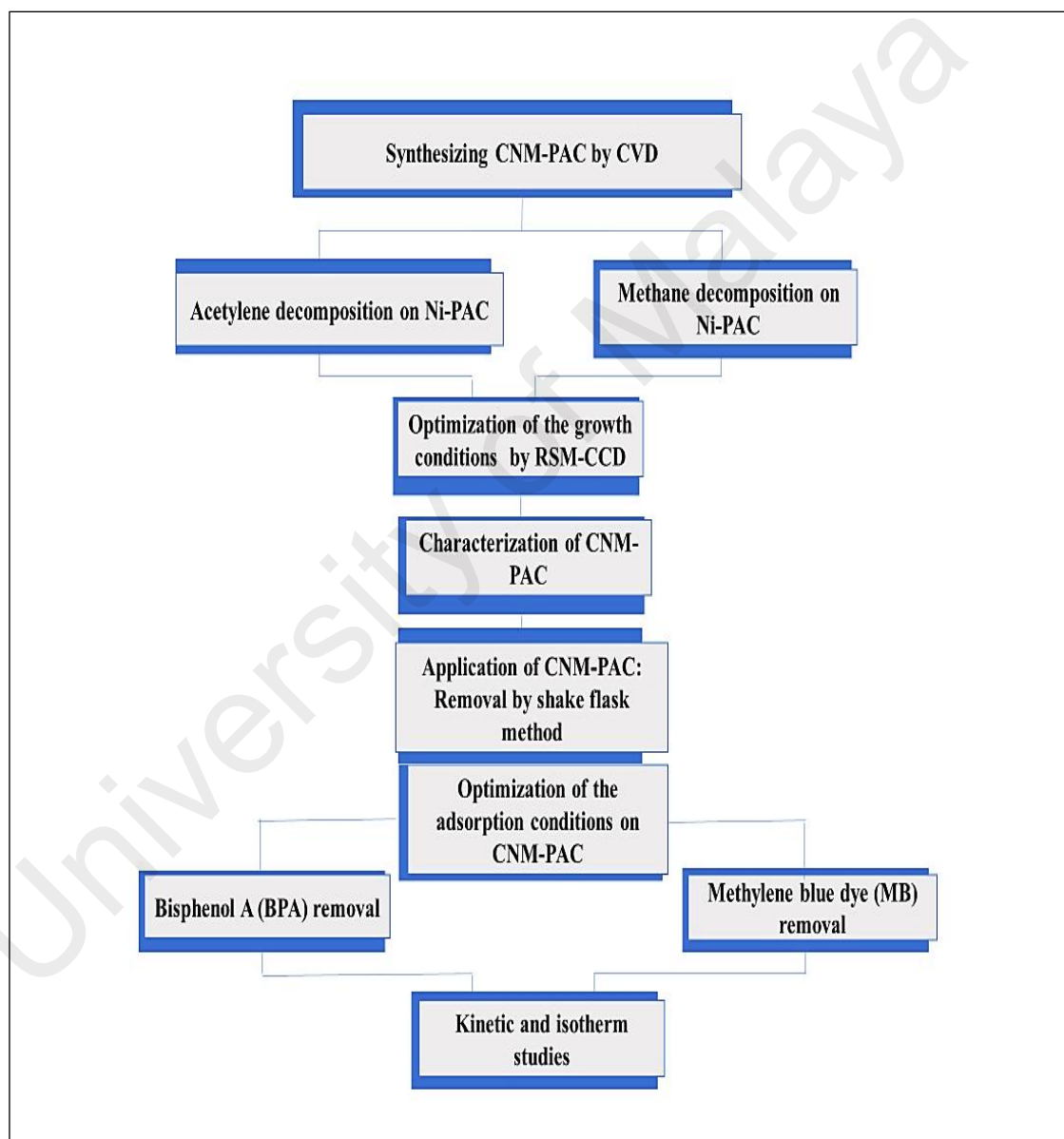


**Figure 3.9: Schematic diagram of the methodology adopted.**

## CHAPTER 4: SYNTHESIZING AND ADSORPTION STUDIES FOR CNM-PAC FROM METHANE DECOMPOSITION

### 4.1 Screening of CNM-PAC synthesis conditions

In the first phase of this study, two sets of experimental design matrix were applied for synthesizing CNM over PAC substrate by using response surface methodology (RSM). The fabrication factors were varied according to the experimental runs. However, the range of variables (growth temperature-A, growth time-B and feed stock gas ratio-C) were preselected based on literature. The adsorption capacity property of CNM-PAC is a prime concern along the yield percentage. Thus, the study considered the following responses <sup>1</sup>:

- 1-  $Y_{CH_4}$ : CNM-PAC yield %
- 2- RV1: removal percentage of BPA

DOE was used to evaluate the statistical variables gained from the model regression analysis and the surface plots constructed based on the synthesizing conditions and responses for each adsorbent-adsorbate interaction at the optimal conditions.

#### 4.1.1 Design of Experiment (DOE) for Production of CNM-PAC from methane decomposition

The conditions in Table 4.1 were suggested by the DOE software covers the growth temperature from 750 °C to 1000 °C, time 20 min to 60 min, and feed stock gas ratio ( $H_2/CH_4$ ) 1.0 to 4.0 to produce CNM on Ni-PAC using the CVD tubular reactor. The responses for evaluation the effect of growth parameter were the yield and removal

---

<sup>1</sup> Hybridizing carbon nanomaterial with powder activated carbon for an efficient removal of Bisphenol A from water: The optimum growth and adsorption conditions. Desalination and Water Treatment Journal. 2017 (95),128-143.

efficiency of BPA from water for each as-grown-sample. The nanostructure production conditions were optimized using a 2-level CCD with one central point. The collected samples after growth were weighed and the experimental yield percentage was calculated using the following formula:

$$\text{Yield \%} = \frac{m_{after}^{catal} - 143}{143} \times 100 \quad (4.1)$$

where the weight of the PAC substrate treated similarly as in growth reaction conditions but without introducing any type of carbon sources was found 143.0 mg.

#### 4.1.2 Adsorption of BPA for DOE Screening

The removal efficiency % of BPA (50 mg/L) from water as a second response was adopted onto the as-grown CNM-PAC samples to evaluate the optimum growth conditions. The batch removal experiments were conducted on the CNM-PAC samples produced from the DOE (Table 4.1).

**Table 4.1: Experimental CCD data for synthesis parameters from CH<sub>4</sub> decomposition.**

Run	Variables			Response	
	A Temperature °C	B Time min	C Gas Ratio	CNM-PAC yield Y <sub>CH<sub>4</sub></sub> (%)	BPA removal efficiency RV (%)
1	850	40	2.5	10.3	70.4
2	950	20	4.0	15.9	83.5
3	750	60	4.0	11.7	85.1
4	850	20	2.5	11.6	78.4
5	1000	20	1.0	27.7	5.6
6	750	20	4.0	12.9	78.0
7	750	60	1.0	9.7	76.2
8	950	60	4.0	21.4	42.1
9	750	40	2.5	9.1	76.3
10	950.0	20.0	1.0	22.9	87.6
11	850.0	40.0	4.0	8.4	83.9
12	950.0	60.0	1.0	37.3	14.7
13	850.0	60.0	2.5	14.1	78.5
14	750.0	20.0	1.0	10.02	60.8

Fourteen shake flasks were prepared, each flask contains 10 mg of as grown CNM-PAC sample and 50 mL of BPA at pH of 6.0. The flasks were placed in a mechanical shaker system for 120 min at room temperature with a shaking speed of 180 rpm. The experimental results of removal efficiency % presented in Table 4.1 was determined by applying equations (3.4). It is observed that the CNM-PAC sample produced from run 10 had the best performance in terms of BPA removal (~ 88%).

## 4.2 Statistical Analysis for the CNM-PAC growth

### 4.2.1 Analysis of variance (ANOVA) for the yield of CNM-PAC

The analysis of variance (ANOVA) was applied to justify the competence of the proposed models. The significance of the developed models was evaluated by the F-test value which is a statistical indication of how well the suggested model represents the variation in the data about the mean. The greater the F-value and smaller P value, the more the model explains adequately the variation of the data and the predicted significant terms of the growth variables are closer to the actual value (Angulakshmi et al., 2012). The growth yield of CNM-PAC is studied through analyzing the data shown in Table 4.1. The corresponding analysis of variance (ANOVA) for yield of CNM-PAC is listed in Table 4.2. The F-value of 210.54 and values of "Prob > F" less than 0.05 confirmed that the suggested model is statistically significant and there is only 0.05 % chance that the "model F-value" can occur due to noise for the CNM-PAC yield. The value of signal to noise ratio is presented by the "Adequate Precision" which should be greater than 4 for desirable value. The model showed adequate signal value of 46.61.

The relationship between the independent variables and the yield of CNM-PAC is given by Equation (4.2):

$$\ln(Y_{CH4}) = 2.36 + 0.370 A + 0.0857 B - 0.27 C + 0.116 AB - 0.169 AC - 0.0329 BC + 0.199A^2 + 0.184 B^2 + 0.0288 C^2 + 0.212 A^2C \quad (4.2)$$

where A, B, C represents growth temperature (°C), growth time (min) and H<sub>2</sub>/CH<sub>4</sub> ratio, respectively.

**Table 4.2: ANOVA results for the yield of CNM-PAC growth.**

*Source	Sum of Squares	df	Mean Square	F Value	p-value Prob > F
Model	2.71	10	0.27	210.54	0.0005
A	1.18	1	1.18	914.87	< 0.0001
B	0.074	1	0.074	57.22	0.0048
C	0.068	1	0.068	52.94	0.0054
AB	0.11	1	0.11	84.02	0.0027
AC	0.23	1	0.23	178.35	0.0009
BC	8.713x10 <sup>-3</sup>	1	8.713x10 <sup>-3</sup>	6.76	0.0804
A <sup>2</sup>	0.090	1	0.009	69.48	< 0.0036
B <sup>2</sup>	0.043	1	0.043	33.05	0.0105
C <sup>2</sup>	1.144 x10 <sup>-3</sup>	1	1.144 x10 <sup>-3</sup>	0.89	0.4158
A <sup>2</sup> C	0.048	1	0.048	37.40	0.0088
R- Squared 0.998				Std.Dev. 0.0359	
Adj. R-Squared 0.994				C.V. % 1.35	
Pred. R-Squared 0.938				Adeq. Precesion 46.61	

\*A: Temperature; (°C), B: Time; (min) and C: H<sub>2</sub>/CH<sub>4</sub>

The predicted values of the CNM-PAC yield calculated from ANOVA model equation along with actual values are listed in Table 4.3. The correlation coefficient R<sup>2</sup> value for the yield of CNM-PAC growth is greater than 0.98 suggests that the obtained model provides a good estimation of the response. Moreover, it can be seen from Figure 4.1 that the experimental data for the examined CNM-PAC sample are close to the predicted values suggested by the proposed model.

**Table 4.3: List of the actual and predicted values of the CNM-PAC yield.**

Run No.	Actual		Predicted	
	Yield %	(ln Yield)	Yield %	ln (yield)
1	10.28	2.33	10.59	2.36
2	15.96	2.77	15.64	2.75
3	11.70	2.46	11.59	2.45
4	11.59	2.45	11.70	2.46
5	27.66	3.32	27.94	3.33
6	12.94	2.56	13.20	2.58
7	9.68	2.27	9.87	2.29
8	21.33	3.06	21.76	3.08
9	9.12	2.21	8.94	2.19
10	22.87	3.13	22.87	3.13
11	8.41	2.13	8.33	2.12
12	37.34	3.62	36.60	3.60
13	14.15	2.65	13.87	2.63
14	9.97	2.30	9.87	2.29

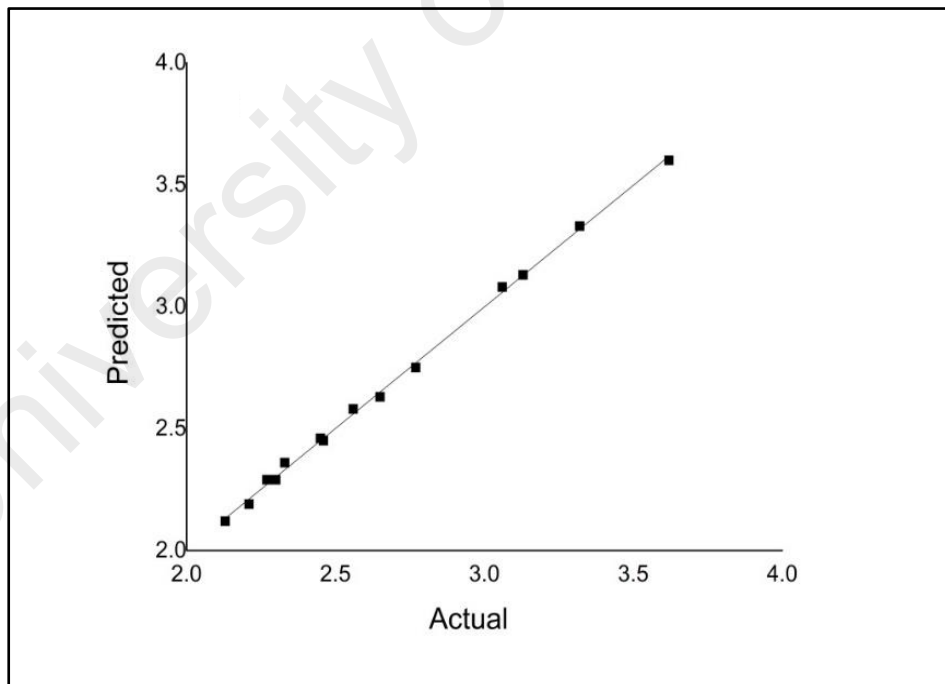


**Figure 4.1: Predicted values vs. actual values CNM-PAC growth response.**

#### 4.2.2 Analysis of variance (ANOVA) for the removal of BPA onto CNM-PAC

The second response was the removal (%) of BPA from water. Each sample of CNM-PAC was used as an adsorbent and the results of removal % were entered the software, as given in Table 4.1. By referring to the corresponding (ANOVA) for removal of BPA, presented in Table 4.4, the Model F-value of 13.87 implies the model is significant. There is only a 0.26 % chance that a "Model F-Value" this large could occur due to noise. The desirable value of signal to noise ratio "Adeq Precesion" for this response showed a value of 11.923.

This model can be used to navigate the design space and it is represented by the following equation:

$$\begin{aligned} \mathbf{BPA\ RV\ \%} = & 76.21 + 24.55 A - 9.17 B + 6.34 C - 17.10 AB - 0.35 AC - \\ & 10.09 A^2 - 33.70 A^3 \end{aligned} \quad (4.3)$$

where RV % is the removal efficiency of BPA from water, A, B and C are temperature of growth (°C), time (min) and gas ratio (H<sub>2</sub>/CH<sub>4</sub>), respectively. Table 4.5 lists the predicted values of removal efficiency % calculated from ANOVA model equation along with the actual values. Furthermore, the predicted values were plotted against the experimental data (Figure 4.2). It can be seen a good relationship between the experimental and predicted values since the data points has good distribution near to the straight line. The coefficient of determination (R<sup>2</sup>) of BPA removal % was 0.9418. The high R<sup>2</sup> values and the low coefficient of variation (CV= 5.47 %) suggest that the obtained model provides a good estimation of the response which can be reproducible as long CV values are not greater than 10% (Angulakshmi et al., 2012).



**Table 4.4: ANOVA results for BPA removal % for CNM-PAC growth optimization**

<b>*Source</b>	<b>Sum of Squares</b>	<b>df</b>	<b>Mean Square</b>	<b>F Value</b>	<b>p-value Prob &gt; F</b>
Model	8494.09	7	1213.44	13.87	0.0025
A	510.83	1	510.83	5.84	0.0521
B	840.89	1	840.89	9.61	0.0211
C	352.03	1	352.03	4.02	0.0917
AB	2339.28	1	2339.28	26.74	0.0021
AC	0.98	1	0.98	0.011	0.9192
A <sup>2</sup>	275.25	1	275.25	3.15	0.1265
A <sup>3</sup>	1324.83	1	1324.83	14.14	0.0081
	R- Squared 0.9418			Std.Dev.3.35	
	Adj. R-Squared 0.8379			C.V. % 5.47	
	Pred. R-Squared 0.7977			Adeq. Precesion 11.932	
*A: Temperature; (°C), B: Time; (min) and C: H <sub>2</sub> /CH <sub>4</sub>					

**Table 4.5: List of the actual and predicted values of the BPA removal efficiency.**

<b>Run No.</b>	<b>RV%</b>	
	<b>Actual</b>	<b>Predicted</b>
1	70.4	76.2
2	83.5	89.2
3	85.1	89.9
4	78.4	85.4
5	5.60	5.60
6	78.0	74.0
7	76.2	76.5
8	42.1	36.7
9	76.3	75.3
10	87.6	77.3
11	83.9	82.6
12	14.7	24.7
13	78.5	67.0
14	60.8	60.7

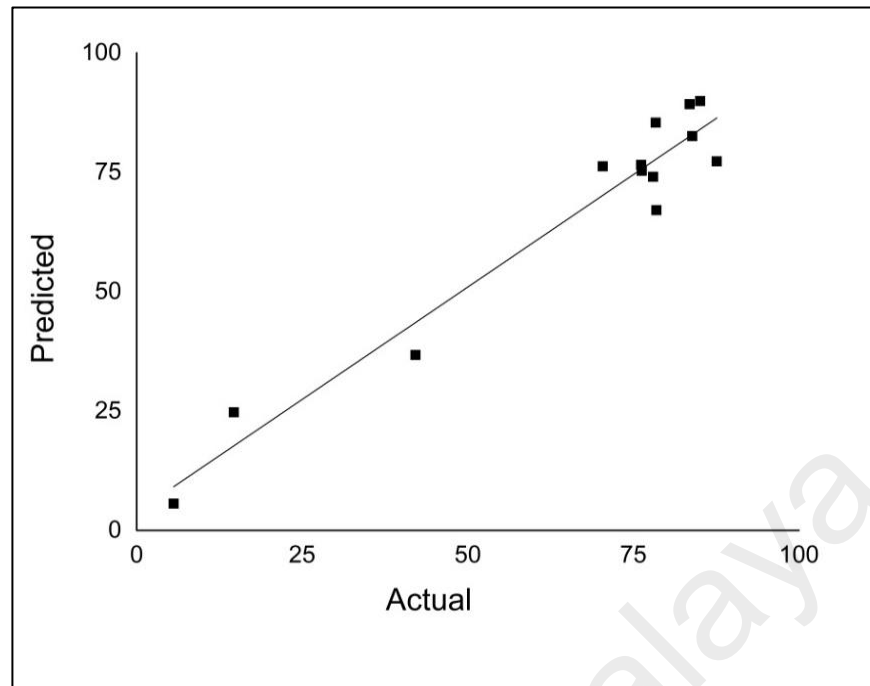


**Figure 4.2: Predicted values vs. actual values BPA removal response.**

#### **4.2.3 The interactive effects of selected parameters on the CNM-PAC growth and BPA adsorption**

The yield % of CNM-PAC and the removal efficiency % of BPA over the independent variables were presented by three-dimension view of response surface plot as a function of two independent variables (Figure 4.3). Generally, if the F function is greater than 4, the product is significantly influenced by the parameter variations (Zare, Sadegh, et al., 2015). ANOVA Tables 4.2 and 4.4 showed that the studied parameters affect the CNM-PAC yield and BPA removal significantly. Among these parameters, the reactor temperature, and growth duration are the most important. It is obvious that the high F-value for the linear terms of A (temperature) and B (time) (914.87, 57.22, respectively) indicates their large effect on the CNM-PAC yield. Furthermore, it is noticed from their corresponding F values that the removal of BPA increases with the increase in temperature and time of synthesis (5.84 and 9.61). The interaction effect of growth temperature and growth time (AB) has the greatest impact on the CNM-PAC yield and

on BPA removal efficiency as was justified by the “Prob. > F” values which were less than 0.0027 and 0.0021, respectively (Roosta et al., 2014).

RSM results, as displayed in Figure 4.3 (a), suggested that the yield increased proportionally with the increase in growth time, and then dropped as the reaction proceeds. However longer reaction times was found to cause the deposition of amorphous carbon (Hussein et al., 2012). Figure 4.3 (b) shows the yield versus temperature and gas ratio. Increasing the gas ratio ( $H_2/CH_4$ ) did not provide a respected enhancement in the yield of CNM-PAC as compared with the reaction temperature. The concentration of carbon atoms in CVD reactor is an important factor for the rate of growth. Therefore, a high content of hydrogen in the carbon precursor contributes, together with the  $H_2$  produced during the reaction, to move the reaction backward again towards the methane formation reducing the number of active carbon atoms on the catalyst surface and consequently the amount of grown CNM-PAC (Dikonimos Makris et al., 2005). Figure 4.3 (c) demonstrates that the reaction duration has notable effect than that observed by the feed stock gas ratio (Ashik, Wan Daud, & Hayashi, 2017)

Furthermore, Figure 4.3 (d) indicates that the removal of BPA increased with increasing the growth temperature and time. Nevertheless, high growth temperature has more positive effect on promoting the BPA removal efficiency comparing with the impact of growth duration parameter. Figure 4.3 (e) shows the removal of BPA versus temperature and gas ratio. The interaction between those two parameters (AC) have more significant effect as compared with the time- gas ratio (BC) interaction presented in Figure 4.3 (f). From the study of interaction of different parameters of CNM-PAC synthesis, it was noticed that the behavior of surface response of removal as function of reaction conditions is different from that of yield. This indicated that the quality of higher yield product is not necessary to be sufficient for removal process.

Table 4.6 shows the main constraints and their importance levels for optimization five goals namely; growth temperature, growth time, gas ratio, CNM-PAC yield and removal efficiency of BPA to select the optimum conditions for CNM-PAC production. Based on the equations (4.2) and (4.3) and the constraints presented in Table 4.6, the software suggested ten solutions listed in Table 4.7. The more likely suggested solution by DOE software to predict the maximum yield of CNMs-PAC and BPA removal efficiency be feasible is was found reliable at reaction conditions: temperature 933°C, synthesis duration 20 min, and H<sub>2</sub> to CH<sub>4</sub> flow ratio 1.0. The predicted optimization condition was validated by the final run and the percentage values of carbon yield and the removal efficiency of BPA were 22.14 and 89.33%, respectively, implying good agreement between the predicted and the experimental values.

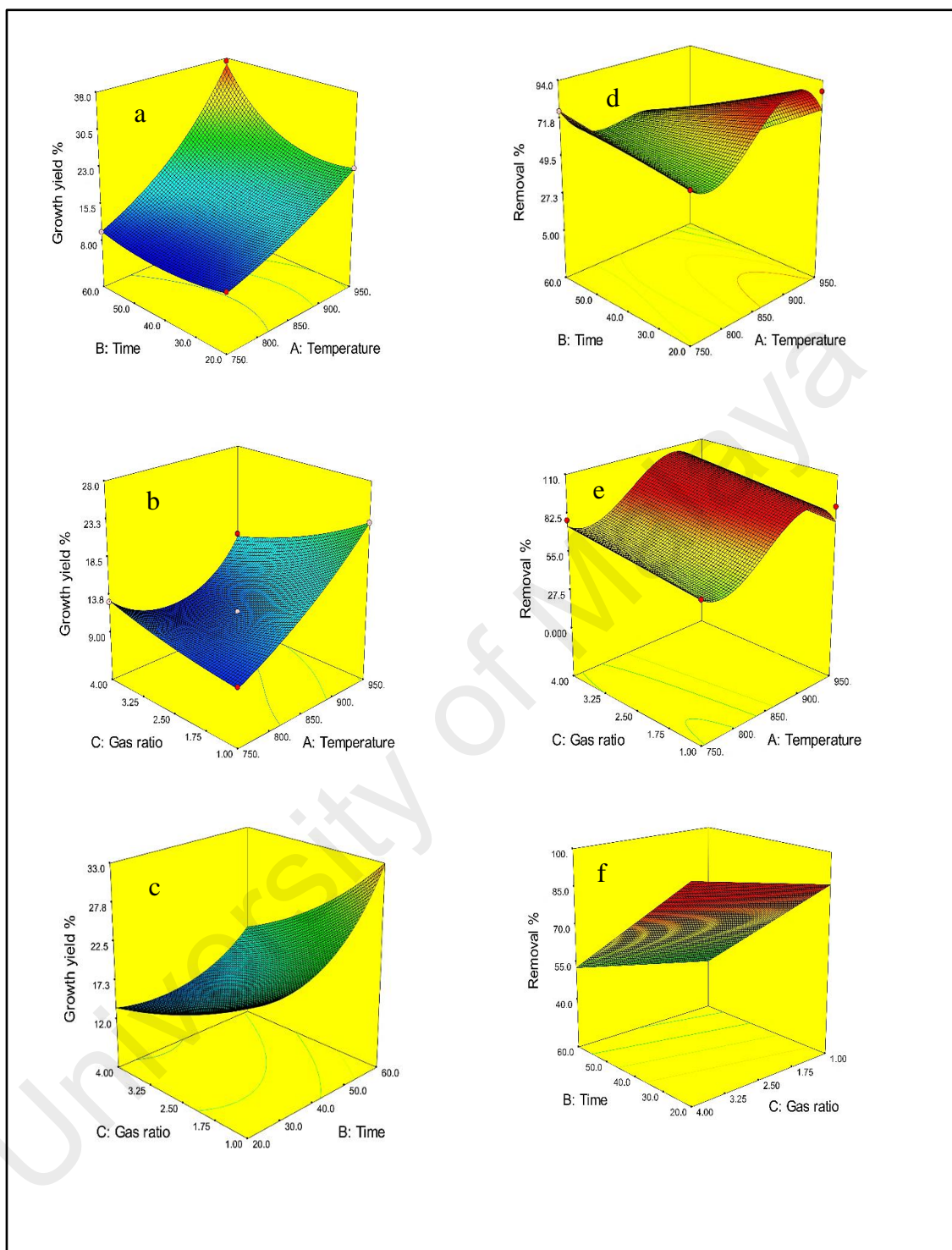


**Figure 4.3: Three-dimensional response surface representation for: CNM-PAC growth yield (Y), and BPA removal efficiency (RV %); (a, b) interaction with growth temperature and time, (c, d) interaction with growth temperature and gas ratio and (e, f) interaction with time and gas ratio.**

**Table 4.6: Constraints for optimization of production conditions for CNM-PAC for BPA removal.**

Name	Goal	Lower limit	Upper limit	Importance out of 5
Temperature (A)	In range	750	1000	3
Time (B)	In range	20	60	3
Gas ratio (C)	In range	1	4	3
Yield % (Y)	Maximize	8.4	37.3	3
Removal % (RV)	Maximize	5.6	87.6	5

**Table 4.7: Solutions for the optimum conditions suggested by DOE software for CNM-PAC growth.**

No.	A	B	C	Y %	RV%	Desirability
1	933.0	20.0	1.0	21.5	87.6	0.876 Selected
2	933.0	20.2	1.0	21.4	87.6	0.875
3	934.0	20.0	1.07	21.3	87.6	0.873
4	930.0	21.0	1.0	21.1	87.6	0.871
5	927.0	20.0	1.0	21.0	89.9	0.870
6	936.0	20.0	1.0	21.7	86.2	0.868
7	925.0	22.9	1.0	20.3	87.6	0.862
8	939.20	20.0	1.78	19.2	87.6	0.845
9	750.0	60.0	3.96	11.5	89.6	0.643
10	842.0	20.0	3.87	9.59	87.6	0.501

A: Temperature, B: time, C: gas ratio

#### 4.2.4 Summary of the optimization conditions for CNM-PAC synthesis from methane decomposition

Based on this study, the influences of the operating variables are optimized for synthesizing CNM on powdered activated carbon substrate. In this context, different range of growth variables were predetermined to get maximum yield of CNM-PAC and BPA removal efficiency. The experimental design results for synthesizing CNM-PAC revealed that all the three variables showed significant effects on the yield of CNM-PAC. However, the growth temperature is the most important factor influencing the removal efficiency. Thus, the variables investigated must be taken into consideration due to their

significant impact on the production of CNM-PAC hybrid. The decomposition of methane is an endothermic reaction. Hence, the chemical conversion improves when increasing the temperature. Similarly, decreasing the inlet gas flow rate or the CH<sub>4</sub> mole fraction increases the contact time, and hence results in higher conversion.

The process optimization produced CNM-PAC hybrid with maximum adsorption efficiency and yield within the experimental ranges studied. Consequently, this would minimize the industrial production costs of this type of hybrid materials. The produced CNM-PAC hybrid at the optimal synthesizing conditions (temperature 933°C, synthesis duration 20 min, and H<sub>2</sub> to CH<sub>4</sub> flow ratio 1.0) was used to optimize the conditions of BPA adsorption such as, the solution pH, adsorbent dose and contact time in the next section.

### 4.3 Adsorption of bisphenol A (BPA)

#### 4.3.1 Design of experiment (DOE) for BPA adsorption

The adsorption of BPA (50 mg/L) from aqueous solution by the optimum CNM-PAC hybrid was studied using DOE to determine the optimum adsorption conditions. The study considered the operating factors including pH; X<sub>1</sub> (2-11), CNM-PAC dose; X<sub>2</sub> (5-20 mg) and contact time; X<sub>3</sub> (10-120 min) (Table 4.8).

**Table 4.8: Summary of CCD for parameters of BPA adsorption on CNM-PAC.**

Factor	Name	Units	Low actual	High actual	Low coded	High coded
X <sub>1</sub>	pH	-	2	11	-1	+1
X <sub>2</sub>	Dose	mg	5	20	-1	+1
X <sub>3</sub>	Contact time	min	10	120	-1	+1

The parameters presented in Table 4.8 were selected based on literature review (Bautista-Toledo et al., 2005; Cai et al., 2003; Dong et al., 2010; Kwon & Lee, 2015). Two-level central composite design (CCD) was used to evaluate the adsorption

performance of BPA by CNM-PAC for two responses, the removal efficiency % of BPA (RV1) and adsorption capacity (Q1). The summary of CCD of experiments produced by DOE software are summarized in Table 4.9. The removal efficiency and adsorption capacity were found to be in the ranges of 62.4 - 97.8 % and 87.4 -323.7 mg/g, respectively.

**Table 4.9: CCD of experimental parameters for BPA removal by CNM-PAC.**

Run No.	pH	Dose (mg)	Contact time (min)	Response 1 (RV1) Removal %	Response 2 (Q1) Adsorption capacity (mg/g)
1	2	20.0	10	89.67	112.08
2	3	5.0	120	64.74	323.68
3	7	10.0	65	62.43	156.07
4	11	20.0	120	74.42	93.02
5	7	12.5	20	67.83	135.66
6	7	10.0	40	67.04	167.61
7	2	20.0	120	97.80	122.25
8	3	5.0	10	47.91	239.54
9	11	5.0	120	44.81	224.06
10	6	12.5	40	74.14	148.29
11	7	12.5	40	72.05	144.10
12	5	15.0	65	86.31	143.86
13	7	15.0	20	84.70	141.18
14	11	20.0	10	69.93	87.41
15	10	15.0	20	73.10	121.83

#### 4.3.2 Analysis of variance (ANOVA)

The analysis of variance was used to investigate the adequacy of models that suggested for two responses, the removal efficiency and adsorption capacity. The responses were studied through analyzing the data given in Table 4.9. The adopted ANOVA model for the removal efficiency % and adsorption capacity (Q1) by CNM-PAC is presented in Tables 4.10 and 4.11. The model F-values of 34.4 and 104.0 confirmed that the models are statistically significant. There is only a 0.01% chance that a "Model F-Value" can



occur due to noise for both the removal efficiency and adsorption capacity. Values of "Prob > F" less than 0.05 indicate the model terms are significant. For the removal % efficiency, the cases  $X_1$  (pH),  $X_2$  (dosage),  $X_3$  (contact time),  $X_2X_3$ , and  $X_2^2$  offered significant model terms. However, the adsorption capacity showed significant terms for  $X_1$ ,  $X_2$ ,  $X_3$ ,  $X_1 X_2$ ,  $X_2 X_3$  and  $X_3^2$ . Values greater than 0.1 indicate that the model terms are not significant. The coefficient of variation for these two models (CV) is the error expressed as a percentage of the mean. In the present study, the (CV) value for RV1 % and Q1 was 5.54 % and, 5.86 % respectively. The desirable value of signal to noise ratio presented by "Adeq Precision" should be greater than 4. The models showed a ratio of 20.4 and 36.3 which indicates an adequate signal. These models can be used to navigate the design space and are expressed by Equations (4.4) and (4.5):

$$RV1 \% = 67.9 - 9.65 X_1 + 18.3 X_2 + 2.28 X_3 - 0.642 X_2 X_3 - 5.04 X_2^2 \quad (4.4)$$

$$Q1 = 170.0 - 35.8 X_1 - 39.8 X_2 + 2.98 X_3 + 12.2 X_1 X_2 - 4.54 X_2 X_3 + 2.78 X_3^2 \quad (4.5)$$

Where  $X_1$ ,  $X_2$  and  $X_3$  represents pH, dosage (mg) and contact time (min).

**Table 4.10: ANOVA results for BPA Removal % (RV1) by CNM-PAC.**

*Source	Sum of Squares	df	Mean Square	F Value	p-value Prob > F
Model	2720.0	5	545.0	34.4	< 0.0001
$X_1$	707.0	1	707.0	44.6	< 0.0001
$X_2$	1550.0	1	1550.0	97.7	< 0.0001
$X_3$	208.0	1	208.0	12.52	0.0076
$X_2 X_3$	44.2	1	44.2	2.79	0.0176
$X_2^2$	320.0	1	320.0	20.2	0.00151
	R- Squared 0.950			Std.Dev. 3.98	
	Adj. R-Squared 0.923			C.V. % 5.54	
	Pred. R-Squared 0.865			Adeq. Precesion 20.4	

\* $X_1$ : pH,  $X_2$ : adsorbent dosage and  $X_3$ : contact time; (min)

**Table 4.11: ANOVA results for BPA adsorption capacity (Q1) on CNM-PAC.**

*Source	Sum of Squares	df	Mean Square	F Value	p-value Prob > F
Model	53000.0	6	8840.0	104.0	< 0.0001
X <sub>1</sub>	6420.0	1	6420.0	75.5	< 0.0001
X <sub>2</sub>	16500.0	1	16500.0	194.0	< 0.0001
X <sub>3</sub>	86.9	1	86.9	1.02	0.342
X <sub>1</sub> X <sub>2</sub>	19500.0	1	19500.0	23.0	0.00137
X <sub>2</sub> X <sub>3</sub>	1990.0	1	1990.0	23.5	0.00128
X <sub>3</sub> <sup>2</sup>	873.0	1	873.0	10.3	0.0125
R- Squared 0.987			Std.Dev.6.5		
Adj. R-Squared 0.978			C.V. % 5.86		
Pred. R-Squared 0.941			Adeq. Precesion 36.3		
*X <sub>1</sub> : pH, X <sub>2</sub> : adsorbent dosage and X <sub>3</sub> : contact time; (min)					

The predicted values of the removal efficiency % and adsorption capacity determined from ANOVA model equations along with the variables values against the experimental values are listed in Table 4.12.

**Table 4.12: List of the actual and predicted values for BPA removal (RV1) and adsorption capacity responses (Q1).**

Run No.	RV1 %		Q1 (mg/g)	
	Actual	Predicted	Actual	Predicted
1	89.67	92.4	112.08	118.0
2	64.74	63.5	323.68	321.0
3	62.43	68.3	156.07	169.0
4	74.42	76.2	93.02	96.6
5	67.83	71.4	135.66	145.0
6	67.04	65.5	167.61	161.0
7	97.80	95.5	122.25	119.0
8	47.91	47.4	239.54	241.0
9	44.81	44.2	224.06	225.0
10	74.14	75.8	148.29	150.0
11	72.05	73.4	144.10	143.0
12	86.31	85.6	143.86	139.0
13	84.70	77.1	141.18	129.0
14	69.93	70.7	87.41	91.9
15	73.10	69.8	121.83.	111.0

Figure 4.4 shows the predicted values plotted versus the experimental values for BPA removal % and adsorption capacity on CNM-PAC hybrid. It can be observed that the experimental data are close to the predicted values suggested by the developed models. The correlation coefficient  $R^2$  value for the removal efficiency and adsorption capacity was 0.950 and 0.987 which confirms the good agreement between predicted and actual values and the models proved to be successfully reliable to represent the relation between the adsorption variables and the targeted responses.

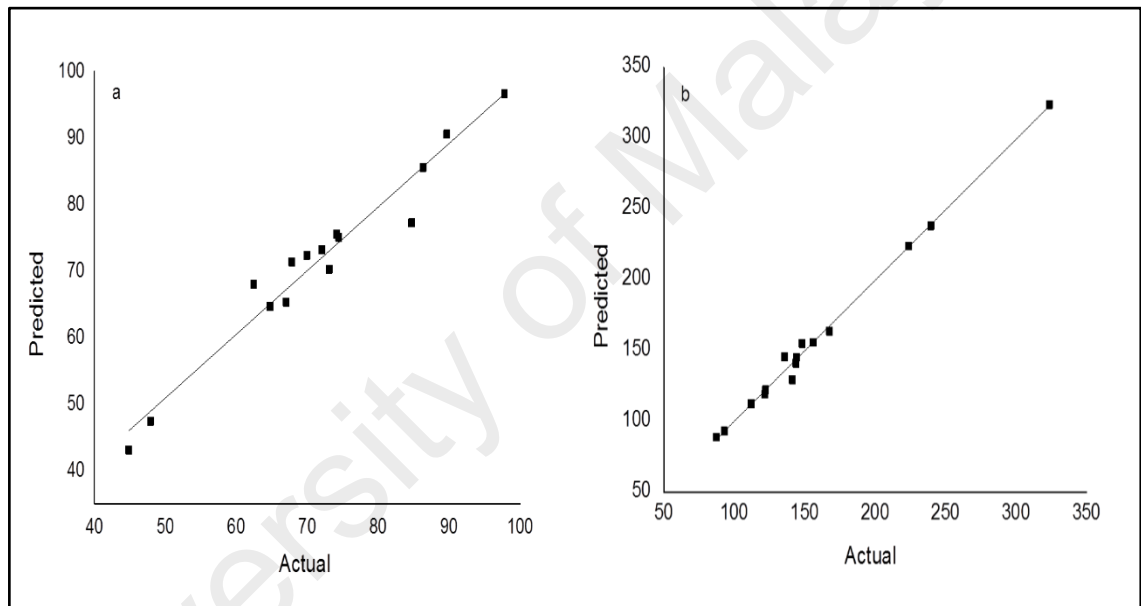


**Figure 4.4: Predicted values vs. actual values for (a) BPA removal efficiency (RV1 %) and (b) adsorption capacity (Q1) on CNM-PAC.**

The statistical analysis of CCD gave several potential solutions for optimum conditions of BPA adsorption by CNM-PAC. Table (4.13) shows set of constrains and different importance levels which were defined for optimization of five potential targets namely, pH, CNM-PAC dosage, contact time, removal efficiency and adsorption capacity to select the optimum conditions for BPA adsorption on the as-grown CNM-PAC hybrid. The software suggested fourteen solutions based on the process constraints (Table 4.14)

for the optimum adsorption process conditions values. In this context, the first choice with the highest desirability was selected; pH of 3.0, adsorbent dosage of 15.6 mg and contact time of 120 min. These conditions were further used for isotherm and kinetics study.

**Table 4.13: Constraints for optimization process based on CCD for BPA adsorption.**

Name	Goal	Low limit	Upper limit	Importance
X <sub>1</sub> (pH)	In range	2	11	3
X <sub>2</sub> (dosage)	In range	5	20	3
X <sub>3</sub> (time)	In range	10	120	3
RV1	Maximize	62.4294	97.8	5
Q1	Maximize	87.41	323.680	3

**4.14: Potential optimization conditions based on CCD for BPA removal.**

No.	pH	Dose (mg)	Contact time (min)	RV1 %	Q1 (mg/g)	Desirability
1	3.00	15.6	120.	95.5	179.	0.964 Selected
2	3.00	15.5	120.	95.5	179.	0.963
3	3.00	15.5	120.	95.4	179.	0.963
4	3.00	15.7	120.	95.6	178.	0.963
5	3.00	15.6	120.	95.5	178.	0.963
6	3.03	15.5	120.	95.4	179.	0.962
7	3.00	15.8	120.	95.7	176.	0.962
8	3.01	15.8	120.	95.7	176.	0.961
9	3.11	15.5	120.	95.2	179.	0.959
10	3.39	15.4	120.	94.4	179.	0.946
11	3.46	15.4	120.	94.2	179.	0.943
12	3.00	14.5	96.3	92.3	172.	0.901
13	3.00	13.0	79.2	88.0	179.	0.844
14	3.00	14.2	45.9	87.5	156.	0.795

### 4.3.3 The interactive effects of selected parameters on BPA adsorption

The removal efficiency % of BPA (50 mg/L) and adsorption capacity of CNM-PAC hybrid adsorbent over different sets of independent parameters were described by three-dimension view of response surface plot as a function of two variables (Figure 4.5 and Figure 4.6).

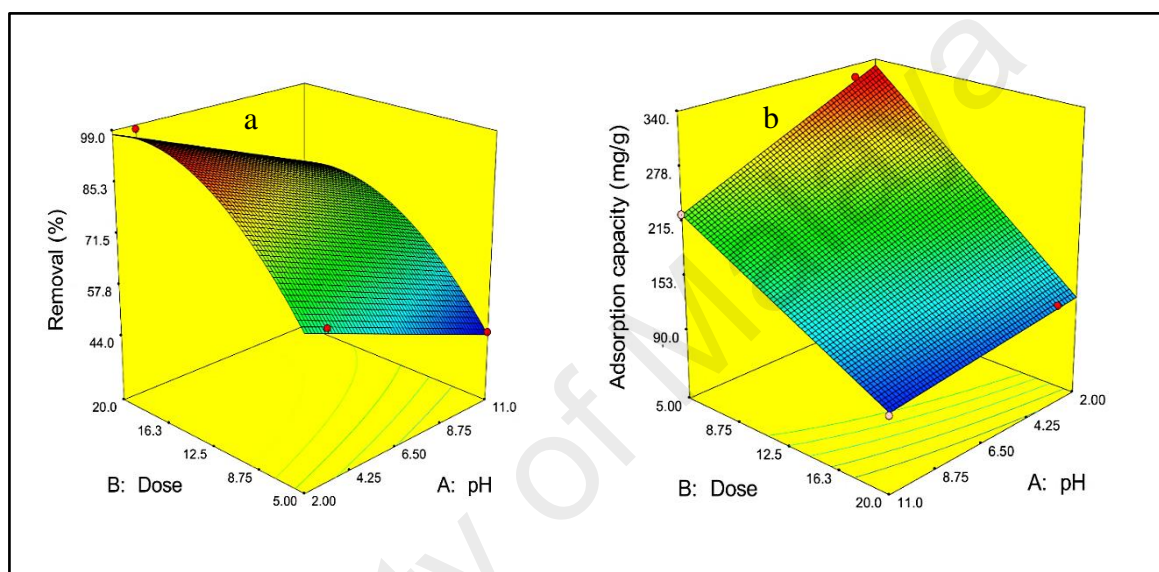


**Figure 4.5: RSM plots of (a) BPA removal efficiency (RV1 %), and (b) adsorbent capacity (Q1) considering the effect of pH and dosage.**

The impact of pH was noticeable on the removal efficiency and adsorption capacity as it affects the properties of both adsorbate and adsorbent. The adsorption of BPA was apparently weakened with increasing pH. This can be due to the deprotonation of some adsorbent surface functional groups resulting in more negatively charged surface (Li, Gong, et al., 2015). As well as, the reduction of BPA removal was observed in the alkaline pH range due to the ionization of BPA molecules to mono- or divalent anions leading to an increase in the repulsive electrostatic interactions between the bisphenolate anion and the negatively charged surface of adsorbents (Chang et al., 2012; Dehghani et al., 2015). Furthermore, it was obvious that the adsorption of BPA was enhanced with decreasing

pH and the removal efficiency and the adsorption capacity reached to a maximum at 3.0 and the worst removal of BPA was obtained at pH up to 11 (Figure 4.5). This can be assigned to the presence of BPA in molecular form and to the highly protonation of adsorbent surface at acidic pH value, leading high attraction between the adsorbent and adsorbate (Qiu et al., 2016). Meanwhile, Figure 4.6 (a) shows the increasing in BPA removal efficiency along with adsorbent dose was less conspicuous than that displayed by the pH. The increase in the removal efficiency can be referred to the increase in creation of more adsorptive sites as a result of the increase in surface area, on the other hand, the adsorption capacity decreased as the adsorbent dosage increased. Thus, the effect of pH is more obvious than the adsorbent dose as can be seen in Figure 4.6 (b). These observations agree with other reported studies (Joseph, Zaib, et al., 2011; Tsai, Lai, & Su, 2006).

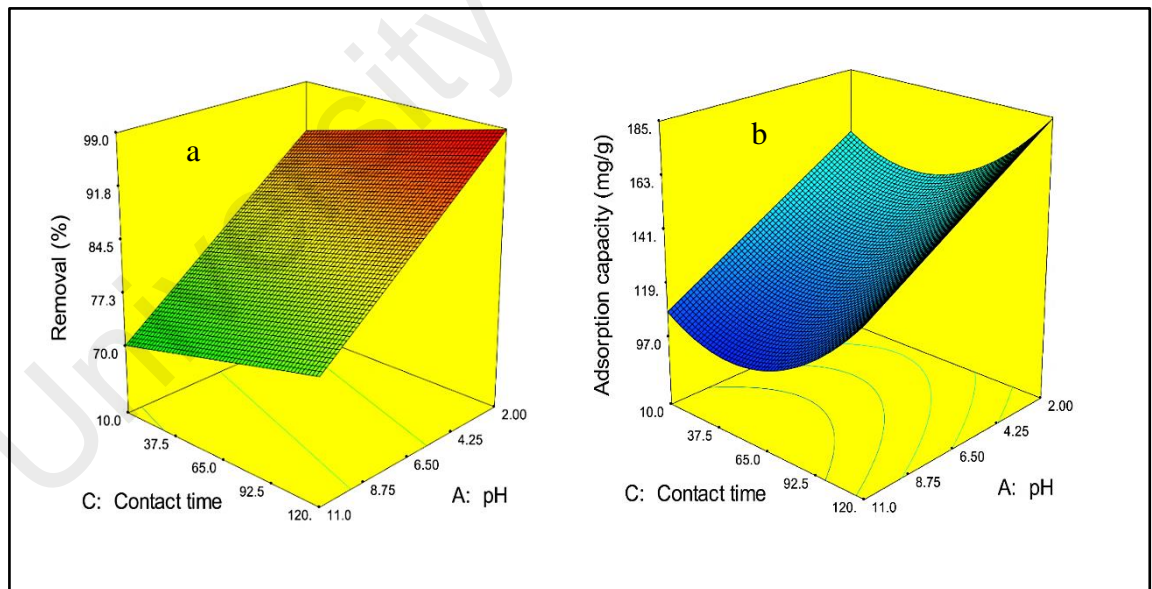


**Figure 4.6: RSM plots of (a) BPA removal efficiency (RV1 %), and (b) adsorbent capacity (Q1) considering the effect of pH and contact time.**

Also, the suggested ANOVA models were used to interpret and support the RSM findings for the interaction of the adsorption parameters. A significant effect for the linear variable terms of the removal efficiency response was observed, along with  $X_2^2$ , as shown in Table 4.10. The high F- values of the pH (44.68) and the adsorbent dosage (97.7) confirmed their significant effect compared to the of contact time (12.52). The combined effect of the pH-adsorbent amount ( $X_2X_3$ ) on removal efficiency was respectable since the P value of 0.0176. This can be attributed to the fact that adsorbent dosage provides a direct reflection to the surface area, while the pH corresponds to surface charge. Meanwhile, the most significant interaction terms for adsorbent capacity (Table 4.11) were observed for pH-adsorbent dosage ( $X_1X_2$ ) and adsorbent dosage-contact time ( $X_1X_3$ ) owing to their low “P values”; 0.00137 and 0.00128, respectively.

#### 4.3.4 Adsorption Kinetics

The adsorption kinetic was investigated to study the adsorption equilibrium time and analyze the uptake behavior of BPA on CNM-PAC hybrid. The kinetic studies were conducted at the optimal conditions for BPA adsorption (initial BPA concentration 50 mg/L, adsorbent dosage 15.6 mg, and pH of 3.0). Three kinetic models, which are: pseudo-first order, pseudo-second order and intraparticle diffusion model (Figure 4.7, Figure 4.8 and Figure 4.9) were applied to the experimental data. As can be observed from Table 4.15 the correlation coefficient ( $R^2$ ) value of Pseudo-second order model was (0.999) which is much higher than the other models (0.825 and 0.821). Thus, the pseudo-second order model is ideally representing the adsorption of BPA on CNM-PAC due to the good agreement between this model and experimental data. This behavior agrees with several previously-reported studies which used carbonaceous adsorbents for BPA removal (Joseph, Heo, et al., 2011; Kwon & Lee, 2015; Sui et al., 2011). The well fitted pseudo-second-order model for BPA adsorption on CNM-PAC suggests the following:

(i) the involvement of the adsorbent and adsorbate in the adsorption process and (ii) the adsorption process rate could be controlled by chemisorption involving valence forces through sharing or exchange of electrons (Chowdhury & Balasubramanian, 2014).

**Table 4.15: Linearized equations of studied kinetic models for BPA adsorption on CNM-PAC.**

Model	Equation	Parameters	Values
Pseudo-First-Order	$\ln(q_e - q_t) = \ln q_e - K_1 t$	$R^2$	0.825
		$K_1$	0.0161
		$q_e$	27.107
Pseudo-Second-Order	$\frac{t}{q_t} = \frac{1}{K_2 q_e^2} + \frac{1}{q_e} t$	$R^2$	0.999
		$K_2$	0.001608
		$q_e$	144.928
Intraparticle diffusion	$q_t = K_d t^{\frac{1}{2}} + C$	$R^2$	0.821
		$K_d$	2.4
		$q_e$	151.98
		$C$	113.24

$q_e$  (experimental) = 144.39 mg/g

It is worth to mention that the intraparticle diffusion model provides further description to the adsorption mechanism (Figure 4.9). The model suggests three adsorption regions: (i) the boundary layer diffusion where the instant adsorption takes place from the bulk solution to the external surface of the adsorbent, (ii) the gradual adsorption through intraparticle diffusion where the adsorbate diffuses on the sorptive sites, and (iii) the equilibrium region accompanied by slow diffusion rate due to the diminishes of BPA concentration in the solution (Kuo, 2009; Ocampo-Pérez et al., 2012). It is obvious from Figure 4.9 that the linear plot is not passing through the origin which indicates that there are other mechanisms involved in the rate limiting process along with the intraparticle diffusion. Meanwhile, the boundary layer thickness has significant impact as can be observed from the high value of the of the intercept ( $C = 113.24$ ) which proposes that the



boundary layer diffusion dominated the BPA removal to some point (Balarak, 2016; Qin et al., 2015).

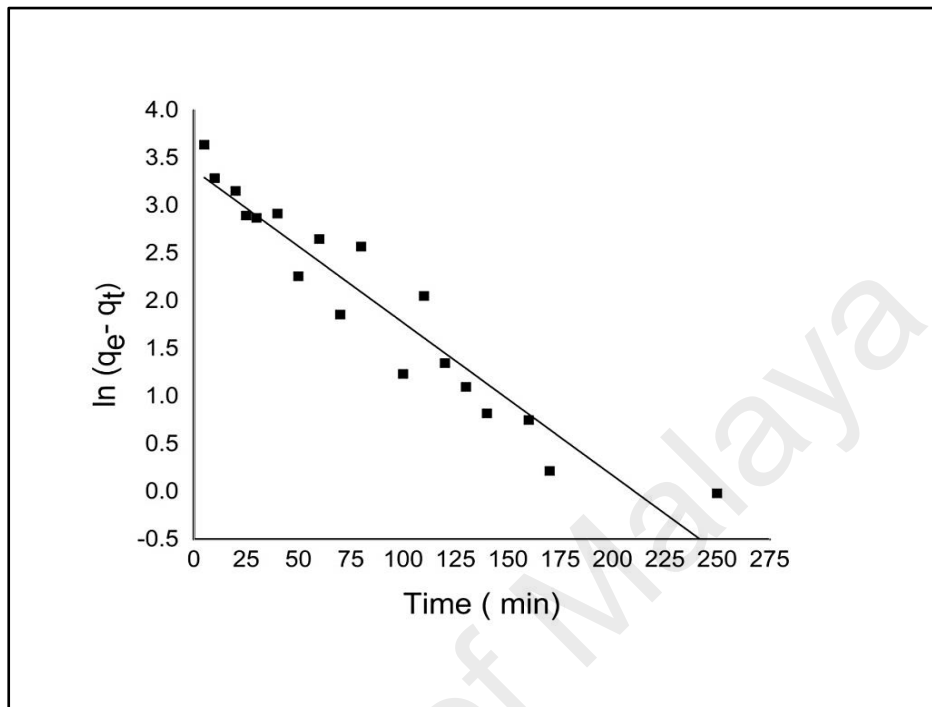


**Figure 4.7: Pseudo-first order kinetic model for BPA adsorption.**

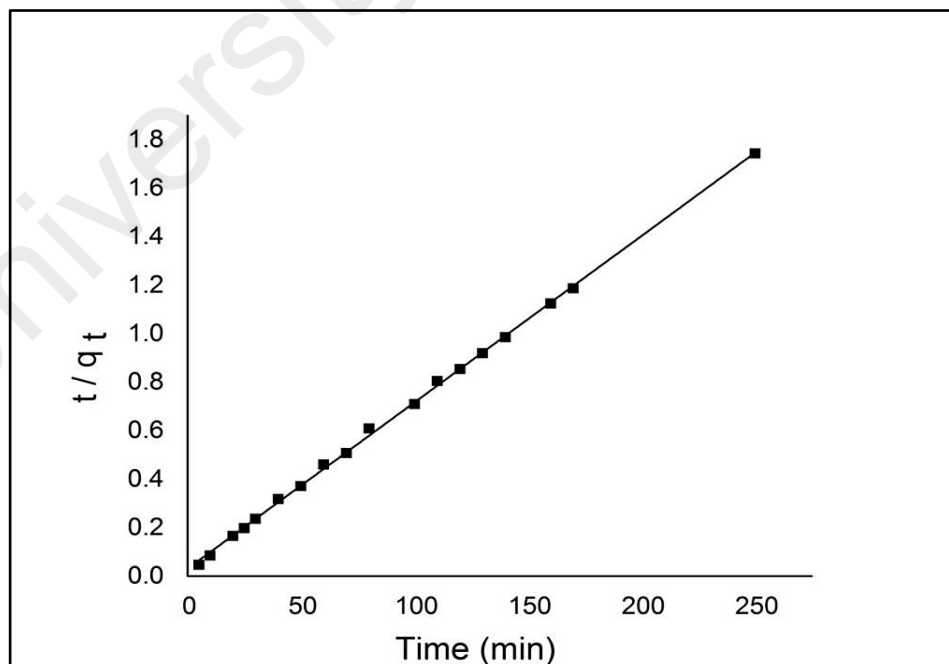


**Figure 4.8: Pseudo-second order kinetic model for BPA adsorption.**

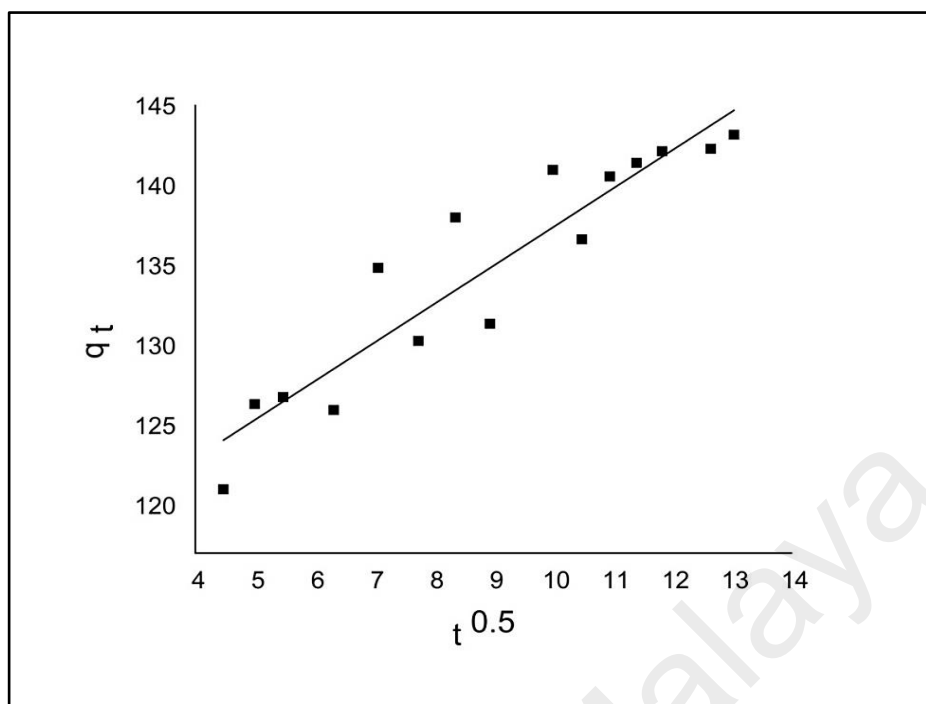


**Figure 4.9: Intraparticle diffusion kinetic model for BPA adsorption.**

#### 4.3.5 Adsorption isotherms

The interaction between the adsorbent and adsorbate up to the equilibrium point was demonstrated by applying three isotherm models namely, Langmuir, Freundlich and Temkin. The best fitted isotherm model to the experimental data was extracted from the highest correlation coefficient  $R^2$ . Figure 4.10, Figure 4.11 and Figure 4.12 show the plot of each model as well as their correlation factors and constants are presented in Table 4.16. The validation of the adsorption favorability of BPA on CNM-PAC under working conditions was confirmed by the values of the separation factor of Langmuir model ( $R_L$ ) and the heterogeneity factor of Freundlich isotherm ( $n$ ) (Zhou et al., 2011). However, the Langmuir model produced the best fit with a high correlation coefficient  $R^2$  (0.994), indicating a monolayer adsorption of BPA onto the CNM-PAC surface. On the other hand, according to the Freundlich  $n$  value ( $n > 1$ ), the adsorptive behavior is dominated by a physical adsorption process, implying that the adsorbent attains heterogeneous surface associated with active sites of different adsorption affinities to the BPA molecules

(Shen et al., 2015). Similar isotherm results were reported for the adsorption of BPA onto activated carbon (AC) derived from rice straw agricultural waste (Chang et al., 2012). Table 4.17 provides a comparison of the maximum adsorption capacity of BPA onto several adsorbents. The CNM-PAC adsorbent synthesized in the present study showed a high maximum adsorption capacity of 181.81 mg/g comparing with other types of adsorbents, indicating a good adsorption performance for BPA removal from water.

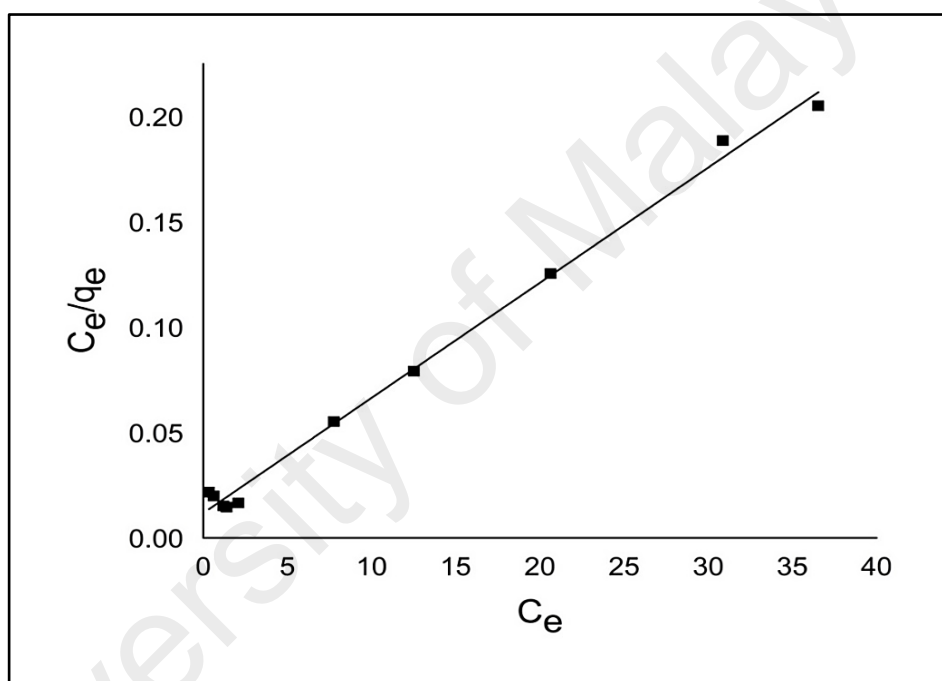


**Figure 4.10: Langmuir isotherm model for BPA adsorption.**

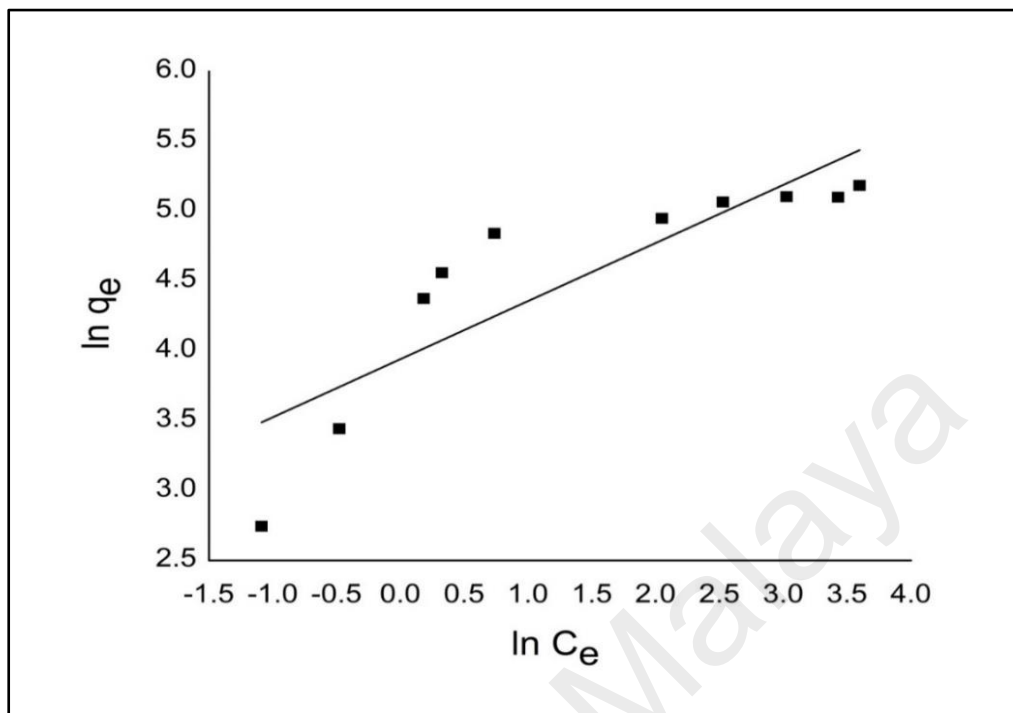


**Figure 4.11: Freundlich isotherm model for BPA adsorption.**

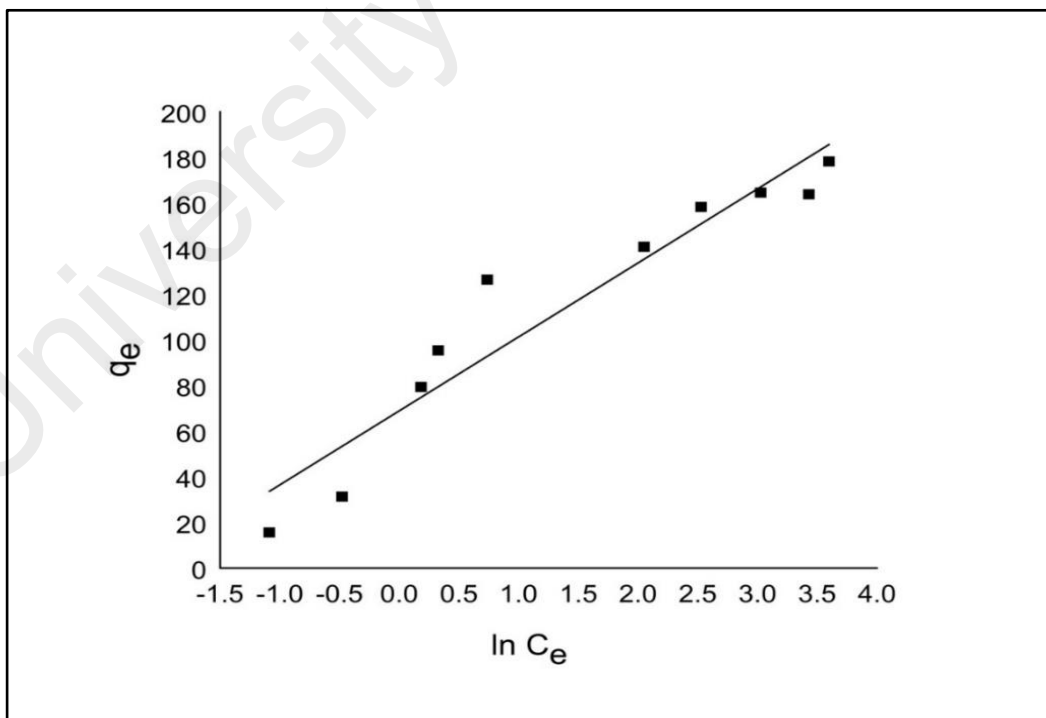


**Figure 4.12: Temkin isotherm model for BPA adsorption.**

**Table 4.16: Linearized equations of studied isotherm models for BPA adsorption on CNM-PAC.**

Model	Equation	Parameters	Values
Langmuir	$\frac{C_e}{q_e} = \frac{1}{K_L q_m} + \left(\frac{1}{q_m}\right) C_e$	$R^2$	0.9941
		$q_m$	181.81
		$K_L$	0.514
		$R_L$	0.0375
Freundlich	$\ln q_e = \ln K_f + \frac{1}{n} \ln C_e$	$R^2$	0.7316
		$K_f$	56.48
		$n$	2.63
Temkin	$q_e = B_1 \ln K_T + B_1 \ln C_e$	$R^2$	0.921
		$K_T$	8.667
		$B_1$	31.954

**Table 4.17: Previously reported maximum adsorption capacities of various adsorbents for Bisphenol A removal.**

Adsorbent	$q_m$ (mg/g)	Reference
CNM-PAC	181.81	Present work
CNTs/Fe <sub>3</sub> O <sub>4</sub>	43.76	(Li, Gong, et al., 2015)
SWCNTs	22.6- 44.8	(Joseph, Zaib, et al., 2011)
Powdered Activated Carbon (PAC)	129.6	(Bautista-Toledo et al., 2005)
reduced graphene	96.2	(Kwon & Lee, 2015)
oxide graphene	58.2	(Jin et al., 2015)
molecularly imprinted polymers (MMIPs)	142.9	(Guo et al., 2011)
Chitosan	34.48	(Dehghani et al., 2016)
Fibric peat	31.40	(Zhou et al., 2011)
Hydrophobic Y type zeolite	111.11	(Tsai, Hsu, et al., 2006)
Organo-montmorillonite	151.522	(Park et al., 2014)

#### 4.3.6 Mechanisms

The adsorption of BPA onto the synthesized CNM-PAC adsorbent was greatly affected by the characteristics of the adsorbent, removal conditions, as well as the molecular properties of BPA. Thus, CNM-PAC has oxygen-functional groups, which enhance its dispersibility in water. Moreover,  $-OH$  is an electron-donating functional group that can increase the sorption affinity of BPA by increasing the  $\pi$ -donating strength of the host aromatic ring (Yu et al., 2017). The molecular size of BPA, its  $pK_a$  ( $pK_a = 9.5$  for BPA) and its rotating structure influenced its affinity towards the surface of CNM-PAC (Apul & Karanfil, 2015). Thus, the wedging of BPA into the groove regions of the adsorbent is allowed by the rotating structure of BPA molecule. The  $\pi$ - $\pi$  interactions between the benzene rings of BPA and the graphene planes includes the polar and charge interactions that may be responsible for the adsorption of BPA onto CNM-PAC. Moreover, the pH of the background solution is another major factor controlling the adsorption process. BPA is a weak acid and the non-dissociated species form dominates in acidic solutions. It is worth to mention that the highest removal efficiency of BPA was obtained at the optimum pH (pH 3.0) value which is less than the  $pK_a$  value of BPA. This observation confirms that the adsorption mechanism was dominated by the  $\pi$ - $\pi$  interaction effects (Apul & Karanfil, 2015). This observation was confirmed by the value of point of zero of charge (PZC) of the synthesized CNM-PAC, which was found at pH 9.2. This implies that our adsorbent acquires positive surface charge as long as the working pH of solution  $< pH_{PZC}$ . Furthermore, Lin et al., (2008) reported that decreases in adsorption affinities for phenolic compounds over their  $pK_a$  values could be attributed to the increased electrostatic repulsion between dissociated adsorbates and negatively charged MWCNTs (Lin & Xing, 2008). In addition, at pH3 the methyl groups on BPA

are protonated and increase the electron density of resonating  $\pi$  electrons in the benzene ring, enhancing the attraction between positive CNM-PAC surfaces.

#### **4.3.7 Summary of the adsorption of BPA onto CNM-PAC**

The synthesized CNM-PAC at the optimum growth conditions was used to perform optimization study on removal of BPA from water using CCD experimental design. The optimum conditions were pH 3.0, adsorbent dose 15.6 mg and contact time 120 min. Three kinetic models, which are: Pseudo-first order, Pseudo-second order and intraparticle diffusion. The adsorption of BPA on CNM-PAC was ideally obeying the Pseudo-second-order model with  $R^2 = 0.999$ ,  $q_e = 144.93$  (mg/g) and  $K_2 = 0.0016$  (g/mg.min). Also, the Langmuir, Freundlich and Temkin adsorption isotherm models were tested. The BPA adsorption system was best fitted with Langmuir model with  $R^2 = 0.994$ ,  $q_m = 181.81$  mg/g,  $K_L = 0.514$  and  $R_L = 0.0375$ . The highest removal efficiency of BPA was achieved at the optimum pH (3.0) which is less than the  $pK_a$  value of BPA, leading to conclude that the adsorption mechanism of BPA was governed by the strong  $\pi$ - $\pi$  interaction between the electron in the aromatic rings of BPA and the graphene layer of the synthesized CNM-PAC and it might involve polar electrostatic components, charge transfer and dispersive force.

#### **4.4 Adsorption of methylene blue (MB)**

##### **4.4.1 Design of experiment (DOE) for MB adsorption**

The adsorption performance of the synthesized CNM-PAC hybrid was comprehensively examined for the removal of methylene blue (MB) from water. The adsorption experiments were conducted according to the CCD matrix selected by the DOE software to analyze the behavior of the removal efficiency (RV2) and adsorption capacity (Q2) under three distinct factors pH (2-11), dose (5-20), and contact time (10-

120) (Table 4.18). The summary of CCD of experiments produced by DOE software are summarized in Table 4.19. The removal efficiency and adsorption capacity were found to be in the ranges of 33.3 - 97.8 % and 107.5 -323.3 mg /g, respectively.

**Table 4.18: Summary of CCD for MB adsorption variables on CNM-PAC.**

Factor	Name	Units	Low	High	Low	High
			actual	actual	coded	coded
X <sub>1</sub>	pH	-	2	11	-1	+1
X <sub>2</sub>	Dose	mg	5	20	-1	+1
X <sub>3</sub>	Contact time	min	10	120	-1	+1

**Table 4.19: CCD of experimental variables for MB removal by CNM-PAC.**

Run No.	pH	Dose (mg)	Contact time (min)	Response 1 (RV2) Removal %	Response 2 (Q2) Adsorption capacity (mg/g)
1	6	10	70	69.2	173.1
2	7	10	120	88.6	221.6
3	7	10	40	78.4	196.1
4	2	5	20	33.3	166.4
5	11	15	20	86.4	144.0
6	6	15	70	93.2	155.3
7	3	20	40	43.1	107.5
8	11	15	120	97.8	162.9
9	3	15	120	88.8	147.9
10	7	10	70	67.9	169.8
11	11	5	120	54.0	270.2
12	3	5	120	36.6	182.9
13	7	15	70	82.6	137.7
14	3	10	70	68.9	172.4
15	11	5	20	64.7	323.3

#### 4.4.2 Analysis of variance (ANOVA)

The optimization of MB removal parameters was conducted using RSM and the regression of the obtained data were performed by the analysis of variance (ANOVA).



Thus, an empirical formula relating the removal efficiency of MB (RV2 %) and the adsorption capacity (Q2) to the three input variables were described by the following regression Equations:

$$\begin{aligned} \mathbf{RV2 \%} = & 77.5 + 10.4 X_1 + 18.8 X_2 + 4.847 X_3 - 4.15 X_1 X_3 + 6.26 X_2 X_3 \\ & - 11.9 X_2^2 \end{aligned} \quad (4.6)$$

$$\begin{aligned} \mathbf{Q2 \%} = & 192.0 + 33.4 X_1 - 44.9 X_2 + 4.02 X_3 - 26.9 X_1 X_2 - 9.85 X_1 X_3 \\ & + 10.1 X_2 X_3 \end{aligned} \quad (4.7)$$

Where  $X_1$ ,  $X_2$  and  $X_3$  represents pH, adsorbent dosage and contact time, respectively.

The results for RV2 % and Q2 regression models were presented in Table 4.20 and Table 4.21, respectively. The F-values were 21.5 and 22.5 which implied that both responses were significant. There is only 0.02 % and 0.01 % chance that the “Model F- value” of the removal efficiency of MB and adsorption capacity of CNM-PAC could occur due to noise. The adequacy of the models was also confirmed by the P-value of both responses (0.000159 and 0.000134) which provides further confirmation that the models were highly significant. The correlation coefficient ( $R^2$ ) demonstrates the model strength and the competence of its response prediction (Dutta et al., 2011). The  $R^2$  value for the removal efficiency and adsorption capacity was higher than 91% which indicates a good predictability of the suggested model. Also, the reasonable agreement of the predicted  $R^2$  with the adjusted  $R^2$  supports the close relationship between the obtained experimental values and the values predicted by the proposed model (Table 4.22 and Figure 4.13). These observations demonstrate the sufficiency of the model to describe the performance of the studied responses according to the defined variables. The low coefficient of variation (CV= 8.4 and 9.01 %) suggest that the obtained model provides a good estimation of the response which can be reproducible and can be applied for further analysis as long the CV values are not greater than 10%.

**Table 4.20: ANOVA results for MB Removal % (RV2) by CNM-PAC.**

<b>*Source</b>	<b>Sum of Squares</b>	<b>df</b>	<b>Mean Square</b>	<b>F Value</b>	<b>p-value Prob &gt; F</b>
Model	5630.0	6	939.0	21.5	0.000159
X <sub>1</sub>	930.0	1	930.0	21.3	0.00173
X <sub>2</sub>	3280.0	1	3280.0	75.0	< 0.0001
X <sub>3</sub>	187.0	1	187.0	4.28	0.0723
X <sub>1</sub> X <sub>3</sub>	118.0	1	118.0	2.69	0.14
X <sub>2</sub> X <sub>3</sub>	284.0	1	284.0	6.5	0.0342
X <sub>2</sub> <sup>2</sup>	1150.0	1	1150.0	26.4	0.00089
	R- Squared 0.942			Std.Dev.6.61	
	Adj. R-Squared 0.90			C.V. % 8.4	
	Pred. R-Squared 0.87			Adeq. Precesion 15.1	
*X <sub>1</sub> : pH, X <sub>2</sub> : adsorbent dosage and X <sub>3</sub> : contact time; (min)					

**4.21: ANOVA results for MB adsorption capacity (Q2) by CNM-PAC.**

<b>*Source</b>	<b>Sum of Squares</b>	<b>df</b>	<b>Mean Square</b>	<b>F Value</b>	<b>p-value Prob &gt; F</b>
Model	39000.0	6	6500.0	22.5	0.000134
X <sub>1</sub>	9850.0	1	9850.0	34.1	0.000388
X <sub>2</sub>	23000.0	1	23000.0	79.6	< 0.0001
X <sub>3</sub>	139.0	1	139.0	0.48	0.508
X <sub>1</sub> X <sub>2</sub>	7260.0	1	7260.0	25.1	0.00103
X <sub>1</sub> X <sub>3</sub>	704.0	1	704.0	2.44	0.157
X <sub>2</sub> X <sub>3</sub>	823.0	1	823.0	2.85	0.130
	R- Squared 0.944			Std.Dev.12.0	
	Adj. R-Squared 0.902			C.V. 9.01	
	Pred. R-Squared 0.813			Adeq. Precesion 18.2	
*X <sub>1</sub> : pH, X <sub>2</sub> : adsorbent dosage and X <sub>3</sub> : contact time; (min)					

**Table 4.22: List of the actual and predicted values for MB removal (RV2) and adsorption capacity responses (Q2).**

Run No.	RV2 %		Q2 (mg/g)	
	Actual	Predicted	Actual	Predicted
1	69.2	74.9	173.1	183.0
2	88.6	82.4	221.6	196.0
3	78.4	74.6	196.1	189.0
4	33.3	33.7	166.4	173.0
5	86.4	87.9	144.0	149.0
6	93.2	81.8	155.3	145.0
7	43.1	44.2	107.5	102.0
8	97.8	98.13	162.9	158.0
9	88.8	89.3	147.9	164.0
10	67.9	77.5	169.8	192.0
11	54.0	51.7	270.2	281.0
12	36.6	39.2	182.9	180.0
13	82.6	84.4	137.7	147.0
14	68.9	67.1	172.4	158.0
15	64.7	62.9	323.3	313.0

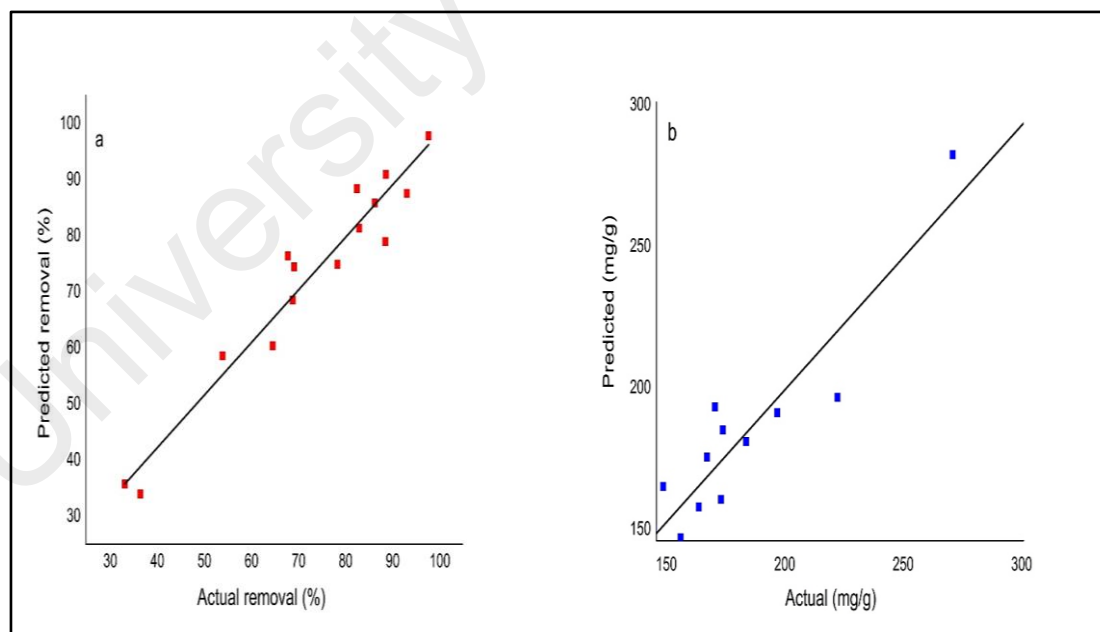


**Figure 4.13: Predicted values versus actual values for (a) removal response and (b) adsorption capacity response.**

#### 4.4.3 The interactive effects of selected parameters on MB adsorption

RSM was used to explore all the significant interactions in the CCD and evaluate the relation between input parameters and the obtained response surfaces. Figure 4.14 represents the response surface plots of RV2 % and Q2 versus the selected independent variables. The role of pH and adsorbent dose are the most influencing variables in the adsorption process. It is notable that the pH has a significant effect on the removal efficiency and adsorbent capacity (Figure 4.14 (a) and 4.14 (b)). The removal efficiency improved by increasing pH value until it reached the maximum at pH 11. The solution pH can affect the adsorbent surface charge, the degree of pollutants ionization, the dissociation of the adsorbent functional groups besides the structure of the dye molecule (Ge et al., 2017). Hence, the observed high MB removal at pH 11 can be explained by the deprotonation of some surface functional groups resulting in more negatively charged adsorbents surface ( $\text{pH} > \text{pH}_{\text{pzc}}$ ) as well as, high pH leads to more dissociation of MB molecules ( $\text{pK}_a = 3.8$  for MB), subsequently increasing the electrostatic attraction between the negatively charged active adsorption sites of CNM-PAC adsorbent and the cationic dye molecule (Kuppusamy et al., 2016). Furthermore, in acidic solutions, the competitive effects of excess  $\text{H}^+$  ions and the electrostatic repulsion between the cationic dye would result in a decrease in the removal efficiency of dye (Liu et al., 2015).

At constant pH values (Figure 4.14 c and 4.15 c), the increase in removal efficiency % and adsorbent capacity occur by increasing the amount of adsorbent. The significant effect of adsorbent dose on both responses is confirmed by the high F-values (98.22 and 64.36) presented in in Tables 4.20 and 4.21, respectively. The adsorption enhancement could be due to the availability of more adsorption sites. Whereas, at low adsorbent dosage, the removal percentage decreased significantly as longer time is required for adsorption to reach the equilibrium due to the reduction of reactive sites with respect to

the dye molecules (Krishni, Foo, & Hameed, 2014; Liu, Wang, & Wang, 2012). The interaction effect of pH- adsorbent dosage ( $X_1 X_2$ ) was also valuable for the adsorbent capacity analysis since it represented an F-value of 19.43. However, this interaction term was insignificant to the removal efficiency response ( $P \geq 0.05$ ).

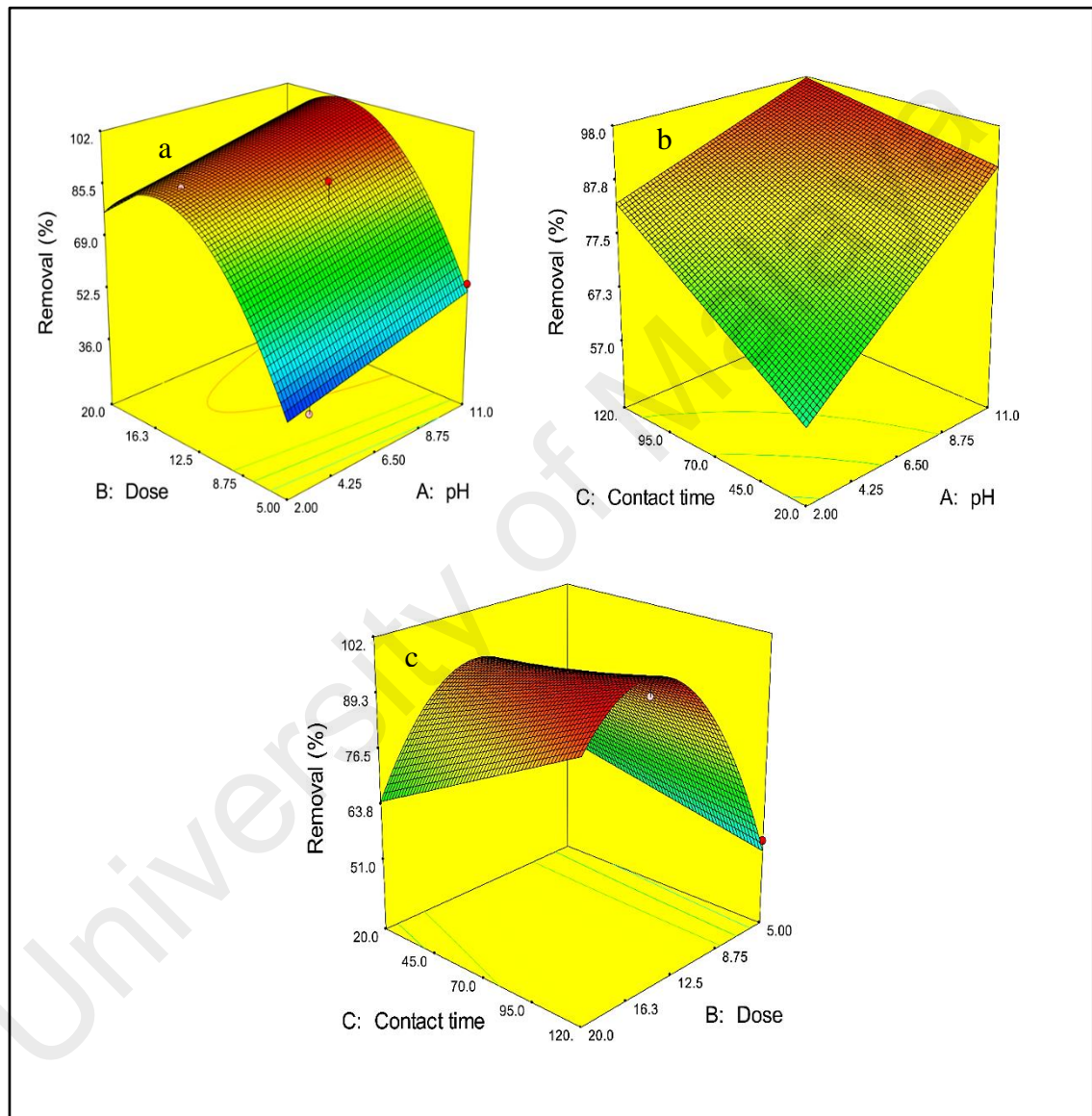


**Figure 4.14: RSM plots of MB removal efficiency and adsorbent capacity considering the effect of (a) pH and dose, (b) pH and contact time and (c) dose and contact time.**

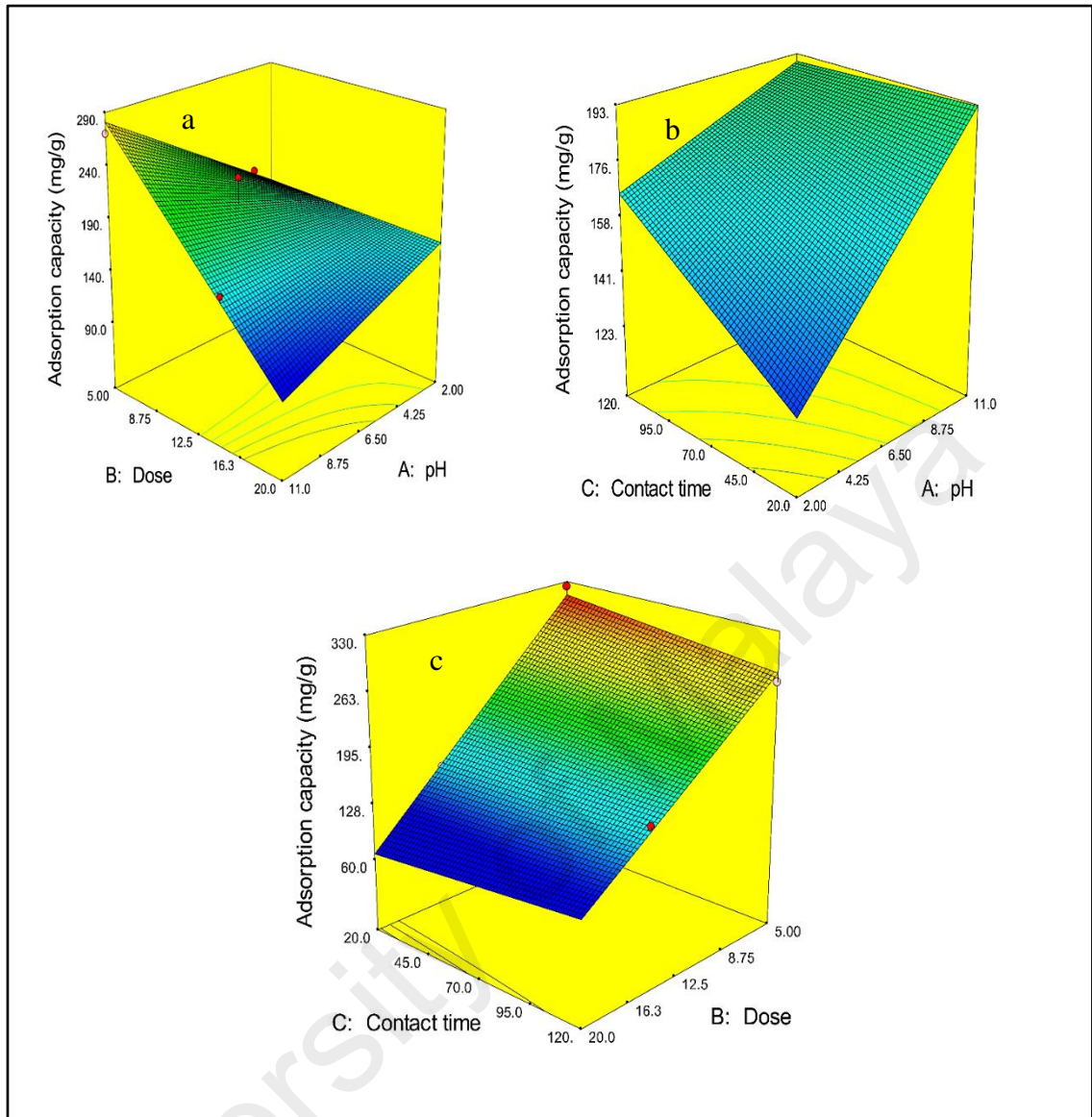


**Figure 4.15: RSM plots of the adsorption capacity considering the effect of (a) pH and dose, (b) pH and contact time and (c) dose and contact time.**

The optimum variable values for MB ( $50 \text{ mg L}^{-1}$ ) removal process was selected by setting some constraints parallel with different importance levels for the independent parameters along with the process responses (Table 4.23). The software suggested twelve solutions based on the process constraints for the optimum adsorption process conditions values (Table 4.24). In this context, the first choice was pH of 11.0, adsorbent dosage of 12.3 mg and contact time of 120 min. These conditions were further used for isotherm

and kinetics study. At these optimum values, the predicted and observed MB removal efficiency and adsorbent capacity were 97.8, 190.0 % and 94.97, 182.22 mg/g, respectively.

**Table 4.23: Constraints for optimization process based on CCD for MB adsorption.**

Name	Goal	Low limit	Upper limit	Importance
X <sub>1</sub> (pH)	In range	2	11	3
X <sub>2</sub> (dosage)	In range	5	20	3
X <sub>3</sub> (time)	In range	20	120	3
RV2	Maximize	36.6	97.8	5
Q2	Maximize	143.9	323.3	3

**4.24: Potential optimization conditions based on CCD for MB removal.**

No.	pH	Dose (mg)	Contact time (min)	RV2 %	Q2 (mg/g)	Desirability
1	11	12.3	120	97.8	190	0.826 Selected
2	11	12.3	120	97.6	191	0.826
3	11	12.4	119	97.8	190	0.826
4	11.0	12.4	119	97.8	190	0.825
5	11.0	12.4	119	97.8	190	0.825
6	11.0	12.4	117	97.8	190	0.824
7	11.0	12.4	117	97.7	190	0.824
8	11.0	12.4	116	97.7	190	0.823
9	10.8	12.5	120	98.1	189	0.823
10	10.9	12.6	112	97.8	188	0.820
11	10.7	12.5	120	97.8	187	0.810
12	7.10	137	120	94.5	170	0.749

#### 4.4.4 Adsorption kinetics

Kinetic modeling estimates the sorption rate of contamination removal from aqueous effluents and predicts the suitable rate expressions of reaction mechanisms. In this respect, in order to investigate the adsorption process of MB dye (50 mg/L) onto CNM-PAC adsorbent, kinetic analyses were conducted at the optimal removal conditions

suggested by DOE using the pseudo-first-order, pseudo-second-order and the intraparticle diffusion models (Ma et al., 2012; Zhang et al., 2015). The experiments were conducted for 7 h to ensure adsorption system reached equilibrium. The experimental data were fitted to the kinetic equations and the characteristic parameters of each model, the linear coefficient of determination ( $R^2$ ) and non-linear Chi-square ( $X^2$ ) were summarized in Table 4.25. Figure 4.16 shows the plots of studied kinetic models.

The error functions  $R^2$  and  $X^2$  were used to select the best kinetic models fitted with the experimental data. The chi-square statistic ( $X^2$ ) can be expressed in Equation 4.8 (Boulinguez, Le Cloirec, & Wolbert, 2008):

$$X^2 = \sum \frac{(q_{e,exp} - q_{e,cal})^2}{q_{e,cal}} \quad (4.8)$$

where  $q_{e,exp}$  and  $q_{e,cal}$  are the experimental and calculated adsorption capacity of CNM-PAC adsorbent (mg /g), respectively. The kinetic model is well fitted to the experimental data when high  $R^2$  and low  $X^2$  values are obtained (Ho, Chiu, & Wang, 2005). It is obvious from Table 4.25 that the adsorption of MB by CNM-PA was fitted better with the pseudo-second order kinetic model due to the highest correlation coefficient value  $R^2$  than other models and the smallest  $X^2$  value obtained (0.998 and 5.75). Therefore, the adsorption of MB on CNM-PAC adsorbent is ideally obeying the Pseudo-second-order kinetic model, and this is in agreement with some reported kinetics results for MB adsorption on carbonaceous adsorbents (Li, Du, et al., 2013; Liu, Chung, et al., 2012). This agreement with the Pseudo-second order model assumes the chemical sorption being rate controlling step which involve valence forces between the dye and the adsorbent through sharing or exchange of electrons (Bedin et al., 2016; Xiong et al., 2010). It was also observed from Figure 4.16 (c) that a good linear plot is obtained from the regression of  $q_t$  versus  $t^{0.5}$  ( $R^2 = 0.914$ ), however the line does not pass through the origin, suggesting that the external mass transfer might be also significant in the adsorption process as well as the



intraparticle diffusion (Ma et al., 2012). This observation is confirmed by the large intercepts of linear portion of the plot ( $C = 101.79$ ) which indicates the more involvement of the CNM-PAC surface in MB removal and supports the crucial effect of the boundary layer diffusion (Salama, 2017).

**Table 4.25: Linearized equations of studied kinetic models for MB adsorption on CNM-PAC.**

Model	Equation	Parameters	Values
Pseudo-First-Order	$\ln(q_e - q_t) = \ln q_e - K_1 t$	$R^2$	0.884
		$X^2$	16.91
		$K_1$	0.012
		$q_e$	51.79
Pseudo-Second-Order	$\frac{t}{q_t} = \frac{1}{K_2 q_e^2} + \frac{1}{q_e} t$	$R^2$	0.998
		$X^2$	5.75
		$K_2$	$6.34 \times 10^{-4}$
		$q_e$	163.93
Intraparticle diffusion	$q_t = K_d t^{\frac{1}{2}} + C$	$R^2$	0.914
		$X^2$	7.1
		$K_d$	4.08
		$C$	101.79
$q_e$ (experimental) = 166.11 mg/g			

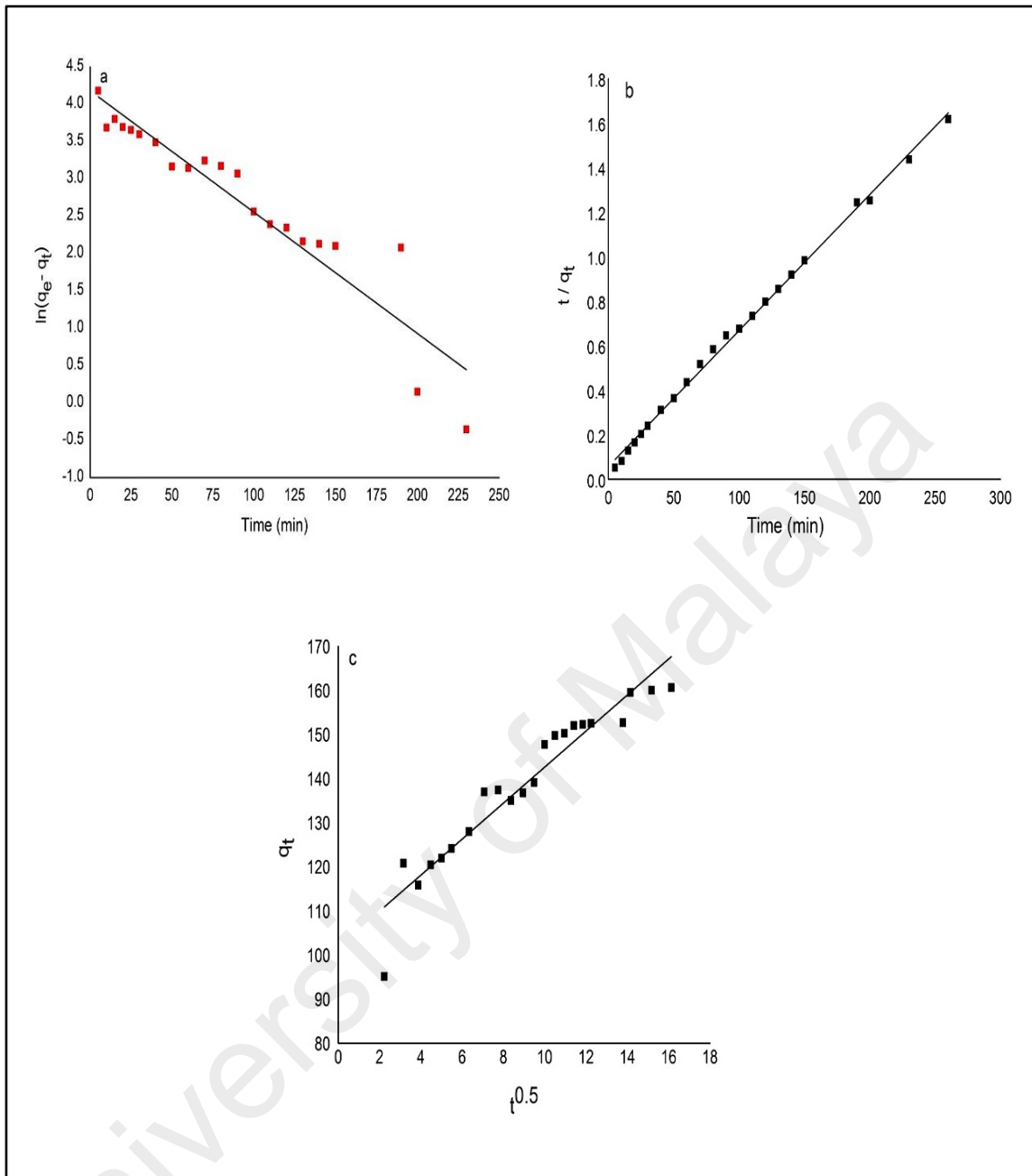


**Figure 4.16: Fittings of different kinetics models for MB adsorption on the synthesized CNM-PAC; (a) Pseudo-first order, (b) Pseudo-second order and (c) Intraparticle diffusion at optimum conditions.**

#### 4.4.5 Adsorption isotherms

Studying the isotherm is important to determine the adsorption equilibrium correlation that can be helpful for designing purposes and evaluating the behavior of adsorbent systems (Zhao et al., 2013). The equilibrium adsorption data was tested using the Langmuir, Freundlich and Temkin models as shown in Figures 4.17 (a), (b) and (c), respectively. Also, the linearized equations of the studied models and related parameters are presented in Table 4.26. As can be observed from the results, Freundlich isotherm shows respectable adsorption favorability of MB onto CNM-PAC adsorbent under experimental conditions which is confirmed by the values of Freundlich constants ( $R_L=0.031$  and  $n = 2.8$ ) (Feng et al., 2012). However, Langmuir isotherm produced better fit with the highest correlation coefficient ( $R^2 = 0.989$ ) as compared to the other isotherms at a significant maximum adsorption capacity of 250 mg/g. This is an indication of a monolayer adsorption of MB onto the homogeneous surface of the prepared adsorbent. In addition, according to  $n$  value ( $>1$ ) obtained from Freundlich model the adsorptive behavior is dominated as a physical adsorption with several adsorption energies related to different sites (Marrakchi et al., 2017). A similar equilibrium result was obtained for the adsorption of MB onto low cost bio-waste adsorbent (Krishni et al., 2014). The validity of models was determined also by calculating the standard deviation (S.D., %) using Equation 4.9:

$$S.D. \% = \sqrt{\frac{\sum(q_{exp}-q_{cal})/q_{exp}}{n-1}} \quad (4.9)$$

where the subscripts *exp* and *cal* refer to the experimental and the calculated data, and  $n$  is the number of data points. The *S.D.* value for Langmuir model was the smallest suggesting that the model is closely fitted with the experimental results. Thus, it can be argued that Langmuir isotherm can preeminently describe the adsorption of MB on CNM-

PAC. A comparison of the maximum adsorption capacity of MB on various adsorbent is listed in Table 4.27.

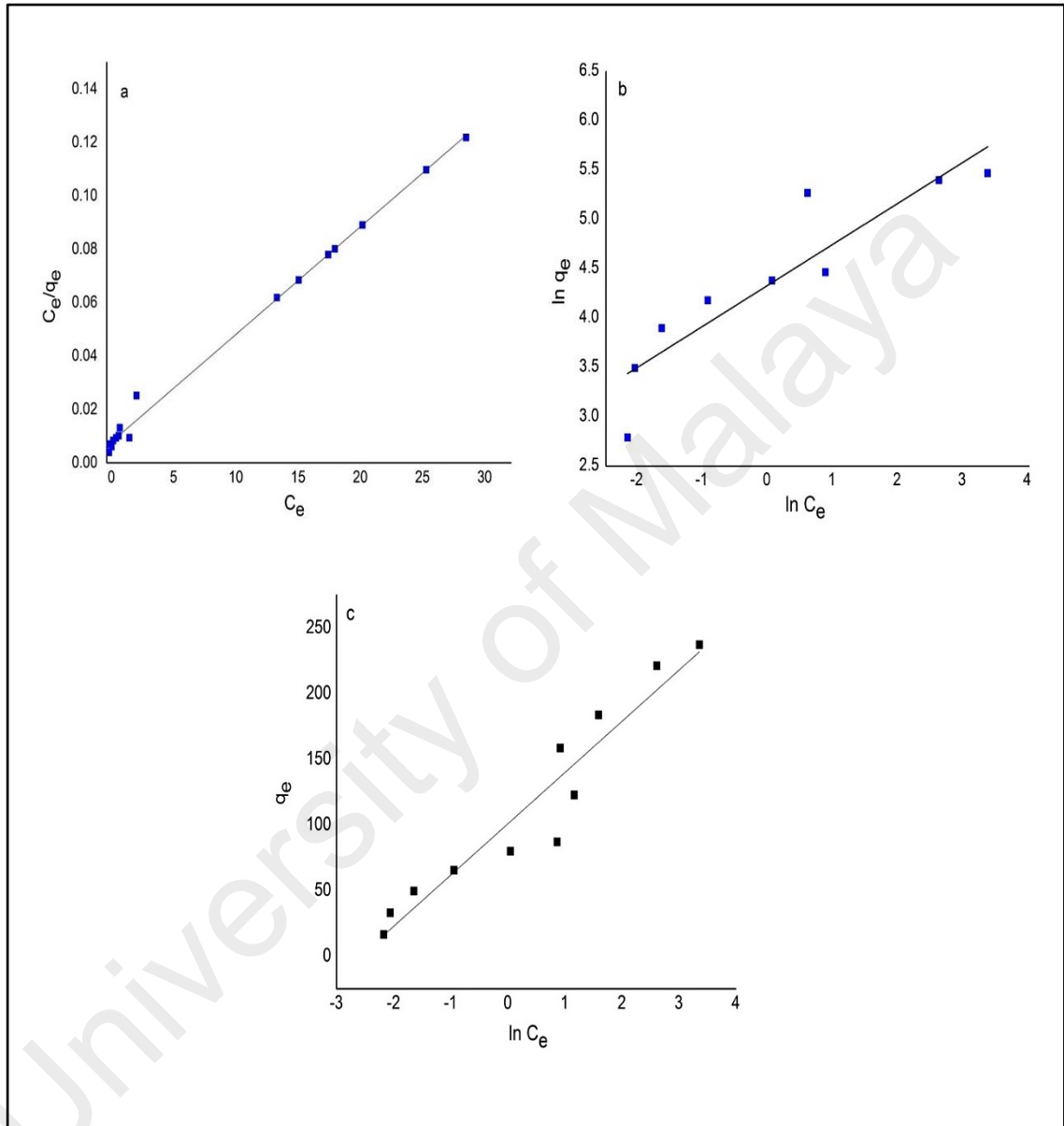


**Figure 4.17: The isotherm plots for MB adsorption on CNM-PAC following (a) Langmuir, (b) Freundlich, and (c) Temkin model.**

**Table 4.26: Linearized equations of studied isotherm models for MB adsorption on CNM-PAC.**

Model	Equation	Parameters	Values
Langmuir	$\frac{C_e}{q_e} = \frac{1}{K_L q_m} + \left(\frac{1}{q_m}\right) C_e$	$q_m$	250.0
		$K_L$	0.645
		$R^2$	0.989
		$R_L$	0.031
		S.D %	13.80
Freundlich	$\ln q_e = \ln K_f + \frac{1}{n} \ln C_e$	$R^2$	0.855
		$K_f$	85.038
		n	2.832
		S.D %	18.89
Temkin	$q_e = B_1 \ln K_T + B_1 \ln C_e$	$R^2$	0.859
		$K_T$	2.695
		$B_1$	39.401
		S.D %	25.69

**Table 4.27: Comparison between the maximum adsorption capacity ( $q_m$ ) of CNM-PAC and other reported adsorbents for MB removal.**

Adsorbent	$q_m$ (mg/g)	Reference
CNM-PAC	250	The present work
CA-APT	207.48	(Zhang et al., 2015)
MMT@C nanocomposites	194.2	(Dalaran et al., 2009)
Attapulgate / bentonite (50%)	168.63	(Liu et al., 2014)
Titanate nanotubes	133.33	(Xiong et al., 2010)
Activated carbon/NiFe <sub>2</sub> O <sub>4</sub>	182.82	(Jiang, Liang, et al., 2015)
Powdered activated carbon	91.0	(Yener et al., 2008)
Oxidized MWCNTs	188.68	(Li, Du, et al., 2013)
CNTs from acetylene cracking	35.4 - 64.7	(Yao et al., 2010)
Activated carbon/OPW	90.1	(Ahmad, Loh, & Aziz, 2007)
Luffa cylindrica fibers	49.0	(Demir et al., 2008)
Palygorskyte	50.80	(Al-Futaisi, Jamrah, & Al-Hanai, 2007)
halloysite nanotubes (HNTs)	84.32	(Zhao & Liu, 2008)

#### 4.4.6 Mechanisms

The mechanism for adsorption of MB involves the migration of dye from bulk of the solution to the surface of the adsorbent CNM-PAC followed by diffusion through the boundary layer to the surface of the adsorbent. Then the dye is adsorbed on an active site on the surface of the adsorbent and diffused by intraparticle diffusion into the interior pores. The molecular size (width, depth and thickness) of MB according to Pelekani and Snoeyink, are equal to 1.43, 0.61, and 0.4 nm, respectively (Pelekani & Snoeyink, 2000). These dimensions allow the dye to easily access within the porous structure of CNM-PAC. In addition, the substituent groups present in CNM-PAC play an important role in the adsorption capacity and the removal mechanism of the adsorbates.

The high adsorption of MB on CNM-PAC may be attributed to the  $\pi$ - $\pi$  stacking interactions between the electron of the carbon surface and the free electrons of the dye molecule (aromatic rings and  $-N=N-$  or  $-N=C-C=C-$  bonds). Carbon based materials has amphoteric character; thus, depending on the pH of the solution, their surfaces might be positively or negatively charged. At the working pH 11 in our study the  $pH > pH_{pzc}$  ( $PZC = 9.2$ ), and  $pH > pK_a$  ( $pK_a = 3.8$ ); subsequently the carbon surface becomes negatively charged favoring the adsorption of the dominant dissociated MB cationic species (Jung et al., 2016). Thence, the good adsorption performance of the prepared CNM-PAC is attributed to the existence of two adsorption mechanisms involving dispersive and electrostatic interactions. Not to mention, the results obtained from the kinetic studies indicated to the involvement of other mechanisms in MB adsorption on CNM-PAC adsorbent along with the intraparticle diffusion.

#### 4.4.7 Summary of the adsorption of MB onto CNM-PAC

The CNM-PAC synthesized at the optimum growth conditions was used to perform optimization study on removal of MB from water using CCD experimental design. The

optimum conditions were pH 11.0, adsorbent dose 12.3 mg and contact time 120 min. Three kinetic models, which are: Pseudo-first order, Pseudo-second order and intraparticle diffusion were tested. The Pseudo-second-order model was ideally fitting the experimental data of MB adsorption on CNM-PAC with  $R^2 = 0.998$ ,  $X^2 = 5.75$ ,  $q_e = 163.93$  (mg/g) and  $K_2 = 6.34 \times 10^{-4}$  (g/mg min). Also, the Langmuir, Freundlich and Temkin adsorption isotherm models were studied. The MB adsorption system showed the best agreement with Langmuir model with  $R^2 = 0.989$ ,  $R_L = 0.031$ ,  $q_m = 250.0$  mg/g,  $K_L = 0.645$  and  $S.D. = 13.8$ . It was observed lower adsorption capacity of MB at lower pH value which could be due to the protons competition with the cationic MB for the available adsorption sites on the CNM-PAC hybrid surface. Thus, the highest removal efficiency of MB was achieved at the optimum pH (11) which is higher than the  $pK_a$  value of MB, leading to conclude that the adsorption mechanism of MB was governed by the strong electrostatic interactions between the cations of the MB and the negatively charged surface of CNM-PAC ( $pH > pH_{PZC}$ ).

## CHAPTER 5: CHARACTERIZATION OF CNM-PAC SYNTHESIZED FROM METHANE DECOMPOSITION

The synthesis of CNM-PAC was adopted in parallel with growth optimization to achieve the best production yield and pollutant removal efficiency. The CNM-PAC produced under the optimal conditions, namely: reaction temperature of 933°C, reaction time of 20 min and  $H_2/CH_4$  of 1.0. Based on the optimization study, the selected samples were characterized to identify their morphology, surface area, surface charge and surface functional groups.

### 5.1.1 Morphology and surface elemental analysis

The depicted FESEM and TEM images of the impregnated powder activated carbon (Ni-PAC) before the growth reaction are presented in Figure 5.1 (a) and (b). The PAC support has irregular pores and rough areas with well dispersion of Ni particles. It is obvious that the catalyst was successfully trapped into PAC. The large surface area and high porosity of PAC prevent the agglomeration of the catalyst particles and help to produce good catalyst distribution. Furthermore, the low concentration of utilized catalyst (1%), confirmed the catalyzing role of PAC in the formation of CNM (Song et al., 2010) and produced more uniform distribution of Ni crystals. Thus, the sintering of Ni clusters will be reduced by creating uniform bed temperature along with medium hot spots (Allaadini, Tasirin, & Aminayi, 2015; Colomer et al., 2000).

The images of the synthesized CNM-PAC after  $CH_4$  decomposition at the optimized growth conditions are shown in Figure 5.2 (a) and (b). The porous structure of the resulting CNM-PAC hybrid was revealed by FESEM image. The network structure composed of hierarchical pores: the macropores with the diameter in the range of several micrometres are embedded in PAC matrix and their solid walls are composed of randomly



oriented CNTs. The short intercalated CNTs are well dispersed and stabilized uniformly in the PAC matrix.

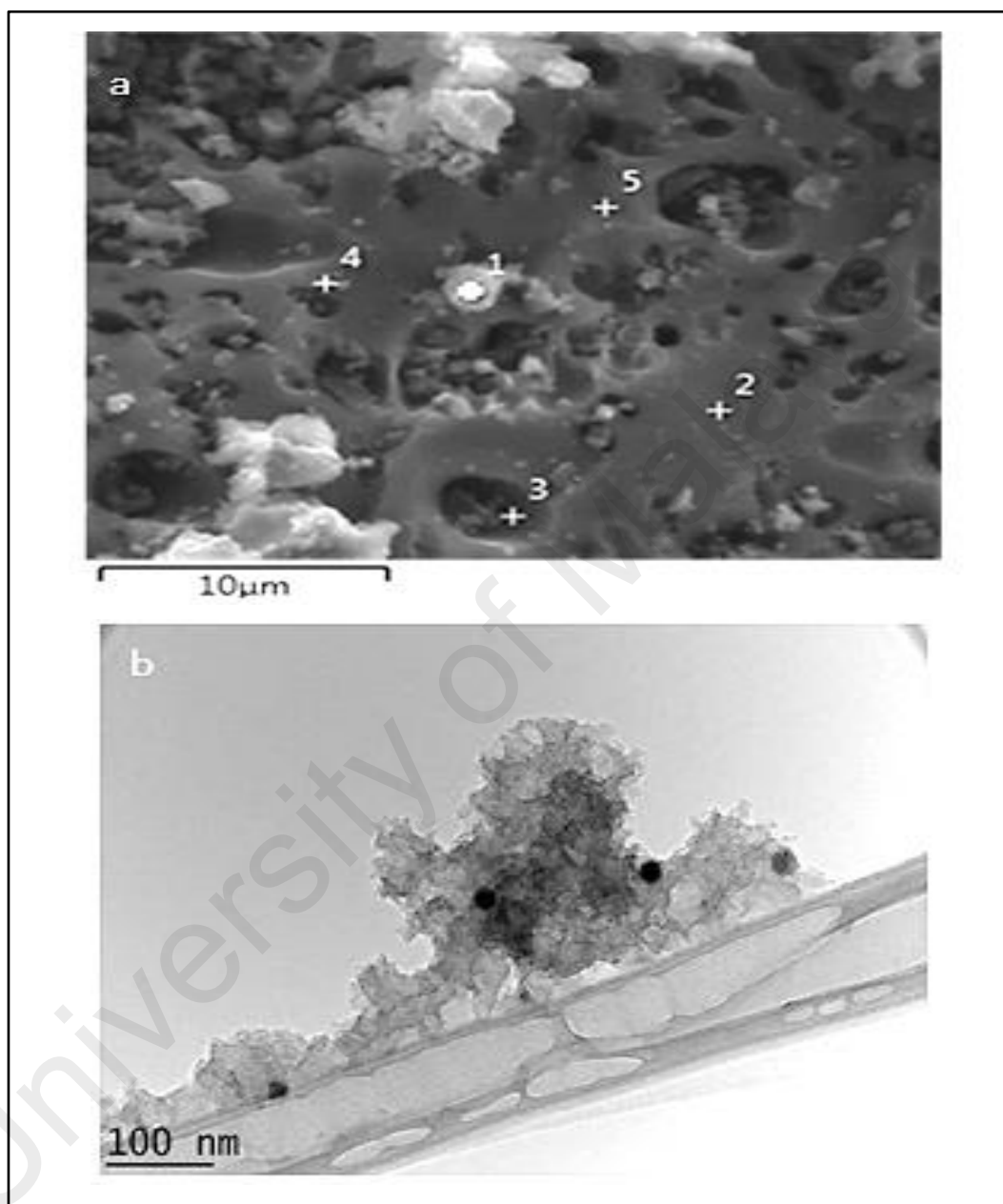


**Figure 5.1: (a) FESEM and (b) TEM images for Ni-PAC before growth reaction.**

TEM images reveals the internal structure of CNTs and CNFs attached to amorphous carbon of the PAC surface. PAC possesses an abundant porous structure hence the produced CNMs are liable to insert into the pores of the activated carbon. The grown

CNMs has groove-like feature microstructures and closely related to the porous structures and surface conditions of the PAC support (Narkiewicz et al., 2010; Shah & Tali, 2016a).

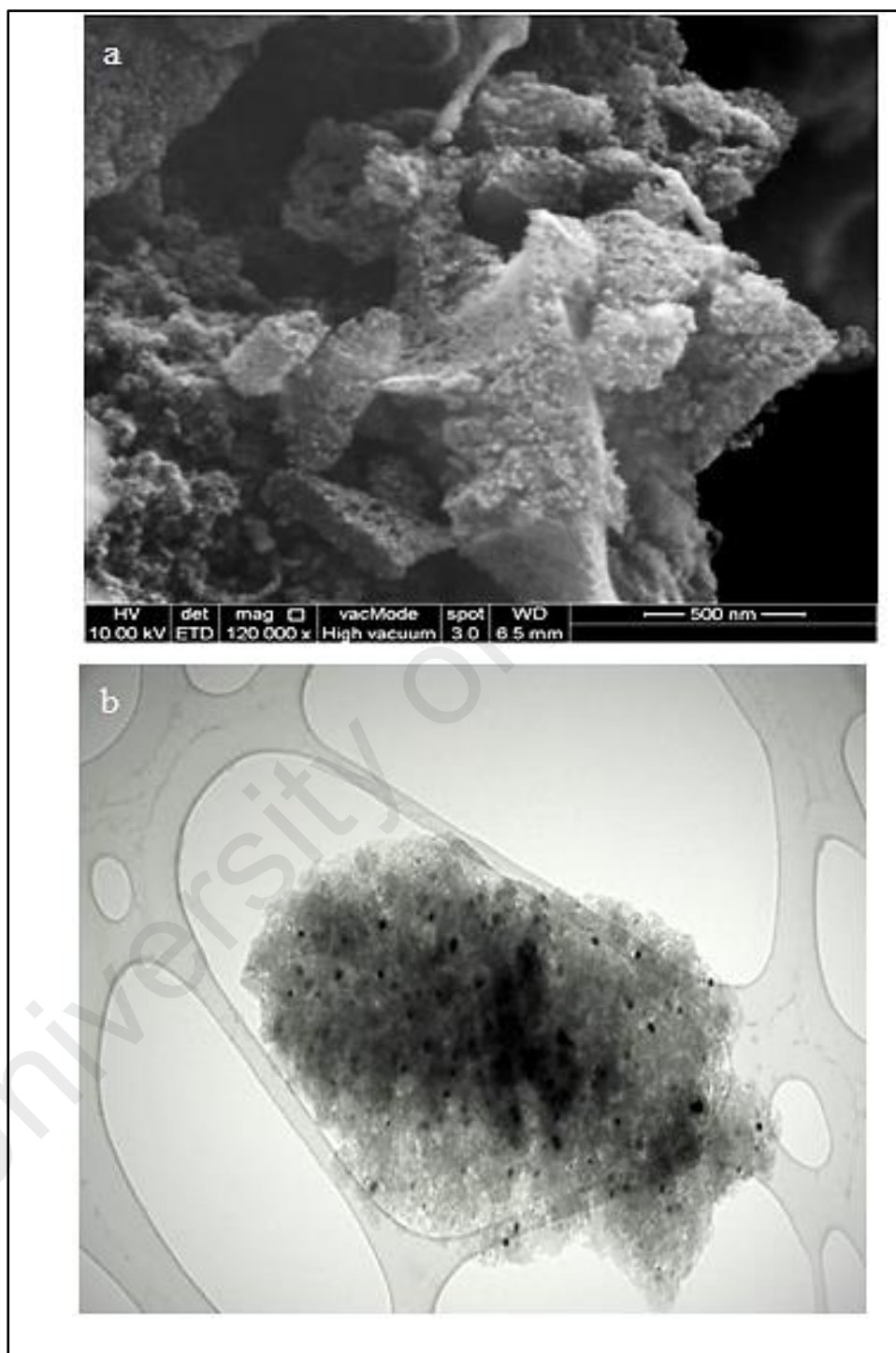


**Figure 5.2: (a) FESEM and (b) TEM images of CNM-PAC obtained at optimal conditions.**

The dark spots in the TEM images represents the metallic catalyst clusters where the carbon atoms build up to form the CNTs and other CNMs structure around it. Furthermore, conducting the growth of CNM on PAC at high reaction temperatures was suitable and unlike other studies, the Ni catalyst was not deactivated at higher temperatures (Chai et al., 2011; Villacampa et al., 2003). Thus, utilizing the PAC as a support is proved to be effective even at high temperatures due to its role in minimizing catalyst deactivation by creating a PAC network around Ni catalyst (Taleshi et al., 2013).

EDX analysis was performed for PAC, Ni-PAC, and the optimized CNM-PAC (Figure 5.3 (a), (b), and (c)). The elemental surface analysis of PAC substrate contains only carbon and oxygen-content (Figure 5.3 (a)). The results demonstrate that the intensity of carbon peak is very high, indicating that the main component of the support is carbon, the highest percentage recorded was for carbon (91.6%). However, trace oxygen was detected in most of the samples because of oxygen adsorption from the surrounding environment during processing. In Ni-PAC (Figure 5.3 (b)), the nickel particles contributed to a total content of 2.1%. The Ni content has fallen after growth to 0.9% as seen in the synthesized CNM-PAC (Figure 5.3 (c)). The decrease in content of Ni catalyst after the growth of CNM could be used as evidence interaction between  $H_2/CH_4$  gases and Ni catalyst, leading to the formation of carbon species on the metal surface (Bigdeli & Fatemi, 2015). In the meanwhile, the SEM results also illustrated that most big Ni particles disappeared and some small uniform Ni particles were dispersed on the surface PAC support. Figure 5.3 (c) also illustrates an increase in the carbon content after the formation CNM-PAC hybrid. The conversion of methane which was accelerated by the existence of the Ni catalyst contributes to the higher yield of carbon.

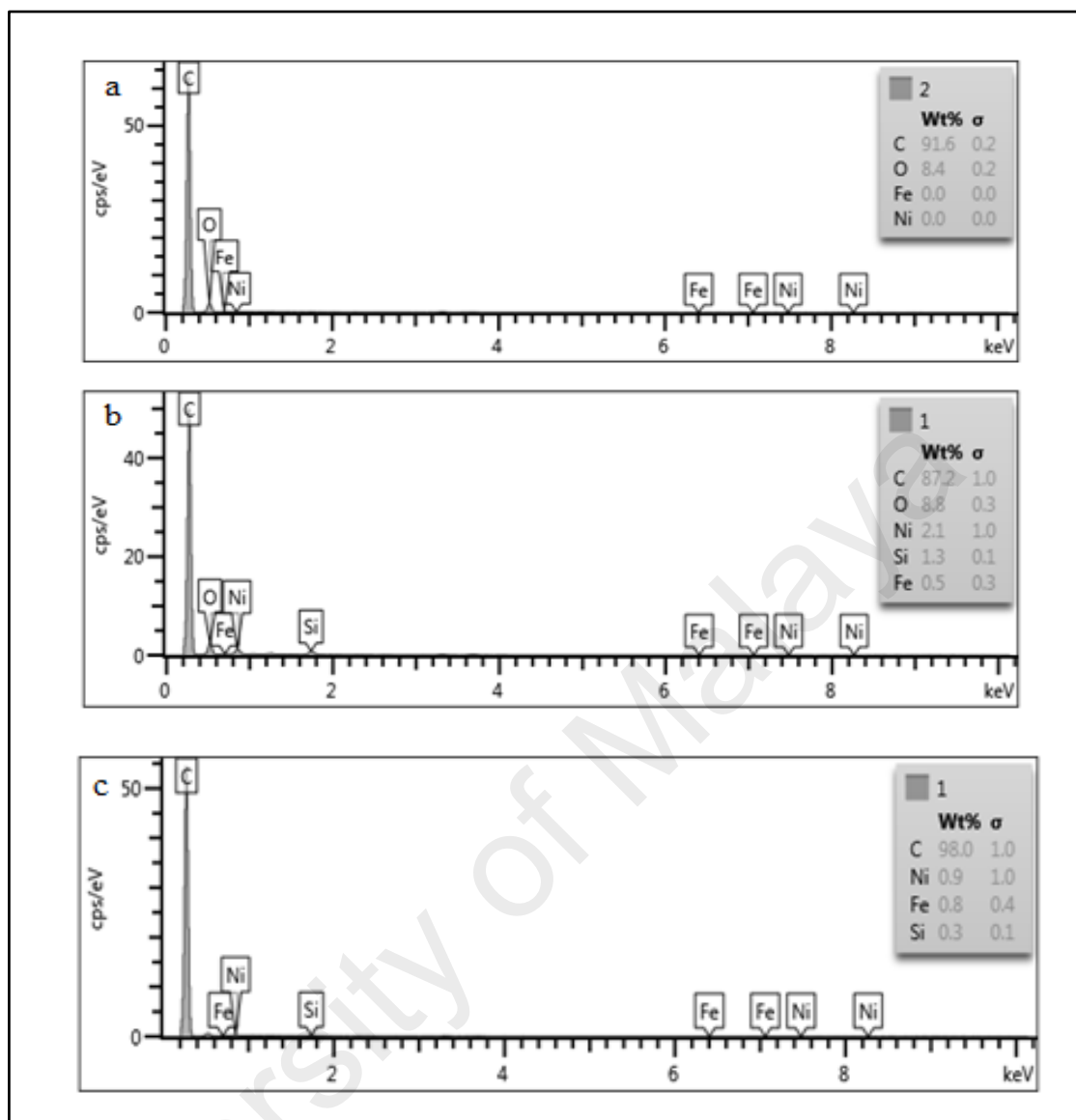


**Figure 5.3: EDX analyses for (a) PAC, (b) Ni-PAC and (c) CNM-PAC synthesized at optimal conditions.**

### 5.1.2 Raman spectroscopy

Raman spectroscopy was conducted to identify the characteristic of the carbon hybrid based nanostructure. The Raman spectra for PAC, Ni-PAC and the synthesized CNM-PAC at the optimum conditions is presented in Figure 5.4. The figure shows two obvious sharp peaks with high intensity near  $1360\text{ cm}^{-1}$  and  $1590\text{ cm}^{-1}$  and broad peaks at  $2500\text{--}3200\text{ cm}^{-1}$  wavelength. The peak at  $1300\text{--}1400\text{ cm}^{-1}$  is the D band which is related to defective nature of the obtained structure which might have originated from the

distorted hexagonal  $sp^3$  carbon network along with the Ni particle-size effects in addition to the effect of the presence of amorphous carbon (Dresselhaus et al., 2010; Lee et al., 2013). While the G band which is raised from the stretching of C=C bond in graphitic materials and related to the common tangential mode to all  $sp^2$  carbon system is detected at  $1550\text{-}1680\text{ cm}^{-1}$  (Costa et al., 2008). Moreover, the degree of carbon-containing defects in the carbon-based nanostructure by determining the ratio of intensities of D to G band ( $I_D/I_G$ ).

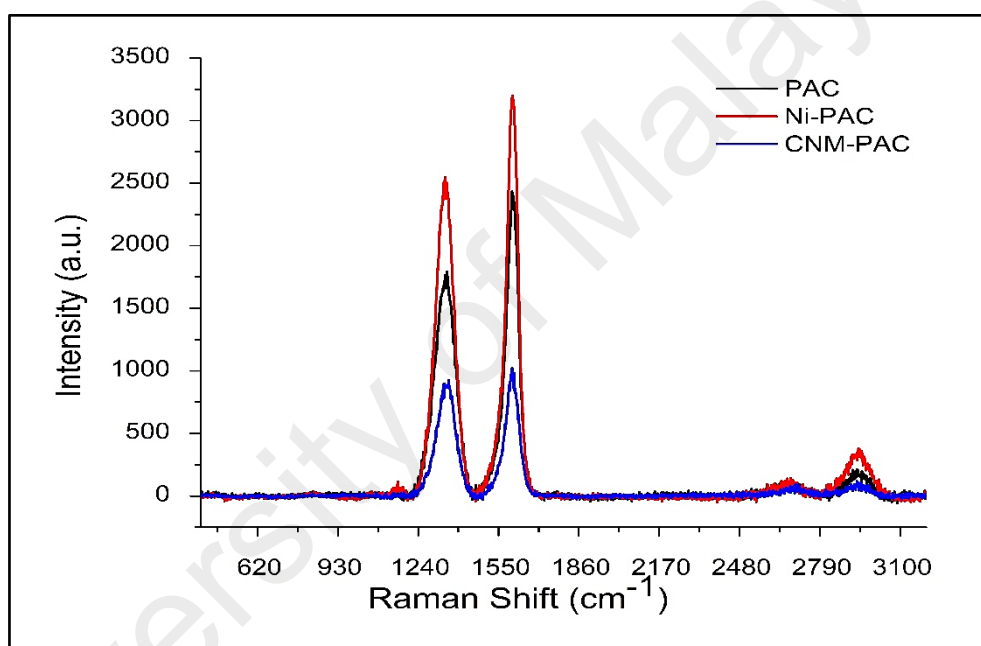


**Figure 5.4: Raman spectra of Ni-PAC and CNM-PAC.**

For Ni-PAC, the doping of Ni did not obstruct the overall structure of PAC, since it shows an  $I_D/I_G$  value of 0.81. The Raman shift of CNM-PAC is composed of the two characteristic D and G peaks. The radial breathing mode (RBM) ( $< 400\text{ cm}^{-1}$ ), which is identifying the SWCNTs was not detected, suggesting that the CNM-PAC may possessed a multiwall structure with large diameter (Ziebro et al., 2010). It is noted the high intensity of the G band, which can be explained by the fact that more  $sp^2$  carbons are formed. The  $I_D/I_G$  ratio for the CNM-PAC obtained from methane decomposition was of 0.93,

similarly to a previously reported study (Izadi et al., 2011). In addition, the  $I_D/I_G$  ratio of CNM-PAC hybrid shifts to some higher extent in comparison with PAC and Ni-PAC, reflecting a significant interaction between CNM and PAC and increased functionalities on the obtained hybrid (Sui et al., 2012). The appearance of unusually shaped 2D ( $G'$ ) peak at  $2500\text{--}3200\text{ cm}^{-1}$  is a graphitic index due to strain structure-induced effects and the higher position corresponds to a larger crystal lateral thickness which propose a better stacking order for the graphitic structures. (Hernandez et al., 2013; Zhou, Liu, et al., 2016).

### 5.1.3 Thermogravimetric analysis (TGA)

The oxidation behavior was investigated using thermal gravimetric analysis (TGA) under oxygen flow rate of 50 mL/min at temperature range between 25 to 800 °C with a heating rate of 10 °C/min. It is well known that the well graphitized carbon structures require high oxidizing activation energies. All samples PAC, Ni-PAC and CNM-PAC exhibited single step degradation as displayed in Figure 5.5 and no weight loss was observed for Ni-PAC or CNM-PAC at a degassing temperature range of 100 to 400°C, suggesting the absence of oxygenated functional groups (Hruzewicz-Kołodziejczyk et al., 2012). The oxidation temperatures of CNMs characterize thermal stability and describe the differences in their crystalline properties. The TGA profile for each sample can be characterized by three main regions: (i) initial gradual loss of 2 % for Ni-PAC and CNM-PAC and ~ 8 % for PAC is observed in the first region because of the adsorbed water, followed by constant declines of the weight to the onset combustion temperature at 430.3, 489.4 and 507.2 °C for PAC, Ni-PAC and CNM-PAC, respectively. (ii) the feature of the second region is presented by a steep drop due to elimination of the functional groups (Zhang et al., 2009) and (iii) the final combustion region for oxidizing the remaining amorphous carbon which starts at temperature higher than 500°C (Zhou et al., 2014b).

The combustion profiles of all samples indicate that the CNM-PAC acquires the highest thermal stability. The synthesized CNM-PAC can sustain a temperature as high as 800°C because of the embedded CNM in the PAC matrix (Inyang et al., 2014).

The remaining weight after exposure to high temperatures (> 650 °C) during thermogravimetric tests represents the catalyst residuals (McKee & Vecchio, 2006). According to the TGA curves for PAC samples, the weight residue remaining after the test was about 7% reflecting impurities in the substrate. This percentage increased to 21% after the catalyst particles were impregnated in the structure. However, after growth using CH<sub>4</sub> decomposition, the remaining weight recorded above 650°C was approximately 14%. The reduction in residual percentage can be explained by the growth of CNM on the catalyst surface, thus, a change in the overall composition occurs. The same degradation trend was previously reported for CNT prepared on Ni catalyst (Bom et al., 2002).

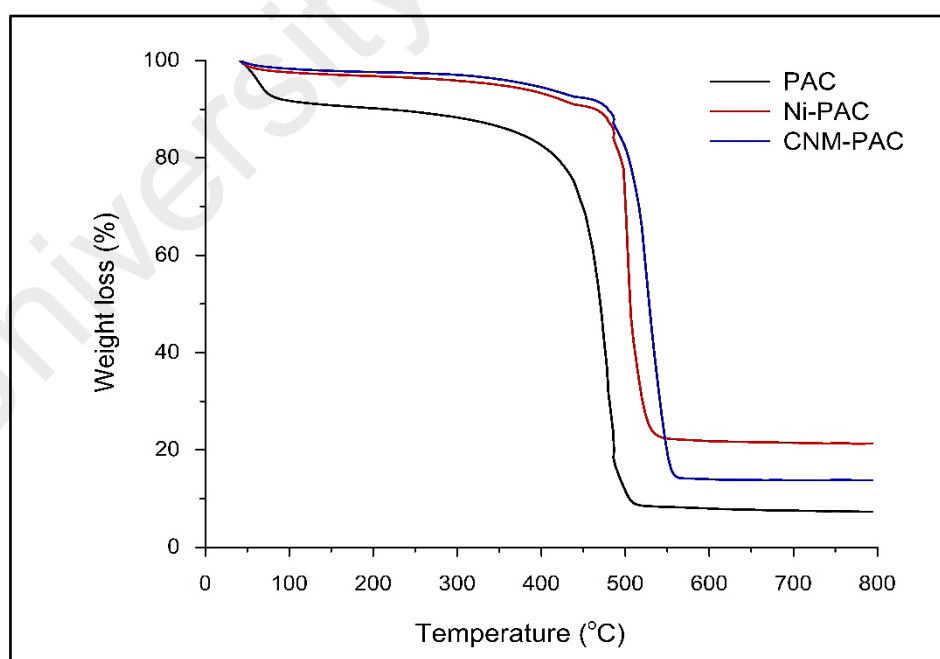


**Figure 5.5: TGA curves for PAC, Ni-PAC and CNM-PAC.**

#### 5.1.4 Surface chemistry analysis (FTIR) for BPA adsorption

The chemical reactivity of the adsorbent surface in term of the attached functional groups is a requisite feature to assess its adsorption efficiency (Stobinski et al., 2010). Figure 5.6 displays the FTIR spectra of BPA and the CNM-PAC before and after BPA adsorption. Obvious peaks were detected on the carbon surface (CNM-PAC) before BPA adsorption at around  $2350\text{ cm}^{-1}$  and within the wavenumber range of  $2800 - 2900\text{ cm}^{-1}$ , reflecting the presence of aromatic  $sp^2$  C–H stretching vibration and the asymmetric and symmetric stretching vibrations of  $\text{CH}_2$ , respectively (Koduru et al., 2016). The peak at  $1515\text{ cm}^{-1}$  reflects the existence of carbon double bonds (C=C) in the graphitic structure. The band at  $\sim 1710\text{ cm}^{-1}$  with a high intensity can be attributed to the stretching vibration of a carboxylic group (Jung et al., 2015). The peaks at  $1200$  and  $3450\text{ cm}^{-1}$  are associated with O–H. Some characteristics related to BPA molecule were also detected on the adsorbent surface, including aromatic C=C bonds (at  $1600-1400\text{ cm}^{-1}$ ), benzene ring C–H bonds (at  $900-650\text{ cm}^{-1}$ ), phenolic C–O bonds (at  $1250\text{ cm}^{-1}$ ), CH stretching vibration (at  $2990\text{ cm}^{-1}$ ), and  $-\text{CH}_3$  stretching vibrations at  $1387\text{ cm}^{-1}$  (Jung et al., 2015).

FTIR spectra of CNM-PAC after BPA adsorption show an intense peak at  $3747\text{ cm}^{-1}$  which can be attributed to the O–H stretching vibration originating from chemisorbed phenolic groups. The wide peak at  $3412\text{ cm}^{-1}$  corresponding to the stretching vibration of O–H groups of CNM-PAC shifted to  $3360\text{ cm}^{-1}$ . The shift indicated that the hydroxyl take part in the adsorption as hydrogen bonding sites. Also, the peak of carbonyl shifted from  $1719$  to  $1723\text{ cm}^{-1}$  after adsorption, indicating that carbonyl is a proton acceptor as well. The peaks at  $1150\text{ cm}^{-1}$  which is assigned to the stretching vibration of C–C bonds had a small shift toward larger wavenumber (from  $1160$  to  $1168\text{ cm}^{-1}$  for C–C bonds). This could be believed to be the influence of hydrophobic interactions. The intensity of the bands in the region between  $500$  and  $850\text{ cm}^{-1}$ , indicative of the C–H bending in



substituted aromatic rings, is increased with the presence of BPA (Bautista-Toledo et al., 2014).

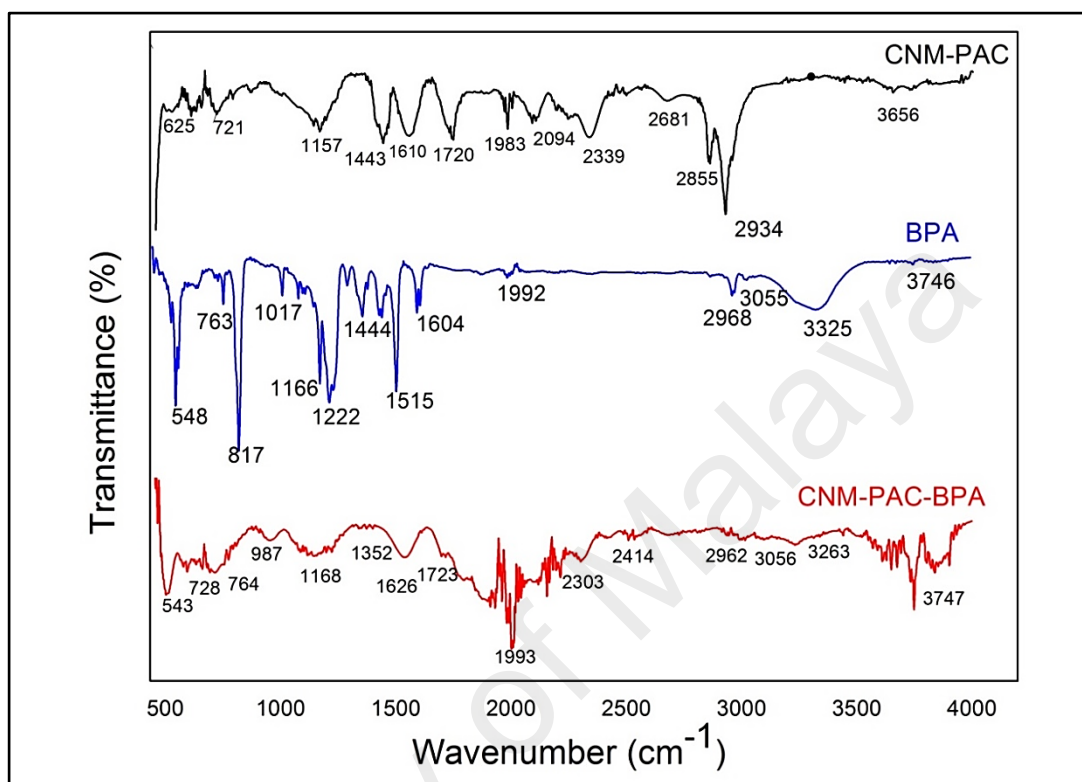


**Figure 5.6: FTIR spectra of BPA, CNM-PAC before, and after BPA adsorption.**

#### 5.1.5 Surface chemistry analysis (FTIR) for MB adsorption

Figure 5.7 show the FTIR spectra in the range 4000–400  $\text{cm}^{-1}$  for the CNM-PAC, free-MB and MB-loaded adsorbent (CNM-PAC-MB) sample. The bands from 1400 to 1735  $\text{cm}^{-1}$  were assigned to the C=O stretch mode of carboxylic acid and carbonyl moieties. The bands for CNM-PAC and CNM-PAC-MB at (3500 to 3700)  $\text{cm}^{-1}$  were due to hydroxyl groups (Yao et al., 2010). CNM-PAC adsorption presents the existence of symmetric stretching vibration of C=O groups band at 1420  $\text{cm}^{-1}$  and the band at 1580  $\text{cm}^{-1}$  is assigned to C=C skeletal stretching (Colomer et al., 2000). The two CH<sub>2</sub> stretching bands at 2918 and 2850  $\text{cm}^{-1}$  were assigned to asymmetric and symmetric stretching of the CH<sub>2</sub> groups, respectively, which presented the same wavenumbers before and after

adsorption, indicating that this group did not participate in the adsorption process. Small bands at 1734 and 1729  $\text{cm}^{-1}$ , before and after absorption, respectively, were assigned to the carbonyl groups of carboxylic acid. The band at about 1110  $\text{cm}^{-1}$  represents the C-O vibration of various oxygen-containing groups (Wang, Wang, et al., 2015). The peaks at 2922 and 2855  $\text{cm}^{-1}$  in CNM-PAC are related to the symmetric alkane stretching of C-H bond which become less strong after the adsorption of MB (Yao et al., 2010).

The spectrum of MB displays several bands in the region between 675 and 900  $\text{cm}^{-1}$  corresponding to axial-deformation vibrations of the C-H bond in the aromatic rings. The C-C axial deformation vibrations and the angular deformation bands in the C-H plane for aromatic compounds which was observed in the CNM-PAC spectrum, also appear in MB spectrum due to the presence of three condensed rings in the MB structure. The bands in the regions 1020-1250  $\text{cm}^{-1}$  and 1266-1342  $\text{cm}^{-1}$  were attributed to the axial deformation vibrations of the C-N bond of aliphatic amines and to the axial deformation of the C-N bond of aromatic amines, respectively (Auta & Hameed, 2012a).

The spectrum for MB adsorbed onto CNM-PAC shows new bands when compared to the spectrum of CNM-PAC alone. It can be observed the presence of the adsorbed dye as well as some bands previously described for CNM-PAC and MB. The bands between 3300 and 3600  $\text{cm}^{-1}$ , are assigned to both phenolic groups and carboxylic acid, decreases in intensity because these groups interact with MB. For this reason, the band between 1550 and 1650  $\text{cm}^{-1}$  can be attributed to the asymmetric axial deformation of the carboxylate anion, and the weaker band at 1400  $\text{cm}^{-1}$  can be attributed to the symmetrical axial deformation of the same anion (Li, Du, et al., 2013). The vibration of aromatic ring C-N can be clearly observed in CNM-PAC at the peak 1398  $\text{cm}^{-1}$ , became weaker after its adsorption onto the CNM-PAC adsorbent. Furthermore, the band at 1454  $\text{cm}^{-1}$  present on the CNM-PAC adsorbent that was assigned to the ring mode of the aromatic ring was

shifted to higher wavenumbers ( $1465\text{ cm}^{-1}$ ), and the relative intensity of this band was also remarkably diminished after adsorption of the dye (Li, Du, et al., 2013; Ma et al., 2012). The MB is a planar cationic dye molecule, therefore can be easily adsorbed by CNM-PAC by  $\pi$ - $\pi$  stacking interactions (Cottet et al., 2014; Jiang, Xiao, et al., 2015; Manilo et al., 2016). Table 5.1 summarizes the main functional groups detected on the as-synthesized CNM-PAC and after removal BPA and MB pollutants.

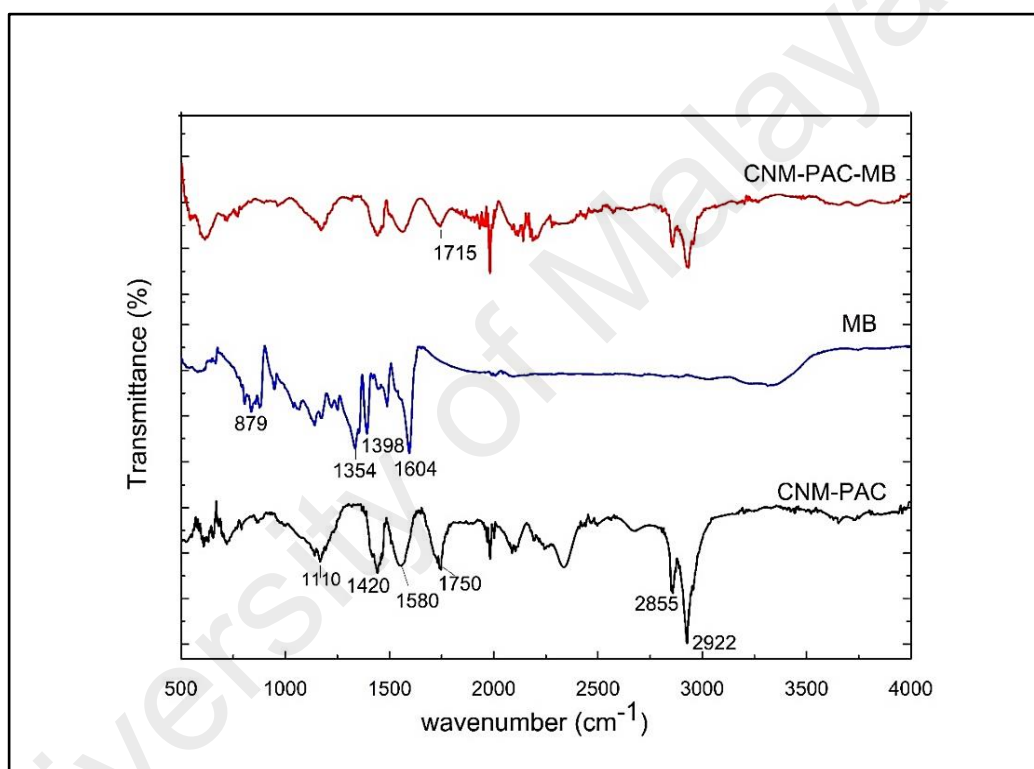


**Figure 5.7: FTIR spectrums for free MB and CNM-PAC before and after adsorption.**

**Table 5.1: Some of the predicted functional groups on the surface of synthesized CNM-PAC before and after adsorption of organic pollutants.**

<b>Expected functional groups</b>	<b>Involving adsorbents</b>
Overlapping of O–H and N–H stretching	All (3187 cm <sup>-1</sup> )
C–H stretching	ALL (2800-2900 cm <sup>-1</sup> )
C=O	ALL (1727 cm <sup>-1</sup> )
C=C–C Aromatic ring stretch	ALL (1622 cm <sup>-1</sup> )
O=C–O Carboxyl	All (1383 cm <sup>-1</sup> )
O–H (phenolic)	CNM-PAC-BPA (3747 cm <sup>-1</sup> )
Phenolic –C–O bonds	CNM-PAC-BPA (1250 cm <sup>-1</sup> )
–CH <sub>3</sub> stretching	CNM-PAC-BPA (1387 cm <sup>-1</sup> )
NH <sub>2</sub> group	CNM-PAC-MB (1463 cm <sup>-1</sup> )
C–N	CNM-PAC-MB (1490, 1394 cm <sup>-1</sup> )
Aromatic ring vibration of MB	CNM-PAC-MB (1604 cm <sup>-1</sup> )
CH <sub>3</sub> group vibrations	CNM-PAC-MB (1354, 1342 cm <sup>-1</sup> )

#### 5.1.6 BET Surface area

The surface area of the substrate, catalyst impregnated substrate and the synthesized CNM-PAC were evaluated using the BET method. BET surface area were studied via nitrogen adsorption-desorption experiments (Shah & Tali, 2016b). Table 5.2 lists the surface area of various samples for PAC, Ni-PAC, and CNM-PAC. The loading of Ni onto PAC support decreased the pore volume of the support, likely due to the blockage of the PAC pores by the impregnated catalyst resulting in a reduced surface area. However, the growth of CNM on Ni-PAC has enhanced the surface area to reach 164.6 m<sup>2</sup>/g due to the additional active surface added on the PAC. Song et al. results proposed that the good activity of activated carbon to catalyze the formation of CNTs was attributed to their porous structure which is likely similar to the catalytic effects of the CNTs themselves (Song et al., 2010). The total pore volume of CNM-PAC reached 0.29 cm<sup>3</sup>/g compared to PAC (0.09 cm<sup>3</sup>/g). Thus, an excellent sorption capacity is expected for our material due to the enhancement of the surface area. Allaedini et al., (2015) reported that the transition metals such as Fe and Ni are effective in removing organic and inorganic

contaminants in water and are used as catalysts for promoting pollutant removal. This is due to the small particle size of the impregnated catalyst and to their effect in enhancing the surface area which will provide a sufficient interaction between the catalyst and the pollutant molecules (Allaadini, Tasirin, et al., 2015).

**Table 5.2: Summary of BET results for PAC, Ni-PAC and CNM-PAC.**

Property	PAC	Ni-PAC	CNM-PAC
BET surface Area (m <sup>2</sup> /g)	101.1	97.2	164.6
Total pore volume (cm <sup>3</sup> /g)	0.09	0.07	0.29
Average pore diameter (°A)	34.89	21.29	96.19

#### 5.1.7 Point of zero of charge (PZC)

Since carbon based materials are amphoteric in nature due to the various functional groups on their surfaces and the presence of a  $\pi$ -electron system that confers them with Lewis basic properties, it is always important to evaluate their point of zero charge at which the zeta potential is zero. The points of zero charge ( $\text{pH}_{\text{pzc}}$ ) of CNM-PAC was established by means of pH shift analysis by adding 20 mg of the adsorbent to several Erlenmeyer flasks containing 20.00 mL of 0.050 mol /L NaCl. A range of initial pH ( $\text{pH}_i$ ) values of the prepared solutions were adjusted from 2 to 12 by adding either HCl and NaOH, which were securely capped immediately. The suspensions were shaken to reach equilibrium for 48 h and centrifuged at 4000 rpm for 10 min. The final pH ( $\text{pH}_f$ ) values of the supernatant liquid were recorded. The value of  $\text{pH}_{\text{pzc}}$  is the point where the curve of pH ( $\text{pH}_f - \text{pH}_i$ ) versus  $\text{pH}_i$  crosses the line equal to zero (Tran et al., 2017).

From Figure 5.8 the point of zero charge ( $\text{pH}_{\text{PZC}}$ ) of the CNM-PAC was calculated to be about 9.2. This value indicated that the synthesized CNM-PAC has a basic chemical nature with a negative charge at  $\text{pH} > 9.2$ . In this context, the decrease of the BPA

adsorption at basic pH ranges ( $\text{pH} > 10$ ) is attributed to the repulsive electrostatic interaction between the negatively charged surface of CNM-PAC ( $\text{pH} > \text{pH}_{\text{PZC}}$ ) and the bisphenolate anion. Therefore, it can be argued the mechanism of BPA removal could be mainly due to the hydrophobic  $\pi$ - $\pi$  dispersion interaction between the aromatic ring of BPA and the aromatic structure of the graphene layers of the CNM-PAC adsorbent (Bohdziewicz & Kamińska, 2013). However, for the removal of MB at the optimum pH 11, The negatively charged surface of the CNM-PAC ( $\text{pH} > \text{pH}_{\text{PZC}}$ ) can enhance the adsorption properties of the positively charged MB cations by the adsorbents through electrostatic forces of attraction (Zhang, Zhang, et al., 2010).

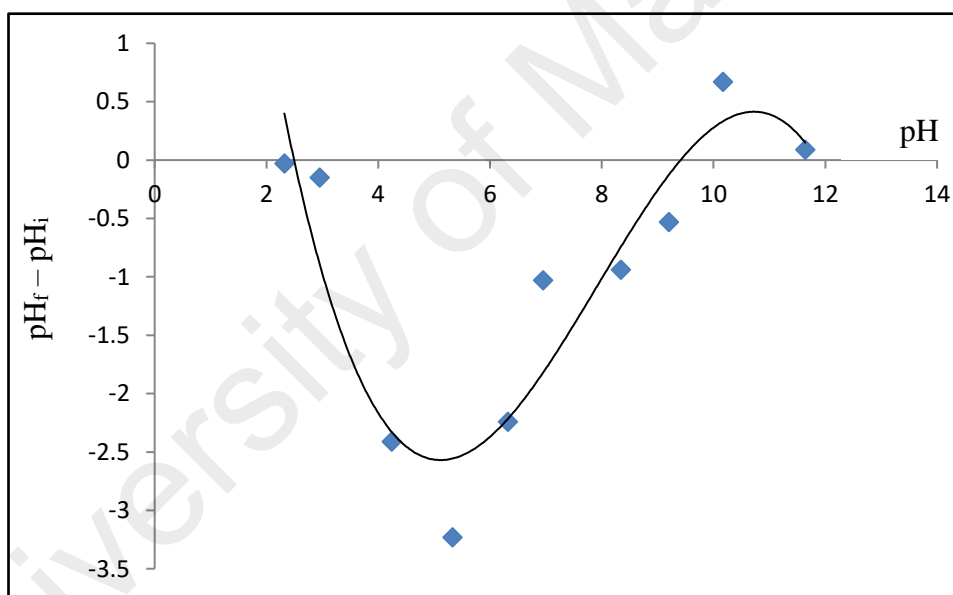


**Figure 5.8: Determination of the point of zero charge of the CNM-PAC by the pH drift analysis.**

### 5.1.8 Zeta potential

Zeta potential is the potential difference between the stationary fluid layer attached to the nanoadsorbent particles and the dispersion medium (Kyzas & Matis, 2015). The zeta potential presented in Table 5.3 was determined by dispersing 10 mg of PAC, Ni-PAC and CNM-PAC in 20 mL of deionized water (Li et al., 2008). Negative zeta potential

value for PAC before catalyst impregnation and thermal treatment is well understood. Most of the PAC surface is covered by oxygen containing groups such as carboxyl, carbonyl, alcohol and ethers, which were confirmed by the FTIR analysis, generated during the PAC production and acid washing. Thus, the negative zeta potential can be explained due to the dissociation of these carboxyl (COOH) and carbonyl (C=O) groups. Nevertheless, the Ni-impregnated PAC and CNM-PAC showed a noticeable reduction in its zeta potential along with positive values. This observation is expected due to the thermal treatment process including calcination and reduction. Heat-treatment seems to have removed some oxygen-containing surface groups as evidenced by the low oxygen ratio in the elemental analysis results. Reduction of oxygen groups after heat-treatment has also been reported by Pradhan and Menéndez (Menendez et al., 1996; Pradhan & Sandle, 1999). In addition, the positive zeta potential and the CNM-PAC basicity could be attributed to the electron-donor-acceptor (EDA) complex. Accordingly, the  $\pi$ -electron-rich regions (oxygen-free carbon) located in the basal planes, can absorb  $H_3O^+$  ions to produce surface with positive charge and basic properties (Li, Liu, et al., 2014; Montes-Moran et al., 1998). The removal of oxygen not only renders an activated carbon surface more basic but also less polar, a desirable merit when the adsorption of organic contaminants from aqueous solution is the primary objective (Li, Quinlivan, & Knappe, 2002). Meanwhile, the adsorption of BPA on the CNM-PAC via the hydrophobic interaction has increased the zeta potential absolute value by increasing the functionality of the adsorbent surface through the addition of more oxygen-containing groups. However, the enhancement in the absolute value of zeta potential was more substantial for the interaction of CNM-PAC with MB. Besides the hydrophobic interaction, MB can stably be adsorbed on the CNM-PAC through charge-transfer in which CNM-PAC is the

electron donor and the polynuclear aromatic MB is the electron acceptor (Wang, Chen, & Chen, 2014; Yan et al., 2005).

**Table 5.3: Zeta potential results for PAC and the different carbon structures produced**

Sample	Zeta potential
PAC	- 42.6
Ni-PAC	+ 1.67
CNM-PAC	+ 9.64
CNM-PAC-BPA	- 13.7
CNM-PAC-MB	- 46.8

### 5.1.9 Summary of characterization

The synthesized CNM-PAC at the optimum growth conditions was characterized with FESEM and TEM to verify the growth of CNM on PAC substrate and to identify surface morphology. The synthesized multi-structure possessed a graphitic structure with high surface area and large pore volume. The low fraction of catalyst would prevent catalyst aggregation and produce more uniform distribution of Ni particles.

The synthesized CNM-PAC can sustain a temperature as high as 800°C which is attributed to the embedded CNM in the PAC matrix. The chemical reactivity of the adsorbent surface in term of FTIR analysis displayed the characteristic functional groups and confirmed the adsorption of BPA and MB.

The BET study for CNM-PAC showed an improvement in specific surface area when compared with the raw PAC. In addition, the positive zeta potential of the CNM-PAC could be attributed to the electron-donor-acceptor (EDA) complex.



## CHAPTER 6: SYNTHESIZING AND ADSORPTION STUDIES FOR CNM-PAC FROM ACETYLENE DECOMPOSITION

### 6.1 Screening of CNM-PAC synthesis conditions

Two sets of experimental design matrix were carried out for synthesizing CNM over PAC substrate from acetylene pyrolysis by using response surface methodology (RSM). The fabrication variables were changed according to the experimental runs. However, the range of variables (growth temperature-A, growth time-B and feed stock gas ratio-C) were preselected based on literature. The responses which were considered in this part as follows <sup>2</sup>:

- 1-  $Y_{C_2H_2}$ : CNM-PAC yield %
- 2-  $RV_{C_2H_2}$ : removal percentage of MB

The DOE was used to evaluate the statistical parameters obtained from the model regression analysis and estimate the surface contour plots constructed based on the synthesizing conditions preparation variables and responses for each adsorbent-adsorbate interaction at the optimal conditions.

#### 6.1.1 DOE for production of CNM-PAC from acetylene decomposition

The CNM-PAC production conditions were optimized using a 2-level CCD with one central point. Table 6.1 presents the experimental runs to cover the following parameter ranges; temperature from 550 °C to 750 °C, time from 20 min to 60 min, and gas ratio ( $H_2/C_2H_2$ ) from 1.0 to 4.0 (AlSaadi et al., 2011). The collected samples after growth were weighed and the experimental yield ( $Y_{C_2H_2}$ ) was calculated using equation (4.1). It

---

<sup>2</sup> The formation of hybrid carbon nanomaterial by chemical vapor deposition: An efficient adsorbent for enhanced removal of methylene blue from aqueous solution. *Water Science and Technology Journal*. 2018, 77 (6), 1714-1723.

is observed that the highest yield of CNM-PAC synthesized from the decomposition of  $C_2H_2$  was (173 %).

### 6.1.2 Adsorption of MB for DOE Screening

The removal efficiency % of MB (50 mg/L) from water as a second response was adopted onto the as-grown CNM-PAC samples to evaluate the optimum growth conditions. The batch removal experiments were conducted on the CNM-PAC samples produced from the DOE (Table 6.1) by preparing 11 shake flasks. Each flask contains 10 mg of as grown CNM-PAC sample and 50 mL of MB at pH of 6.0. The flasks were placed in a mechanical shaker system for 120 min at room temperature with a shaking speed of 180 rpm. The experimental results of % removal efficiency was determined by applying equations (3.4). It is observed that the CNM-PAC sample produced from run 2 had the best performance in terms of MB removal (95.5 %).

**Table 6.1: Experimental CCD data for the synthesis parameters from  $C_2H_2$  decomposition.**

Run	Variables			Response	
	A Temperature °C	B Time min	C Gas Ratio	CNM-PAC yield $Y_{C_2H_2}$ (%)	MB Removal $RV_{C_2H_2}$ (%)
1	650	40	2.5	114.0	88.6
2	550	20	1	150.0	95.5
3	550	60	4	89.8	89.3
4	750	60	1	155.0	77.5
5	650	20	1	89.4	87.2
6	550	20	4	148.0	90.4
7	750	20	4	142.0	73.3
8	750	20	1	90.3	70.6
9	650	60	1	160.0	85.6
10	750	60	4	120.0	65.7
11	550	60	1	173.0	91.7

## 6.2 Statistical Analysis for the CNM-PAC growth

### 6.2.1 Analysis of variance (ANOVA) for the yield of CNM-PAC

Table 6.2 shows the ANOVA for the growth factors; temperature (A), duration of synthesis (B), gases flow ratio (C), and their higher-order terms along with the CNM-PAC yield as model response ( $Y_{C_2H_2}$ ). The larger F value and smaller P value, the more significant is the corresponding coefficient term (Kalavathy M et al., 2009). The F-value for  $Y_{C_2H_2}$  was 101 and the value of "Prob > F" is less than 0.05 confirming that the model is statistically significant. The analysis of ANOVA for the  $Y_{C_2H_2}$  response displayed in Table 6.2 indicates that the effects of the linear terms of (A), (B), and (C) on this response were significant, as their Prob > F values less than 0.05. However, the combined effect of the growth temperature and reaction time with gas ratio (AC) and (BC) are strongly significant (Prob > F = 0.0092 and 0.0037, respectively), thence it can be concluded that they could be considered as major determinants of  $Y_{C_2H_2}$  over the studied range.

**Table 6.2: ANOVA results for the yield of CNM-PAC growth from  $C_2H_2$  decomposition.**

*Source	Sum of Squares	df	Mean Square	F Value	p-value Prob > F
Model	0.692	8	0.0865	101	0.00986
A	0.0176	1	0.0176	20.4	0.0456
B	0.0522	1	0.0522	60.8	0.0160
C	0.0334	1	0.0334	38.9	0.0247
AB	0.0654	1	0.0654	76.1	0.0129
AC	0.0921	1	0.0921	107.0	0.00920
BC	0.231	1	0.231	269.0	0.00370
A <sup>2</sup>	0.0197	1	0.0197	23.0	0.0409
A <sup>2</sup> B	0.0428	1	0.0428	49.9	0.0195
R- Squared 0.998				Std.Dev.0.0293	
Adj. R-Squared 0.988				C.V. % 0.604	
Pred. R-Squared 0.929				Adeq. Precesion 26.4	

\* A: Temperature; (°C), B: Time; (min) and C:  $H_2/C_2H_2$

The final empirical model equation constructed of the actual parameters for  $Y_{C_2H_2}$  (%) is given in Equation (6.1):

$$\begin{aligned} \ln Y_{C_2H_2} \% = & 4.77 - 0.0468 A + 0.181 B - 0.0621 C + 0.0904 AB \\ & + 0.107 AC - 0.17 BC + 0.1 A^2 - 0.179 A^2B \end{aligned} \quad (6.1)$$

The coefficient of determination ( $R^2$ ) and coefficient of variation (CV) of were at 0.998 and 0.604 % respectively. The high  $R^2$  values and the low coefficient of variation suggest that the obtained model provides a good estimation of the response  $Y_{C_2H_2}$  (Angulakshmi et al., 2012). The predicted values of CNM-PAC yield % from  $C_2H_2$  decomposition calculated from ANOVA model equation along with the experimental values is listed in Table 6.3. In addition, a comparison of the experimental results with the model values of  $Y_{C_2H_2}$  is depicted in Figure 6.1. The plot demonstrates a good convergence between the experimental and predicted values and the proposed model has successfully created adequate correlation between the process variables.

**Table 6.3: List of the actual and predicted values of the CNM-PAC yield from  $C_2H_2$  decomposition.**

Run No.	Actual		Predicted	
	Yield %	(ln Yield)	Yield %	ln (yield)
1	114.0	4.74	117.92	4.77
2	150.0	5.01	148.41	5.00
3	89.8	4.49	88.23	4.48
4	155.0	5.04	154.47	5.04
5	89.4	4.49	89.12	4.49
6	148.0	5.00	148.41	5.00
7	142.0	4.96	139.77	4.94
8	90.3	4.50	90.92	4.51
9	160.0	5.07	167.68	5.12
10	120.0	4.78	120.30	4.79
11	173.0	5.15	174.16	5.16

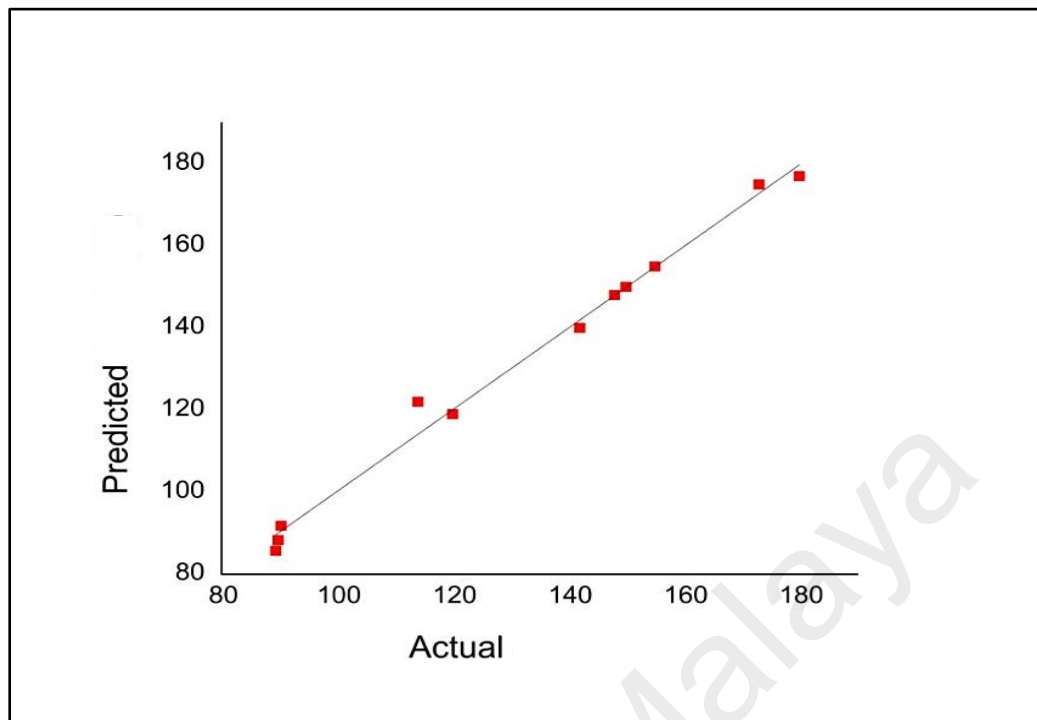


**Figure 6.1: Predicted vs. actual values for CNM-PAC yield ( $Y_{C_2H_2}$  %).**

### 6.2.2 Analysis of variance (ANOVA) for the removal of MB onto CNM-PAC

Each sample of the CNM-PAC suggested from the DOE was used as an adsorbent for removal of MB from water and the results of the removal% were statistically analyzed using the CCD method. By referring to the corresponding (ANOVA) results for MB removal presented in Table 6.4, the Model F-value of 16.3 implies the model is significant. There is only a 0.26 % chance that a "Model F-Value" this large could occur due to noise. The desirable value of signal to noise ratio "Adeq Precision" for this response showed a value of 10.3.

This model can be used to navigate the design space and it is represented by the following Equation:

$$\begin{aligned}
 MB\ RV_{C_2H_2}\ \% = & 86.7 - 10.0 A - 1.08 B - 1.77 C - 0.0967 BC + \\
 & 4.87 A^2
 \end{aligned}
 \tag{6.2}$$

where  $RV_{C_2H_2}$  % is the removal percentage of MB from water while, A, B and C are temperature of growth ( $^{\circ}C$ ), time (min) and gas ratio ( $H_2/C_2H_2$ ), respectively.

**Table 6.4: ANOVA results for MB removal % for CNM-PAC growth optimization.**

*Source	Sum of Squares	df	Mean Square	F Value	p-value Prob > F
Model	930.0	5	186.0	16.3	0.00407
A	806.0	1	806.0	70.8	0.000389
B	11.3	1	11.3	0.99	0.366
C	27.2	1	27.2	2.39	0.183
BC	8.97	1	8.97	0.788	0.415
A <sup>2</sup>	46.6	1	46.6	4.09	0.0490
	R- Squared 0.942			Std.Dev.3.37	
	Adj. R-Squared 0.885			C.V. % 4.04	
	Pred. R-Squared 0.798			Adeq. Precision 10.3	
* A: Temperature; ( $^{\circ}C$ ), B: Time; (min) and C: $H_2/C_2H_2$					

Table 6.5 lists the predicted values of removal efficiency % calculated from ANOVA model equation along with the actual values. Furthermore, the predicted values were plotted against the experimental data (Figure 6.2). It can be seen a good relationship between the experimental and predicted values since the data points has good distribution near to the straight line. The coefficient of determination ( $R^2$ ) of MB removal % was 0.942. The high  $R^2$  values and the low coefficient of variation ( $CV= 4.04$  %) suggest that the obtained model provides a good estimation of the response which can be reproducible as long CV values are not greater than 10% (Angulakshmi et al., 2012).

**Table 6.5: List of the actual and predicted values of the MB removal efficiency.**

Run No.	RV <sub>C2H2</sub> %	
	Actual	Predicted
1	88.6	86.7
2	95.5	93.7
3	89.3	88.6
4	77.5	73.4
5	87.2	88.0
6	90.4	92.1
7	73.3	72.1
8	70.6	73.7
9	85.6	88.3
10	65.7	68.0
11	91.7	93.5

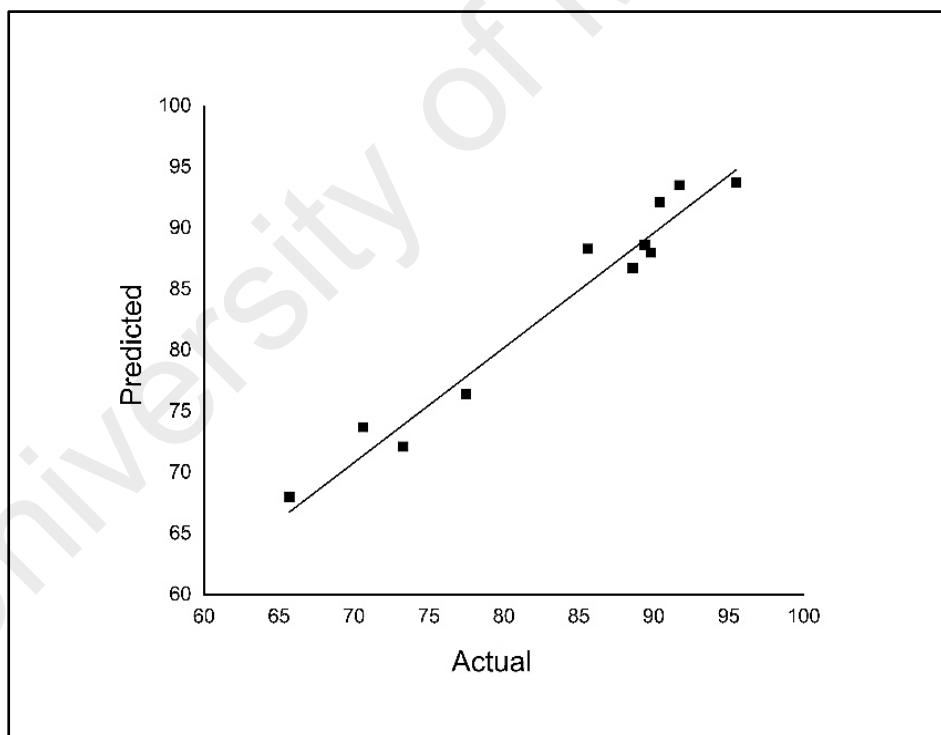


**Figure 6.2: Predicted values vs. actual values MB removal response.**

### 6.2.3 Effects of reaction temperature, reaction time and gas Ratio

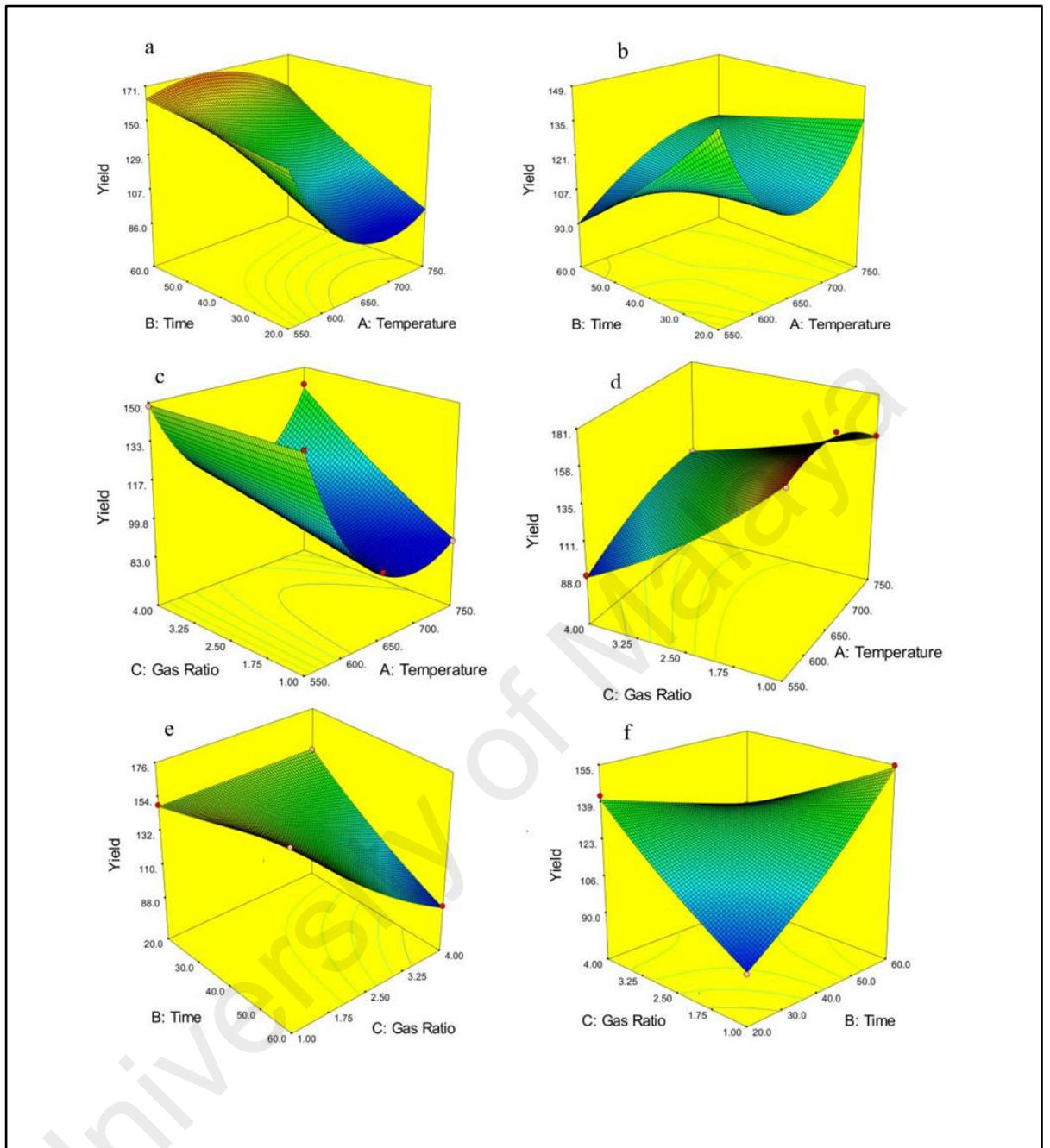
The effects of the process parameters on  $Y_{C_2H_2}$  were investigated to determine the conditions that favored the growth of carbon nanomaterials on the PAC substrate. The interaction effects of the process parameters on the yield were graphically illustrated by RSM plots as a function of two independent parameters (Figure 6.3). The effects of reaction temperature and time on the product yield at fixed gas ratio (1.0 and 4.0) were displayed in Figure 6.3 (a) and (b). There was a notable increase in  $Y_{C_2H_2}$  with increasing reaction temperatures from 550 to 650°C. A temperature increase from 650 to 750 °C led to small reduction in the yield. Furthermore, the plots showed that, the greatest amount of CNM-PAC percentage is observed at low growth temperature. In addition to the fact that Ni possess low melting point among other transition metals, these observations suggest that PAC is an effective support for Ni catalyst even at higher temperature and deactivation of Ni catalyst can be minimized by creating PAC network around the Ni catalyst. These findings agree with those reported in previous studies (Aiello et al., 2000; Reshetenko et al., 2003; Seidel et al., 2004).

Figure 6.3 (c) and (d) showed the effects of reaction temperature and gas ratio on  $Y_{C_2H_2}$  at fixed reaction time (20 and 60 min). The effect of gas ratio on the yield was insignificant for growth duration 20 min, as the higher yield was seen at almost the same at gas ratio 1.0 and 4.0. It was well known that the presence of higher  $H_2$  gas along with  $C_2H_2$  could facilitate suppression of catalyst poisoning effect which in turn results in increased yield of the CNTs (Taleshi et al., 2013), however, the lower observed yield in CNM-PAC at high hydrogen concentration is due to the competition between  $H_2$  and  $C_2H_2$  for the metallic surface sites. Not to mention that the high hydrogen fraction would affect the reaction kinetics and suppress the  $C_2H_2$  decomposition (Jung et al., 2001; Zhang et al., 2017). It is worthy to point out that the present study demonstrated that using PAC



as a support could potentially minimize the suppression of catalyst poisoning by motivating Ni catalyst protection even at higher flow of  $H_2/C_2H_2$  gas. Also, a small  $Y_{C_2H_2}$  was found at longer reaction time (60 min), therefore, lowering the reaction time will be convenient for achieving the highest growth rate along with minimizing the carbonaceous particle formation (Piao et al., 2002).

Figure 6.3 (e) and (f) show the effects of reaction time and gas ratio on  $Y_{C_2H_2}$  at growth temperature of 550 and 750 °C. There was a steady increase in the yield with increasing reaction time for the gas ratio of 1.0 at lower temperature (550 °C). However, lower yield is observed with gas ratio of 4.0 at higher temperature (750 °C). This may be due to the rapid reduction of metal oxides by  $H_2$  gas, thereby makes  $C_2H_2$  to decompose at a faster rate, subsequently, cause pyrolytic carbons deposition onto the active catalytic sites, which in turn reducing the catalyst activity. Figure 6.3 (e) indicated that for growth temperature of 550 °C, a high reaction time was unfavorable at maximum gas ratio 4.0 that was used at ratio of 750. Typically, the rate of diffusion of carbon into the catalyst decreases with increasing reaction time and eventually terminates to zero giving rise to no additional increase in the yield (Chen et al., 2015; Sharma & Lakkad, 2009).



**Figure 6.3: Response surface plots for the effects of reaction temperature and reaction time on CNM-PAC ( $Y_{C_2H_2}$ ); at fixed gas ratio 1.0 (a) and 4.0 (b), effects of deposition temperature and gas ratio at fixed reaction time 20 (c) and 60 min (d), and effects reaction time and gas ratio at fixed growth temperature 550°C (e) and 750°C (f).**

#### 6.2.4 Optimization of the selected parameters and study their interactive effects on the CNM-PAC growth

The yield of the CNM-PAC response under the combination of the independent growth variables was presented by RSM plots. Table 6.6 shows the optimization criteria and their importance levels of the growth parameters along with the process response namely; growth temperature, time, feed stock gas ratio and the yield of the CNM-PAC to select the optimum conditions for the growth of CNM-PAC under  $C_2H_2$  decomposition. The plots showed that, the maximum growth percentage is observed when all the preparation variables were set at low values. It is obvious from the plots (Figure 6.3 (a)) that increasing the temperature above 560 °C will cause the following: (i) reduction in the yield and enhancement of the soot formation which may inhibit the growth process, (ii) the ability to conduct the growth at low temperatures will reduce the interaction between the catalyst and the underlayer metallic alloying as this kind of interaction hinder the growth of the CNM and (iii) high reaction temperatures increase the decomposition rate of acetylene, and hence the C supply rate will exceed the C diffusion rate, so as C accumulates on the metal surface and partly deactivates the nickel catalyst, leading to the observed yield deterioration (Wang, Yang, et al., 2017). The plots (6.3 (b)) also indicated that short reaction times has favorable effect on the yield indicating that the catalyst is very active at early stage. Furthermore, longer reaction times will promote the formation of amorphous carbon (Khedr, Halim, & Soliman, 2008; Mubarak, Abdullah, et al., 2014; Nessim et al., 2009).

Based on the specified constrains in Table 6.6, there were several sets of selected solutions predicted to be the optimum conditions; these were listed in Table 6.7 and ranked by the desirability. The highest yield CNM-PAC of 160 % was found at the optimum process conditions of a reaction temperature 550°C, a reaction time 37.3 and a

gas ratio 1.0. Sets of experiments in which the optimum reaction condition based on the RSM study were conducted using the procedure discussed in the experiment section. The CNM-PAC from the optimized reaction was calculated to be 156.56 % which were close to the RSM analysis result with a mean error of 2%. It is believed that C<sub>2</sub>H<sub>2</sub> is an active compound with low thermal stability. Therefore, high reaction temperature and long reaction time will result in rapid decomposition of C<sub>2</sub>H<sub>2</sub>, leading to the deactivation of the catalyst. This deactivation is higher when the feedstock gases flow rate increase due to particle absorption of too much carbon or conversion of the metal into other non-catalytic form (Ahmad et al., 2017; Kang et al., 2015). Accordingly, the sample obtained at the optimized growth condition is identified as O-CNT to be investigated in the MB adsorption study.

**Table 6.6: Optimization constraints for CNM-PAC production.**

Name	Goal	Lower limit	Upper limit	Importance out of 5
Temperature (A)	In range	550	750	3
Time (B)	In range	20	60	3
Gas ratio (C)	In range	1	4	3
Yield % (Y <sub>C<sub>2</sub>H<sub>2</sub></sub> )	Maximize	89.4	173	3
MB removal % (RV <sub>C<sub>2</sub>H<sub>2</sub></sub> )	Maximize	65.7	95.5	5

**Table 6.7: The optimum conditions suggested by DOE for CNM-PAC growth.**

No.	A	B	C	Y %	RV%	Desirability	
1	550.	37.3	1.00	160.	93.6	0.918	Selected
2	550.	36.1	1.00	159.	93.6	0.917	
3	550.	31.9	1.00	156.	93.7	0.913	
4	550.	25.5	1.00	152.	93.7	0.907	
5	550.	21.5	1.00	150.	93.7	0.903	
6	550.	20.3	1.00	149.	93.7	0.902	
7	554.	20.0	1.00	144.	93.7	0.890	
8	550.	20.0	2.54	149.	92.9	0.879	
9	550.	20.0	2.65	149.	92.9	0.878	

A: Temperature, B: time, C: gas ratio

Furthermore, Figure 6.4 (a) and (b) indicate that the removal of MB increased with increasing the growth temperature. Thus, the high growth temperature has more positive effect on promoting the MB removal efficiency comparing with the impact of growth duration parameter and gas ratio. Figure 6.4 (c) shows that the interaction between those the parameters (BC) has smaller effect as compared with the temperature-time (AB) interaction. From the study of interaction of different parameters of CNM-PAC synthesis, it was noticed that the behavior of surface response of removal as function of reaction conditions is different from that of yield. This indicates that the quality of higher yield product is not necessary to be sufficient for removal process (Madannejad et al., 2018).

University of Malaysia

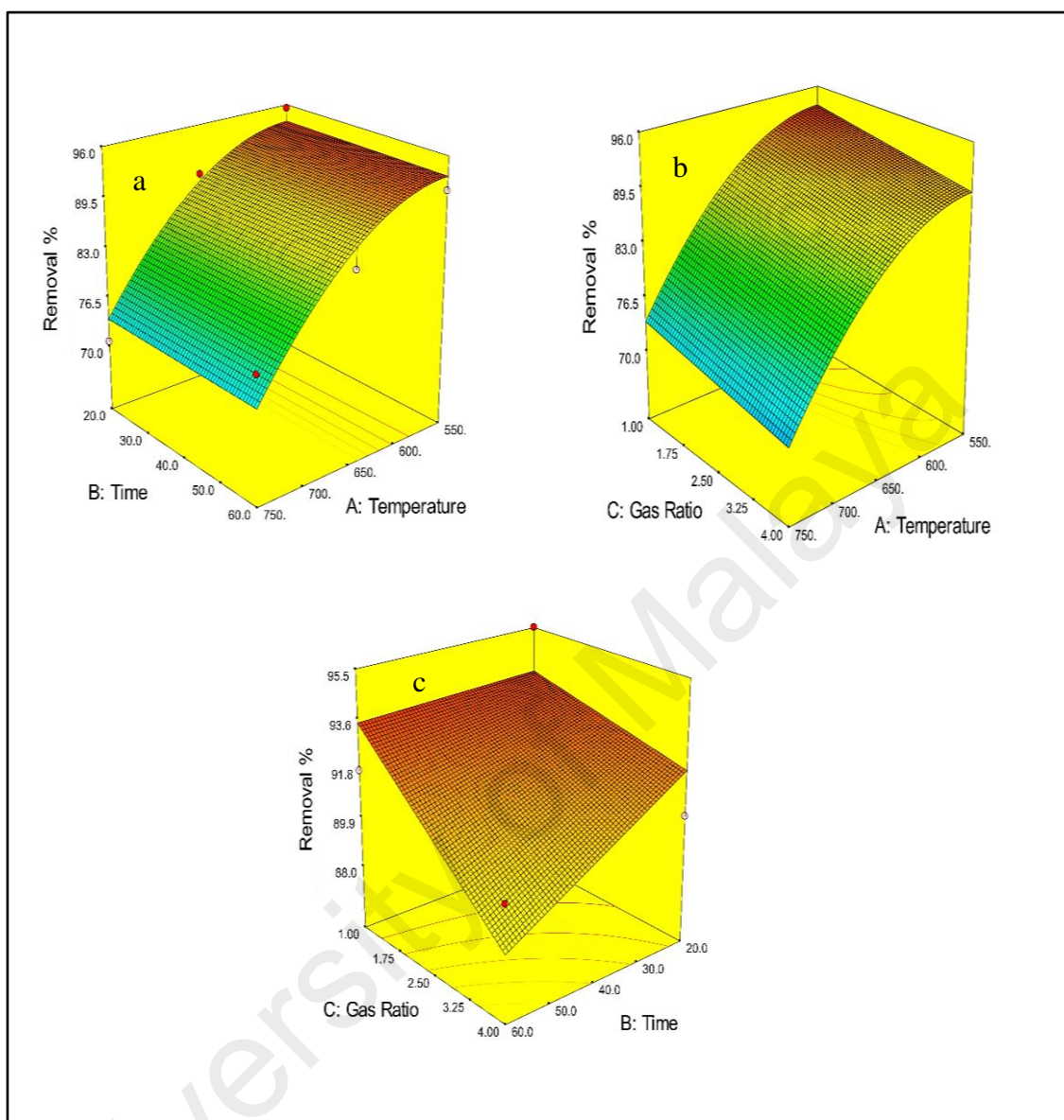


**Figure 6.4: Three-dimensional response surface representation for: MB removal efficiency (RV<sub>C<sub>2</sub>H<sub>2</sub></sub> %) on CNM-PAC; (a) interaction with growth temperature and time, (b) interaction with growth temperature and gas ratio and (c) interaction with time and gas ratio.**

### **6.2.5 Summary of optimization the conditions of CNM-PAC synthesis from acetylene decomposition**

Based on this study, the effects of the operating variables were optimized for preparing CNM on powdered activated substrate from acetylene cracking. In view of this, the findings of this study are:

- 1- different range of process variables were preset to get maximum CNM-PAC yield. temperature from 550 °C to 750 °C, time from 20 min to 60 min, and gas ratio ( $H_2/C_2H_2$ ) from 1.0 to 4.0.
- 2- The experimental design results for synthesizing CNM-PAC revealed that all the three variables showed significant effects on the yield of CNM-PAC. However, the growth temperature is the most important factor influencing yield % and the removal efficiency of MB.
- 3- The process optimization produced CNM-PAC hybrid with maximum possible yield within the experimental ranges studied. The proposed model has successfully created adequate correlation between the process variables.
- 4- The highest yield CNM-PAC of 160.0 % was found at the optimum process conditions of a reaction temperature 550 °C, a reaction time 37.3 and a gas ratio 1.0 min.
- 5- The produced CNM-PAC hybrid at the optimal synthesizing conditions was identified as O-CNT in the MB adsorption study demonstrated in the next section.

### 6.3 Adsorption of Methylene blue (MB)

#### 6.3.1 Primary screening

The primary adsorption screening was conducted as prescribed in section 3.4.5.5 to select the adsorbent with the highest removal efficiency for MB. The screening test was carried out for three adsorbents (O-CNT, KS-CNT, and K-CNT) and the results were described in Figure 6.5. The results demonstrated that the removal percentage was pH dependent. The O-CNT achieved the highest removal percentage at pH 11. KS-CNT recorded the highest removal at pH 3. O-CNT and KS-CNT were characterized by almost the same adsorption capacity but were much higher than K-CNT<sup>3</sup>.

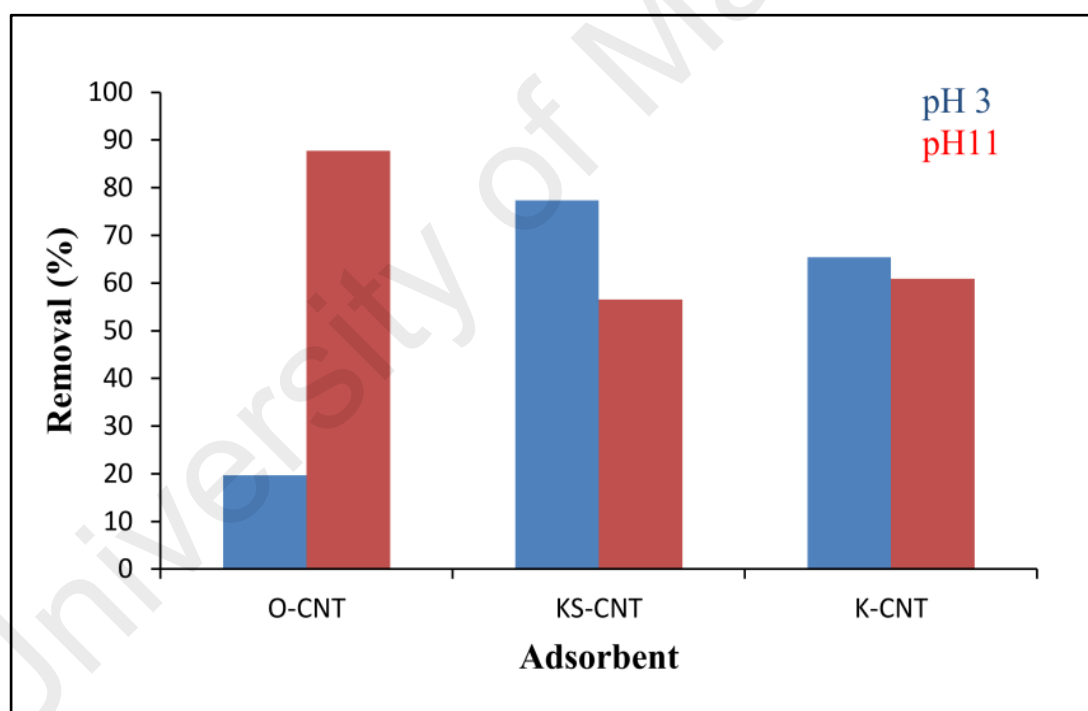


**Figure 6.5: Primary screening study for all adsorbents.**

<sup>3</sup> Growth and optimization of carbon nanotubes in powder activated carbon for an efficient removal of methylene blue from aqueous solution. Environmental Technology Journal. 2018, (38).



Figure 6.6 shows the effect of contact time on the adsorption of MB by the three adsorbents. The initial adsorption rate for KS-CNT was higher than that of the as-grown O-CNT suggesting that the sorption of MB onto KS-CNT was faster than that onto O-CNT. The difference in starting removal efficiency between as-grown O-CNT and KS-CNT might be due to the changes in the surface chemistry of CNTs after  $\text{KMnO}_4/\text{H}_2\text{SO}_4$  oxidization. However, the removal efficiency of KS-CNT decreased, and the removal performance was slightly enhanced at a prolonged contact time. The maximum removal efficiency for O-CNT and KS-CNT after 24 h were 99.65 and 94.5 %, respectively. After oxidization, the surface of CNTs became negatively charged because of the deprotonation of the attached oxygen-containing groups. In this case, the attraction of water molecules is more favorable than the sorption of MB; thus the removal process is more difficult (Shen et al., 2009). The sorption of organic chemicals is depressed on carbon materials because of the presence of oxygen functional groups (Franz, Arafat, & Pinto, 2000; Zhu & Pignatello, 2005), and this depression in removal efficiency can occur via water adsorption, dispersive/repulsive interaction and hydrogen bonding. Cho et al., (2008) observed that the incorporation of surface oxides onto multi-walled carbon nanotubes has reduced the surface area resulted in a decrease in the maximum adsorption capacity of naphthalene by 70 % (Cho et al., 2008). Also, Sheng et al., (2010) reported that the low adsorption affinity of ionizable aromatic compounds on oxidized MWCNTs due to the produced carboxylic groups. These groups can act as electrons withdrawing groups localizing electron from system of MWCNTs, which might be expected to interfere with the dispersion forces between the aromatic ring of the aromatic compounds and the graphitic structure of MWCNTs (Sheng et al., 2010). Furthermore, the lowest removal efficiency of MB was observed for the K-CNT sample which could be due to the extensive presence of  $\text{MnO}_2$ . The  $\text{MnO}_2$  deposition, destroys the hexagonal graphite

structure of CNTs through wrapping the CNTs into a non-stoichiometric amorphous shape (AlOmar et al., 2017). These observations were confirmed by monitoring the removal efficiency of MB onto all the adsorbents and by observing the changes in colour (Figure 6.6). O-CNTs and the functionalized sample with  $\text{KMnO}_4/\text{H}_2\text{SO}_4$  introduced the same adsorption capacity. Therefore, this study focused on the optimization of MB removal onto O-CNTs for further kinetics and isotherm investigation.

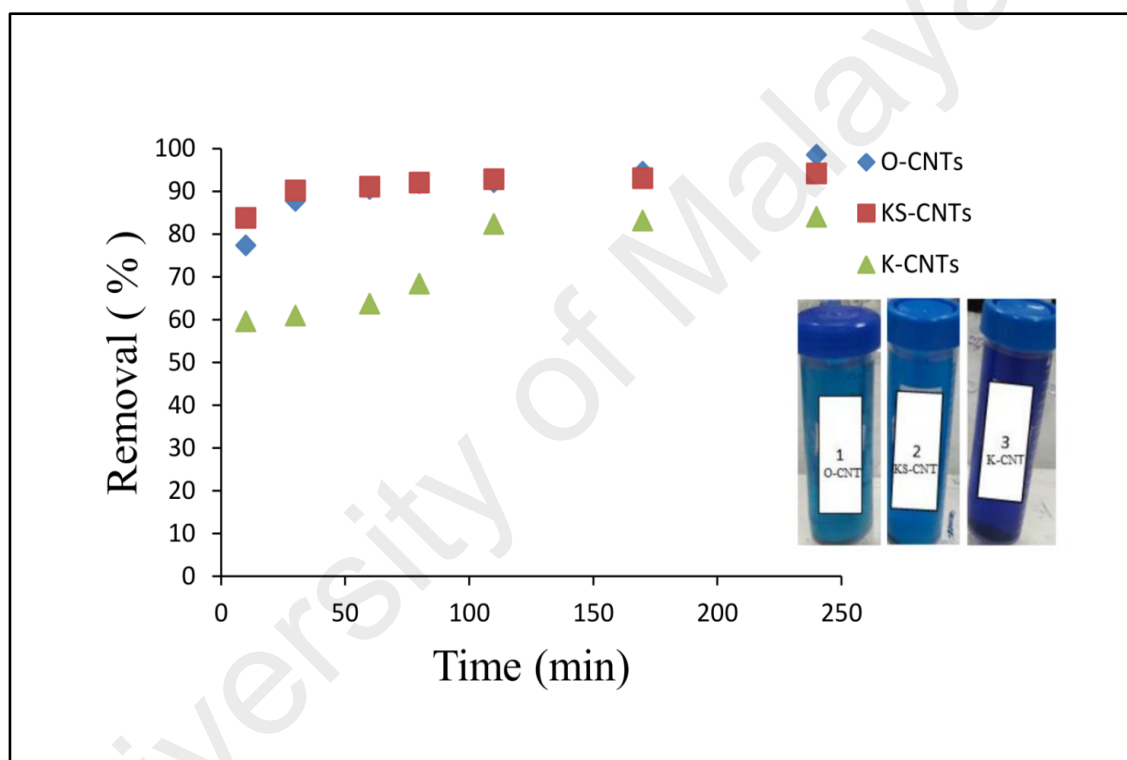


**Figure 6.6: Effect of contact time on the removal efficiency of MB for all adsorbents.**

### 6.3.2 Design of experiment (DOE) for MB adsorption

The adsorption performance of the synthesized O-CNT was evaluated for the removal of methylene blue (MB) from water. The adsorption experiments were conducted according to the CCD matrix selected by the DOE software to analyze the behavior of the removal efficiency (RV3) and adsorption capacity (Q3) under three factors pH (3-11),

dose (5-20), and contact time (10-140). The summary of CCD of experiments produced by DOE software are summarized in Table 6.8. The removal efficiency and adsorption capacity were found to be in the ranges of 20 - 96 % and 49 -148 mg /g, respectively.

**Table 6.8: CCD of experimental parameters for MB removal by O-CNT.**

Run No.	pH	Dose (mg)	Contact time (min)	Removal efficiency % (RV3)	Adsorption capacity (mg/g) (Q3)
1	7	15	140	48.3	80.5
2	8	20	90	54.4	68.0
3	11	15	120	94.3	148.0
4	9	20	90	56.3	70.4
5	11	20	140	96.2	120.3
6	5	15	90	31.0	51.6
7	10	20	60	67.9	84.9
8	8	15	40	33.4	55.7
9	11	10	20	33.2	83.0
10	10	20	60	61.8	86.8
11	11	10	60	59.0	85.3160
12	11	20	135	95.9	119.4
13	11	20	60	87.6	110.0
14	3	5	140	19.8	49.4

### 6.3.3 Analysis of variance (ANOVA)

The regression of the obtained data was performed by the analysis of variance (ANOVA). Thus, an empirical formula relating the removal efficiency of MB (RV3 %) and the adsorption capacity (Q3) to the three input variables were described by the following regression equations:

$$\begin{aligned} \text{Removal efficiency (RV3 \%)} = & 30.9 + 18.7 X_1 + 20.2 X_2 + 20.0 X_3 + \\ & 4.2 X_1 X_2 + 17.6 X_1^2 - 6.36 X_2^2 \end{aligned} \quad (6.3)$$

$$\begin{aligned} \text{O - CNTs adsorption capacity (Q3)} = & 64.3 + 62.7 X_1 - 3.9 X_2 + \\ & 53.2 X_3 - 58.5 X_1 X_2 + 41.9 X_1 X_3 - 80.1 X_2 X_3 + 45.5 X_1^2 \end{aligned} \quad (6.4)$$

Where, the coefficients with pH ( $X_1$ ), adsorbent dose ( $X_2$ ) and contact time ( $X_3$ ) represent the effect of that factor for the adsorption of MB. Coefficients with two factors show the interaction between the two variables.

The competence of the developed models was further justified through analysis of variance (ANOVA) and the results obtained are depicted in Tables 6.9 and 6.10 for both RV3 and Q3, respectively.

**Table 6.9: ANOVA results for MB Removal % (RV3) by O-CNT.**

*Source	Sum of Squares	df	Mean Square	F Value	p-value Prob > F
Model	7060	6	1180	23.1	0.000278
$X_1$	298	1	298	5.85	0.046233
$X_2$	311	1	311	6.11	0.0428
$X_3$	932	1	932	18.3	0.00366
$X_1 X_2$	8.97	1	8.97	0.176	0.687
$X_1^2$	113	1	113	2.23	0.179
$X_2^2$	24.3	1	24.3	0.478	0.511
	R- Squared 0.952			Std.Dev.7.13	
	Adj. R-Squared 0.911			C.V. 12.5	
	Pred. R-Squared 0.833			Adeq. Precesion 15.5	
* $X_1$ : pH, $X_2$ : adsorbent dosage and $X_3$ : contact time; (min)					

**Table 6.10: ANOVA results for the adsorption capacity of O-CNT (Q3).**

*Source	Sum of Squares	df	Mean Square	F Value	p-value Prob > F
Model	10600	7	941	49.3	<0.0001
$X_1$	2490	1	2490	81.4	0.000104
$X_2$	8.96	1	8.96	0.293	0.08
$X_3$	1320	1	1320	43.0	0.000602
$X_1 X_2$	1250	1	1250	40.9	0.00069
$X_1 X_3$	533	1	533	17.4	0.00586
$X_2 X_3$	1400	1	1400	45.7	0.000512
$X_1^2$	676	1	676	22.1	0.00332
	R- Squared 0.983			Std.Dev.5.53	
	Adj. R-Squared 0.963			C.V. 6.37	
	Pred. R-Squared .839			Adeq. Precesion23.5	
* $X_1$ : pH, $X_2$ : adsorbent dosage and $X_3$ : contact time; (min)					

Based on 95% confidence level, the model F-value for MB removal percentage and adsorption capacity were 23.1, 49.3 respectively, which implied that these models were significant. Meanwhile, their probable F values were 0.000278 and  $< 0.0001$  confirming that the model terms are highly significant. The correlation coefficient,  $R^2$  and standard deviation values demonstrate the quality of the model developed.  $R^2$  describes how well the model approximate the actual data points and it describes the ratio between sum of squares (SSR) with total sum of squares (SST). The  $R^2$  values for Equations 6.3 and 6.4 were 0.952 and 0.983 respectively indicating adequate adjustment of the proposed models with the experimental data. The reproducibility of the model was reflected by the small values of the coefficient of variation (CV) and standard deviations. Also, the "Adeq Precision" attained for all the responses suggested that the models can be applied to navigate the design space. The diagnostic test of the performance of the model can also be depicted by the linear plots of the predicted values versus experimental values of the MB removal percentage and adsorption capacity data as shown in Figure 6.7.

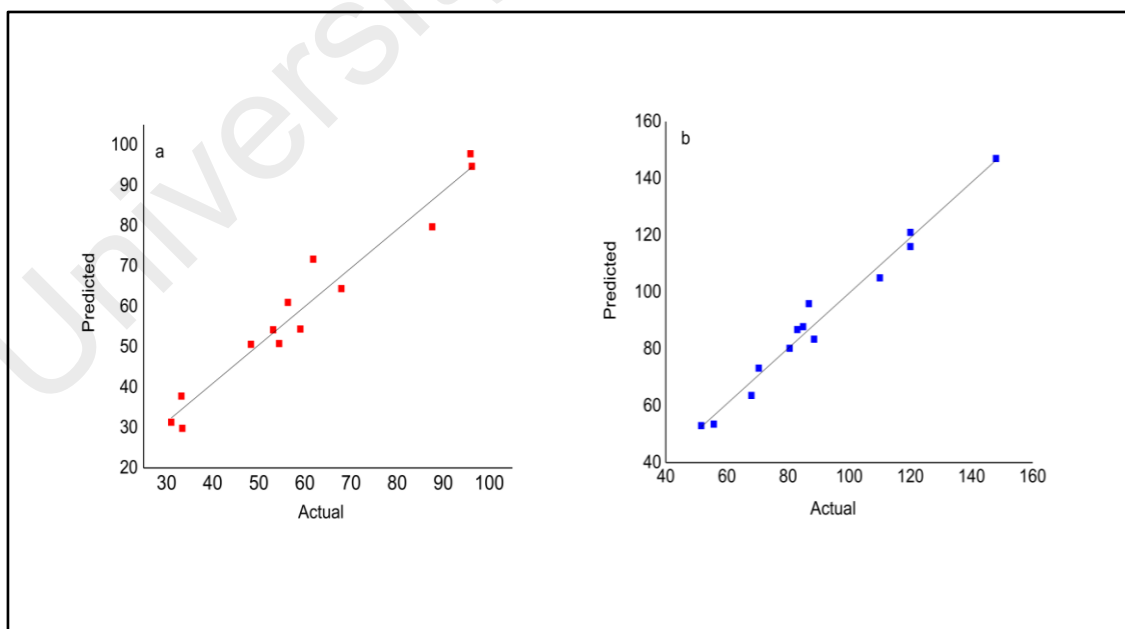


**Figure 6.7: Predicted values vs. actual data for MB adsorption on O-CNT adsorbent (a) removal (%) and (b) adsorbent capacity (mg/g).**

### 6.3.4 The interactive effects of selected parameters on the adsorption of MB on O-CNT

Table 6.11 presents the applied process criteria and their importance levels which were defined for optimization the pH, adsorbent dosage, contact time, RV3% and Q3 to select the optimum conditions for MB removal onto O-CNT adsorbent. Based on the equations (6.3) and (6.4) and the constrains presented in Table 6.11, the software suggested six solutions listed in Table 6.12. Optimal removal conditions were found to be pH 11, adsorbent dosage around 18.1 mg, and contact time of 128 min at initial MB concentration of 50 mg/L. At these optimum values, the predicted and observed MB removal efficiency and adsorbent capacity were 94.7, 148.0 % and 91.63, 146.74 mg/g, respectively.

**Table 6.11: Constraints for optimization process based on CCD for MB adsorption.**

Name	Goal	Low limit	Upper limit	Importance
X <sub>1</sub> (pH)	In range	2	11	3
X <sub>2</sub> (dosage)	In range	5	20	3
X <sub>3</sub> (time)	In range	20	140	3
RV3	Maximize	19.8	96.2	5
Q3	Maximize	49.4	148.0	3

**Table 6.12: Potential optimization conditions based on CCD for MB removal onto O-CNT.**

No.	pH	Dose (mg)	Contact time (min)	RV3 %	Q3 (mg/g)	Desirability	
1	11.0	18.1	128	94.7	148.	0.986	Selected
2	11.0	18.1	139.	94.1	148.	0.982	
3	11.0	18.2	140.	94.5	147.	0.982	
4	11.0	18.0	140.	93.9	148.	0.981	
5	11.0	18.0	135.	93.0	148.	0.974	
6	10.9	17.8	140.	92.1	148.	0.966	

RSM was used to explore all the significant interactions in the CCD and evaluate the relation between input parameters and the obtained response surfaces (Figure 6.8). The enhancement in MB removal and adsorbent capacity in the solution with increasing pH at the optimal time is shown in Figures 6.8 (a) and (b). Figure 6.8 (a) indicates that increasing the solution pH improved the MB removal, and MB was almost completely removed at pH 11. This observation can be attributed to the changes of the adsorbent surface charge and the ionization of the MB dye in basic media (Ansari, Mosayebzadeh, & Mohammad-khah, 2011). At a solution pH higher than the point of the zero charge of the adsorbent ( $pH_{PZC} = 8.0$ ), the adsorbent surface acquired a negative charge. Consequently, electrostatic attraction occurred between the cationic MB molecules and the negatively charged adsorbent surface, leading to an enhanced adsorption. Furthermore, the dye removal efficiency at acidic pH was low probably because of excess  $H^+$  that competed with MB for the adsorption sites of the sorbents (Joseph et al., 2013).

According to the plot of pH versus agitation time at the optimal adsorbent dosage Figure 6.8 (b), the effect of time on adsorption was almost constant (75%) within the pH range of 3.0–8.0, whilst shifting pH to an alkali region led to an enhancement in adsorption regardless of contact time. At pH 11.0 and 128 min of contact time, 96.3% removal was observed. The maximum dyes removed at high pH confirmed the high contribution of the charge and nature of the adsorbent surface during adsorption. The response surface plots demonstrated that the agitation time achieved an enhanced contact between the dye and the adsorbent and the increase in the dose increased the active site concentration. Hence, high values of MB removal were obtained by simultaneously increasing the agitation time and the adsorbent mass.

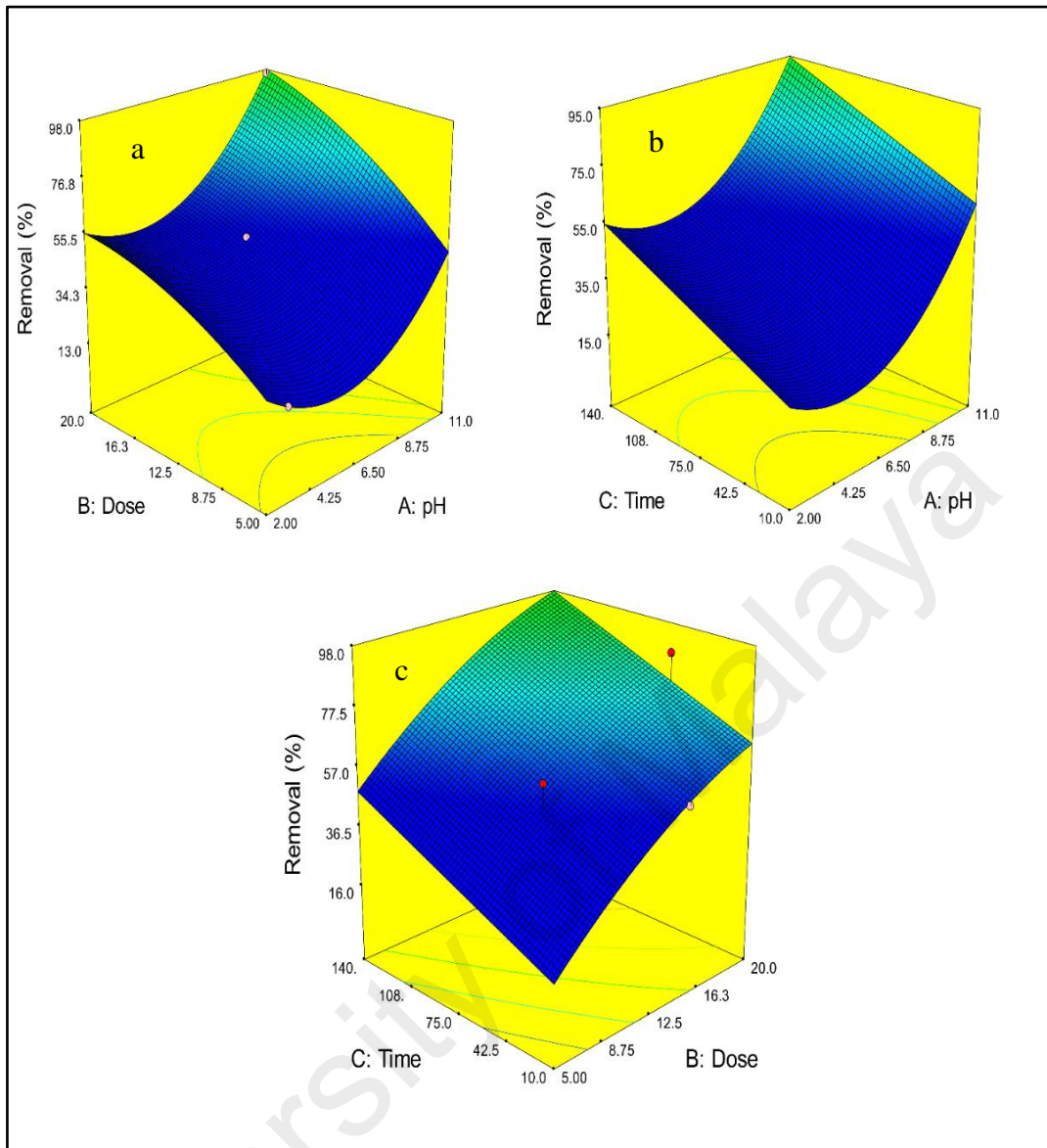


**Figure 6.8: Surface response representation of the interaction of removal efficiency of MB onto O-CNTs with (a) pH and dose, (b) pH and contact time and (c) dose and contact time.**

Referring to Figure 6.9, also the pH has more significant effect on the absorption capacity than the adsorbent dose. In Figure 6.9 (a) the adsorption capacity increased within the range of 5–18.1 mg, and the capacity declined as the O-CNT dosage increased. Similar observations were obtained in a previous literature (Wu, 2007). High adsorbent dosage might increase the viscosity and inhibit the diffusion of MB molecules to the surface of the CNTs (Asmaly et al., 2015). The obtained optimal removal conditions were



used to study the adsorption kinetics and isotherms for MB adsorption on O-CNT adsorbent.

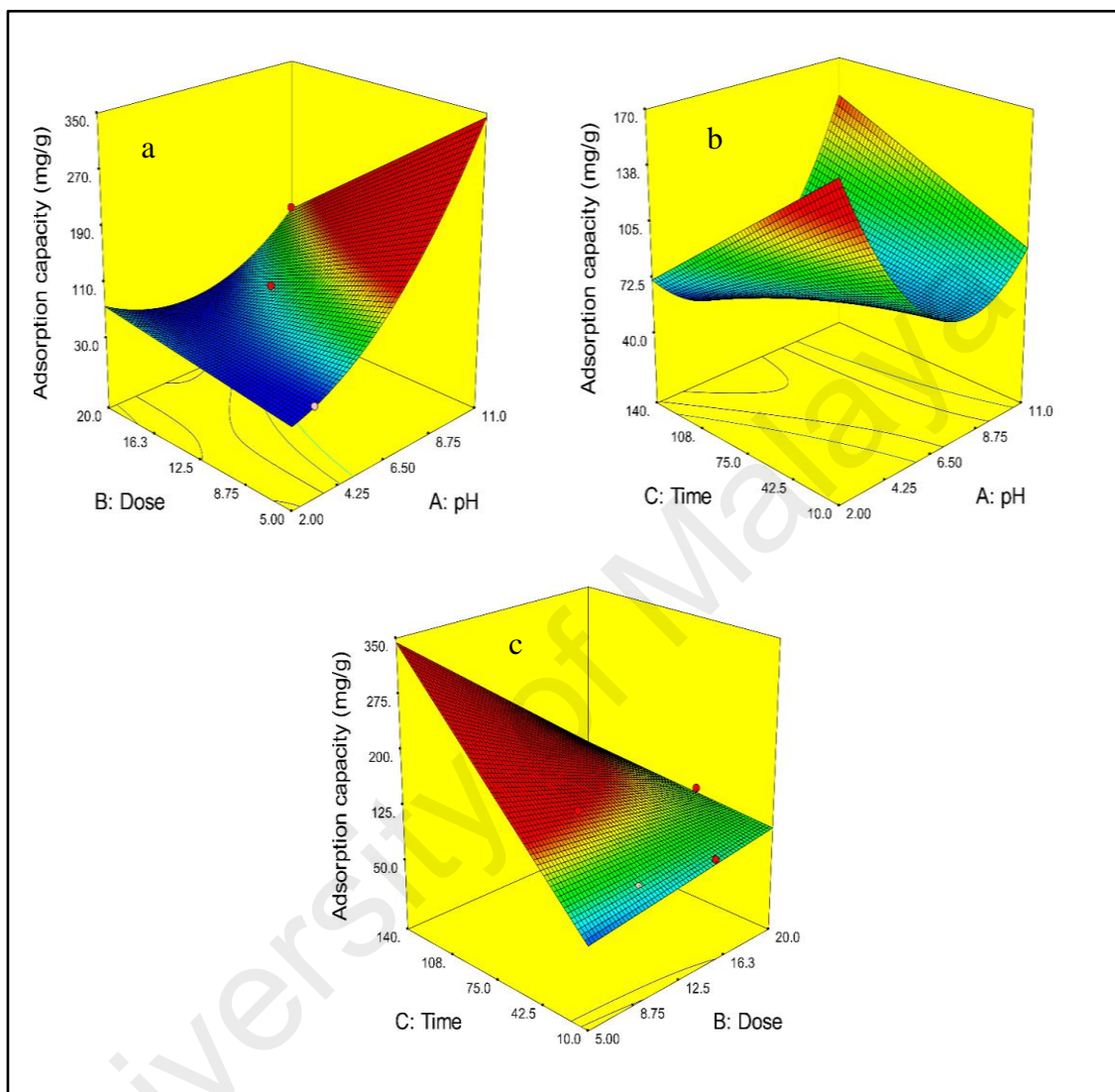


**Figure 6.9: Surface response representation of the interaction of adsorption capacity of MB onto O-CNTs with (a) pH and dose, (b) pH and contact time and (c) dose and contact time.**

### 6.3.5 Adsorption Kinetics

Three well-known kinetic models were utilized at the selected optimum condition to analyze the experimental data for better understanding of the kinetic behavior of MB adsorption on O-CNT; pseudo-first order, pseudo-second order and intraparticle diffusion model. The initial concentration of MB was 50 mg/L and a contact time of 7 h was used to verify the equilibrium condition. Table 6.13 lists all the related kinetic parameters and the correlation coefficients ( $R^2$ ) which were determined by linear regression of the plots displayed in Figure 6.10.

**Table 6.13: Experimental values of constants of adsorption kinetics models.**

Model	Equation	Parameters	Values
Pseudo-First-Order	$\ln(q_e - q_t) = \ln q_e - K_1 t$	$R^2$ $K_1$ $q_e$	0.886 0.027 38.86
Pseudo-Second-Order	$\frac{t}{q_t} = \frac{1}{K_2 q_e^2} + \frac{1}{q_e} t$	$R^2$ $K_2$ $q_e$	0.999 $1.49 \times 10^{-3}$ 122.69
Intraparticle diffusion	$q_t = K_d t^{\frac{1}{2}} + C$	$R^2$ $K_d$ $C$	0.85 1.884 94.736
$q_e$ (experimental) = 120.367 mg/g			

For the pseudo-first-order model, large differences between the experimental and calculated values of the equilibrium adsorption capacity indicated that the adsorption of MB onto the O-CNT did not follow the pseudo-first-order model. By contrast,  $R^2$  of pseudo-second-order model was 0.999, suggesting that the adsorption kinetic was ideally consistent with the pseudo-second-order model. This observation is also in agreement

with some reported kinetic results for MB adsorption on multi-walled CNTs (Fan et al., 2017; Ma et al., 2012). The applicability of pseudo-second-order kinetic model to describe the adsorption of MB implied the possibility of adsorbate and adsorbent involvement in the adsorption mechanism and controlled by chemisorption involving valence forces through exchange or sharing electrons (Zhang, Lan, et al., 2013).

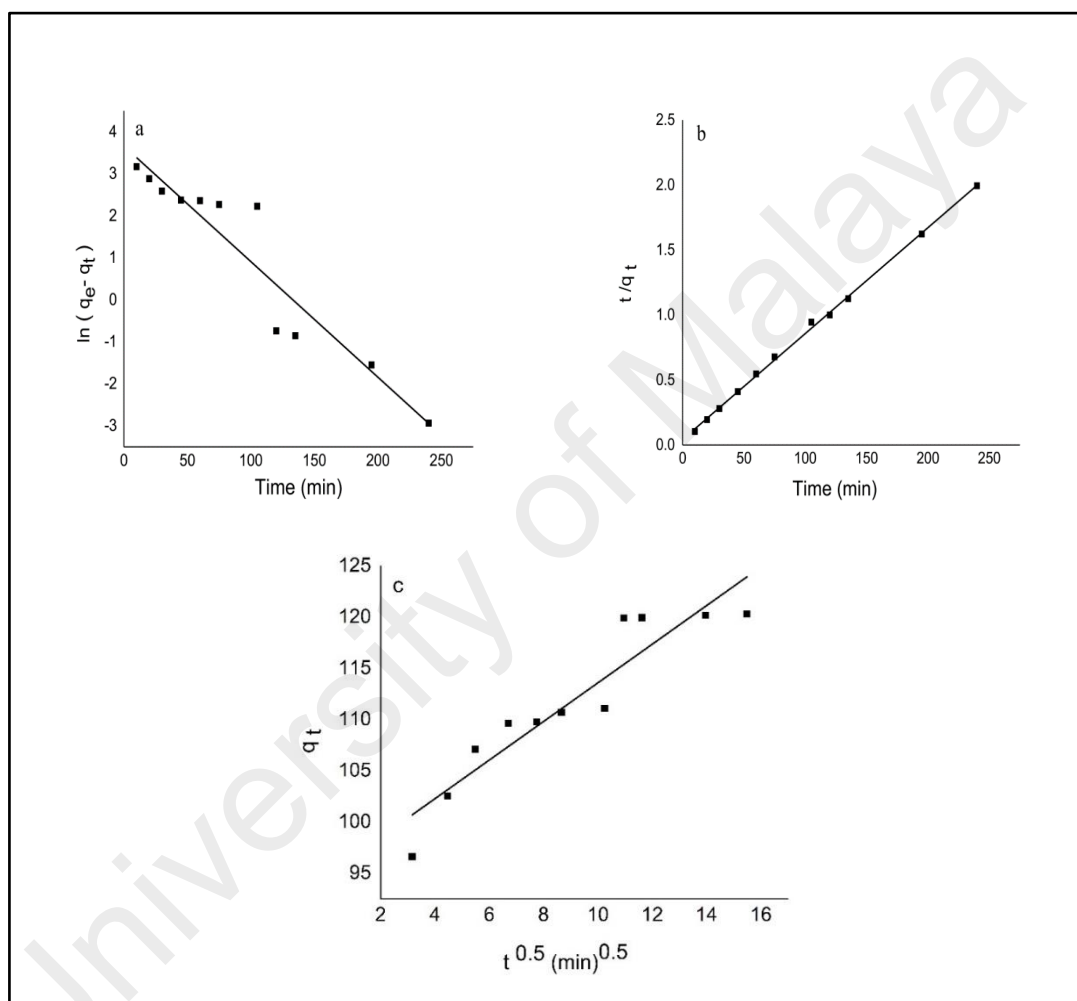


**Figure 6.10: Fittings of different kinetics models for MB adsorption on O-CNT; (a) Pseudo-first order, (b) Pseudo-second order and (c) Intraparticle diffusion at optimum conditions.**

The intraparticle diffusion (ID) model was also investigated for further demonstration of the adsorption behavior of MB on O-CNT adsorbent. The interpretation of the plot of  $q_t$  against  $t^{0.5}$  indicated that the ID was not the only rate-limiting step as long the linear plot did not pass through the origin (Ai & Jiang, 2012b; Altıntug et al., 2017b; Chen & Bai, 2013). Therefore, it can be argued that the adsorption of MB is affected by the involvement of other mechanisms such as the boundary layer diffusion which is confirmed by the high value of the layer thickness ( $C = 94.736$ ). Accordingly, the adsorption of MB begins with rapid diffusion of dye molecules through the bulk solution to the exterior surface of the adsorbent. As result of the saturation of the external surface, a gradual adsorption of the MB through the pores of the interior surface takes place (Vijwani et al., 2015).

### 6.3.6 Adsorption isotherms

The adsorption isotherm describes basically the interaction between the solute and the adsorbent at an equilibrium state. The experimental data was fitted to different types of isotherm models namely Langmuir, Freundlich and Temkin isotherm models. The mathematical equations in the linearized forms were applied to fit the equilibrium data as they are simpler than the nonlinearized form and more commonly used by previous researchers. The linearized plots of the studied isotherms are presented in Figure 6.11 and the associated parameters along with the correlation coefficients are listed in Table 6.14.

The values of Langmuir separation factor ( $R_L$ ) and Freundlich heterogeneity constant ( $n$ ) listed in Table 6.14 confirmed the adsorption favorability of MB for both the Langmuir and Freundlich isotherm models under experimental conditions. This kind of duality is common in adsorption studies (Ai & Jiang, 2012b; Asfaram et al., 2016; Yao et al., 2010). However, the fit of Langmuir isotherm was better with a high  $R^2$  of 0.991 than that of

Freundlich isotherm. This finding indicated the monolayer adsorption of MB onto the homogeneous sites of the O-CNT surface with no interaction between sorbate species. The results agreed well with previous studies which reported that the Langmuir model gave a better fit to explain the experimental data for the adsorption of MB from aqueous solution (Ofomaja, 2008; Rafatullah et al., 2010; Vargas et al., 2011; Zhang et al., 2015). Table 6.15 provides a comparison of the maximum adsorption capacity of MB on several adsorbents. Compared with those in previous studies, a significant maximum adsorption capacity of 174.52 mg/g was observed in the as-prepared O-CNT adsorbent in this study.

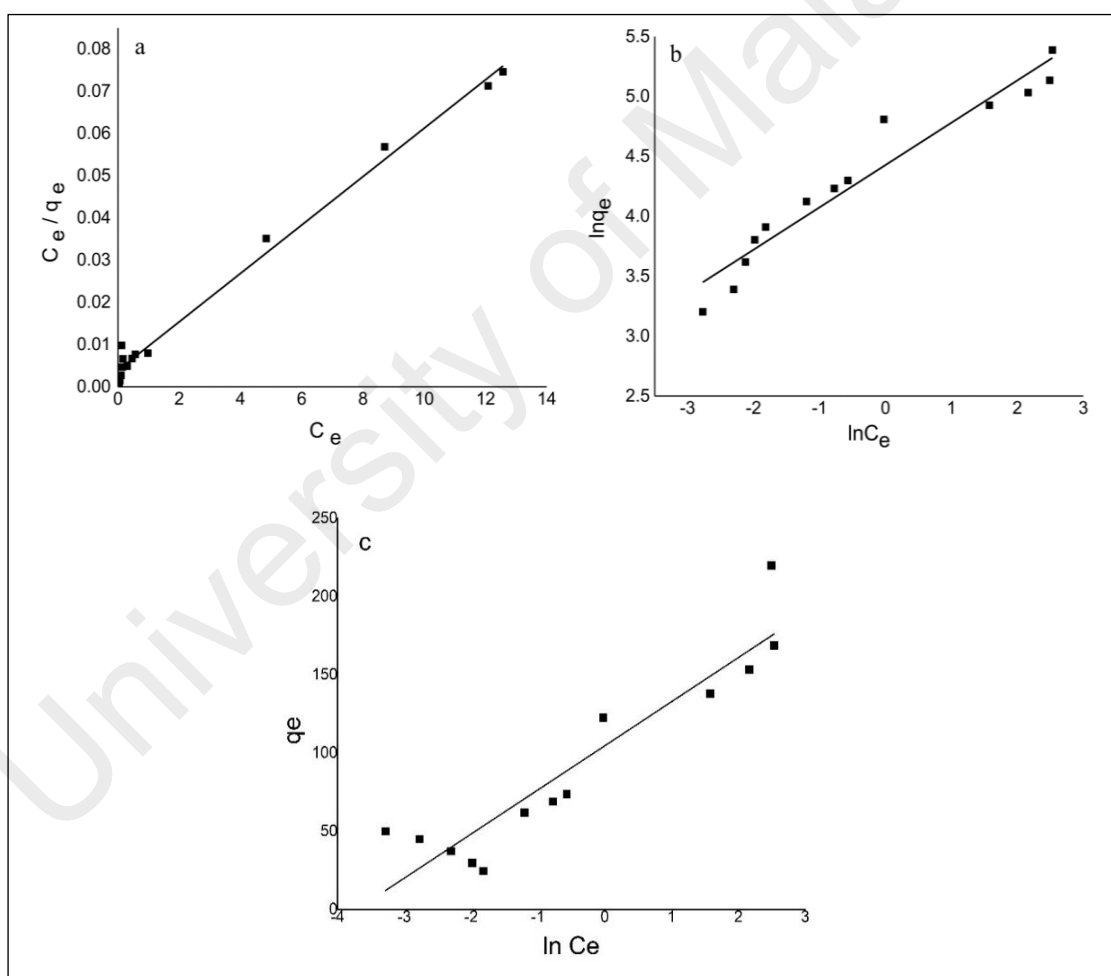


**Figure 6.11: The isotherm plots for MB adsorption on CNM-PAC; (a) Langmuir, (b) Freundlich, and (c) Temkin model.**

**Table 6.14: Linearized equations of studied isotherm models for MB adsorption on O-CNT.**

Model	Equation	Parameters	Values
Langmuir	$\frac{C_e}{q_e} = \frac{1}{K_L q_m} + \left(\frac{1}{q_m}\right) C_e$	$R^2$	0.991
		$q_m$	174.52
		$K_L$	1.454
		$R_L$	0.0138
Freundlich	$\ln q_e = \ln K_f + \frac{1}{n} \ln C_e$	$R^2$	0.932
		$K_f$	83.734
		$n$	2.8
Temkin	$q_e = B_1 \ln K_T + B_1 \ln C_e$	$R^2$	0.854
		$K_T$	40.99
		$B_1$	28.18

**Table 6.15: Comparison between the maximum adsorption capacity ( $q_m$ ) of O-CNT and other reported adsorbents for MB removal.**

Adsorbent	$q_m$ (mg/g)	Reference
O-CNT	174.52	The present work
MWCNTs	109.31	(Zohre, Ataallah, & Mehdi, 2010)
Calcined titanate nanotubes	133.33	(Xiong et al., 2010)
MWCNTs produced by CVD (acetylene cracking on Fe/Si)	50.25	(Liu et al., 2014)
Cotton stalk	147.06	(Deng et al., 2011)
graphene/magnetite composite	43.08	(Ai, Zhang, & Chen, 2011)
Activated carbon	123	(Suresh, Sugumar, & Maiyalagan, 2011)
ZnS:Cu nanoparticles loaded on activated carbon	106.95	(Asfaram et al., 2015)
Sugar beet pulp	714.29	(Vučurović, Razmovski, & Tekić, 2012)
Powdered activated carbon	91.0	(Yener et al., 2008)
polydopamine microspheres	88.89	(Fu et al., 2015)
Self-assembled graphene-CNT	81.97	(Ai & Jiang, 2012a)
Oxidized-CNTs	99.83	(Norzilah et al., 2011)

### 6.3.7 Mechanisms

It is important to understand the mechanism of MB adsorption that results in the apparent behavior of the system. The afore investigations of the impact of different parameters on the adsorption process along with the demonstration of the kinetic models indicated that the pH factor has a remarkable influence on the removal of MB. It is worthy to mention that fitting the experimental data with the intraparticle diffusion model (ID) was useful technique to identify the mechanism involved in the sorption process. The solute transfer in a solid/liquid sorption process is usually designated by either the boundary layer diffusion (external mass transfer) or intraparticle diffusion or both. Thus, the mechanism of MB removal from aqueous phase by adsorption is expected to consist of four steps: (i) transfer of the MB molecules from the bulk solution to the surface of the O-CNT adsorbent, (ii) boundary layer diffusion through the surface of the adsorbent, (iii) adsorption of dye at an active site on the surface of O-CNT and (iv) intraparticle or pore diffusion by which MB adsorption takes place onto the interior sites of the adsorbent (Etim et al., 2013; Sanghi & Verma, 2013; Yagub, Sen, Afroze, et al., 2014). Figure 6.10 (c) showed that the adsorption plot was not linear over the whole-time range and can be divided into two to three linear regions which confirm the multi-stages of adsorption. The rapid earlier stage signified by the external mass transfer through film diffusion followed by the slower intraparticle diffusion through the pore after the adsorbent sites are loaded with dye ions. Moreover, from the same figure, it can be concluded that the film diffusion and intraparticle diffusion happen concurrently as confirmed by the linear plot which did not pass through the origin (Yagub, Sen, & Ang, 2014).

As already mentioned, poor removal efficiency of MB on O-CNT was observed at low pH value and it enhanced as pH value increased until it reached its maximum value at pH11. The ionization degree of the adsorbate molecule and the surface properties of

the adsorbent are highly influenced by the variation of the pH value. Thus, the low pH leads the surface of adsorbent to acquire to an increase positive charge by absorbing  $H^+$  and less amount of cationic dye adsorption takes place. Furthermore, the higher MB adsorption under basic condition may be attributed to the electrostatic attraction between the cationic species of MB with the negatively charged surfaces ( $pH > pH_{PZC}$ ). Meanwhile, MB is a planar molecule with aromatic backbone and the O-CNT adsorbent contains abundant aromatic rings, therefore, the  $\pi$ - $\pi$  stacking interactions could occur between MB molecules and O-CNT adsorbent. A similar behavior was observed for methylene blue adsorption on Neem (*Azadirachta indica*) powder (Bhattacharyya & Sharma, 2005), on sawdust and crushed brick (Hamdaoui, 2006), on cashew nut shell (Kumar, Ramalingam, & Sathishkumar, 2011) and on carbon nanomaterials (Gong, Liu, Chen, et al., 2015; Li, Du, et al., 2013). Furthermore, the high adsorption of MB on as-synthesized O-CNT indicated that there were very strong van der-Waals forces and hydrophobic interactions between the carbon nanomaterial and the dye (Tan et al., 2015). This observation leads to the conclusion that, even though adsorption of cationic species on KSCNT was enhanced by the presence of surface acid groups, O-CNT still present better performances, indicating that dispersive interactions between the delocalized  $\pi$  electrons on the surface of the CNTs and the free electrons of the dye molecule present in the aromatic rings and multiple bonds play a dominant role in the adsorption mechanism (Rajabi, Mahanpoor, & Moradi, 2017). These dispersive interactions were improved by the thermal treatments of the Ni-PAC substrate. Fernando et al, (2003) reported that the thermal treated samples of activated carbon exhibited higher removal performances for the adsorption of basic dyes than the acidic treated samples (Pereira et al., 2003). Their results showed that one of the most important adsorption mechanisms involves the interaction between the delocalized  $\pi$  electron of the carbon surface and the



free electrons of the dye molecule (aromatic rings and  $-N=N-$  or  $-N=C-C=C-$  bonds) (Martín-Jimeno et al., 2015).

### 6.3.8 Summary of the adsorption of MB onto O-CNT

The key findings of this study can be summarized as following:

- 1- The synthesized O-CNT was used to prepare two modified adsorbents:
  - (a) KSCNT produced after modifying O-CNT with  $KMnO_4/H_2SO_4$
  - (b) K-CNT produced after modifying O-CNT with  $KMnO_4$
- 2- Three adsorbents O-CNT, KS-CNT and K-CNT were examined via a separate primary screening study for the removal of MB. The O-CNT demonstrated the highest removal efficiency for MB and was selected for further adsorption studies.
- 3- The optimum removal conditions for MB removal were detected by using RSM-CCD experimental design. The removal efficiency and adsorption capacity were chosen as the adsorption process responses and the ANOVA was used to establish their empirical equations. The optimum conditions suggested by the optimization process were found at pH 11, adsorbent dosage of 18.1 mg and contact time of 128 min.
- 4- The adsorption kinetics for O-CNT adsorbent was well fitted by pseudo-second order model and the equilibrium adsorption data was best described by Langmuir isotherm model indicating a monolayer adsorption of MB on a homogeneous surface with a maximum adsorption capacity of 174.52 mg/g.
- 5- MB adsorbed on O-CNT adsorbent increased with pH values suggested that the adsorption resulted from electrostatic attraction between the negatively charged O-CNT adsorbent surface and the positively charged cationic dyes in addition to dispersive interactions.

## CHAPTER 7: CHARACTERIZATION OF CNM-PAC SYNTHESIZED FROM ACETYLENE DECOMPOSITION

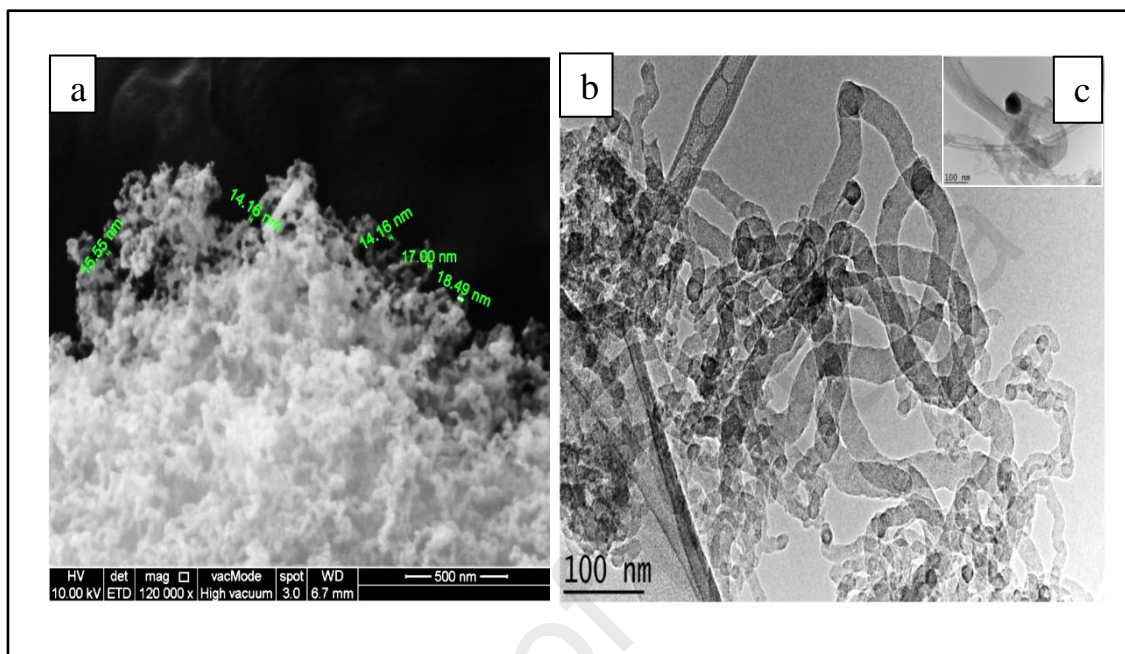
### 7.1 FESEM and TEM analyses

The FESEM and TEM images in Figure 7.1 display the morphology of the deposited product obtained by decomposition of  $C_2H_2$  onto Ni-PAC. At the optimized growth conditions (550 °C, 37.3 min, and gas ratio 1.0), dense CNTs with tubular structures were dominant in the product microscopic analyses (Figure 7.1 (a)). The TEM image presented in Figure 7.1 (b) shows the presence of well-graphitized CNTs with an outer diameter of 10–40 nm with a closed tip tilted from the vertical direction and nucleated from Ni particle of average diameter size of 70 nm (Atthipalli et al., 2011; Sugime et al., 2015).

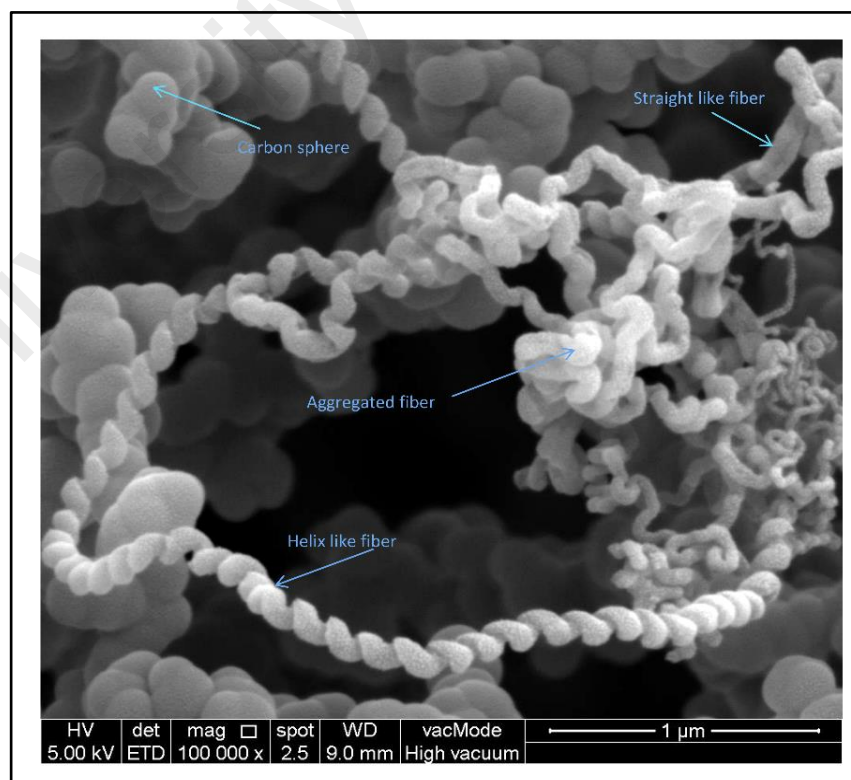
However, the synthesized CNTs walls had some defects because  $H_2$  and  $C_2H_2$  strongly reduced the oxidized catalysts, and the produced oxygen might etch the carbon tube surface into deep pits (De Greef et al., 2015). The encapsulation of catalytic particle at the tip (Figure 7.1 (c)) suggested that the growth of CNTs followed the tip growth mechanism induced by the weak interaction between Ni and PAC (Li et al., 2000; Vander Wal, Ticich, & Curtis, 2001). It is noteworthy the SEM analysis showed no trace of amorphous agglomerated carbon which is attributed to the low synthesis temperature (550 °C) and hence significantly inhibits the spontaneous pyrolysis of gaseous hydrocarbon into amorphous carbon (Pham-Huu et al., 2006). Meanwhile, the synthesis temperature is also closely dependent on the nature of the gaseous carbon source which was confirmed by different optimum growth temperature for  $CH_4$  and  $C_2H_2$  in our study.

Figure 7.2 shows the produced carbon nanomaterials under the decomposition of  $C_2H_2$  at 750 °C, 20 min and gas ratio 1.0. The image confirmed the important role of the reaction temperature on the growth of CNMs. The FESEM image displayed carbon nano-fiber

(CNF) with an average diameter of 75-95 nm, and nano-coil fibre. These observations, unlike those described in previous studies which yielded single type of CNF (Chen, Su, et al., 2007; Chen, Timpe, et al., 2009a).



**Figure 7.1: FESEM and TEM images of O-CNT.**



**Figure 7.2: FESEM image of CNT, CNF, CS and helix cum produced at 750 °C.**

## 7.2 Raman spectroscopy

Raman spectroscopy technique was conducted to analyze O-CNT and KS-CNT. As common with Raman spectra of graphene based materials (Figure 7.3), the prominent peaks at  $\sim 2800\text{ cm}^{-1}$ ,  $1580\text{ cm}^{-1}$ , and  $1340\text{ cm}^{-1}$  refers to G', G and D bands (Dresselhaus et al., 2010). As can be noticed from the figure, two obvious sharp peaks were observed: the first at  $\sim 1340\text{ cm}^{-1}$  (D band) and the second at  $\sim 1600\text{ cm}^{-1}$  (G band). The peak at  $1300\text{--}1400\text{ cm}^{-1}$  is the D band which is a defect-induced mode caused by  $sp^3$ -hybridized carbon atoms in the sidewall of CNT and is often attributed to the disordered structure of graphite. By comparison, the common tangential mode to all  $sp^2$  carbon systems and graphitic layers produce a stretching C–C vibration characterised by the G band at high ranges of Raman shift ( $1550\text{--}1650\text{ cm}^{-1}$ ) (Hernadi et al., 2000; Li et al., 1997). The strong G peak suggested that the CNTs synthesised in activated carbon at  $550\text{ }^\circ\text{C}$  were highly graphitised, and the relatively high intensity of the D band for the CNTs in PAC confirmed the defective and curly structure of CNTs. It seems that the synthesized CNT-PAC can be significantly influenced by the nature of the support (Pham-Huu et al., 2006). The high degree of graphitization of the as-synthesized O-CNT could be attributed to the nature of the support as well as the presence hydrogen in the feed. Park and Keane (Park & Keane, 2004) reported similar findings from their study which demonstrate the contribution of the support in the generation of CNMs by CVD. Another Raman feature to identify the tube diameter is radial breathing mode. No peaks were detected at  $<400\text{ cm}^{-1}$ , indicating that the concerned adsorbents possessed a large diameter (Jorio et al., 2003). The ratio between the areas of these two bands ( $I_G/I_D$ ) was used to quantify the degree of purification of multi-wall CNTs. The lower intensity of D band than that of G band in O-CNT indicated the low amount of amorphous carbon present in the structure.  $I_G/I_D$  for KS-CNT increased from 1.85 to 2.59, implying that the graphitic quality of the

modified CNTs in terms of the amorphous carbon content of the samples is enhanced (Datsyuk et al., 2008; Gómez et al., 2016) .

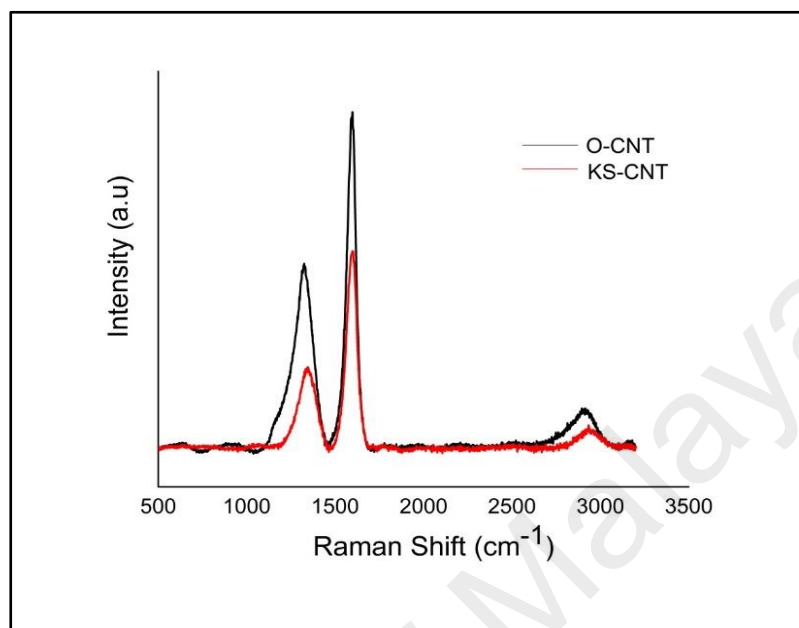


**Figure 7.3: Raman spectrum of O-CNT and KS-CNT.**

### 7.3 Thermogravimetric analysis (TGA)

TGA was performed to measure the purity, defects and overall quality of CNT-PAC. Figure 7.4 shows the TGA results of O-CNTs, KS-CNTs and after-adsorption sample which referred to as O-CNTs-MB. TGA reflects the stability of carbonaceous compounds at a given temperature. No weight loss was observed for O-CNTs at the degassing temperature range from 100 to 400 °C , indicating the absence of oxygenated functional groups (Avilés et al., 2009; Nazal et al., 2016). As reported in previous study, the drastic weight loss in O-CNTs at above 500 °C is related to the oxidation of disordered or amorphous carbon and other metal impurities (Dillon et al., 2000). The initial gradual weight change was reduced by 2% and 5% for O-CNT-MB and KS-CNTs at approximately 100 °C due to moisture evaporation, respectively. Then a steep drop in the weight occurred as the temperature increased. The onset combustion of O-CNTs, O-CNTs-MB and KS-CNTs were 454.97, 449.7 and 423.52 °C, respectively. The

combustion profile of the samples suggested that the thermal stability and purity of O-CNTs were higher than those of O-CNT-MB and KS-CNTs. Functionalization with  $\text{KMnO}_4/\text{H}_2\text{SO}_4$  caused a reduction in the onset of adsorbent combustion due to the presence of various kinds of functional groups that have low activation energy for oxidation, as demonstrated in the FTIR section. The weight loss of KS-CNT adsorbent was 3.21% at  $>690^\circ\text{C}$ , whilst the remaining weight of O-CNTs was 7.36% at the same temperature. This finding indicated that the metal particles were successfully removed through oxidation. After MB was adsorbed (OCNTs-MB), the residues remained almost the same as those of O-CNTs (6.96%), thereby contributing to the metal percentage in the CNT materials.

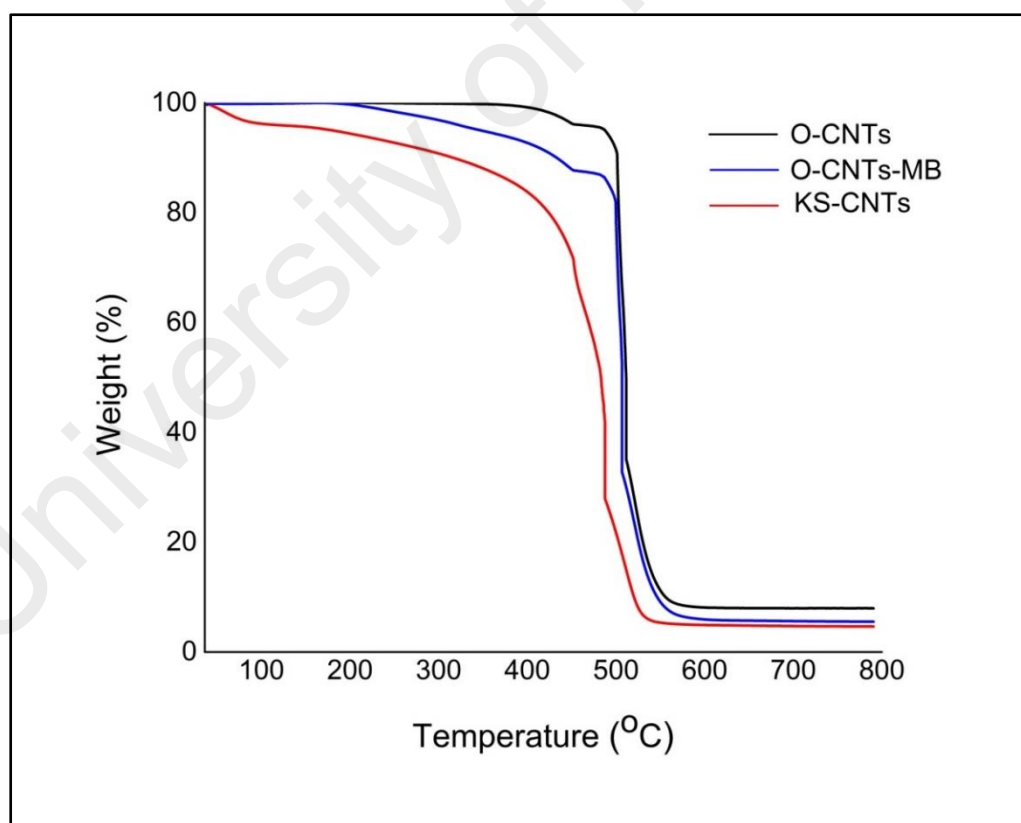


**Figure 7.4: TGA curves for O-CNTs, O-CNTs-MB, and KS-CNTs.**

#### 7.4 Surface chemistry analysis (FTIR)

The corresponding FTIR spectra of O-CNTs, free MB and O-CNTs -MB are shown in Figure 7.5. The spectrum of O-CNTs shows important absorption bands at 3400–3500  $\text{cm}^{-1}$  (assigned to OH stretching), 2854–2960  $\text{cm}^{-1}$  (corresponding to the aliphatic C-H stretch of CH, CH<sub>2</sub> or CH<sub>3</sub>), 1631  $\text{cm}^{-1}$  (attributed to conjugated C=C stretching), and 1097  $\text{cm}^{-1}$  (assigned to C–O stretch in alcohols). The presence of these functional groups on the untreated CNTs implied that they are introduced during manufacturing (Machado et al., 2011a). In addition, O-CNT showed a peak centered around 550  $\text{cm}^{-1}$  ascribed to the stretching of NiO bond because most metal oxides displayed their absorption bands at 400 - 1000  $\text{cm}^{-1}$  (Makino et al., 1992). In MB, the peaks at 1088, 1312 and 1590  $\text{cm}^{-1}$  corresponded to CH<sub>3</sub>–, C–N, C=S, respectively (Gong, Liu, Jiang, et al., 2015). Some peaks shifted or appeared after MB adsorption on CNTs. The peak at 1618  $\text{cm}^{-1}$  shifted to 1602  $\text{cm}^{-1}$  suggesting that nitrogen-containing functional groups might participate in the adsorption. In addition, the peak of the NH<sub>2</sub> group shifted from 1522  $\text{cm}^{-1}$  in the spectrum of O-CNT-MB to 1540  $\text{cm}^{-1}$ . The peaks of 1388 and 1331  $\text{cm}^{-1}$  disappeared, implying that –CH<sub>3</sub> and aromatic nitro groups from MB were involved in the interaction between MB and CNTs. The peaks associated with =CH (681  $\text{cm}^{-1}$ ) and C–O (1066  $\text{cm}^{-1}$ ) of O-CNTs showed a significant decrease in intensity possibly attributed to the electrostatic attraction between O-CNTs and MB. Also, the axial deformation vibrations of the C–N bond of aliphatic amines and the axial deformation of the C–N bond of the aromatic amines were detected at 1020-1250  $\text{cm}^{-1}$  and 1266-1342  $\text{cm}^{-1}$ , respectively.

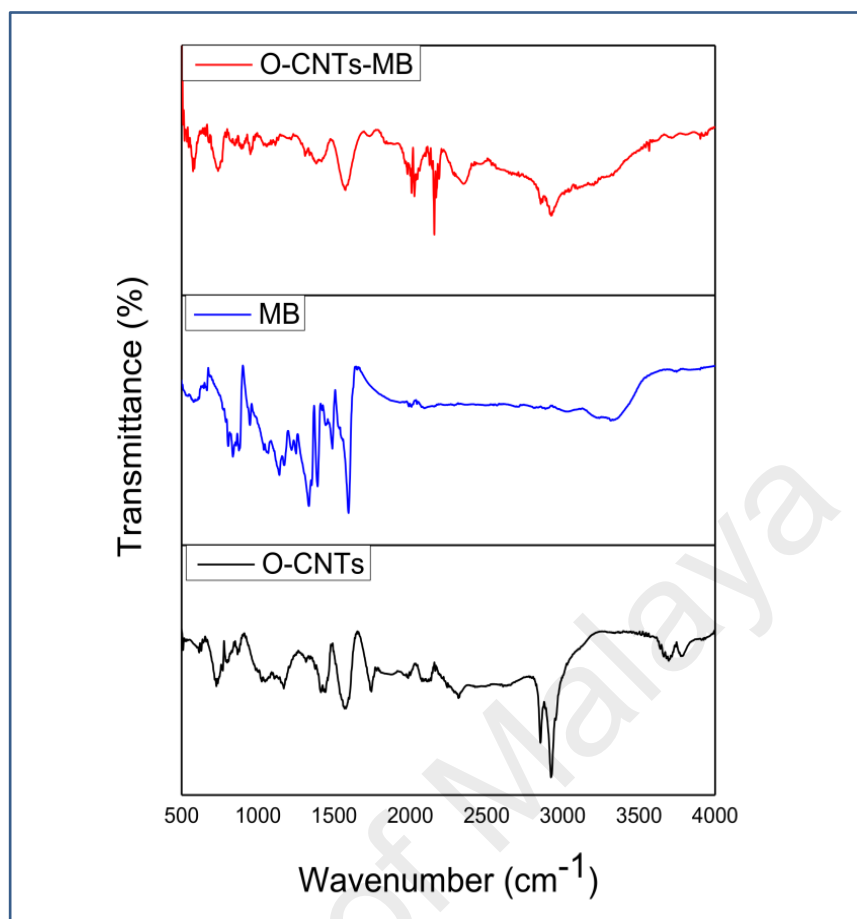


**Figure 7.5: FTIR spectrum for O-CNTs, MB and O -CNTs-MB.**

### 7.5 BET Surface area

The BET surface areas for PAC, Ni-PAC, O-CNTs, and KS-CNTs were investigated. Table 7.1 lists the BET surface area, total pore volume and average pore diameter. The loading of Ni onto the PAC support decreased the pore volume of the support likely because of the blockage of the PAC pores by the impregnated catalyst, resulting in a reduced surface area. The BET surface area of the O-CNTs produced under the optimized conditions significantly enhanced ( $333.83 \text{ m}^2/\text{g}$ ) due to the extra active surface added onto the PAC. Such an enhancement represented the good sorption capacity of such materials. The total pore volume of O-CNTs reached  $0.44 \text{ cm}^3/\text{g}$  compared with that of PAC ( $0.09 \text{ cm}^3/\text{g}$ ). The surface area and the pore volume decreased after  $\text{KMnO}_4/\text{H}_2\text{SO}_4$



was functionalized. The decrease in the surface area is a result of the removal of carbon species with a high chemical potential (Hernadi et al., 2001; Xie, Zhang, & Varadan, 2005).

**Table 7.1: Summary of BET results for PAC, Ni-PAC, O-CNTs, and KS-CNTs.**

Property	PAC	Ni-PAC	O-CNTs	KS-CNTs
BET surface Area (m <sup>2</sup> /g)	101.1	97.2	333.83	198.29
Total pore volume (cm <sup>3</sup> /g)	0.09	0.07	0.44	0.25
Average pore diameter (°A)	34.89	21.29	65.09	69.27

## 7.6 Zeta potential

The adsorption processes are greatly affected by Several factors, including pH, particle surface, ionic strength, conductivity and temperature, influence the measurements of zeta potential (AlOmar et al., 2016). In this study, 10 mg of PAC, Ni-PAC, O-CNTs and KS-CNT was dispersed in deionised water. Table 7.2 shows that high absolute values of zeta potential were obtained at high synthesis temperatures. Subsequently, the dispersibility of the produced material was enhanced. The results showed that the absolute values of zeta potential increased from 34.3 to 46.0 for O-CNTs and KS-CNTs. As revealed in the FTIR spectra, the increase in the absolute value of zeta potential could be due to the presence of numerous oxygen-containing groups, such as carbonyl, carboxyl and hydroxyl groups (Gao et al., 2009). Moreover, the treatment of O-CNTs with KMnO<sub>4</sub>/H<sub>2</sub>SO<sub>4</sub> increased the hydrophilicity of the adsorbent which enhanced the stability of the suspension of O-CNTs in the aqueous solution (Premkumar, Mezzenga, & Geckeler, 2012). The surface charge assessed by the point of zero charge (pH<sub>PZC</sub>) is defined as the point where the zeta potential is zero. When pH < pH<sub>PZC</sub>, the surface charge is positive, and when pH > pH<sub>PZC</sub>, the surface charge is negative. In this case, the pH<sub>PZC</sub>

of O-CNTs determined by the pH drift method (Figure 7.6) is about 8.0 and the analysis revealed a small size mode between 10-100 nm.

**Table 7.2: Zeta potential results for PAC and the different carbon structures produced.**

Sample	Zeta potential (mV)
PAC	- 42.6
Ni-PAC	+1.67
O-CNTs (550°C)	- 34.3
CNF (750°C)	- 38.7
KS-CNTs	- 46.0

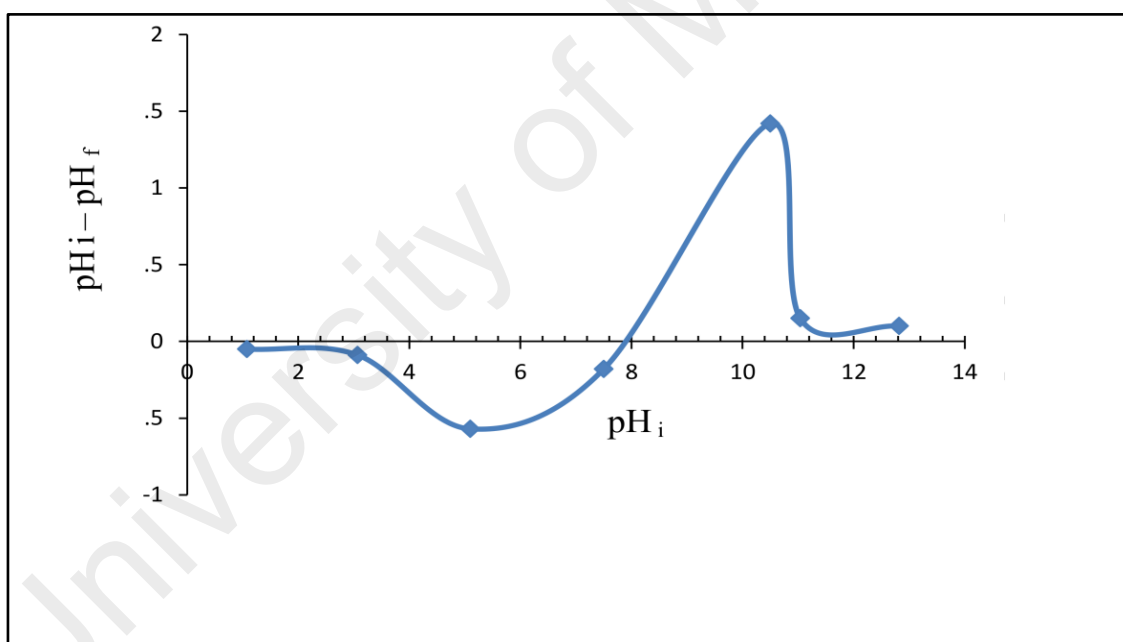


**Figure 7.6: Determination of the point of zero charge of the O-CNTs by the pH drift.**

## 7.7 Summary of characterization

The main findings of the characterization study are:

- 1- The metal-catalyzed CVD growth under acetylene decomposition produced dense CNTs on the PAC substrate. The results showed the pores in PAC can load catalyst particles which exhibit effective catalytic activity to CNTs formation. This observation confirms that utilizing powder activated carbon as a support material seems the most promising.
- 2- Growth temperature has a significant impact on the quality of the synthesized CNMs. Different types of CNMs were observed from the pyrolysis of  $C_2H_2$  at high reaction temperature.
- 3- The high graphitization of O-CNT and the low formation of amorphous carbon produced at the optimum growth conditions could be due to the low reaction temperature and the presence of  $H_2$  in the feed flow. Hydrogen permits the saturation of graphite edges and prevents the formation of amorphous carbon.
- 4- The high temperature (750 °C) was not favorable for the growth of good quality CNTs as the products were fibrous and twisted tubes
- 5- The growth of CNTs onto the carbon support contributes to the improvement on the surface area when compared with the raw PAC, thus the enhancement of adsorption performance is expected.
- 6- The point of zero charge (PZC) of O-CNT determined by the pH drift method was 8.0 and the zeta potential of the KS-CNT sample showed significant improvement in surface double layer negative charge.

## CHAPTER 8: CONCLUSIONS AND RECOMMENDATIONS

### 8.1 Conclusion

In persuasion of developing an affordable technique to treat wastewater containing organic pollutants, synthesizing carbon nanomaterials (CNMs) on the surface of Ni<sup>2+</sup> impregnated powdered activated carbon (PAC) from two different carbon sources was adopted for removal of organic pollutants from water. Statistical analysis of the experimental data was evaluated using ANOVA and the adequacy of the suggested regression models were investigated. The synthesizing conditions were optimized using RSM-CCD method. The as-grown CNM-PAC was used for removal of bisphenol A and methylene blue dye from aqueous solution. The synthesizing approach was conducted by CVD reactor and the adsorption experiments were carried out in conventional shake flasks. The characterization of the selected adsorbent synthesized at the optimal growth conditions included FESEM, TEM, EDA, TGA, Raman spectroscopy, BET and zeta potential. The RSM-CCD experimental design was used to optimize the adsorption parameters including pH of the solution, adsorbent dose and contact time. The removal efficiency and adsorption capacity were chosen as process responses and ANOVA was used to develop the adequate empirical equations. Additionally, kinetic and adsorption isotherm studies were investigated for the adsorption systems at the optimum removal conditions for both pollutant.

#### 8.1.1 Synthesizing of carbon nanomaterials on powder activated substrate from methane decomposition

Based on the overall experimental observations discussed in Chapter 4 and 5, the conclusions can be listed below:

- 1- The RSM- CCD was utilized to optimize the synthesizing conditions of CNM-PAC from CH<sub>4</sub> decomposition. The yield % of the CNM-PAC and removal % of organic pollutant were investigated for the input growth parameters (reaction temperature, growth time and feed stock gas ratio). The optimization method showed the optimal conditions were achieved at reaction temperature of 933°C, growth duration of 20 min and gas ratio of 1.0.
- 2- The DOE clearly revealed that the growth temperature (A), growth time (B) and gas ratio (C) were important parameters influencing the growth of the CNM-PAC and its adsorption performance. However, the effect of growth temperature played the most significant role for producing CNM-PAC.
- 3- The regression models were appropriate and adequate in predicting the responses. They were effectively developed to describe the correlation between the synthesizing variables and the responses of the yield and removal percentage.
- 4- The selected optimum sample characterization demonstrated the following characteristics: The FESEM and TEM images indicated that the synthesized multi-structure possessed of short intercalated CNTs which were well dispersed and stabilized uniformly in the PAC matrix. Raman spectroscopy has confirmed the graphitic structure of CNM-PAC hybrid and the TGA profile proved the stability of the synthesized CNM-PAC hybrid with onset temperature of 507 °C. The CNM-PAC hybrid established surface area of ~165.0 m<sup>2</sup>/g and total pore volume of 0.29 cm<sup>3</sup>/g. FTIR results indicated the presence of different functional groups such as carbonyl, hydroxyl, and carboxylate.
- 5- The optimum process conditions for the adsorption of BPA and MB dye with initial concentration of 50 mg/L on CNM-PAC hybrid were performed by the RSM-CCD approach. The optimization study revealed that the adsorption of BPA

and MB was highly dependent on the pH of the solution and on the surface charge of the adsorbent as well as the  $pK_a$  of the adsorbate. The optimal conditions of BPA removal were obtained at pH of 3.0, adsorbent dose of 15.6 mg and contact time of 120 min. However, the maximum removal efficiency of MB was observed at the optimal conditions of pH 11.0, adsorbent dosage 12.3 mg and contact time of 120 min.

- 6- The BPA and MB adsorption kinetics for the synthesized CNM-PAC hybrid were well presented by pseudo-second order model suggesting chemisorption as the feasible mechanism for adsorption and the adsorbent-adsorbate system studied were mainly governed by external mass transport. The equilibrium adsorption data for BPA and MB dye was well described by Langmuir isotherm model indicating a monolayer adsorption on a homogeneous surface with a maximum adsorption capacity of 181.81 and 250 mg/g, respectively.

It is obvious from the results that the synthesized CNM-PAC hybrid was obtained at the lowest growth time, while the quality of obtained material was not compromised. This reduce the overall cost and energy use for synthesizing CNMs, not to mention that the growth of CNM on PAC produced a multi-structure network and unlike other CNMs prepared on metal oxides or silica substrates can be used directly in the adsorption processes without removing the substrate from the product.

### 8.1.2 Synthesizing of carbon nanomaterials on powder activated substrate from acetylene decomposition

Referring to the experimental observations discussed in Chapter 6 and Chapter 7, the key findings can be summarized as following:

- 1- The synthesizing conditions of CNM-PAC (growth temperature, reaction time and gas ratio) from  $C_2H_2$  decomposition were optimized using the RSM-CCD method. The yield % of the CNM-PAC and removal % of MB were investigated as growth process responses. The optimization method showed the optimal conditions were achieved at reaction temperature of 550, growth duration of 37.3 min and gas ratio of 1.0. The process optimization resulted in CNM-PAC with maximum possible yield and adsorption performance within the experimental ranges studied.
- 2- The experimental design results for the growth process revealed that the reaction temperature was notably influenced the growth of CNM-PAC. However, conducting the reaction at higher temperatures (750 °C) was unsuitable which could be attribute to the catalyst deactivation.
- 3- From the statistical results obtained (ANOVA), it is shown that the regression models proposed were significant and adequate to predict the CNM-PAC yield and MB removal efficiency within the experimental range of variables selected.
- 4- The characterization studies of the synthesized CNM-PAC at the optimal growth conditions (O-CNT) showed that the physiochemical properties such as the surface area, porosity, and thermal stability were enhanced by the growth of the CNTs. TEM images of O-CNT showed the presence of tubular CNT bundles (diameter, 15–20 nm) on the PAC surface which further demonstrates the incorporation and the growth of CNTs in the obtained hybrid. Raman spectroscopy confirmed the high degree of graphitization of the as-synthesized O-CNT which likely

significantly influenced by the nature of the support. The combustion profile suggested the higher thermal stability and purity for O-CNTs and the surface areas O-CNT was about 3 times greater than the PAC substrate and the pore volume also increased with the growth of the CNTs. Results of the zeta potential measurement showed that the surface of the hybrid O-CNT was negatively charged with point of zero charge of 8.0.

- 5- The primary screening adsorption experiments indicated that the as-synthesized O-CNT has the same removal efficiency of MB as the modified sample (KS-CNT). This reduces the overall cost and thus contribute towards fulfilling the optimization, kinetic and isotherm studies on O-CNT adsorbent.
- 6- The optimum MB removal conditions suggested by the RSM-CCD optimization method were found at pH 11, adsorbent dosage of 18.1 mg and contact time of 128 min. The MB adsorption system was accurately fitted by the pseudo-second order kinetic model and the adsorption data was perfectly described by Langmuir isotherm with the maximum adsorption capacity ( $q_m$ ) of 174.52 mg/g.
- 7- The collected data suggests that electrostatic attraction was the dominant mechanism for the removal of MB onto O-CNT adsorbent, but the  $\pi$ - $\pi$  should not be ruled out as a contributing sorption mechanism. Moreover, the intraparticle diffusion was also likely to control the rate at which MB was adsorbed on O-CNT hybrid.

Our findings contribute towards successful developing of hybrid carbon nanomaterial by simple, optimized and inexpensive procedure to be used as an efficient adsorbent for BPA and MB dye from aqueous solution. Furthermore, the utilization of PAC as support provided significantly increases the activity toward the production of carbon nanostructures by enhancing the electronic interaction with the deposited gaseous



reactant mixture. The nanoscopic structure covering the surface of the PAC host is expected to provide a highly accessible surface for reactants, which could significantly increase the catalytic activity. Not to mention, the high reactivity of the prismatic planes of the PAC allowed better dispersion of the metal particles, contributing to the overall improvement in active site density.

## **8.2 Recommendations**

Although the synthesizing of carbon nanomaterials with the aid of powder activated carbon substrate for adsorption Bisphenol A and methylene blue dye was very effective and efficient, there remain scope of further study in this field. Hence, the following are recommendations that can proposed to boost the research:

- 1- The scaling up of the CVD reactor by comprising a continuous reaction to produce substantial quantity of the CNM-PAC hybrid should be considered to meet the requirement of the industry.
- 2- Other metals such as Co, Mo and Fe can be used individually or as mixtures to investigate the effect of catalyst on the morphology of the produced CNM-PAC.
- 3- Different dyes, hazardous organic pollutants and bio-pollutants other than bisphenol A and methylene blue required to be tested on the CNM-PAC.
- 4- It is expected that the growth of such nanostructured material will open opportunities for its use as a catalyst support compared with what is usually obtained on traditional catalyst supports. It is suggested to further investigate the impact of the synthesized CNM-PAC in heterogeneous catalysis.
- 5- The adsorption process can be further augmented by: (i) Desorption study to regenerate the spent CNM-PAC is also required for more sustainable and environment friendly system (ii) utilizing the synthesized CNM-PAC material in a fixed bed column to study the breakthrough conditions of the adsorption system,

(iii) It is recommended to further evaluate the adsorption performance of the synthesized CNM-PAC hybrid in this study for removing BPA and MB dye from different industrial process to analyze the behavior of the synthesized adsorbent in a competitive system.

6- Further investigation of the synthesized CNM-PAC hybrid in this study in other applications including photocatalysis, membrane and sensing systems.

University of Malaya

## REFERENCES

- Abdel-Ghani, N., Rawash, E., & El-Chaghaby, G. (2016). Equilibrium and kinetic study for the adsorption of p-nitrophenol from wastewater using olive cake based activated carbon. *Global Journal of Environmental Science and Management*, 2(1), 11-18.
- Abdel-Ghani, N. T., El-Chaghaby, G. A., & Helal, F. S. (2015). Individual and competitive adsorption of phenol and nickel onto multiwalled carbon nanotubes. *Journal of advanced research*, 6(3), 405-415.
- Abdel-Shafy, H. I., & Mansour, M. S. (2016). A review on polycyclic aromatic hydrocarbons: source, environmental impact, effect on human health and remediation. *Egyptian Journal of Petroleum*, 25(1), 107-123.
- Abdel Salam, M., & Burk, R. C. (2008). Thermodynamics of pentachlorophenol adsorption from aqueous solutions by oxidized multi-walled carbon nanotubes. *Applied Surface Science*, 255(5, Part 1), 1975-1981.
- Abkenar, S. S., Malek, R. M. A., & Mazaheri, F. (2015). Dye adsorption of cotton fabric grafted with PPI dendrimers: Isotherm and kinetic studies. *Journal of environmental management*, 163, 53-61.
- Abou-Gamra, Z., & Ahmed, M. (2016). Synthesis of mesoporous TiO<sub>2</sub>-curcumin nanoparticles for photocatalytic degradation of methylene blue dye. *Journal of Photochemistry and Photobiology B: Biology*, 160, 134-141.
- Acomb, J. C., Wu, C., & Williams, P. T. (2015). Effect of growth temperature and feedstock:catalyst ratio on the production of carbon nanotubes and hydrogen from the pyrolysis of waste plastics. *Journal of Analytical and Applied Pyrolysis*, 113(Supplement C), 231-238.
- Adamska, M., & Narkiewicz, U. (2017). Fluorination of Carbon Nanotubes— A Review. *Journal of Fluorine Chemistry*, 200, 179-189.
- Adeleye, A. S., Conway, J. R., Garner, K., Huang, Y., Su, Y., & Keller, A. A. (2016). Engineered nanomaterials for water treatment and remediation: Costs, benefits, and applicability. *Chemical Engineering Journal*, 286(Supplement C), 640-662.
- Adewale, H. B., Jefferson, W. N., Newbold, R. R., & Patisaul, H. B. (2009). Neonatal Bisphenol-A Exposure Alters Rat Reproductive Development and Ovarian Morphology Without Impairing Activation of Gonadotropin-Releasing Hormone Neurons 1. *Biology of reproduction*, 81(4), 690-699.
- Agnihotri, S., Mota, J. P., Rostam-Abadi, M., & Rood, M. J. (2006). Theoretical and experimental investigation of morphology and temperature effects on adsorption of organic vapors in single-walled carbon nanotubes. *The Journal of Physical Chemistry B*, 110(15), 7640-7647.
- Ago, H., Nakamura, K., Uehara, N., & Tsuji, M. (2004). Roles of metal— support interaction in growth of single-and double-walled carbon nanotubes studied with

diameter-controlled iron particles supported on MgO. *The Journal of Physical Chemistry B*, 108(49), 18908-18915.

- Ahmad, A., Loh, M., & Aziz, J. (2007). Preparation and characterization of activated carbon from oil palm wood and its evaluation on methylene blue adsorption. *Dyes and pigments*, 75(2), 263-272.
- Ahmad, A., Razali, M. H., Kassim, K., & Amin, K. A. M. (2017). Synthesis of multiwalled carbon nanotubes supported on M/MCM-41 (M= Ni, Co and Fe) mesoporous catalyst by chemical vapour deposition method. *Journal of Porous Materials*, 1-9.
- Ahmad, I., Yazdani, B., & Zhu, Y. (2015). Recent advances on carbon nanotubes and graphene reinforced ceramics nanocomposites. *Nanomaterials*, 5(1), 90-114.
- Ai, L., & Jiang, J. (2012a). Removal of methylene blue from aqueous solution with self-assembled cylindrical graphene-carbon nanotube hybrid. *Chemical Engineering Journal*, 192(Supplement C), 156-163.
- Ai, L., & Jiang, J. (2012b). Removal of methylene blue from aqueous solution with self-assembled cylindrical graphene-carbon nanotube hybrid. *Chemical Engineering Journal*, 192, 156-163.
- Ai, L., Zhang, C., & Chen, Z. (2011). Removal of methylene blue from aqueous solution by a solvothermal-synthesized graphene/magnetite composite. *Journal of hazardous materials*, 192(3), 1515-1524.
- Ai, L., Zhang, C., Liao, F., Wang, Y., Li, M., Meng, L., & Jiang, J. (2011). Removal of methylene blue from aqueous solution with magnetite loaded multi-wall carbon nanotube: kinetic, isotherm and mechanism analysis. *Journal of hazardous materials*, 198, 282-290.
- Aiello, R., Fiscus, J. E., zur Loye, H.-C., & Amiridis, M. D. (2000). Hydrogen production via the direct cracking of methane over Ni/SiO<sub>2</sub>: catalyst deactivation and regeneration. *Applied Catalysis A: General*, 192(2), 227-234.
- Akingbemi, B. T., Sottas, C. M., Koulova, A. I., Klinefelter, G. R., & Hardy, M. P. (2004). Inhibition of testicular steroidogenesis by the xenoestrogen bisphenol A is associated with reduced pituitary luteinizing hormone secretion and decreased steroidogenic enzyme gene expression in rat Leydig cells. *Endocrinology*, 145(2), 592-603.
- Al-Futaisi, A., Jamrah, A., & Al-Hanai, R. (2007). Aspects of cationic dye molecule adsorption to palygorskite. *Desalination*, 214(1-3), 327-342.
- Al-Hamadani, Y. A. J., Chu, K. H., Son, A., Heo, J., Her, N., Jang, M., . . . Yoon, Y. (2015). Stabilization and dispersion of carbon nanomaterials in aqueous solutions: A review. *Separation and Purification Technology*, 156, Part 2, 861-874.
- Allaedini, G., Aminayi, P., & Tasirin, S. M. (2015). The effect of alumina and magnesia supported germanium nanoparticles on the growth of carbon nanotubes in the chemical vapor deposition method. *Journal of Nanomaterials*, 2015, 5.

- Allaadini, G., Tasirin, S. M., & Aminayi, P. (2015). Synthesis of Fe–Ni–Ce trimetallic catalyst nanoparticles via impregnation and co-precipitation and their application to dye degradation. *Chemical Papers*, 70(2), 231-242.
- Almeida, C. A. P., Debacher, N. A., Downs, A. J., Cottet, L., & Mello, C. A. D. (2009). Removal of methylene blue from colored effluents by adsorption on montmorillonite clay. *Journal of colloid and interface science*, 332(1), 46-53.
- AlOmar, M. K., Alsaadi, M. A., Hayyan, M., Akib, S., Ibrahim, M., & Hashim, M. A. (2017). Allyl triphenyl phosphonium bromide based DES-functionalized carbon nanotubes for the removal of mercury from water. *Chemosphere*, 167, 44-52.
- AlOmar, M. K., Alsaadi, M. A., Hayyan, M., Akib, S., Ibrahim, R. K., & Hashim, M. A. (2016). Lead removal from water by choline chloride based deep eutectic solvents functionalized carbon nanotubes. *Journal of Molecular Liquids*, 222, 883-894.
- AlSaadi, M. A., Al-Mamun, A., Muyibi, S. A., Alam, M. Z., Sopyan, I., Atieh, M. A., & Ahmed, Y. M. (2011). Synthesis of various carbon nanomaterials (CNMs) on powdered activated carbon. *African Journal of Biotechnology*, 10(81), 18892-18905.
- Altıntığ, E., Altundag, H., Tuzen, M., & Sari, A. (2017a). Effective removal of methylene blue from aqueous solutions using magnetic loaded activated carbon as novel adsorbent. *Chemical Engineering Research and Design*, 122(Supplement C), 151-163.
- Altıntığ, E., Altundag, H., Tuzen, M., & Sari, A. (2017b). Effective removal of methylene blue from aqueous solutions using magnetic loaded activated carbon as novel adsorbent. *Chemical Engineering Research and Design*, 122, 151-163.
- Alvarez, W., Kitiyanan, B., Borgna, A., & Resasco, D. (2001). Synergism of Co and Mo in the catalytic production of single-wall carbon nanotubes by decomposition of CO. *Carbon*, 39(4), 547-558.
- Amara, M. S., Paineau, E., Rouzière, S. p., Guiose, B. a., Krapf, M.-E. M., Taché, O., . . . Thill, A. (2015). Hybrid, tunable-diameter, metal oxide nanotubes for trapping of organic molecules. *Chemistry of Materials*, 27(5), 1488-1494.
- Ampelli, C., Perathoner, S., & Centi, G. (2014). Carbon-based catalysts: Opening new scenario to develop next-generation nano-engineered catalytic materials. *Chinese Journal of Catalysis*, 35(6), 783-791.
- Andrews, R., Jacques, D., Rao, A., Derbyshire, F., Qian, D., Fan, X., . . . Chen, J. (1999). Continuous production of aligned carbon nanotubes: a step closer to commercial realization. *Chemical Physics Letters*, 303(5), 467-474.
- Angulakshmi, V., Sivakumar, N., & Karthikeyan, S. (2012). Response surface methodology for optimizing process parameters for synthesis of carbon nanotubes. *J. Environ. Nanotechnol*, 1(1), 40-45.
- Annadurai, G., & Krishnan, M. (1996). Adsorption of basic dye using chitin. *Indian J. Environ. Protec*, 16(6), 444-449.

- Ansari, R., Mosayebzadeh, Z., & Mohammad-khah, A. (2011). Adsorption of cationic dyes from aqueous solutions using polyaniline conducting polymer as a novel adsorbent. *Journal of Advanced Scientific Research*, 1(2), 27-34.
- Ansari, S. Combination of molecularly imprinted polymers and carbon nanomaterials as a versatile biosensing tool in sample analysis: Recent applications and challenges. *TrAC Trends in Analytical Chemistry*.
- Anwer, F., Chaurasia, S., & Khan, A. A. (2016). Hormonally active agents in the environment: a state-of-the-art review. *Reviews on environmental health*, 31(4), 415-433.
- Apul, O. G., & Karanfil, T. (2015). Adsorption of synthetic organic contaminants by carbon nanotubes: a critical review. *Water research*, 68, 34-55.
- Aqel, A., El-Nour, K. M. A., Ammar, R. A., & Al-Warthan, A. (2012). Carbon nanotubes, science and technology part (I) structure, synthesis and characterisation. *Arabian Journal of Chemistry*, 5(1), 1-23.
- Arora, N., & Sharma, N. (2016). *Synthesis of multiwalled carbon nanotube from different grades of carbon black using arc discharge method*. Paper presented at the AIP Conference Proceedings.
- Asfaram, A., Ghaedi, M., Hajati, S., Rezaeinejad, M., Goudarzi, A., & Purkait, M. K. (2015). Rapid removal of Auramine-O and Methylene blue by ZnS:Cu nanoparticles loaded on activated carbon: A response surface methodology approach. *Journal of the Taiwan Institute of Chemical Engineers*, 53(Supplement C), 80-91.
- Asfaram, A., Ghaedi, M., Yousefi, F., & Dastkhooon, M. (2016). Experimental design and modeling of ultrasound assisted simultaneous adsorption of cationic dyes onto ZnS: Mn-NPs-AC from binary mixture. *Ultrasonics sonochemistry*, 33, 77-89.
- Ashik, U. P. M., Wan Daud, W. M. A., & Hayashi, J.-i. (2017). A review on methane transformation to hydrogen and nanocarbon: Relevance of catalyst characteristics and experimental parameters on yield. *Renewable and Sustainable Energy Reviews*, 76, 743-767.
- Ashraf, A., Salih, H., Nam, S., & Dastgheib, S. A. (2016). Robust carbon nanotube membranes directly grown on Hastelloy substrates and their potential application for membrane distillation. *Carbon*, 106, 243-251.
- Asmaly, H. A., Abussaud, B., Saleh, T. A., Gupta, V. K., & Atieh, M. A. (2015). Ferric oxide nanoparticles decorated carbon nanotubes and carbon nanofibers: from synthesis to enhanced removal of phenol. *Journal of Saudi Chemical Society*, 19(5), 511-520.
- Atchudan, R., Perumal, S., Edison, T. N. J. I., & Lee, Y. R. (2015). Highly graphitic carbon nanosheets synthesized over tailored mesoporous molecular sieves using acetylene by chemical vapor deposition method. *RSC Advances*, 5(113), 93364-93373.

- Atthipalli, G., Epur, R., Kumta, P. N., Yang, M., Lee, J.-K., & Gray, J. L. (2011). Nickel catalyst-assisted vertical growth of dense carbon nanotube forests on bulk copper. *The Journal of Physical Chemistry C*, 115(9), 3534-3538.
- Auta, M., & Hameed, B. (2012a). Modified mesoporous clay adsorbent for adsorption isotherm and kinetics of methylene blue. *Chemical Engineering Journal*, 198, 219-227.
- Auta, M., & Hameed, B. H. (2012b). Modified mesoporous clay adsorbent for adsorption isotherm and kinetics of methylene blue. *Chemical Engineering Journal*, 198(Supplement C), 219-227.
- Avilés, F., Cauch-Rodríguez, J., Moo-Tah, L., May-Pat, A., & Vargas-Coronado, R. (2009). Evaluation of mild acid oxidation treatments for MWCNT functionalization. *Carbon*, 47(13), 2970-2975.
- Avilés, F., de Jesús Kú-Herrera, J., & Oliva-Avilés, A. I. (2017). Deposition of Carbon Nanotubes on Fibers. *Carbon Nanotube-Reinforced Polymers: From Nanoscale to Macroscale*, 117.
- Awadallah, A. E., El-Desouki, D. S., Aboul-Gheit, N. A., Ibrahim, A. H., & Aboul-Gheit, A. K. (2016). Effect of crystalline structure and pore geometry of silica based supported materials on the catalytic behavior of metallic nickel particles during methane decomposition to CO<sub>x</sub>-free hydrogen and carbon nanomaterials. *International Journal of Hydrogen Energy*, 41(38), 16890-16902.
- Azevedo, D. d. A., Lacorte, S., Viana, P., & Barceló, D. (2001). Occurrence of nonylphenol and bisphenol-A in surface waters from Portugal. *Journal of the Brazilian Chemical Society*, 12(4), 532-537.
- Baker, R., Barber, M., Harris, P., Feates, F., & Waite, R. (1972). Nucleation and growth of carbon deposits from the nickel catalyzed decomposition of acetylene. *Journal of catalysis*, 26(1), 51-62.
- Balandin, A. A. (2011). Thermal properties of graphene and nanostructured carbon materials. *Nature materials*, 10(8), 569-581.
- Balarak, D. (2016). Kinetics, isotherm and thermodynamics studies on bisphenol A adsorption using barley husk. *International Journal of ChemTech Research*, 9(5), 681-690.
- Basheer, C., Lee, H. K., & Tan, K. S. (2004). Endocrine disrupting alkylphenols and bisphenol-A in coastal waters and supermarket seafood from Singapore. *Marine pollution bulletin*, 48(11), 1161-1167.
- Bashir, R., & Chisti, H. (2014). Nanotechnology for Environmental Control and Remediation. *Nanotechnology Applications for Improvements in Energy Efficiency and Environmental Management*, 156.
- Bautista-Toledo, I., Ferro-Garcia, M., Rivera-Utrilla, J., Moreno-Castilla, C., & Vegas Fernandez, F. (2005). Bisphenol A removal from water by activated carbon. Effects of carbon characteristics and solution chemistry. *Environmental science & technology*, 39(16), 6246-6250.

- Bautista-Toledo, M. I., Rivera-Utrilla, J., Ocampo-Pérez, R., Carrasco-Marín, F., & Sánchez-Polo, M. (2014). Cooperative adsorption of bisphenol-A and chromium(III) ions from water on activated carbons prepared from olive-mill waste. *Carbon*, 73(Supplement C), 338-350.
- Bayramoglu, G., Arica, M. Y., Liman, G., Celikbicak, O., & Salih, B. (2016). Removal of bisphenol A from aqueous medium using molecularly surface imprinted microbeads. *Chemosphere*, 150, 275-284.
- Bazrafshan, E., Kord Mostafapour, F., Rahdar, S., & Mahvi, A. H. (2015). Equilibrium and thermodynamics studies for decolorization of Reactive Black 5 (RB5) by adsorption onto MWCNTs. *Desalination and Water Treatment*, 54(8), 2241-2251.
- Bedin, K. C., Martins, A. C., Cazetta, A. L., Pezoti, O., & Almeida, V. C. (2016). KOH-activated carbon prepared from sucrose spherical carbon: Adsorption equilibrium, kinetic and thermodynamic studies for Methylene Blue removal. *Chemical Engineering Journal*, 286, 476-484.
- Bele, S., Samanidou, V., & Deliyanni, E. (2016). Effect of the reduction degree of graphene oxide on the adsorption of Bisphenol A. *Chemical Engineering Research and Design*, 109, 573-585.
- Berhane, T. M., Levy, J., Krekeler, M. P., & Danielson, N. D. (2016). Adsorption of bisphenol A and ciprofloxacin by palygorskite-montmorillonite: Effect of granule size, solution chemistry and temperature. *Applied Clay Science*, 132, 518-527.
- Bhatnagar, A., & Anastopoulos, I. (2017). Adsorptive removal of bisphenol A (BPA) from aqueous solution: A review. *Chemosphere*, 168, 885-902.
- Bhattacharyya, K. G., & Sharma, A. (2005). Kinetics and thermodynamics of Methylene Blue adsorption on Neem (*Azadirachta indica*) leaf powder. *Dyes and pigments*, 65(1), 51-59.
- Bigdeli, S., & Fatemi, S. (2015). Fast carbon nanofiber growth on the surface of activated carbon by microwave irradiation: A modified nano-adsorbent for deep desulfurization of liquid fuels. *Chemical Engineering Journal*, 269(Supplement C), 306-315.
- Bina, B., Pourzamani, H., Rashidi, A., & Amin, M. M. (2011). Ethylbenzene removal by carbon nanotubes from aqueous solution. *Journal of environmental and public health*, 2012.
- Bohdziewicz, J., & Kamińska, G. (2013). Kinetics and equilibrium of the sorption of bisphenol A by carbon nanotubes from wastewater. *Water Science and Technology*, 68(6), 1306-1314.
- Bom, D., Andrews, R., Jacques, D., Anthony, J., Chen, B., Meier, M. S., & Selegue, J. P. (2002). Thermogravimetric analysis of the oxidation of multiwalled carbon nanotubes: evidence for the role of defect sites in carbon nanotube chemistry. *Nano letters*, 2(6), 615-619.



- Boulinguez, B., Le Cloirec, P., & Wolbert, D. (2008). Revisiting the Determination of Langmuir Parameters • Application to Tetrahydrothiophene Adsorption onto Activated Carbon. *Langmuir*, 24(13), 6420-6424.
- Bradder, P., Ling, S. K., Wang, S., & Liu, S. (2010). Dye adsorption on layered graphite oxide. *Journal of Chemical & Engineering Data*, 56(1), 138-141.
- Burke, V., Duennbier, U., & Massmann, G. (2012). The effect of aeration on the removal of wastewater-derived pharmaceutical residues from groundwater—A laboratory study. *Water Science and Technology*, 67(3), 658-666.
- Bystrzejewski, M., Rümmele, M., Lange, H., Huczko, A., Baranowski, P., Gemming, T., & Pichler, T. (2008). Single-walled carbon nanotubes synthesis: a direct comparison of laser ablation and carbon arc routes. *Journal of nanoscience and nanotechnology*, 8(11), 6178-6186.
- Cai, Y., Jiang, G., Liu, J., & Zhou, Q. (2003). Multiwalled carbon nanotubes as a solid-phase extraction adsorbent for the determination of bisphenol A, 4-nonylphenol, and 4-tert-octylphenol. *Analytical Chemistry*, 75(10), 2517-2521.
- Careghini, A., Mastorgio, A. F., Saponaro, S., & Sezenna, E. (2015). Bisphenol A, nonylphenols, benzophenones, and benzotriazoles in soils, groundwater, surface water, sediments, and food: a review. *Environmental science and pollution Research*, 22(8), 5711-5741.
- Cassell, A. M., Raymakers, J. A., Kong, J., & Dai, H. (1999). Large scale CVD synthesis of single-walled carbon nanotubes. *The Journal of Physical Chemistry B*, 103(31), 6484-6492.
- Céspedes, R., Lacorte, S., Raldúa, D., Ginebreda, A., Barceló, D., & Piña, B. (2005). Distribution of endocrine disruptors in the Llobregat River basin (Catalonia, NE Spain). *Chemosphere*, 61(11), 1710-1719.
- Chai, S.-P., Lee, K.-Y., Ichikawa, S., & Mohamed, A. R. (2011). Synthesis of carbon nanotubes by methane decomposition over Co–Mo/Al<sub>2</sub>O<sub>3</sub>: Process study and optimization using response surface methodology. *Applied Catalysis A: General*, 396(1), 52-58.
- Chang, K.-L., Hsieh, J.-F., Ou, B.-M., Chang, M.-H., Hsieh, W.-Y., Lin, J.-H., . . . Chen, S.-T. (2012). Adsorption studies on the removal of an endocrine-disrupting compound (Bisphenol A) using activated carbon from rice straw agricultural waste. *Separation Science and Technology*, 47(10), 1514-1521.
- Chellaram, C., Murugaboopathi, G., John, A. A., Sivakumar, R., Ganesan, S., Krithika, S., & Priya, G. (2014). Significance of Nanotechnology in Food Industry. *APCBEE Procedia*, 8(Supplement C), 109-113.
- Chen, C.-C., Kuo, C.-J., Liao, C.-D., Chang, C.-F., Tseng, C.-A., Liu, C.-R., & Chen, Y.-T. (2015). Growth of large-area graphene single crystals in confined reaction space with diffusion-driven chemical vapor deposition. *Chemistry of Materials*, 27(18), 6249-6258.

- Chen, D., Kannan, K., Tan, H., Zheng, Z., Feng, Y.-L., Wu, Y., & Widelka, M. (2016). Bisphenol Analogues Other Than BPA: Environmental Occurrence, Human Exposure, and Toxicity • A Review. *Environmental science & technology*, 50(11), 5438-5453.
- Chen, G.-C., Shan, X.-Q., Pei, Z.-G., Wang, H., Zheng, L.-R., Zhang, J., & Xie, Y.-N. (2011). Adsorption of diuron and dichlobenil on multiwalled carbon nanotubes as affected by lead. *Journal of Hazardous Materials*, 188(1–3), 156-163.
- Chen, G.-C., Shan, X.-Q., Wang, Y.-S., Wen, B., Pei, Z.-G., Xie, Y.-N., . . . Pignatello, J. J. (2009). Adsorption of 2,4,6-trichlorophenol by multi-walled carbon nanotubes as affected by Cu(II). *Water Research*, 43(9), 2409-2418.
- Chen, J., Hamon, M. A., Hu, H., Chen, Y., Rao, A. M., Eklund, P. C., & Haddon, R. C. (1998). Solution properties of single-walled carbon nanotubes. *science*, 282(5386), 95-98.
- Chen, J., Huang, X., & Lee, D. (2008). Bisphenol A removal by a membrane bioreactor. *Process Biochemistry*, 43(4), 451-456.
- Chen, J. S. (2015). *Selective growth of carbon nanotubes via photo-thermal chemical vapour deposition*. University of Surrey (United Kingdom).
- Chen, L., & Bai, B. (2013). Equilibrium, kinetic, thermodynamic, and in situ regeneration studies about methylene blue adsorption by the raspberry-like TiO<sub>2</sub>@ yeast microspheres. *Industrial & engineering chemistry research*, 52(44), 15568-15577.
- Chen, W., Duan, L., & Zhu, D. (2007). Adsorption of polar and nonpolar organic chemicals to carbon nanotubes. *Environmental science & technology*, 41(24), 8295-8300.
- Chen, X.-W., Su, D. S., Hamid, S. B., & Schlögl, R. (2007). The morphology, porosity and productivity control of carbon nanofibers or nanotubes on modified activated carbon. *Carbon*, 45(4), 895-898.
- Chen, X.-W., Timpe, O., Hamid, S. B., Schlögl, R., & Su, D. S. (2009a). Direct synthesis of carbon nanofibers on modified biomass-derived activated carbon. *Carbon*, 47(1), 340-343.
- Chen, X.-W., Timpe, O., Hamid, S. B. A., Schlögl, R., & Su, D. S. (2009b). Direct synthesis of carbon nanofibers on modified biomass-derived activated carbon. *Carbon*, 47(1), 340-343.
- Cheng, H., Li, F., Su, G., Pan, H., He, L., Sun, X., & Dresselhaus, M. (1998). Large-scale and low-cost synthesis of single-walled carbon nanotubes by the catalytic pyrolysis of hydrocarbons. *Applied physics letters*, 72(25), 3282-3284.
- Cheng, J., Zhang, X., Liu, F., Tu, J., Lu, H., Sun, Y., & Chen, F. (2004). Long bundles of aligned carbon nanofibers obtained by vertical floating catalyst method. *Materials Chemistry and Physics*, 87(2), 241-245.

- Cheng, Q., Debnath, S., Gregan, E., & Byrne, H. J. (2010). Ultrasound-assisted SWNTs dispersion: effects of sonication parameters and solvent properties. *The Journal of Physical Chemistry C*, 114(19), 8821-8827.
- Cherifi, H., Fatiha, B., & Salah, H. (2013). Kinetic studies on the adsorption of methylene blue onto vegetal fiber activated carbons. *Applied surface science*, 282, 52-59.
- Cheung, C. L., Kurtz, A., Park, H., & Lieber, C. M. (2002). Diameter-controlled synthesis of carbon nanotubes. *The Journal of Physical Chemistry B*, 106(10), 2429-2433.
- Cho, H.-H., Huang, H., & Schwab, K. (2011). Effects of Solution Chemistry on the Adsorption of Ibuprofen and Triclosan onto Carbon Nanotubes. *Langmuir*, 27(21), 12960-12967.
- Cho, H.-H., Smith, B. A., Wnuk, J. D., Fairbrother, D. H., & Ball, W. P. (2008). Influence of surface oxides on the adsorption of naphthalene onto multiwalled carbon nanotubes. *Environmental science & technology*, 42(8), 2899-2905.
- Chowdhury, S., & Balasubramanian, R. (2014). Recent advances in the use of graphene-family nanoadsorbents for removal of toxic pollutants from wastewater. *Advances in colloid and interface science*, 204(Supplement C), 35-56.
- Chuenchom, L., Kraehnert, R., & Smarsly, B. M. (2012). Recent progress in soft-templating of porous carbon materials. *Soft Matter*, 8(42), 10801-10812.
- Ci, L., Zhu, H., Wei, B., Xu, C., Liang, J., & Wu, D. (2000). Graphitization behavior of carbon nanofibers prepared by the floating catalyst method. *Materials Letters*, 43(5), 291-294.
- Colomer, J.-F., Stephan, C., Lefrant, S., Van Tendeloo, G., Willems, I., Konya, Z., . . . Nagy, J. B. (2000). Large-scale synthesis of single-wall carbon nanotubes by catalytic chemical vapor deposition (CCVD) method. *Chemical Physics Letters*, 317(1), 83-89.
- Cong, H.-P., Ren, X.-C., Wang, P., & Yu, S.-H. (2012). Macroscopic multifunctional graphene-based hydrogels and aerogels by a metal ion induced self-assembly process. *ACS nano*, 6(3), 2693-2703.
- Contreras, J. E., Rodriguez, E. A., & Taha-Tijerina, J. (2017). Nanotechnology applications for electrical transformers—A review. *Electric Power Systems Research*, 143(Supplement C), 573-584.
- Costa, S., Borowiak-Palen, E., Kruszynska, M., Bachmatiuk, A., & Kalenczuk, R. (2008). Characterization of carbon nanotubes by Raman spectroscopy. *Materials Science-Poland*, 26(2), 433-441.
- Cottet, L., Almeida, C., Naidek, N., Viante, M., Lopes, M., & Debacher, N. (2014). Adsorption characteristics of montmorillonite clay modified with iron oxide with respect to methylene blue in aqueous media. *Applied Clay Science*, 95, 25-31.

- Cousins, I., Staples, C., Klečka, G., & Mackay, D. (2002). A multimedia assessment of the environmental fate of bisphenol A. *Human and Ecological Risk Assessment*, 8(5), 1107-1135.
- Couteau, E., Hernadi, K., Seo, J. W., Thien-Nga, L., Mikó, C., Gaal, R., & Forro, L. (2003). CVD synthesis of high-purity multiwalled carbon nanotubes using CaCO<sub>3</sub> catalyst support for large-scale production. *Chemical Physics Letters*, 378(1), 9-17.
- Crini, G. (2008). Kinetic and equilibrium studies on the removal of cationic dyes from aqueous solution by adsorption onto a cyclodextrin polymer. *Dyes and pigments*, 77(2), 415-426.
- Cui, L., Wei, J., Du, X., & Zhou, X. (2016). Preparation and Evaluation of Self-Assembled Porous Microspheres–Fibers for Removal of Bisphenol A from Aqueous Solution. *Industrial & engineering chemistry research*, 55(6), 1566-1574.
- Cumings, J., Mickelson, W., & Zettl, A. (2003). Simplified synthesis of double-wall carbon nanotubes. *Solid State Communications*, 126(6), 359-362.
- Dai, H., Hafner, J. H., Rinzler, A. G., Colbert, D. T., & Smalley, R. E. (1996). Nanotubes as nanoprobe in scanning probe microscopy. *nature*, 384(6605), 147.
- Dalaran, M., Emik, S., Güçlü, G., İyim, T. B., & Özgümüş, S. (2009). Removal of acidic dye from aqueous solutions using poly (DMAEMA–AMPS–HEMA) terpolymer/MMT nanocomposite hydrogels. *Polymer Bulletin*, 63(2), 159-171.
- Das, R., Vecitis, C. D., Schulze, A., Cao, B., Ismail, A. F., Lu, X., . . . Ramakrishna, S. (2017). Recent advances in nanomaterials for water protection and monitoring. *Chemical Society Reviews*.
- Datsyuk, V., Kalyva, M., Papagelis, K., Parthenios, J., Tasis, D., Siokou, A., . . . Galiotis, C. (2008). Chemical oxidation of multiwalled carbon nanotubes. *Carbon*, 46(6), 833-840.
- Davis, W., Slawson, R., & Rigby, G. (1953). An unusual form of carbon. *nature*, 171(4356), 756-756.
- De Greef, N., Zhang, L., Magrez, A., Forró, L., Locquet, J.-P., Verpoest, I., & Seo, J. W. (2015). Direct growth of carbon nanotubes on carbon fibers: Effect of the CVD parameters on the degradation of mechanical properties of carbon fibers. *Diamond and Related Materials*, 51, 39-48.
- De La Cueva Bueno, P., Gillerman, L., Gehr, R., & Oron, G. (2017). Nanotechnology for sustainable wastewater treatment and use for agricultural production: A comparative long-term study. *Water research*, 110(Supplement C), 66-73.
- de la Luz-Asunción, M., Sánchez-Mendieta, V., Martínez-Hernández, A., Castaño, V., & Velasco-Santos, C. (2015). Adsorption of phenol from aqueous solutions by carbon nanomaterials of one and two dimensions: kinetic and equilibrium studies. *Journal of Nanomaterials*, 16(1), 422.

- De Volder, M. F. L., Tawfick, S. H., Baughman, R. H., & Hart, A. J. (2013). Carbon Nanotubes: Present and Future Commercial Applications. *science*, 339(6119), 535-539.
- Dehghani, M. H., Ghadermazi, M., Bhatnagar, A., Sadighara, P., Jahed-Khaniki, G., Heibati, B., & McKay, G. (2016). Adsorptive removal of endocrine disrupting bisphenol A from aqueous solution using chitosan. *Journal of Environmental Chemical Engineering*, 4(3), 2647-2655.
- Dehghani, M. H., Mahvi, A. H., Rastkari, N., Saeedi, R., Nazmara, S., & Irvani, E. (2015). Adsorption of bisphenol A (BPA) from aqueous solutions by carbon nanotubes: kinetic and equilibrium studies. *Desalination and Water Treatment*, 54(1), 84-92.
- Delzeit, L., McAninch, I., Cruden, B. A., Hash, D., Chen, B., Han, J., & Meyyappan, M. (2002). Growth of multiwall carbon nanotubes in an inductively coupled plasma reactor. *Journal of Applied Physics*, 91(9), 6027-6033.
- Demir, H., Top, A., Balköse, D., & Ülkü, S. (2008). Dye adsorption behavior of *Luffa cylindrica* fibers. *Journal of hazardous materials*, 153(1-2), 389-394.
- Deng, H., Lu, J., Li, G., Zhang, G., & Wang, X. (2011). Adsorption of methylene blue on adsorbent materials produced from cotton stalk. *Chemical Engineering Journal*, 172(1), 326-334.
- Dikonimos Makris, T., Giorgi, L., Giorgi, R., Lisi, N., & Salernitano, E. (2005). CNT growth on alumina supported nickel catalyst by thermal CVD. *Diamond and Related Materials*, 14(3), 815-819.
- Dillon, A., Gennett, T., Parilla, P., Alleman, J., Jones, K., & Heben, M. (2000). *Evaluating the purity of single-wall nanotube materials*. Paper presented at the MRS Proceedings.
- Ding, D., Wang, J., Cao, Z., & Dai, J. (2003). Synthesis of carbon nanostructures on nanocrystalline Ni-Ni<sub>3</sub>P catalyst supported by SiC whiskers. *Carbon*, 41(3), 579-582.
- Diring, S., Furukawa, S., Takashima, Y., Tsuruoka, T., & Kitagawa, S. (2010). Controlled multiscale synthesis of porous coordination polymer in nano/micro regimes. *Chemistry of Materials*, 22(16), 4531-4538.
- Dong, Y., Wu, D., Chen, X., & Lin, Y. (2010). Adsorption of bisphenol A from water by surfactant-modified zeolite. *Journal of colloid and interface science*, 348(2), 585-590.
- Dotto, G., Santos, J., Rodrigues, I., Rosa, R., Pavan, F., & Lima, E. (2015). Adsorption of Methylene Blue by ultrasonic surface modified chitin. *Journal of colloid and interface science*, 446, 133-140.
- Doustan, F., & Pasha, M. A. (2016). Growth of carbon nanotubes over Fe-Co and Ni-Co catalysts supported on different phases of TiO<sub>2</sub> substrate by thermal CVD. *Fullerenes, Nanotubes and Carbon Nanostructures*, 24(1), 25-33.

- Dresselhaus, M. S., Jorio, A., Hofmann, M., Dresselhaus, G., & Saito, R. (2010). Perspectives on carbon nanotubes and graphene Raman spectroscopy. *Nano letters*, 10(3), 751-758.
- Duman, O., Tunç, S., Polat, T. G., & Bozoğlan, B. K. (2016). Synthesis of magnetic oxidized multiwalled carbon nanotube- $\kappa$ -carrageenan-Fe<sub>3</sub>O<sub>4</sub> nanocomposite adsorbent and its application in cationic Methylene Blue dye adsorption. *Carbohydrate Polymers*, 147, 79-88.
- Dutta, S., Bhattacharyya, A., Ganguly, A., Gupta, S., & Basu, S. (2011). Application of Response Surface Methodology for preparation of low-cost adsorbent from citrus fruit peel and for removal of Methylene Blue. *Desalination*, 275(1), 26-36.
- Ebele, A. J., Abdallah, M. A.-E., & Harrad, S. (2017). Pharmaceuticals and personal care products (PPCPs) in the freshwater aquatic environment. *Emerging Contaminants*.
- Efremenko, I., & Sheintuch, M. (2006). Predicting solute adsorption on activated carbon: phenol. *Langmuir*, 22(8), 3614-3621.
- Eggen, T., Moeder, M., & Arukwe, A. (2010). Municipal landfill leachates: a significant source for new and emerging pollutants. *Science of the Total Environment*, 408(21), 5147-5157.
- Endo, M., Muramatsu, H., Hayashi, T., Kim, Y., Terrones, M., & Dresselhaus, M. (2005). Nanotechnology: 'Buckypaper' from coaxial nanotubes. *nature*, 433(7025), 476-476.
- Engel, M., & Chefetz, B. (2016). Adsorption and desorption of dissolved organic matter by carbon nanotubes: Effects of solution chemistry. *Environmental Pollution*, 213(Supplement C), 90-98.
- Ersan, G., Apul, O. G., Perreault, F., & Karanfil, T. (2017a). Adsorption of organic contaminants by graphene nanosheets: A review. *Water research*, 126(Supplement C), 385-398.
- Ersan, G., Apul, O. G., Perreault, F., & Karanfil, T. (2017b). Adsorption of organic contaminants by graphene nanosheets: A review. *Water research*.
- Etim, U., Inam, E., Umoren, S., & Eduok, U. (2013). Dye removal from aqueous solution using coconut coir dust extract-modified polyvinyl alcohol: a novel adsorbent. *International Journal of Environment and Bioenergy*, 5(2), 62-79.
- Ezzeddine, Z., Batonneau-Gener, I., Pouilloux, Y., & Hamad, H. (2016). Removal of methylene blue by mesoporous CMK-3: Kinetics, isotherms and thermodynamics. *Journal of Molecular Liquids*, 223(Supplement C), 763-770.
- Fan, S., Wang, Y., Wang, Z., Tang, J., Tang, J., & Li, X. (2017). Removal of methylene blue from aqueous solution by sewage sludge-derived biochar: adsorption kinetics, equilibrium, thermodynamics and mechanism. *Journal of Environmental Chemical Engineering*, 5(1), 601-611.

- Fan, W., Gao, W., Zhang, C., Tjiu, W. W., Pan, J., & Liu, T. (2012). Hybridization of graphene sheets and carbon-coated Fe<sub>3</sub>O<sub>4</sub> nanoparticles as a synergistic adsorbent of organic dyes. *Journal of Materials Chemistry*, 22(48), 25108-25115.
- Farmany, A., Shirmohammadi, M., Kazemi, S., Hatami, M., & Mortazavi, S. (2016). Aminopropyl functionalization of superparamagnetic iron oxide/SiO<sub>2</sub> nanocrystals for adsorption of bisphenol A from water. *Desalination and Water Treatment*, 57(56), 27355-27362.
- Félix-Cañedo, T. E., Durán-Álvarez, J. C., & Jiménez-Cisneros, B. (2013). The occurrence and distribution of a group of organic micropollutants in Mexico City's water sources. *Science of the Total Environment*, 454, 109-118.
- Feng, Y., Zhou, H., Liu, G., Qiao, J., Wang, J., Lu, H., . . . Wu, Y. (2012). Methylene blue adsorption onto swede rape straw (*Brassica napus* L.) modified by tartaric acid: equilibrium, kinetic and adsorption mechanisms. *Bioresource technology*, 125, 138-144.
- Fernandes, R. M., Buzaglo, M., Regev, O., Marques, E. F., & Furó, I. n. (2015). Surface coverage and competitive adsorption on carbon nanotubes. *The Journal of Physical Chemistry C*, 119(38), 22190-22197.
- Flahaut, E., Laurent, C., & Peigney, A. (2005). Catalytic CVD synthesis of double and triple-walled carbon nanotubes by the control of the catalyst preparation. *Carbon*, 43(2), 375-383.
- Fonseca, A., Hernadi, K., Piedigrosso, P., Colomer, J.-F., Mukhopadhyay, K., Doome, R., . . . Thiry, P. (1998). Synthesis of single-and multi-wall carbon nanotubes over supported catalysts. *Applied Physics A*, 67(1), 11-22.
- Foo, K., & Hameed, B. (2010). Insights into the modeling of adsorption isotherm systems. *Chemical Engineering Journal*, 156(1), 2-10.
- Franklin, N. R., Li, Y., Chen, R. J., Javey, A., & Dai, H. (2001). Patterned growth of single-walled carbon nanotubes on full 4-inch wafers. *Applied physics letters*, 79(27), 4571-4573.
- Franz, M., Arafat, H. A., & Pinto, N. G. (2000). Effect of chemical surface heterogeneity on the adsorption mechanism of dissolved aromatics on activated carbon. *Carbon*, 38(13), 1807-1819.
- Freundlich, H. (1906). Over the adsorption in solution. *J. Phys. Chem*, 57(385471), 1100-1107.
- Fu, J., Chen, Z., Wang, M., Liu, S., Zhang, J., Zhang, J., . . . Xu, Q. (2015). Adsorption of methylene blue by a high-efficiency adsorbent (polydopamine microspheres): kinetics, isotherm, thermodynamics and mechanism analysis. *Chemical Engineering Journal*, 259, 53-61.
- Fu, M., Li, Z., & Gao, H. (2007). Distribution characteristics of nonylphenol in Jiaozhou Bay of Qingdao and its adjacent rivers. *Chemosphere*, 69(7), 1009-1016.

- Gao, B., Zhou, H., Chen, D., & Yang, J. (2017). Porous carbon with small mesopores as an ultra-high capacity adsorption medium. *Applied surface science*, 420(Supplement C), 535-541.
- Gao, Z., Bandosz, T. J., Zhao, Z., Han, M., & Qiu, J. (2009). Investigation of factors affecting adsorption of transition metals on oxidized carbon nanotubes. *Journal of hazardous materials*, 167(1), 357-365.
- Garg, V. K., Amita, M., Kumar, R., & Gupta, R. (2004). Basic dye (methylene blue) removal from simulated wastewater by adsorption using Indian Rosewood sawdust: a timber industry waste. *Dyes and pigments*, 63(3), 243-250.
- Ge, F., Ye, H., Li, M.-M., & Zhao, B.-X. (2012). Efficient removal of cationic dyes from aqueous solution by polymer-modified magnetic nanoparticles. *Chemical Engineering Journal*, 198, 11-17.
- Ge, M., Du, M., Zheng, L., Wang, B., Zhou, X., Jia, Z., . . . Jahangir Alam, S. M. (2017). A maleic anhydride grafted sugarcane bagasse adsorbent and its performance on the removal of methylene blue from related wastewater. *Materials Chemistry and Physics*, 192(Supplement C), 147-155.
- Ghaedi, M., Ghayedi, M., Kokhdan, S. N., Sahraei, R., & Daneshfar, A. (2013). Palladium, silver, and zinc oxide nanoparticles loaded on activated carbon as adsorbent for removal of bromophenol red from aqueous solution. *Journal of Industrial and Engineering Chemistry*, 19(4), 1209-1217.
- Ghasemian, E., & Palizban, Z. (2016). Comparisons of azo dye adsorptions onto activated carbon and silicon carbide nanoparticles loaded on activated carbon. *International Journal of Environmental Science and Technology*, 13(2), 501-512.
- Gómez, S., Rendtorff, N. M., Aglietti, E. F., Sakka, Y., & Suárez, G. (2016). Surface modification of multiwall carbon nanotubes by sulfonitric treatment. *Applied surface science*, 379(Supplement C), 264-269.
- Gong, J.-L., Wang, B., Zeng, G.-M., Yang, C.-P., Niu, C.-G., Niu, Q.-Y., . . . Liang, Y. (2009). Removal of cationic dyes from aqueous solution using magnetic multi-wall carbon nanotube nanocomposite as adsorbent. *Journal of hazardous materials*, 164(2), 1517-1522.
- Gong, J., Liu, J., Chen, X., Jiang, Z., Wen, X., Mijowska, E., & Tang, T. (2015). Converting real-world mixed waste plastics into porous carbon nanosheets with excellent performance in the adsorption of an organic dye from wastewater. *Journal of Materials Chemistry A*, 3(1), 341-351.
- Gong, J., Liu, J., Jiang, Z., Wen, X., Mijowska, E., Tang, T., & Chen, X. (2015). A facile approach to prepare porous cup-stacked carbon nanotube with high performance in adsorption of methylene blue. *Journal of colloid and interface science*, 445, 195-204.
- Gong, Z., Li, S., Ma, J., & Zhang, X. (2016). Synthesis of recyclable powdered activated carbon with temperature responsive polymer for bisphenol A removal. *Separation and Purification Technology*, 157, 131-140.



- Gotovac, S., Song, L., Kanoh, H., & Kaneko, K. (2007). Assembly structure control of single wall carbon nanotubes with liquid phase naphthalene adsorption. *Colloids and Surfaces A: Physicochemical and Engineering Aspects*, 300(1), 117-121.
- Griffith, D. R. (2013). *Natural and synthetic estrogens in wastewater treatment plant effluent and the coastal ocean*. Massachusetts Institute of Technology and Woods Hole Oceanographic Institution.
- Gromov, D. G., Bulyarskii, S., Pavlov, A., Scorik, S., Shulyat'ev, A., & Trifonov, A. Y. (2016). Catalytic CVD-growth of array of multiwall carbon nanotubes on initially amorphous film Co–Zr–N–O. *Diamond and Related Materials*, 64(Supplement C), 97-102.
- Guerra, J., & Herrero, M. A. (2010). Hybrid materials based on Pd nanoparticles on carbon nanostructures for environmentally benign C–C coupling chemistry. *Nanoscale*, 2(8), 1390-1400.
- Guerra, P., Kim, M., Teslic, S., Alaei, M., & Smyth, S. A. (2015). Bisphenol-A removal in various wastewater treatment processes: Operational conditions, mass balance, and optimization. *Journal of environmental management*, 152, 192-200.
- Gui, C.-X., Wang, Q.-Q., Hao, S.-M., Qu, J., Huang, P.-P., Cao, C.-Y., . . . Yu, Z.-Z. (2014). Sandwichlike magnesium silicate/reduced graphene oxide nanocomposite for enhanced Pb<sup>2+</sup> and methylene blue adsorption. *ACS applied materials & interfaces*, 6(16), 14653-14659.
- Gulnaz, O., Kaya, A., Matyar, F., & Arıkan, B. (2004). Sorption of basic dyes from aqueous solution by activated sludge. *Journal of hazardous materials*, 108(3), 183-188.
- Guo, W., Hu, W., Pan, J., Zhou, H., Guan, W., Wang, X., . . . Xu, L. (2011). Selective adsorption and separation of BPA from aqueous solution using novel molecularly imprinted polymers based on kaolinite/Fe<sub>3</sub>O<sub>4</sub> composites. *Chemical Engineering Journal*, 171(2), 603-611.
- Gupta, V., & Nayak, A. (2012). Cadmium removal and recovery from aqueous solutions by novel adsorbents prepared from orange peel and Fe<sub>2</sub>O<sub>3</sub> nanoparticles. *Chemical Engineering Journal*, 180, 81-90.
- Gupta, V. K., Ali, I., Saleh, T. A., Nayak, A., & Agarwal, S. (2012). Chemical treatment technologies for waste-water recycling—an overview. *RSC Advances*, 2(16), 6380-6388.
- Gupta, V. K., Jain, R., Mittal, A., Saleh, T. A., Nayak, A., Agarwal, S., & Sikarwar, S. (2012). Photo-catalytic degradation of toxic dye amaranth on TiO<sub>2</sub>/UV in aqueous suspensions. *Materials Science and Engineering: C*, 32(1), 12-17.
- Gupta, V. K., Jain, R., Nayak, A., Agarwal, S., & Shrivastava, M. (2011). Removal of the hazardous dye—tartrazine by photodegradation on titanium dioxide surface. *Materials Science and Engineering: C*, 31(5), 1062-1067.

- Gupta, V. K., Kumar, R., Nayak, A., Saleh, T. A., & Barakat, M. (2013). Adsorptive removal of dyes from aqueous solution onto carbon nanotubes: a review. *Advances in colloid and interface science*, 193, 24-34.
- Gupta, V. K., Mittal, A., & Gajbe, V. (2005). Adsorption and desorption studies of a water soluble dye, Quinoline Yellow, using waste materials. *Journal of colloid and interface science*, 284(1), 89-98.
- Gupta, V. K., Nayak, A., & Agarwal, S. (2015). Bioadsorbents for remediation of heavy metals: current status and their future prospects. *Environmental Engineering Research*, 20(1), 1-18.
- Gupta, V. K., & Saleh, T. A. (2013). Sorption of pollutants by porous carbon, carbon nanotubes and fullerene- An overview. *Environmental science and pollution Research*, 20(5), 2828-2843.
- Gurr, E. (2012). *Synthetic dyes in biology, medicine and chemistry*: Elsevier.
- Hamdaoui, O. (2006). Batch study of liquid-phase adsorption of methylene blue using cedar sawdust and crushed brick. *Journal of hazardous materials*, 135(1), 264-273.
- Hamdaoui, Q., & Chiha, M. (2007). Removal of methylene blue from aqueous solutions by wheat bran. *Acta Chimica Slovenica*, 54(2), 407.
- Hameed, B., Din, A. M., & Ahmad, A. (2007). Adsorption of methylene blue onto bamboo-based activated carbon: kinetics and equilibrium studies. *Journal of hazardous materials*, 141(3), 819-825.
- Hameed, B. H. (2009). Spent tea leaves: a new non-conventional and low-cost adsorbent for removal of basic dye from aqueous solutions. *Journal of hazardous materials*, 161(2), 753-759.
- Han, S., Wu, D., Li, S., Zhang, F., & Feng, X. (2014). Porous graphene materials for advanced electrochemical energy storage and conversion devices. *Advanced Materials*, 26(6), 849-864.
- Hanelt, S., Friedrich, J. F., Orts-Gil, G., & Meyer-Plath, A. (2012). Study of Lewis acid catalyzed chemical bromination and bromoalkylation of multi-walled carbon nanotubes. *Carbon*, 50(3), 1373-1385.
- Haseman, J., Tharrington, E., Huff, J., & McConnell, E. (1986). Comparison of site-specific and overall tumor incidence analyses for 81 recent National Toxicology Program carcinogenicity studies. *Regulatory toxicology and pharmacology*, 6(2), 155-170.
- Haynes, W. M. (2014). *CRC handbook of chemistry and physics*: CRC press.
- Hayyan, M., Abo-Hamad, A., AlSaadi, M., & Hashim, M. (2015). Functionalization of graphene using deep eutectic solvents. *Nanoscale research letters*, 10(1), 1-26.
- He, D., Li, H., Li, W., Haghi-Ashtiani, P., Lejay, P., & Bai, J. (2011). Growth of carbon nanotubes in six orthogonal directions on spherical alumina microparticles. *Carbon*, 49(7), 2273-2286.

- Heemken, O., Reincke, H., Stachel, B., & Theobald, N. (2001). The occurrence of xenoestrogens in the Elbe river and the North Sea. *Chemosphere*, 45(3), 245-259.
- Helal, H. O. (2015). *Design of an electrical sensor for scale deposition detection using Carbon Nanotubes*. The Petroleum Institute (United Arab Emirates).
- Hernadi, K., Fonseca, A., Nagy, J. B., Siska, A., & Kiricsi, I. (2000). Production of nanotubes by the catalytic decomposition of different carbon-containing compounds. *Applied Catalysis A: General*, 199(2), 245-255.
- Hernadi, K., Siska, A., Thien-Nga, L., Forro, L., & Kiricsi, I. (2001). Reactivity of different kinds of carbon during oxidative purification of catalytically prepared carbon nanotubes. *Solid State Ionics*, 141, 203-209.
- Hernandez, J. M. M., San German, C. M. R., Arceo, L. D. B., Villalobos, L. Z., & Flores, M. E. (2013). Synthesis and characterization of carbon nanospheres obtained by microwave radiation. *Carbon*, 54, 168-174.
- Hiraoka, T., Kawakubo, T., Kimura, J., Taniguchi, R., Okamoto, A., Okazaki, T., . . . Shinohara, H. (2003). Selective synthesis of double-wall carbon nanotubes by CCVD of acetylene using zeolite supports. *Chemical Physics Letters*, 382(5), 679-685.
- Ho, S.-M., Tang, W.-Y., De Frausto, J. B., & Prins, G. S. (2006). Developmental exposure to estradiol and bisphenol A increases susceptibility to prostate carcinogenesis and epigenetically regulates phosphodiesterase type 4 variant 4. *Cancer research*, 66(11), 5624-5632.
- Ho, Y.-S., Chiu, W.-T., & Wang, C.-C. (2005). Regression analysis for the sorption isotherms of basic dyes on sugarcane dust. *Bioresource technology*, 96(11), 1285-1291.
- Ho, Y.-S., & McKay, G. (1999). Pseudo-second order model for sorption processes. *Process Biochemistry*, 34(5), 451-465.
- Honma, S., Suzuki, A., Buchanan, D. L., Katsu, Y., Watanabe, H., & Iguchi, T. (2002). Low dose effect of in utero exposure to bisphenol A and diethylstilbestrol on female mouse reproduction. *Reproductive toxicology*, 16(2), 117-122.
- Hruzewicz-Kołodziejczyk, A., Ting, V. P., Bimbo, N., & Mays, T. J. (2012). Improving comparability of hydrogen storage capacities of nanoporous materials. *International Journal of Hydrogen Energy*, 37(3), 2728-2736.
- Hu, H., Yu, B., Ye, Q., Gu, Y., & Zhou, F. (2010). Modification of carbon nanotubes with a nanothin polydopamine layer and polydimethylamino-ethyl methacrylate brushes. *Carbon*, 48(8), 2347-2353.
- Huang, Q., & Weber, W. J. (2005). Transformation and removal of bisphenol A from aqueous phase via peroxidase-mediated oxidative coupling reactions: efficacy, products, and pathways. *Environmental science & technology*, 39(16), 6029-6036.

- Huang, Y., Wong, C., Zheng, J., Bouwman, H., Barra, R., Wahlström, B., . . . Wong, M. (2012). Bisphenol A (BPA) in China: a review of sources, environmental levels, and potential human health impacts. *Environment international*, 42, 91-99.
- Hussain, C. M., & Mitra, S. (2011). Micropreconcentration units based on carbon nanotubes (CNT). *Analytical and bioanalytical chemistry*, 399(1), 75-89.
- Hussein, A. K. (2015). Applications of nanotechnology in renewable energies—A comprehensive overview and understanding. *Renewable and Sustainable Energy Reviews*, 42(Supplement C), 460-476.
- Hussein, M., Zakarya, S., Sarijo, S., & Zainal, Z. (2012). Parameter optimisation of carbon nanotubes synthesis via hexane decomposition over minerals generated from Anadara granosa shells as the catalyst support. *Journal of Nanomaterials*, 2012, 90.
- Iijima, S. (1991). Helical microtubules of graphitic carbon. *nature*, 354(6348), 56-58.
- Inyang, M., Gao, B., Zimmerman, A., Zhang, M., & Chen, H. (2014). Synthesis, characterization, and dye sorption ability of carbon nanotube–biochar nanocomposites. *Chemical Engineering Journal*, 236, 39-46.
- Isobe, T., Takada, H., Kanai, M., Tsutsumi, S., Isobe, K. O., Boonyatumanond, R., & Zakaria, M. P. (2007). Distribution of polycyclic aromatic hydrocarbons (PAHs) and phenolic endocrine disrupting chemicals in South and Southeast Asian mussels. *Environmental Monitoring and Assessment*, 135(1), 423-440.
- Izadi, N., Rashidi, A. M., Horri, B. A., Mosoudi, M. R., Bozorgzadeh, H. R., & Zeraatkar, A. (2011). Growth of single-walled carbon nanotubes on a Co–Mo–MgO supported catalyst by the CVD of methane in a fixed bed reactor: Model setting and parameter estimation. *Solid State Sciences*, 13(6), 1242-1250.
- Jafari, M., & Aghamiri, S. (2011). Evaluation of carbon nanotubes as solid-phase extraction sorbent for the removal of cephalexin from aqueous solution. *Desalination and Water Treatment*, 28(1-3), 55-58.
- Ji, L., Chen, W., Bi, J., Zheng, S., Xu, Z., Zhu, D., & Alvarez, P. J. (2010). Adsorption of tetracycline on single-walled and multi-walled carbon nanotubes as affected by aqueous solution chemistry. *Environmental Toxicology and Chemistry*, 29(12), 2713-2719.
- Jiang, T., Liang, Y.-d., He, Y.-j., & Wang, Q. (2015). Activated carbon/NiFe<sub>2</sub>O<sub>4</sub> magnetic composite: A magnetic adsorbent for the adsorption of methyl orange. *Journal of Environmental Chemical Engineering*, 3(3), 1740-1751.
- Jiang, W., Xiao, F., Wang, D., Wang, Z., & Cai, Y. (2015). Removal of emerging contaminants by pre-mixed PACl and carbonaceous materials. *RSC Adv.*, 5(45), 35461-35468.
- Jin, Z., Wang, X., Sun, Y., Ai, Y., & Wang, X. (2015). Adsorption of 4-n-nonylphenol and bisphenol-A on magnetic reduced graphene oxides: a combined experimental and theoretical studies. *Environmental science & technology*, 49(15), 9168-9175.

- Jorio, A., Pimenta, M. A., Souza Filho, A. G., Saito, R., Dresselhaus, G., & Dresselhaus, M. S. (2003). Characterizing carbon nanotube samples with resonance Raman scattering. *New Journal of Physics*, 5(1), 139.
- José-Yacamán, M., Miki-Yoshida, M., Rendon, L., & Santiesteban, J. (1993). Catalytic growth of carbon microtubules with fullerene structure. *Applied physics letters*, 62(6), 657-659.
- Joseph, L., Boateng, L. K., Flora, J. R. V., Park, Y.-G., Son, A., Badawy, M., & Yoon, Y. (2013). Removal of bisphenol A and 17 $\alpha$ -ethinyl estradiol by combined coagulation and adsorption using carbon nanomaterials and powdered activated carbon. *Separation and Purification Technology*, 107, 37-47.
- Joseph, L., Heo, J., Park, Y.-G., Flora, J. R. V., & Yoon, Y. (2011). Adsorption of bisphenol A and 17 $\alpha$ -ethinyl estradiol on single walled carbon nanotubes from seawater and brackish water. *Desalination*, 281, 68-74.
- Joseph, L., Zaib, Q., Khan, I. A., Berge, N. D., Park, Y.-G., Saleh, N. B., & Yoon, Y. (2011). Removal of bisphenol A and 17 $\alpha$ -ethinyl estradiol from landfill leachate using single-walled carbon nanotubes. *Water research*, 45(13), 4056-4068.
- Jourdain, V., & Bichara, C. (2013a). Current understanding of the growth of carbon nanotubes in catalytic chemical vapour deposition. *Carbon*, 58, 2-39.
- Jourdain, V., & Bichara, C. (2013b). Current understanding of the growth of carbon nanotubes in catalytic chemical vapour deposition. *Carbon*, 58(Supplement C), 2-39.
- Jung, C., Son, A., Her, N., Zoh, K.-D., Cho, J., & Yoon, Y. (2015). Removal of endocrine disrupting compounds, pharmaceuticals, and personal care products in water using carbon nanotubes: A review. *Journal of Industrial and Engineering Chemistry*, 27, 1-11.
- Jung, K.-W., Choi, B. H., Hwang, M.-J., Jeong, T.-U., & Ahn, K.-H. (2016). Fabrication of granular activated carbons derived from spent coffee grounds by entrapment in calcium alginate beads for adsorption of acid orange 7 and methylene blue. *Bioresource technology*, 219(Supplement C), 185-195.
- Jung, M., Eun, K. Y., Lee, J.-K., Baik, Y.-J., Lee, K.-R., & Park, J. W. (2001). Growth of carbon nanotubes by chemical vapor deposition. *Diamond and Related Materials*, 10(3), 1235-1240.
- Kabir, E. R., Rahman, M. S., & Rahman, I. (2015). A review on endocrine disruptors and their possible impacts on human health. *Environmental toxicology and pharmacology*, 40(1), 241-258.
- Kalavathy M, H., Regupathi, I., Pillai, M. G., & Miranda, L. R. (2009). Modelling, analysis and optimization of adsorption parameters for H<sub>3</sub>PO<sub>4</sub> activated rubber wood sawdust using response surface methodology (RSM). *Colloids and Surfaces B: Biointerfaces*, 70(1), 35-45.
- Kang, C.-S., Fujisawa, K., Ko, Y.-I., Muramatsu, H., Hayashi, T., Endo, M., . . . Kim, Y. A. (2016). Linear carbon chains inside multi-walled carbon nanotubes:

Growth mechanism, thermal stability and electrical properties. *Carbon*, 107(Supplement C), 217-224.

- Kang, J., Han, R., Wang, J., Yang, L., Fan, G., & Li, F. (2015). In situ synthesis of nickel carbide-promoted nickel/carbon nanofibers nanocomposite catalysts for catalytic applications. *Chemical Engineering Journal*, 275(Supplement C), 36-44.
- Kannan, N., & Sundaram, M. M. (2001). Kinetics and mechanism of removal of methylene blue by adsorption on various carbons—a comparative study. *Dyes and pigments*, 51(1), 25-40.
- Karima, B., Mossab, B. L., & A-Hassen, M. (2010). *Removal of methylene blue from aqueous solutions using an acid activated algerian bentonite: Equilibrium and kinetic studies*. Paper presented at the International renewable energy congress.
- Karousis, N., Suarez-Martinez, I., Ewels, C. P., & Tagmatarchis, N. (2016). Structure, properties, functionalization, and applications of carbon nanohorns. *Chemical Reviews*, 116(8), 4850-4883.
- Karousis, N., Tagmatarchis, N., & Tasis, D. (2010). Current Progress on the Chemical Modification of Carbon Nanotubes. *Chemical Reviews*, 110(9), 5366-5397.
- Kathyayini, H., Reddy, K. V., Nagy, J., & Nagaraju, N. (2008). Synthesis of carbon nanotubes over transition metal ions supported on Al (OH)<sub>3</sub>.
- Kawahata, H., Ohta, H., Inoue, M., & Suzuki, A. (2004). Endocrine disrupter nonylphenol and bisphenol A contamination in Okinawa and Ishigaki Islands, Japan—within coral reefs and adjacent river mouths. *Chemosphere*, 55(11), 1519-1527.
- Keleşoğlu, S., Kes, M., Sütçü, L., & Polat, H. (2012). Adsorption of methylene blue from aqueous solution on high lime fly ash: Kinetic, equilibrium, and thermodynamic studies. *Journal of Dispersion Science and Technology*, 33(1), 15-23.
- Khajeh, M., Laurent, S., & Dastafkan, K. (2013). Nanoadsorbents: classification, preparation, and applications (with emphasis on aqueous media). *Chemical Reviews*, 113(10), 7728-7768.
- Khalaj, Z., Monajjemi, M., & Diudea, M. V. (2016). Main Allotropes of Carbon: A Brief Review. *Sustainable Nanosystems Development, Properties, and Applications*, 185.
- Khan, Z. U., Kausar, A., & Ullah, H. (2016). A review on composite papers of graphene oxide, carbon nanotube, polymer/GO, and polymer/CNT: Processing strategies, properties, and relevance. *Polymer-Plastics Technology and Engineering*, 55(6), 559-581.
- Khedr, M., Halim, K. A., & Soliman, N. (2008). Effect of temperature on the kinetics of acetylene decomposition over reduced iron oxide catalyst for the production of carbon nanotubes. *Applied surface science*, 255(5), 2375-2381.

- Kim, C.-H., & Choi, J.-H. (2017). Effects of dispersion methods and surface treatment of carbon nano-tubes on defect detectability and static strengths of adhesive joints. *Composite Structures*, 176, 684-691.
- Kim, C., Yang, K. S., Kojima, M., Yoshida, K., Kim, Y. J., Kim, Y. A., & Endo, M. (2006). Fabrication of Electrospinning-Derived Carbon Nanofiber Webs for the Anode Material of Lithium-Ion Secondary Batteries. *Advanced functional materials*, 16(18), 2393-2397.
- Kim, P., Shi, L., Majumdar, A., & McEuen, P. (2001). Thermal transport measurements of individual multiwalled nanotubes. *Physical Review Letters*, 87(21), 215502.
- Kim, Y., Hayashi, T., Endo, M., Kaburagi, Y., Tsukada, T., Shan, J., . . . Tsuruoka, S. (2005). Synthesis and structural characterization of thin multi-walled carbon nanotubes with a partially faceted cross section by a floating reactant method. *Carbon*, 43(11), 2243-2250.
- Kimura, Y., Yamamoto, M., Shimazaki, R., Kashiwada, A., Matsuda, K., & Yamada, K. (2012). Use of chitosan for removal of bisphenol a from aqueous solutions through quinone oxidation by polyphenol oxidase. *Journal of Applied Polymer Science*, 124(1), 796-804.
- Koduru, J. R., Lingamdinne, L. P., Singh, J., & Choo, K.-H. (2016). Effective removal of bisphenol A (BPA) from water using a goethite/activated carbon composite. *Process Safety and Environmental Protection*, 103, 87-96.
- Krishni, R., Foo, K., & Hameed, B. (2014). Adsorption of cationic dye using a low-cost biowaste adsorbent: equilibrium, kinetic, and thermodynamic study. *Desalination and Water Treatment*, 52(31-33), 6088-6095.
- Kubo, K., Arai, O., Omura, M., Watanabe, R., Ogata, R., & Aou, S. (2003). Low dose effects of bisphenol A on sexual differentiation of the brain and behavior in rats. *Neuroscience research*, 45(3), 345-356.
- Kudo, A. (2016). *Growth Mechanisms of Carbon Nano-fibers, -tubes, and Graphene on Metal Oxide Nano-particles and-wires*. Massachusetts Institute of Technology.
- Kudo, A., Steiner III, S. A., Bayer, B. C., Kidambi, P. R., Hofmann, S., Strano, M. S., & Wardle, B. L. (2014). CVD growth of carbon nanostructures from zirconia: mechanisms and a method for enhancing yield. *Journal of the American Chemical Society*, 136(51), 17808-17817.
- Kukovecz, A., Konya, Z., Nagaraju, N., Willems, I., Tamasi, A., Fonseca, A., . . . Kiricsi, I. (2000). Catalytic synthesis of carbon nanotubes over Co, Fe and Ni containing conventional and sol-gel silica-aluminas. *Physical Chemistry Chemical Physics*, 2(13), 3071-3076.
- Kumar, A., & Xagorarakis, I. (2010). Pharmaceuticals, personal care products and endocrine-disrupting chemicals in US surface and finished drinking waters: a proposed ranking system. *Science of the Total Environment*, 408(23), 5972-5989.

- Kumar, A. S. K., Jiang, S.-J., & Tseng, W.-L. (2015). Effective adsorption of chromium (VI)/Cr (III) from aqueous solution using ionic liquid functionalized multiwalled carbon nanotubes as a super sorbent. *Journal of Materials Chemistry A*, 3(13), 7044-7057.
- Kumar, M., & Ando, Y. (2003). A simple method of producing aligned carbon nanotubes from an unconventional precursor—Camphor. *Chemical Physics Letters*, 374(5), 521-526.
- Kumar, M., & Ando, Y. (2005). Controlling the diameter distribution of carbon nanotubes grown from camphor on a zeolite support. *Carbon*, 43(3), 533-540.
- Kumar, M., & Ando, Y. (2010). Chemical vapor deposition of carbon nanotubes: a review on growth mechanism and mass production. *Journal of nanoscience and nanotechnology*, 10(6), 3739-3758.
- Kumar, M., Kakamu, K., Okazaki, T., & Ando, Y. (2004). Field emission from camphor-pyrolyzed carbon nanotubes. *Chemical Physics Letters*, 385(3), 161-165.
- Kumar, P. S., Ramalingam, S., & Sathishkumar, K. (2011). Removal of methylene blue dye from aqueous solution by activated carbon prepared from cashew nut shell as a new low-cost adsorbent. *Korean Journal of Chemical Engineering*, 28(1), 149-155.
- Kunduru, K. R., Nazarkovsky, M., Farah, S., Pawar, R. P., Basu, A., & Domb, A. J. (2017). 2 - Nanotechnology for water purification: applications of nanotechnology methods in wastewater treatment A2 - Grumezescu, Alexandru Mihai *Water Purification* (pp. 33-74): Academic Press.
- Kuo, C.-S., Bai, A., Huang, C.-M., Li, Y.-Y., Hu, C.-C., & Chen, C.-C. (2005). Diameter control of multiwalled carbon nanotubes using experimental strategies. *Carbon*, 43(13), 2760-2768.
- Kuo, C.-Y. (2009). Comparison with as-grown and microwave modified carbon nanotubes to removal aqueous bisphenol A. *Desalination*, 249(3), 976-982.
- Kuo, C.-Y., Wu, C.-H., & Wu, J.-Y. (2008). Adsorption of direct dyes from aqueous solutions by carbon nanotubes: Determination of equilibrium, kinetics and thermodynamics parameters. *Journal of colloid and interface science*, 327(2), 308-315.
- Kuppusamy, S., Thavamani, P., Megharaj, M., Venkateswarlu, K., Lee, Y. B., & Naidu, R. (2016). Potential of *Melaleuca diosmifolia* as a novel, non-conventional and low-cost coagulating adsorbent for removing both cationic and anionic dyes. *Journal of Industrial and Engineering Chemistry*, 37(Supplement C), 198-207.
- Kushwaha, A. K., Gupta, N., & Chattopadhyaya, M. (2014). Removal of cationic methylene blue and malachite green dyes from aqueous solution by waste materials of *Daucus carota*. *Journal of Saudi Chemical Society*, 18(3), 200-207.



- Kwon, J., & Lee, B. (2015). Bisphenol A adsorption using reduced graphene oxide prepared by physical and chemical reduction methods. *Chemical Engineering Research and Design*, 104, 519-529.
- Kyzas, G. Z., & Matis, K. A. (2015). Nanoadsorbents for pollutants removal: A review. *Journal of Molecular Liquids*, 203, 159-168.
- Lacerda, R., Teo, K., Teh, A., Yang, M., Dalal, S., Jefferson, D., . . . Amaratunga, G. (2004). Thin-film metal catalyst for the production of multi-wall and single-wall carbon nanotubes. *Journal of Applied Physics*, 96(8), 4456-4462.
- Lagergren, S. (1898). About the theory of so-called adsorption of soluble substances.
- Langmuir, I. (1918). The adsorption of gases on plane surfaces of glass, mica and platinum. *Journal of the American Chemical Society*, 40(9), 1361-1403.
- Laurila, T., Sainio, S., & Caro, M. A. (2017). Hybrid carbon based nanomaterials for electrochemical detection of biomolecules. *Progress in Materials Science*, 88, 499-594.
- Lee, C. J., Lyu, S. C., Kim, H.-W., Park, C.-Y., & Yang, C.-W. (2002). Large-scale production of aligned carbon nanotubes by the vapor phase growth method. *Chemical Physics Letters*, 359(1-2), 109-114.
- Lee, C. J., & Park, J. (2000). Growth model of bamboo-shaped carbon nanotubes by thermal chemical vapor deposition. *Applied physics letters*, 77(21), 3397-3399.
- Lee, J., Choi, K., Park, J., Moon, H.-B., Choi, G., Lee, J. J., . . . Kim, S. (2017). Bisphenol A distribution in serum, urine, placenta, breast milk, and umbilical cord serum in a birth panel of mother–neonate pairs. *Science of the Total Environment*.
- Lee, O., Jung, J., Doo, S., Kim, S.-S., Noh, T.-H., Kim, K.-I., & Lim, Y.-S. (2010). Effects of temperature and catalysts on the synthesis of carbon nanotubes by chemical vapor deposition. *Metals and Materials International*, 16(4), 663-667.
- Lee, S., Hong, J., Koo, J. H., Lee, H., Lee, S., Choi, T., . . . Kim, H. (2013). Synthesis of few-layered graphene nanoballs with copper cores using solid carbon source. *ACS applied materials & interfaces*, 5(7), 2432-2437.
- Leranth, C., Hajszan, T., Szigeti-Buck, K., Bober, J., & MacLusky, N. J. (2008). Bisphenol A prevents the synaptogenic response to estradiol in hippocampus and prefrontal cortex of ovariectomized nonhuman primates. *Proceedings of the National Academy of Sciences*, 105(37), 14187-14191.
- Li, C., Zhong, H., Wang, S., Xue, J., & Zhang, Z. (2015). Removal of basic dye (methylene blue) from aqueous solution using zeolite synthesized from electrolytic manganese residue. *Journal of Industrial and Engineering Chemistry*, 23, 344-352.
- Li, D.-C., Dai, L., Huang, S., Mau, A. W., & Wang, Z. L. (2000). Structure and growth of aligned carbon nanotube films by pyrolysis. *Chemical Physics Letters*, 316(5), 349-355.

- Li, D., Mueller, M. B., Gilje, S., Kaner, R. B., & Wallace, G. G. (2008). Processable aqueous dispersions of graphene nanosheets. *Nature nanotechnology*, 3(2), 101-105.
- Li, H., He, D., Li, T., Genestoux, M., & Bai, J. (2010). Chemical kinetics of catalytic chemical vapor deposition of an acetylene/xylene mixture for improved carbon nanotube production. *Carbon*, 48(15), 4330-4342.
- Li, H., Zhang, D., Han, X., & Xing, B. (2014). Adsorption of antibiotic ciprofloxacin on carbon nanotubes: pH dependence and thermodynamics. *Chemosphere*, 95, 150-155.
- Li, J., Jiang, L., Xiang, X., Xu, S., Wen, R., & Liu, X. (2013). Competitive sorption between 17 $\alpha$ -ethinyl estradiol and bisphenol A/4-n-nonylphenol by soils. *Journal of Environmental Sciences*, 25(6), 1154-1163.
- Li, L., Quinlivan, P. A., & Knappe, D. R. U. (2002). Effects of activated carbon surface chemistry and pore structure on the adsorption of organic contaminants from aqueous solution. *Carbon*, 40(12), 2085-2100.
- Li, M., Liu, Q., Lou, Z., Wang, Y., Zhang, Y., & Qian, G. (2014). Method to characterize acid–base behavior of biochar: site modeling and theoretical simulation. *ACS Sustainable Chemistry & Engineering*, 2(11), 2501-2509.
- Li, S., Gong, Y., Yang, Y., He, C., Hu, L., Zhu, L., . . . Shu, D. (2015). Recyclable CNTs/Fe<sub>3</sub>O<sub>4</sub> magnetic nanocomposites as adsorbents to remove bisphenol A from water and their regeneration. *Chemical Engineering Journal*, 260, 231-239.
- Li, W., Zhang, H., Wang, C., Zhang, Y., Xu, L., Zhu, K., & Xie, S. (1997). Raman characterization of aligned carbon nanotubes produced by thermal decomposition of hydrocarbon vapor. *Applied Physics Letters*, 70(20), 2684-2686.
- Li, W., & Zhao, D. (2013). An overview of the synthesis of ordered mesoporous materials. *Chemical Communications*, 49(10), 943-946.
- Li, X., Chen, S., Fan, X., Quan, X., Tan, F., Zhang, Y., & Gao, J. (2015). Adsorption of ciprofloxacin, bisphenol and 2-chlorophenol on electrospun carbon nanofibers: In comparison with powder activated carbon. *Journal of colloid and interface science*, 447, 120-127.
- Li, Y., Du, Q., Liu, T., Peng, X., Wang, J., Sun, J., . . . Xia, L. (2013). Comparative study of methylene blue dye adsorption onto activated carbon, graphene oxide, and carbon nanotubes. *Chemical Engineering Research and Design*, 91(2), 361-368.
- Li, Y., Zhao, Y., Hu, W., Ahmad, I., Zhu, Y., Peng, X., & Luan, Z. (2007). *Carbon nanotubes-the promising adsorbent in wastewater treatment*. Paper presented at the Journal of physics: conference series.

- Li, Z., Gondal, M. A., & Yamani, Z. H. (2014). Preparation of magnetic separable CoFe<sub>2</sub>O<sub>4</sub>/PAC composite and the adsorption of bisphenol A from aqueous solution. *Journal of Saudi Chemical Society*, 18(3), 208-213.
- Li, Z., Liu, Z., Sun, H., & Gao, C. (2015). Superstructured assembly of nanocarbons: fullerenes, nanotubes, and graphene. *Chemical Reviews*, 115(15), 7046-7117.
- Liang, Y., Han, Q., & Xin, H. (2013). Elastic properties of carbon nanotubes. *Journal of Computational and Theoretical Nanoscience*, 10(5), 1061-1071.
- Libbrecht, W., Vandaele, K., De Buysser, K., Verberckmoes, A., Thybaut, J. W., Poelman, H., . . . Van Der Voort, P. (2015). Tuning the pore geometry of ordered mesoporous carbons for enhanced adsorption of bisphenol-A. *Materials*, 8(4), 1652-1665.
- Libbrecht, W., Verberckmoes, A., Thybaut, J. W., Van Der Voort, P., & De Clercq, J. (2017). Soft templated mesoporous carbons: Tuning the porosity for the adsorption of large organic pollutants. *Carbon*, 116, 528-546.
- Lin, D., & Xing, B. (2008). Adsorption of phenolic compounds by carbon nanotubes: role of aromaticity and substitution of hydroxyl groups. *Environmental science & technology*, 42(19), 7254-7259.
- Lin, Z., Zeng, Z., Gui, X., Tang, Z., Zou, M., & Cao, A. (2016). Carbon nanotube sponges, aerogels, and hierarchical composites: Synthesis, properties, and energy applications. *Advanced Energy Materials*, 6(17).
- Liu, F., Chung, S., Oh, G., & Seo, T. S. (2012). Three-dimensional graphene oxide nanostructure for fast and efficient water-soluble dye removal. *ACS applied materials & interfaces*, 4(2), 922-927.
- Liu, G., Ma, J., Li, X., & Qin, Q. (2009). Adsorption of bisphenol A from aqueous solution onto activated carbons with different modification treatments. *Journal of hazardous materials*, 164(2), 1275-1280.
- Liu, H., Jin, X., & Ding, B. (2016). Application of nanotechnology in petroleum exploration and development. *Petroleum Exploration and Development*, 43(6), 1107-1115.
- Liu, L., Gao, Z. Y., Su, X. P., Chen, X., Jiang, L., & Yao, J. M. (2015). Adsorption removal of dyes from single and binary solutions using a cellulose-based bioadsorbent. *ACS Sustainable Chemistry & Engineering*, 3(3), 432-442.
- Liu, S., Sun, J., & Huang, Z. (2010). Carbon spheres/activated carbon composite materials with high Cr (VI) adsorption capacity prepared by a hydrothermal method. *Journal of hazardous materials*, 173(1), 377-383.
- Liu, T., Li, Y., Du, Q., Sun, J., Jiao, Y., Yang, G., . . . Wang, K. (2012). Adsorption of methylene blue from aqueous solution by graphene. *Colloids and Surfaces B: Biointerfaces*, 90, 197-203.
- Liu, X., Wang, M., Zhang, S., & Pan, B. (2013). Application potential of carbon nanotubes in water treatment: A review. *Journal of Environmental Sciences*, 25(7), 1263-1280.

- Liu, Y., Kang, Y., Mu, B., & Wang, A. (2014). Attapulgite/bentonite interactions for methylene blue adsorption characteristics from aqueous solution. *Chemical Engineering Journal*, 237, 403-410.
- Liu, Y., Wang, W., & Wang, A. (2012). Effect of dry grinding on the microstructure of palygorskite and adsorption efficiency for methylene blue. *Powder technology*, 225, 124-129.
- Liu, Y., Zhong, G., Liu, Z., Meng, M., Liu, F., & Ni, L. (2016). Facile synthesis of novel photoresponsive mesoporous molecularly imprinted polymers for photo-regulated selective separation of bisphenol A. *Chemical Engineering Journal*, 296, 437-446.
- Locatelli, M., Sciascia, F., Cifelli, R., Malatesta, L., Bruni, P., & Croce, F. (2016). Analytical methods for the endocrine disruptor compounds determination in environmental water samples. *Journal of Chromatography A*, 1434, 1-18.
- Louis, B., Gulino, G., Vieira, R., Amadou, J., Dintzer, T., Galvagno, S., . . . Pham-Huu, C. (2005). High yield synthesis of multi-walled carbon nanotubes by catalytic decomposition of ethane over iron supported on alumina catalyst. *Catalysis Today*, 102, 23-28.
- Lu, C., Chung, Y.-L., & Chang, K.-F. (2005). Adsorption of trihalomethanes from water with carbon nanotubes. *Water research*, 39(6), 1183-1189.
- Lu, C., Chung, Y.-L., & Chang, K.-F. (2006). Adsorption thermodynamic and kinetic studies of trihalomethanes on multiwalled carbon nanotubes. *Journal of hazardous materials*, 138(2), 304-310.
- Luo, X., Wang, C., Wang, L., Deng, F., Luo, S., Tu, X., & Au, C. (2013). Nanocomposites of graphene oxide-hydrated zirconium oxide for simultaneous removal of As (III) and As (V) from water. *Chemical Engineering Journal*, 220, 98-106.
- Luo, Y., Guo, W., Ngo, H. H., Nghiem, L. D., Hai, F. I., Zhang, J., . . . Wang, X. C. (2014). A review on the occurrence of micropollutants in the aquatic environment and their fate and removal during wastewater treatment. *Science of the Total Environment*, 473, 619-641.
- Lyu, S. C., Liu, B. C., Lee, C. J., Kang, H. K., Yang, C.-W., & Park, C. Y. (2003). High-quality double-walled carbon nanotubes produced by catalytic decomposition of benzene. *Chemistry of Materials*, 15(20), 3951-3954.
- Ma, J., Yu, F., Zhou, L., Jin, L., Yang, M., Luan, J., . . . Chen, J. (2012). Enhanced adsorptive removal of methyl orange and methylene blue from aqueous solution by alkali-activated multiwalled carbon nanotubes. *ACS applied materials & interfaces*, 4(11), 5749-5760.
- Machado, F. M., Bergmann, C. P., Fernandes, T. H., Lima, E. C., Royer, B., Calvete, T., & Fagan, S. B. (2011a). Adsorption of Reactive Red M-2BE dye from water solutions by multi-walled carbon nanotubes and activated carbon. *Journal of hazardous materials*, 192(3), 1122-1131.

- Machado, F. M., Bergmann, C. P., Fernandes, T. H. M., Lima, E. C., Royer, B., Calvete, T., & Fagan, S. B. (2011b). Adsorption of Reactive Red M-2BE dye from water solutions by multi-walled carbon nanotubes and activated carbon. *Journal of Hazardous Materials*, 192(3), 1122-1131.
- Madannejad, S., Rashidi, A., Sadeghhassani, S., Shemirani, F., & Ghasemy, E. (2018). Removal of 4-chlorophenol from water using different carbon nanostructures: A comparison study. *Journal of Molecular Liquids*, 249(Supplement C), 877-885.
- Majewska, M. M. (2015). *Functionalizing carbon nanotubes for crosslinking and properties control*: Yale University.
- Makino, T., Edamura, M., Kato, A., & Yoshida, A. (1992). Thermal radiation properties of molten salt (properties of alkali metal carbonates). *Heat transfer. Japanese research*, 21(4), 331-339.
- Makinwa, T., & Uadia, P. (2015). A Survey of the Level of Bisphenol A (BPA) in Effluents, Soil Leachates, Food Samples, Drinking Water and Consumer Products in South-Western Nigeria. *World Environment*, 5(4), 135-139.
- Mallakpour, S., & Khadem, E. (2016). Carbon nanotube–metal oxide nanocomposites: Fabrication, properties and applications. *Chemical Engineering Journal*, 302(Supplement C), 344-367.
- Manilo, M., Lebovka, N., & Barany, S. (2016). Mechanism of Methylene Blue adsorption on hybrid laponite-multi-walled carbon nanotube particles. *Journal of Environmental Sciences*, 42, 134-141.
- Manzano-Ramírez, A., Moreno-Barcenas, A., Apatiga-Castro, M., Mauricio Rivera-Munoz, E., Nava-Mendoza, R., & Velázquez-Castillo, R. (2013). An overview of carbon nanotubes: synthesis, purification and characterization. *Current Organic Chemistry*, 17(17), 1858-1866.
- Markey, C. M., Wadia, P. R., Rubin, B. S., Sonnenschein, C., & Soto, A. M. (2005). Long-Term Effects of Fetal Exposure to Low Doses of the Xenoestrogen Bisphenol-A in the Female Mouse Genital Tract 1. *Biology of reproduction*, 72(6), 1344-1351.
- Marrakchi, F., Ahmed, M. J., Khanday, W. A., Asif, M., & Hameed, B. H. (2017). Mesoporous-activated carbon prepared from chitosan flakes via single-step sodium hydroxide activation for the adsorption of methylene blue. *International Journal of Biological Macromolecules*, 98(Supplement C), 233-239.
- Martín-Jimeno, F., Suárez-García, F., Paredes, J., Martínez-Alonso, A., & Tascón, J. (2015). Activated carbon xerogels with a cellular morphology derived from hydrothermally carbonized glucose-graphene oxide hybrids and their performance towards CO<sub>2</sub> and dye adsorption. *Carbon*, 81, 137-147.
- Mattevi, C., Wirth, C. T., Hofmann, S., Blume, R., Cantoro, M., Ducati, C., . . . Castellarin-Cudia, C. (2008). In-situ X-ray photoelectron spectroscopy study of catalyst– support interactions and growth of carbon nanotube forests. *The Journal of Physical Chemistry C*, 112(32), 12207-12213.

- McKay, G., Porter, J., & Prasad, G. (1999). The removal of dye colours from aqueous solutions by adsorption on low-cost materials. *Water, Air, & Soil Pollution*, 114(3), 423-438.
- McKee, G. S., & Vecchio, K. S. (2006). Thermogravimetric analysis of synthesis variation effects on CVD generated multiwalled carbon nanotubes. *The Journal of Physical Chemistry B*, 110(3), 1179-1186.
- Melo, S. M., & Brito, N. M. (2014). Analysis and occurrence of endocrine disruptors in Brazilian water by HPLC-fluorescence detection. *Water, Air, & Soil Pollution*, 225(1), 1783.
- Menendez, J. A., Radovic, L. R., Xia, B., & Phillips, J. (1996). Low-temperature generation of basic carbon surfaces by hydrogen spillover. *The Journal of Physical Chemistry*, 100(43), 17243-17248.
- Meshot, E. R., Zwissler, D. W., Bui, N., Kuykendall, T. R., Wang, C., Hexemer, A., . . . Fornasiero, F. (2017). Quantifying the Hierarchical Order in Self-Aligned Carbon Nanotubes from Atomic to Micrometer Scale. *ACS nano*.
- Meunier, V., Souza Filho, A., Barros, E., & Dresselhaus, M. (2016). Physical properties of low-dimensional sp<sup>2</sup>-based carbon nanostructures. *Reviews of Modern Physics*, 88(2), 025005.
- Meyyappan, M., Delzeit, L., Cassell, A., & Hash, D. (2003). Carbon nanotube growth by PECVD: a review. *Plasma Sources Science and Technology*, 12(2), 205.
- Mickelson, E., Huffman, C., Rinzler, A., Smalley, R., Hauge, R., & Margrave, J. (1998). Fluorination of single-wall carbon nanotubes. *Chemical Physics Letters*, 296(1), 188-194.
- Mishra, S. (2016). Nanotechnology in medicine. *Indian Heart Journal*, 68(3), 437-439.
- Mleczko, L., & Lolli, G. (2013). Carbon nanotubes: an example of multiscale development—a mechanistic view from the subnanometer to the meter scale. *Angewandte Chemie International Edition*, 52(36), 9372-9387.
- MOE, B. (1997). Environmental Management Act, Contaminated Sites Regulation. *BC Reg*, 375, 96.
- Moghaddam, S. S., Moghaddam, M. A., & Arami, M. (2010). Coagulation/flocculation process for dye removal using sludge from water treatment plant: optimization through response surface methodology. *Journal of hazardous materials*, 175(1), 651-657.
- Mohmood, I., Lopes, C. B., Lopes, I., Ahmad, I., Duarte, A. C., & Pereira, E. (2013). Nanoscale materials and their use in water contaminants removal—a review. *Environmental science and pollution Research*, 20(3), 1239-1260.
- Montes-Moran, M. A., Menéndez, J. A., Fuente, E., & Suarez, D. (1998). Contribution of the basal planes to carbon basicity: An ab Initio study of the H<sub>3</sub>O<sup>+</sup>– $\pi$  interaction in cluster models. *The Journal of Physical Chemistry B*, 102(29), 5595-5601.

- Mubarak, N., Sahu, J., Abdullah, E., & Jayakumar, N. (2014). Removal of heavy metals from wastewater using carbon nanotubes. *Separation & Purification Reviews*, 43(4), 311-338.
- Mubarak, N. M., Abdullah, E. C., Jayakumar, N. S., & Sahu, J. N. (2014). An overview on methods for the production of carbon nanotubes. *Journal of Industrial and Engineering Chemistry*, 20(4), 1186-1197.
- Mukhopadhyay, S. M., & Karumuri, A. K. (2010). Nanotube attachment for prevention of interfacial delamination. *Journal of Physics D: Applied Physics*, 43(36), 365301.
- Mulzer, C. R., Shen, L., Bisbey, R. P., McKone, J. R., Zhang, N., Abruña, H. D., & Dichtel, W. R. (2016). Superior charge storage and power density of a conducting polymer-modified covalent organic framework. *ACS central science*, 2(9), 667-673.
- Muñoz-de-Toro, M., Markey, C. M., Wadia, P. R., Luque, E. H., Rubin, B. S., Sonnenschein, C., & Soto, A. M. (2005). Perinatal exposure to bisphenol-A alters peripubertal mammary gland development in mice. *Endocrinology*, 146(9), 4138-4147.
- Murakami, T., Sako, T., Harima, H., Kisoda, K., Mitikami, K., & Isshiki, T. (2004). Raman study of SWNTs grown by CCVD method on SiC. *Thin solid films*, 464, 319-322.
- Murray, T. J., Maffini, M. V., Ucci, A. A., Sonnenschein, C., & Soto, A. M. (2007). Induction of mammary gland ductal hyperplasias and carcinoma in situ following fetal bisphenol A exposure. *Reproductive toxicology*, 23(3), 383-390.
- Murty, B., Shankar, P., Raj, B., Rath, B., & Murday, J. (2013). Applications of nanomaterials *Textbook of nanoscience and nanotechnology* (pp. 107-148): Springer.
- Nagaraju, N., Fonseca, A., Konya, Z., & Nagy, J. (2002). Alumina and silica supported metal catalysts for the production of carbon nanotubes. *Journal of molecular catalysis A: Chemical*, 181(1), 57-62.
- Nagel, S. C., vom Saal, F. S., Thayer, K. A., Dhar, M. G., Boechler, M., & Welshons, W. V. (1997). Relative binding affinity-serum modified access (RBA-SMA) assay predicts the relative in vivo bioactivity of the xenoestrogens bisphenol A and octylphenol. *Environmental health perspectives*, 105(1), 70.
- Narkiewicz, U., Podsiadły, M., Jędrzejewski, R., & Pelech, I. (2010). Catalytic decomposition of hydrocarbons on cobalt, nickel and iron catalysts to obtain carbon nanomaterials. *Applied Catalysis A: General*, 384(1), 27-35.
- Nazal, M. K., Oweimreen, G. A., Khaled, M., Atieh, M. A., Aljundi, I. H., & Abulkibash, A. M. (2016). Adsorption isotherms and kinetics for dibenzothiophene on activated carbon and carbon nanotube doped with nickel oxide nanoparticles. *Bulletin of Materials Science*, 39(2), 437-450.

- Nessim, G. D. (2010). Properties, synthesis, and growth mechanisms of carbon nanotubes with special focus on thermal chemical vapor deposition. *Nanoscale*, 2(8), 1306-1323.
- Nessim, G. D., Seita, M., O'Brien, K. P., Hart, A. J., Bonaparte, R. K., Mitchell, R. R., & Thompson, C. V. (2009). Low temperature synthesis of vertically aligned carbon nanotubes with electrical contact to metallic substrates enabled by thermal decomposition of the carbon feedstock. *Nano letters*, 9(10), 3398-3405.
- Newbold, R. R., Jefferson, W. N., & Padilla-Banks, E. (2009). Prenatal exposure to bisphenol a at environmentally relevant doses adversely affects the murine female reproductive tract later in life. *Environmental health perspectives*, 117(6), 879.
- Norzilah, A., Fakhru'l-Razi, A., Choong, T. S., & Chuah, A. L. (2011). Surface modification effects on CNTs adsorption of methylene blue and phenol. *Journal of Nanomaterials*, 2011, 55.
- O'Connell, M. J. (2012). *Carbon nanotubes: properties and applications*: CRC press.
- Oberlin, A., Endo, M., & Koyama, T. (1976). Filamentous growth of carbon through benzene decomposition. *Journal of crystal growth*, 32(3), 335-349.
- Ocampo-Pérez, R., Rivera-Utrilla, J., Méndez-Díaz, J. D., & Sánchez-Polo, M. (2012). Modeling adsorption rate of organic micropollutants present in landfill leachates onto granular activated carbon. *Journal of colloid and interface science*, 385(1), 174-182.
- Oei, B. C., Ibrahim, S., Wang, S., & Ang, H. M. (2009). Surfactant modified barley straw for removal of acid and reactive dyes from aqueous solution. *Bioresource technology*, 100(18), 4292-4295.
- Ofomaja, A. E. (2008). Sorptive removal of Methylene blue from aqueous solution using palm kernel fibre: Effect of fibre dose. *Biochemical Engineering Journal*, 40(1), 8-18.
- Onundi, Y. B., Mamun, A., Al Khatib, M., Al Saadi, M., & Suleyman, A. (2011). Heavy metals removal from synthetic wastewater by a novel nano-size composite adsorbent. *International Journal of Environmental Science and Technology:(IJEST)*, 8(4), 799.
- Palanza, P. L., Howdeshell, K. L., Parmigiani, S., & vom Saal, F. S. (2002). Exposure to a low dose of bisphenol A during fetal life or in adulthood alters maternal behavior in mice. *Environmental health perspectives*, 110(Suppl 3), 415.
- Palizdar, M., Ahgababazadeh, R., Mirhabibi, A., Brydson, R., & Pilehvari, S. (2011). Investigation of Fe/MgO catalyst support precursors for the chemical vapour deposition growth of carbon nanotubes. *Journal of nanoscience and nanotechnology*, 11(6), 5345-5351.
- Pan, B., Lin, D., Mashayekhi, H., & Xing, B. (2008). Adsorption and hysteresis of bisphenol A and 17 $\alpha$ -ethinyl estradiol on carbon nanomaterials. *Environmental science & technology*, 42(15), 5480-5485.



- Pan, B., & Xing, B. (2008). Adsorption mechanisms of organic chemicals on carbon nanotubes. *Environmental science & technology*, 42(24), 9005-9013.
- Park, C., & Keane, M. A. (2004). Catalyst support effects in the growth of structured carbon from the decomposition of ethylene over nickel. *Journal of catalysis*, 221(2), 386-399.
- Park, H.-S., Koduru, J. R., Choo, K.-H., & Lee, B. (2015). Activated carbons impregnated with iron oxide nanoparticles for enhanced removal of bisphenol A and natural organic matter. *Journal of hazardous materials*, 286, 315-324.
- Park, S., Vosguerichian, M., & Bao, Z. (2013). A review of fabrication and applications of carbon nanotube film-based flexible electronics. *Nanoscale*, 5(5), 1727-1752.
- Park, Y., Sun, Z., Ayoko, G. A., & Frost, R. L. (2014). Bisphenol A sorption by organo-montmorillonite: implications for the removal of organic contaminants from water. *Chemosphere*, 107, 249-256.
- Patrolecco, L., Capri, S., Angelis, S. D., Pagnotta, R., Polesello, S., & Valsecchi, S. (2006). Partition of nonylphenol and related compounds among different aquatic compartments in Tiber River (Central Italy). *Water, Air, & Soil Pollution*, 172(1), 151-166.
- Pelekani, C., & Snoeyink, V. L. (2000). Competitive adsorption between atrazine and methylene blue on activated carbon: the importance of pore size distribution. *Carbon*, 38(10), 1423-1436.
- Peng, H., Pan, B., Wu, M., Liu, R., Zhang, D., Wu, D., & Xing, B. (2012). Adsorption of ofloxacin on carbon nanotubes: Solubility, pH and cosolvent effects. *Journal of Hazardous Materials*, 211–212(0), 342-348.
- Peng, X., Li, Y., Luan, Z., Di, Z., Wang, H., Tian, B., & Jia, Z. (2003). Adsorption of 1, 2-dichlorobenzene from water to carbon nanotubes. *Chemical Physics Letters*, 376(1), 154-158.
- Peng, X., Luan, Z., Di, Z., Zhang, Z., & Zhu, C. (2005). Carbon nanotubes-iron oxides magnetic composites as adsorbent for removal of Pb (II) and Cu (II) from water. *Carbon*, 43(4), 880-883.
- Peng, X., Luan, Z., Ding, J., Di, Z., Li, Y., & Tian, B. (2005). Ceria nanoparticles supported on carbon nanotubes for the removal of arsenate from water. *Materials Letters*, 59(4), 399-403.
- Pereira, M. F. R., Soares, S. F., Órfão, J. J., & Figueiredo, J. L. (2003). Adsorption of dyes on activated carbons: influence of surface chemical groups. *Carbon*, 41(4), 811-821.
- Peretz, J., Vrooman, L., Ricke, W. A., Hunt, P. A., Ehrlich, S., Hauser, R., . . . VandeVoort, C. A. (2014). Bisphenol A and reproductive health: update of experimental and human evidence, 2007–2013. *Environmental health perspectives*, 122(8), 775.

- Pham-Huu, C., Vieira, R., Louis, B., Carvalho, A., Amadou, J., Dintzer, T., & Ledoux, M. J. (2006). About the octopus-like growth mechanism of carbon nanofibers over graphite supported nickel catalyst. *Journal of catalysis*, 240(2), 194-202.
- Piao, L., Li, Y., Chen, J., Chang, L., & Lin, J. Y. (2002). Methane decomposition to carbon nanotubes and hydrogen on an alumina supported nickel aerogel catalyst. *Catalysis Today*, 74(1), 145-155.
- Piao, L., Liu, Q., & Li, Y. (2012). Interaction of amino acids and single-wall carbon nanotubes. *The Journal of Physical Chemistry C*, 116(2), 1724-1731.
- Pichon, V., & Chapuis-Hugon, F. (2008). Role of molecularly imprinted polymers for selective determination of environmental pollutants—a review. *Analytica chimica acta*, 622(1), 48-61.
- Pignatello, J., Mitch, W. A., & Xu, W. (2017). Activity and reactivity of pyrogenic carbonaceous matter toward organic compounds. *Environmental science & technology*, 51(16), 8893-8908.
- Pignotti, E., Farré, M., Barceló, D., & Dinelli, E. (2017). Occurrence and distribution of six selected endocrine disrupting compounds in surface-and groundwaters of the Romagna area (North Italy). *Environmental science and pollution Research*, 24(26), 21153-21167.
- Pinault, M., Mayne-L'Hermite, M., Reynaud, C., Pichot, V., Launois, P., & Ballutaud, D. (2005). Growth of multiwalled carbon nanotubes during the initial stages of aerosol-assisted CCVD. *Carbon*, 43(14), 2968-2976.
- Pochorovski, I., Wang, H., Feldblyum, J. I., Zhang, X., Antaris, A. L., & Bao, Z. (2015). H-bonded supramolecular polymer for the selective dispersion and subsequent release of large-diameter semiconducting single-walled carbon nanotubes. *Journal of the American Chemical Society*, 137(13), 4328-4331.
- Pop, E., Mann, D., Wang, Q., Goodson, K., & Dai, H. (2006). Thermal conductance of an individual single-wall carbon nanotube above room temperature. *Nano letters*, 6(1), 96-100.
- Pradhan, B. K., & Sandle, N. (1999). Effect of different oxidizing agent treatments on the surface properties of activated carbons. *Carbon*, 37(8), 1323-1332.
- Prasek, J., Drbohlavova, J., Chomoucka, J., Hubalek, J., Jasek, O., Adam, V., & Kizek, R. (2011). Methods for carbon nanotubes synthesis—review. *Journal of Materials Chemistry*, 21(40), 15872-15884.
- Premkumar, T., Mezzenga, R., & Geckeler, K. E. (2012). Carbon nanotubes in the liquid phase: addressing the issue of dispersion. *Small*, 8(9), 1299-1313.
- Prieto, G., Shakeri, M., De Jong, K. P., & De Jongh, P. E. (2014). Quantitative relationship between support porosity and the stability of pore-confined metal nanoparticles studied on CuZnO/SiO<sub>2</sub> methanol synthesis catalysts. *ACS nano*, 8(3), 2522-2531.
- Pullket, S. (2015). Sewage sludge as source of activated carbon for the removal of endocrine disrupting chemical in wastewater.

- Qian, D. (2001). Multiwalled carbon nanotube CVD synthesis, modification, and composite applications.
- Qin, F.-X., Jia, S.-Y., Liu, Y., Li, H.-Y., & Wu, S.-H. (2015). Adsorptive removal of bisphenol A from aqueous solution using metal-organic frameworks. *Desalination and Water Treatment*, 54(1), 93-102.
- Qiu, F., Peng, M., Wei, Z., Wang, X., & Yang, J. (2016). Preparation of polyethersulfone/sulfonated polyethersulfonephenylethane microspheres and its application for the adsorption of bisphenol A. *Journal of Applied Polymer Science*, 133(9).
- Qu, S., Huang, F., Yu, S., Chen, G., & Kong, J. (2008). Magnetic removal of dyes from aqueous solution using multi-walled carbon nanotubes filled with Fe<sub>2</sub>O<sub>3</sub> particles. *Journal of hazardous materials*, 160(2), 643-647.
- Qu, X., Alvarez, P. J., & Li, Q. (2013). Applications of nanotechnology in water and wastewater treatment. *Water research*, 47(12), 3931-3946.
- Rafatullah, M., Sulaiman, O., Hashim, R., & Ahmad, A. (2010). Adsorption of methylene blue on low-cost adsorbents: a review. *Journal of hazardous materials*, 177(1), 70-80.
- Rajabi, M., Mahanpoor, K., & Moradi, O. (2017). Removal of dye molecules from aqueous solution by carbon nanotubes and carbon nanotube functional groups: critical review. *RSC Advances*, 7(74), 47083-47090.
- Rajbhandari, R., Shrestha, L. K., Pokharel, B. P., & Pradhananga, R. R. (2013). Development of Nanoporous Structure in Carbons by Chemical Activation with Zinc Chloride. *Journal of nanoscience and nanotechnology*, 13(4), 2613-2623.
- Ramesha, G., Kumara, A. V., Muralidhara, H., & Sampath, S. (2011). Graphene and graphene oxide as effective adsorbents toward anionic and cationic dyes. *Journal of colloid and interface science*, 361(1), 270-277.
- Rao, C., Gopalakrishnan, K., & Maitra, U. (2015). Comparative study of potential applications of graphene, MoS<sub>2</sub>, and other two-dimensional materials in energy devices, sensors, and related areas. *ACS applied materials & interfaces*, 7(15), 7809-7832.
- Rathnayake, S. I., Xi, Y., Frost, R. L., & Ayoko, G. A. (2016). Environmental applications of inorganic–organic clays for recalcitrant organic pollutants removal: Bisphenol A. *Journal of colloid and interface science*, 470, 183-195.
- Raty, J.-Y., Gygi, F., & Galli, G. (2005). Growth of carbon nanotubes on metal nanoparticles: a microscopic mechanism from ab initio molecular dynamics simulations. *Physical Review Letters*, 95(9), 096103.
- Ravi, S., & Vadukumpully, S. (2016). Sustainable carbon nanomaterials: Recent advances and its applications in energy and environmental remediation. *Journal of Environmental Chemical Engineering*, 4(1), 835-856.

- Ren, X., Chen, C., Nagatsu, M., & Wang, X. (2011). Carbon nanotubes as adsorbents in environmental pollution management: A review. *Chemical Engineering Journal*, 170(2–3), 395-410.
- Reshetenko, T. V., Avdeeva, L. B., Ismagilov, Z. R., Chuvilin, A. L., & Ushakov, V. A. (2003). Carbon capacious Ni-Cu-Al<sub>2</sub>O<sub>3</sub> catalysts for high-temperature methane decomposition. *Applied Catalysis A: General*, 247(1), 51-63.
- Robinson, T., McMullan, G., Marchant, R., & Nigam, P. (2001). Remediation of dyes in textile effluent: a critical review on current treatment technologies with a proposed alternative. *Bioresource technology*, 77(3), 247-255.
- Rodriguez, A., Ovejero, G., Sotelo, J., Mestanza, M., & García, J. (2010). Adsorption of dyes on carbon nanomaterials from aqueous solutions. *Journal of Environmental Science and Health Part A*, 45(12), 1642-1653.
- Romero Rodríguez, P. (2017). Synthesis of carbon nanomaterials by catalytic chemical vapor deposition: growth mechanisms on metal powders and foils.
- Ronix, A., Pezoti, O., Souza, L. S., Souza, I. P., Bedin, K. C., Souza, P. S., . . . Almeida, V. C. (2017). Hydrothermal carbonization of coffee husk: Optimization of experimental parameters and adsorption of methylene blue dye. *Journal of Environmental Chemical Engineering*, 5(5), 4841-4849.
- Roosta, M., Ghaedi, M., Daneshfar, A., Sahraei, R., & Asghari, A. (2014). Optimization of the ultrasonic assisted removal of methylene blue by gold nanoparticles loaded on activated carbon using experimental design methodology. *Ultrasonics Sonochemistry*, 21(1), 242-252.
- Rosenzweig, S., Sorial, G. A., Sahle-Demessie, E., & Mack, J. (2013). Effect of acid and alcohol network forces within functionalized multiwall carbon nanotubes bundles on adsorption of copper (II) species. *Chemosphere*, 90(2), 395-402.
- Rubin, B. S. (2011). Bisphenol A: an endocrine disruptor with widespread exposure and multiple effects. *The Journal of steroid biochemistry and molecular biology*, 127(1), 27-34.
- Ruoff, R. S., Qian, D., & Liu, W. K. (2003). Mechanical properties of carbon nanotubes: theoretical predictions and experimental measurements. *Comptes Rendus Physique*, 4(9), 993-1008.
- Sadegh, H., Ali, G. A., Gupta, V. K., Makhlof, A. S. H., Shahryari-ghoshekandi, R., Nadagouda, M. N., . . . Megiel, E. (2017). The role of nanomaterials as effective adsorbents and their applications in wastewater treatment. *Journal of Nanostructure in Chemistry*, 7(1), 1-14.
- Sadegh, H., Shahryari-ghoshekandi, R., & Kazemi, M. (2014). Study in synthesis and characterization of carbon nanotubes decorated by magnetic iron oxide nanoparticles. *International Nano Letters*, 4(4), 129-135.
- Saha, A., Jiang, C., & Martí, A. A. (2014). Carbon nanotube networks on different platforms. *Carbon*, 79, 1-18.

- Salama, A. (2017). New sustainable hybrid material as adsorbent for dye removal from aqueous solutions. *Journal of colloid and interface science*, 487(Supplement C), 348-353.
- Saleh, T. A., & Gupta, V. K. (2012). Photo-catalyzed degradation of hazardous dye methyl orange by use of a composite catalyst consisting of multi-walled carbon nanotubes and titanium dioxide. *Journal of colloid and interface science*, 371(1), 101-106.
- Salehinia, S., Ghoreishi, S. M., Maya, F., & Cerdà, V. (2016). Hydrophobic magnetic montmorillonite composite material for the efficient adsorption and microextraction of bisphenol A from water samples. *Journal of Environmental Chemical Engineering*, 4(4), 4062-4071.
- Samadi, M. T., Shokoohi, R., Poormohammadi, A., Azarian, G., Harati, M., & Shanesaz, S. (2016). Removal of Bisphenol A using Antimony Nanoparticle Multi-walled Carbon Nanotubes composite from aqueous solutions. *Oriental Journal of Chemistry*, 32(2), 1015-1024.
- Sanghi, R., & Verma, P. (2013). Decolorisation of aqueous dye solutions by low-cost adsorbents: a review. *Coloration Technology*, 129(2), 85-108.
- Santangelo, S., Messina, G., Faggio, G., Abdul Rahim, S., & Milone, C. (2012). Effect of sulphuric–nitric acid mixture composition on surface chemistry and structural evolution of liquid-phase oxidised carbon nanotubes. *Journal of Raman Spectroscopy*, 43(10), 1432-1442.
- Santangelo, S., Messina, G., Faggio, G., Lanza, M., Pistone, A., & Milone, C. (2010). Calibration of reaction parameters for the improvement of thermal stability and crystalline quality of multi-walled carbon nanotubes. *Journal of Materials Science*, 45(3), 783.
- Santhosh, C., Velmurugan, V., Jacob, G., Jeong, S. K., Grace, A. N., & Bhatnagar, A. (2016). Role of nanomaterials in water treatment applications: A review. *Chemical Engineering Journal*, 306, 1116-1137.
- Satishkumar, B., Govindaraj, A., Sen, R., & Rao, C. (1998). Single-walled nanotubes by the pyrolysis of acetylene-organometallic mixtures. *Chemical Physics Letters*, 293(1), 47-52.
- Satishkumar, B., Thomas, P. J., Govindaraj, A., & Rao, C. (2000). Y-junction carbon nanotubes. *Applied physics letters*, 77(16), 2530-2532.
- Schultzenberger, P., & Schultzenberger, L. (1890). Sur quelques faits relatifs a l'histoire du carbon. *CR Acad Sci Paris*, 111, 774.
- Schütt, F., Signetti, S., Krüger, H., Röder, S., Smazna, D., Kaps, S., . . . Adelung, R. (2017). Hierarchical self-entangled carbon nanotube tube networks. *Nature communications*, 8(1), 1215.
- Seah, C.-M., Chai, S.-P., & Mohamed, A. R. (2014). Mechanisms of graphene growth by chemical vapour deposition on transition metals. *Carbon*, 70(Supplement C), 1-21.

- Seidel, R., Duesberg, G. S., Unger, E., Graham, A. P., Liebau, M., & Kreupl, F. (2004). Chemical vapor deposition growth of single-walled carbon nanotubes at 600 C and a simple growth model. *The Journal of Physical Chemistry B*, 108(6), 1888-1893.
- Seow, T. W., & Lim, C. K. (2016). Removal of dye by adsorption: a review. *International Journal of Applied Engineering Research*, 11(4), 2675-2679.
- Shah, K. A., & Tali, B. A. (2016a). Synthesis of carbon nanotubes by catalytic chemical vapour deposition: A review on carbon sources, catalysts and substrates. *Materials Science in Semiconductor Processing*, 41, 67-82.
- Shah, K. A., & Tali, B. A. (2016b). Synthesis of carbon nanotubes by catalytic chemical vapour deposition: A review on carbon sources, catalysts and substrates. *Materials Science in Semiconductor Processing*(41), 67-82.
- Shah, K. A., & Tali, B. A. (2016c). Synthesis of carbon nanotubes by catalytic chemical vapour deposition: A review on carbon sources, catalysts and substrates. *Materials Science in Semiconductor Processing*, 41(Supplement C), 67-82.
- Sharma, J., Mishra, I., & Kumar, V. (2015). Degradation and mineralization of Bisphenol A (BPA) in aqueous solution using advanced oxidation processes: UV/H<sub>2</sub>O<sub>2</sub> and oxidation systems. *Journal of environmental management*, 156, 266-275.
- Sharma, S., & Lakkad, S. (2009). Morphology study of carbon nanospecies grown on carbon fibers by thermal CVD technique. *Surface and Coatings Technology*, 203(10), 1329-1335.
- Shen, X.-E., Shan, X.-Q., Dong, D.-M., Hua, X.-Y., & Owens, G. (2009). Kinetics and thermodynamics of sorption of nitroaromatic compounds to as-grown and oxidized multiwalled carbon nanotubes. *Journal of colloid and interface science*, 330(1), 1-8.
- Shen, X., Guo, X., Zhang, M., Tao, S., & Wang, X. (2015). Sorption mechanisms of organic compounds by carbonaceous materials: site energy distribution consideration. *Environmental science & technology*, 49(8), 4894-4902.
- Sheng, G., Shao, D., Ren, X., Wang, X., Li, J., Chen, Y., & Wang, X. (2010). Kinetics and thermodynamics of adsorption of ionizable aromatic compounds from aqueous solutions by as-prepared and oxidized multiwalled carbon nanotubes. *Journal of hazardous materials*, 178(1), 505-516.
- Shindy, A. (2017). Problems and solutions in colors, dyes and pigments chemistry: a review. *Chem. Int.*, 3, 97-105.
- Shirazi, Y., Tofighy, M. A., Mohammadi, T., & Pak, A. (2011). Effects of different carbon precursors on synthesis of multiwall carbon nanotubes: Purification and Functionalization. *Applied surface science*, 257(16), 7359-7367.
- Shukla, B., Saito, T., Ohmori, S., Koshi, M., Yumura, M., & Iijima, S. (2010). Interdependency of gas phase intermediates and chemical vapor deposition

growth of single wall carbon nanotubes. *Chemistry of Materials*, 22(22), 6035-6043.

Shunin, Y., Bellucci, S., Gruodis, A., & Lobanova-Shunina, T. (2018). Nanotechnology Application Challenges: Nanomanagement, Nanorisks and Consumer Behaviour *Nonregular Nanosystems* (pp. 337-395): Springer.

Sigmund, G., Sun, H., Hofmann, T., & Kah, M. (2016). Predicting the sorption of aromatic acids to noncarbonized and carbonized sorbents. *Environmental science & technology*, 50(7), 3641-3648.

Sing, K. S. (2014). Adsorption by active carbons *In: Adsorption by Powders and Porous solids—Principles, Methodology and Applications* (pp. 321-391): Academic Press Massachusetts, US.

Sivakumar, V., Abdullah, A., Mohamed, A., & Chai, S. (2011). Optimized parameters for carbon nanotubes synthesis over Fe and Ni catalysts VIA methane CVD. *Rev. Adv. Mater. Sci*, 27, 25-30.

Smith, S. C., & Rodrigues, D. F. (2015a). Carbon-based nanomaterials for removal of chemical and biological contaminants from water: A review of mechanisms and applications. *Carbon*, 91(Supplement C), 122-143.

Smith, S. C., & Rodrigues, D. F. (2015b). Carbon-based nanomaterials for removal of chemical and biological contaminants from water: A review of mechanisms and applications. *Carbon*, 91, 122-143.

Soma, K., Radhakrishnan, T., & Sarat Chandra Babu, J. (2017). Carbon nanotubes: Their role in engineering applications and challenges ahead. *Inorganic and Nano-Metal Chemistry*, 47(2), 188-196.

Song, J., Feng, S., Zhao, J., Zheng, J., & Zhu, Z. (2010). Activated carbon catalyzing the formation of carbon nanotubes. *Materials Research Bulletin*, 45(9), 1234-1239.

Song, M., Tang, X., Xu, J., Yu, L., & Wei, Y. (2016). The formation of novel carbon/carbon composite by chemical vapor deposition: An efficient adsorbent for enhanced desulfurization performance. *Journal of Analytical and Applied Pyrolysis*, 118, 34-41.

Soni, H., & Padmaja, P. (2014). Palm shell based activated carbon for removal of bisphenol A: an equilibrium, kinetic and thermodynamic study. *Journal of Porous Materials*, 21(3), 275-284.

Sotelo, J. L., Rodríguez, A. R., Mateos, M. M., Hernández, S. D., Torrellas, S. A., & Rodríguez, J. G. (2012). Adsorption of pharmaceutical compounds and an endocrine disruptor from aqueous solutions by carbon materials. *Journal of Environmental Science and Health, Part B*, 47(7), 640-652.

Speltini, A., Sturini, M., Maraschi, F., & Profumo, A. (2016). Recent trends in the application of the newest carbonaceous materials for magnetic solid-phase extraction of environmental pollutants. *Trends in Environmental Analytical Chemistry*, 10, 11-23.

- Stackelberg, P. E., Gibs, J., Furlong, E. T., Meyer, M. T., Zaugg, S. D., & Lippincott, R. L. (2007). Efficiency of conventional drinking-water-treatment processes in removal of pharmaceuticals and other organic compounds. *Science of the Total Environment*, 377(2), 255-272.
- Staples, C. A., Dorn, P. B., Klecka, G. M., Sondra, T., Branson, D. R., & Harris, L. R. (2000). Bisphenol A concentrations in receiving waters near US manufacturing and processing facilities. *Chemosphere*, 40(5), 521-525.
- Stobinski, L., Lesiak, B., Kövér, L., Tóth, J., Biniak, S., Trykowski, G., & Judek, J. (2010). Multiwall carbon nanotubes purification and oxidation by nitric acid studied by the FTIR and electron spectroscopy methods. *Journal of Alloys and Compounds*, 501(1), 77-84.
- Su, F., Lu, C., & Hu, S. (2010). Adsorption of benzene, toluene, ethylbenzene and p-xylene by NaOCl-oxidized carbon nanotubes. *Colloids and Surfaces A: Physicochemical and Engineering Aspects*, 353(1), 83-91.
- Subramani, S., & Thinakaran, N. (2017). Isotherm, kinetic and thermodynamic studies on the adsorption behaviour of textile dyes onto chitosan. *Process Safety and Environmental Protection*, 106, 1-10.
- Sugime, H., Esconjauregui, S., D'Arzié, L., Yang, J., Robertson, A. W., Oliver, R. A., . . . Robertson, J. (2015). Low-temperature growth of carbon nanotube forests consisting of tubes with narrow inner spacing using Co/Al/Mo catalyst on conductive supports. *ACS applied materials & interfaces*, 7(30), 16819-16827.
- Suhrhoff, T. J., & Scholz-Böttcher, B. M. (2016). Qualitative impact of salinity, UV radiation and turbulence on leaching of organic plastic additives from four common plastics—A lab experiment. *Marine pollution bulletin*, 102(1), 84-94.
- Sui, Q., Huang, J., Liu, Y., Chang, X., Ji, G., Deng, S., . . . Yu, G. (2011). Rapid removal of bisphenol A on highly ordered mesoporous carbon. *Journal of Environmental Sciences*, 23(2), 177-182.
- Sui, Z., Meng, Q., Zhang, X., Ma, R., & Cao, B. (2012). Green synthesis of carbon nanotube-graphene hybrid aerogels and their use as versatile agents for water purification. *Journal of Materials Chemistry*, 22(18), 8767-8771.
- Sun, C.-F., Meany, B., & Wang, Y. (2014). Characteristics and applications of carbon nanotubes with different numbers of walls. *Carbon Nanotubes and Graphene*, 313-339.
- Sun, K., Zhang, Z., Gao, B., Wang, Z., Xu, D., Jin, J., & Liu, X. (2012). Adsorption of diuron, fluridone and norflurazon on single-walled and multi-walled carbon nanotubes. *Science of The Total Environment*, 439(0), 1-7.
- Suresh, S., Sugumar, R. W., & Maiyalagan, T. (2011). Equilibrium and Kinetic studies on the adsorption of Methylene blue from aqueous solution onto activated carbon prepared from *Murraya koenigii* (curry tree) stems. *Asian Journal of Chemistry*, 23(10), 4486.



- Suzuki, M., Sugiyama, T., Musashi, E., Kobiyama, Y., Kashiwada, A., Matsuda, K., & Yamada, K. (2010). Use of chitosan for removal of bisphenol A and bisphenol derivatives through tyrosinase-catalyzed quinone oxidation. *Journal of Applied Polymer Science*, 118(2), 721-732.
- Swati, S. S. (2017). *STUDY OF ENVIRONMENTAL PARAMETERS OF WASTE WATER GENERATED AFTER DYEING WITH REACTIVE DYES*. Daffodil International university.
- Szabó, A., Perri, C., Csató, A., Giordano, G., Vuono, D., & Nagy, J. B. (2010). Synthesis methods of carbon nanotubes and related materials. *Materials*, 3(5), 3092-3140.
- Szyguła, A., Guibal, E., Palacín, M. A., Ruiz, M., & Sastre, A. M. (2009). Removal of an anionic dye (Acid Blue 92) by coagulation–flocculation using chitosan. *Journal of environmental management*, 90(10), 2979-2986.
- Taleshi, F., Hosseini, A., Mohammadi, M., & Pashae, M. (2013). Effect of hydrocarbon gas on synthesis and diameter of carbon nanotubes. *Indian Journal of Physics*, 87(9), 873-877.
- Tan, C. W., Tan, K. H., Ong, Y. T., Mohamed, A. R., Zein, S. H. S., & Tan, S. H. (2012). Energy and environmental applications of carbon nanotubes. *Environmental chemistry letters*, 10(3), 265-273.
- Tan, I., Ahmad, A., & Hameed, B. (2008). Optimization of preparation conditions for activated carbons from coconut husk using response surface methodology. *Chemical Engineering Journal*, 137(3), 462-470.
- Tan, K. B., Vakili, M., Horri, B. A., Poh, P. E., Abdullah, A. Z., & Salamatinia, B. (2015). Adsorption of dyes by nanomaterials: Recent developments and adsorption mechanisms. *Separation and Purification Technology*, 150(Supplement C), 229-242.
- Tang, J., Jin, G.-Q., Wang, Y.-Y., & Guo, X.-Y. (2010). Tree-like carbon grown from camphor. *Carbon*, 48(5), 1545-1551.
- Tang, L., Cai, Y., Yang, G., Liu, Y., Zeng, G., Zhou, Y., . . . Fang, Y. (2014). Cobalt nanoparticles-embedded magnetic ordered mesoporous carbon for highly effective adsorption of rhodamine B. *Applied surface science*, 314, 746-753.
- Tang, L., Xie, Z., Zeng, G., Dong, H., Fan, C., Zhou, Y., . . . Wei, X. (2016). Removal of bisphenol A by iron nanoparticle-doped magnetic ordered mesoporous carbon. *RSC Advances*, 6(31), 25724-25732.
- Tang, S. C., & Lo, I. M. (2013). Magnetic nanoparticles: essential factors for sustainable environmental applications. *Water research*, 47(8), 2613-2632.
- Tang, Z., Poh, C. K., Tian, Z., Lin, J., Ng, H. Y., & Chua, D. H. (2011). In situ grown carbon nanotubes on carbon paper as integrated gas diffusion and catalyst layer for proton exchange membrane fuel cells. *Electrochimica Acta*, 56(11), 4327-4334.

- Taty-Costodes, V. C., Fauduet, H., Porte, C., & Delacroix, A. (2003). Removal of Cd (II) and Pb (II) ions, from aqueous solutions, by adsorption onto sawdust of *Pinus sylvestris*. *Journal of hazardous materials*, *105*(1), 121-142.
- Temkin, M., & Pyzhev, V. (1940). Recent modifications to Langmuir isotherms.
- Thines, R. K., Mubarak, N. M., Nizamuddin, S., Sahu, J. N., Abdullah, E. C., & Ganesan, P. (2017). Application potential of carbon nanomaterials in water and wastewater treatment: A review. *Journal of the Taiwan Institute of Chemical Engineers*, *72*(Supplement C), 116-133.
- Titirici, M.-M., White, R. J., Brun, N., Budarin, V. L., Su, D. S., del Monte, F., . . . MacLachlan, M. J. (2015). Sustainable carbon materials. *Chemical Society Reviews*, *44*(1), 250-290.
- Tomie, T., Inoue, S., Kohno, M., & Matsumura, Y. (2010). Prospective growth region for chemical vapor deposition synthesis of carbon nanotube on C–H–O ternary diagram. *Diamond and Related Materials*, *19*(11), 1401-1404.
- Tran, H. N., Wang, Y.-F., You, S.-J., & Chao, H.-P. (2017). Insights into the mechanism of cationic dye adsorption on activated charcoal: The importance of  $\pi$ - $\pi$  interactions. *Process Safety and Environmental Protection*, *107*(Supplement C), 168-180.
- Tričković, J., Isakovski, M. K., Watson, M., Maletić, S., Rončević, S., Dalmacija, B., . . . Kukovecz, Á. (2016). Sorption behaviour of trichlorobenzenes and polycyclic aromatic hydrocarbons in the absence or presence of carbon nanotubes in the aquatic environment. *Water, Air, & Soil Pollution*, *227*(10), 374.
- Tripathi, P. K., Gan, L., Liu, M., Ma, X., Zhao, Y., Zhu, D., . . . Rao, N. N. (2014). One-pot assembly of silica@ two polymeric shells for synthesis of hollow carbon porous nanospheres: Adsorption of bisphenol A. *Materials Letters*, *120*, 108-110.
- Tsai, W.-T., Hsu, H.-C., Su, T.-Y., Lin, K.-Y., & Lin, C.-M. (2006). Adsorption characteristics of bisphenol-A in aqueous solutions onto hydrophobic zeolite. *Journal of colloid and interface science*, *299*(2), 513-519.
- Tsai, W.-T., Lai, C.-W., & Su, T.-Y. (2006). Adsorption of bisphenol-A from aqueous solution onto minerals and carbon adsorbents. *Journal of hazardous materials*, *134*(1), 169-175.
- Umar, M., Roddick, F., Fan, L., & Aziz, H. A. (2013). Application of ozone for the removal of bisphenol A from water and wastewater—a review. *Chemosphere*, *90*(8), 2197-2207.
- Usman, A., & Ahmad, M. (2016). From BPA to its analogues: Is it a safe journey? *Chemosphere*, *158*, 131-142.
- Vander Wal, R. L., Ticich, T. M., & Curtis, V. E. (2001). Substrate–support interactions in metal-catalyzed carbon nanofiber growth. *Carbon*, *39*(15), 2277-2289.
- Varandas, E. S. G. R. V. (2014). Low-dose effects of Bisphenol A on human primary vascular endothelial cells and colon cancer cells.

- Vargas, A. M. M., Cazetta, A. L., Kunita, M. H., Silva, T. L., & Almeida, V. C. (2011). Adsorption of methylene blue on activated carbon produced from flamboyant pods (*Delonix regia*): Study of adsorption isotherms and kinetic models. *Chemical Engineering Journal*, 168(2), 722-730.
- Varshney, K. (2014). Carbon nanotubes: a review on synthesis, properties and applications. *International Journal of Engineering Research*, 2(4), 660-677.
- Verschueren, K. (1983). Handbook of environmental data on organic chemicals.
- Veziri, C. M., Karanikolos, G., Pilatos, G., Vermisoglou, E., Giannakopoulos, K., Stogios, C., & Kanellopoulos, N. (2009). Growth and morphology manipulation of carbon nanostructures on porous supports. *Carbon*, 47(9), 2161-2173.
- Veziri, C. M., Pilatos, G., Karanikolos, G., Labropoulos, A., Kordatos, K., Kasselouri-Rigopoulou, V., & Kanellopoulos, N. (2008). Growth and optimization of carbon nanotubes in activated carbon by catalytic chemical vapor deposition. *Microporous and Mesoporous Materials*, 110(1), 41-50.
- Vijwani, H., Nadagouda, M. N., Namboodiri, V., & Mukhopadhyay, S. M. (2015). Hierarchical hybrid carbon nano-structures as robust and reusable adsorbents: Kinetic studies with model dye compound. *Chemical Engineering Journal*, 268, 197-207.
- Villacampa, J. I., Royo, C., Romeo, E., Montoya, J. A., Del Angel, P., & Monzon, A. (2003). Catalytic decomposition of methane over Ni-Al<sub>2</sub>O<sub>3</sub> coprecipitated catalysts: reaction and regeneration studies. *Applied Catalysis A: General*, 252(2), 363-383.
- Von Sonntag, C., & Von Gunten, U. (2012). *Chemistry of ozone in water and wastewater treatment*: IWA publishing.
- Voutsas, D., Hartmann, P., Schaffner, C., & Giger, W. (2006). Benzotriazoles, alkylphenols and bisphenol A in municipal wastewaters and in the Glatt River, Switzerland. *Environmental science and pollution Research*, 13(5), 333-341.
- Vučurović, V. M., Razmovski, R. N., & Tekić, M. N. (2012). Methylene blue (cationic dye) adsorption onto sugar beet pulp: Equilibrium isotherm and kinetic studies. *Journal of the Taiwan Institute of Chemical Engineers*, 43(1), 108-111.
- Wagner, R., & Ellis, W. (1964). Vapor-liquid-solid mechanism of single crystal growth. *Applied physics letters*, 4(5), 89-90.
- Wang, C., Feng, C., Gao, Y., Ma, X., Wu, Q., & Wang, Z. (2011). Preparation of a graphene-based magnetic nanocomposite for the removal of an organic dye from aqueous solution. *Chemical Engineering Journal*, 173(1), 92-97.
- Wang, C., Yang, S., Ma, Q., Jia, X., & Ma, P.-C. (2017). Preparation of carbon nanotubes/graphene hybrid aerogel and its application for the adsorption of organic compounds. *Carbon*, 118(Supplement C), 765-771.
- Wang, H., Zhang, H., Jiang, J.-Q., & Ma, X. (2016). Adsorption of bisphenol A onto cationic-modified zeolite. *Desalination and Water Treatment*, 57(54), 26299-26306.

- Wang, J., Chen, Z., & Chen, B. (2014). Adsorption of polycyclic aromatic hydrocarbons by graphene and graphene oxide nanosheets. *Environmental science & technology*, 48(9), 4817-4825.
- Wang, N., Pandit, S., Ye, L., Edwards, M., Mokkalapati, V. R. S. S., Murugesan, M., . . . Liu, J. (2017). Efficient surface modification of carbon nanotubes for fabricating high performance CNT based hybrid nanostructures. *Carbon*, 111(Supplement C), 402-410.
- Wang, S., Ng, C. W., Wang, W., Li, Q., & Hao, Z. (2012). Synergistic and competitive adsorption of organic dyes on multiwalled carbon nanotubes. *Chemical Engineering Journal*, 197, 34-40.
- Wang, W., Wang, F., Kang, Y., & Wang, A. (2015). Enhanced adsorptive removal of methylene blue from aqueous solution by alkali-activated palygorskite. *Water, Air, & Soil Pollution*, 226(3), 1-13.
- Wang, X., Qin, Y., Zhu, L., & Tang, H. (2015). Nitrogen-doped reduced graphene oxide as a bifunctional material for removing bisphenols: synergistic effect between adsorption and catalysis. *Environmental science & technology*, 49(11), 6855-6864.
- Weber, T. W., & Chakravorti, R. K. (1974). Pore and solid diffusion models for fixed-bed adsorbers. *AIChE Journal*, 20(2), 228-238.
- Weber, W. J., & Morris, J. C. (1963). Kinetics of adsorption on carbon from solution. *Journal of the Sanitary Engineering Division*, 89(2), 31-60.
- Weiss, N. O., Zhou, H., Liao, L., Liu, Y., Jiang, S., Huang, Y., & Duan, X. (2012). Graphene: An Emerging Electronic Material. *Advanced Materials*, 24(43), 5782-5825.
- Wiles, P., & Abrahamson, J. (1978). Carbon fibre layers on arc electrodes—I: their properties and cool-down behaviour. *Carbon*, 16(5), 341-349.
- Willems, I., Konya, Z., Colomer, J.-F., Van Tendeloo, G., Nagaraju, N., Fonseca, A., & Nagy, J. (2000). Control of the outer diameter of thin carbon nanotubes synthesized by catalytic decomposition of hydrocarbons. *Chemical Physics Letters*, 317(1), 71-76.
- Wirasnita, R., Hadibarata, T., Yusoff, A. R. M., & Yusop, Z. (2014). Removal of bisphenol A from aqueous solution by activated carbon derived from oil palm empty fruit bunch. *Water, Air, & Soil Pollution*, 225(10), 2148.
- Wirth, C. T., Bayer, B. C., Gamalski, A. D., Esconjauregui, S., Weatherup, R. S., Ducati, C., . . . Hofmann, S. (2012). The phase of iron catalyst nanoparticles during carbon nanotube growth. *Chemistry of Materials*, 24(24), 4633-4640.
- Wolska, J., & Bryjak, M. (2014). Removal of bisphenol A from aqueous solution by molecularly imprinted polymers. *Separation Science and Technology*, 49(11), 1643-1653.

- Wong, Y., Szeto, Y., Cheung, W., & McKay, G. (2004). Pseudo-first-order kinetic studies of the sorption of acid dyes onto chitosan. *Journal of Applied Polymer Science*, 92(3), 1633-1645.
- Wu, C.-H. (2007). Adsorption of reactive dye onto carbon nanotubes: equilibrium, kinetics and thermodynamics. *Journal of hazardous materials*, 144(1), 93-100.
- Wu, W., Chen, W., Lin, D., & Yang, K. (2012). Influence of surface oxidation of multiwalled carbon nanotubes on the adsorption affinity and capacity of polar and nonpolar organic compounds in aqueous phase. *Environmental science & technology*, 46(10), 5446-5454.
- Wu, W., Yang, K., Chen, W., Wang, W., Zhang, J., Lin, D., & Xing, B. (2016). Correlation and prediction of adsorption capacity and affinity of aromatic compounds on carbon nanotubes. *Water research*, 88, 492-501.
- Xie, J., Zhang, N., & Varadan, V. K. (2005). Functionalized carbon nanotubes in platinum decoration. *Smart materials and structures*, 15(1), S5.
- Xiong, L., Yang, Y., Mai, J., Sun, W., Zhang, C., Wei, D., . . . Ni, J. (2010). Adsorption behavior of methylene blue onto titanate nanotubes. *Chemical Engineering Journal*, 156(2), 313-320.
- Xu, J., Wang, L., & Zhu, Y. (2012). Decontamination of bisphenol A from aqueous solution by graphene adsorption. *Langmuir*, 28(22), 8418-8425.
- Xu, X.-j., & Huang, S.-m. (2007). Carbon dioxide as a carbon source for synthesis of carbon nanotubes by chemical vapor deposition. *Materials Letters*, 61(21), 4235-4237.
- Xu, Z.-X., Lin, J.-D., Roy, V., Ou, Y., & Liao, D.-W. (2005). Catalytic synthesis of carbon nanotubes and carbon spheres using Kaolin supported catalyst. *Materials Science and Engineering: B*, 123(2), 102-106.
- Yagub, M. T., Sen, T. K., Afroze, S., & Ang, H. M. (2014). Dye and its removal from aqueous solution by adsorption: a review. *Advances in colloid and interface science*, 209, 172-184.
- Yagub, M. T., Sen, T. K., & Ang, M. (2014). Removal of cationic dye methylene blue (MB) from aqueous solution by ground raw and base modified pine cone powder. *Environmental earth sciences*, 71(4), 1507-1519.
- Yan, X. M., Shi, B. Y., Lu, J. J., Feng, C. H., Wang, D. S., & Tang, H. X. (2008). Adsorption and desorption of atrazine on carbon nanotubes. *Journal of Colloid and Interface Science*, 321(1), 30-38.
- Yan, Y., Miao, J., Yang, Z., Xiao, F.-X., Yang, H. B., Liu, B., & Yang, Y. (2015). Carbon nanotube catalysts: recent advances in synthesis, characterization and applications. *Chemical Society Reviews*, 44(10), 3295-3346.
- Yan, Y., Zhang, M., Gong, K., Su, L., Guo, Z., & Mao, L. (2005). Adsorption of methylene blue dye onto carbon nanotubes: a route to an electrochemically functional nanostructure and its layer-by-layer assembled nanocomposite. *Chemistry of Materials*, 17(13), 3457-3463.

- Yang, J., & Qiu, K. (2010). Preparation of activated carbons from walnut shells via vacuum chemical activation and their application for methylene blue removal. *Chemical Engineering Journal*, 165(1), 209-217.
- Yang, K., Wu, W., Jing, Q., & Zhu, L. (2008). Aqueous adsorption of aniline, phenol, and their substitutes by multi-walled carbon nanotubes. *Environmental science & technology*, 42(21), 7931-7936.
- Yang, K., & Xing, B. (2010). Adsorption of organic compounds by carbon nanomaterials in aqueous phase: Polanyi theory and its application. *Chemical Reviews*, 110(10), 5989-6008.
- Yang, K., Zhu, L., & Xing, B. (2006). Adsorption of polycyclic aromatic hydrocarbons by carbon nanomaterials. *Environmental science & technology*, 40(6), 1855-1861.
- Yang, S.-T., Chen, S., Chang, Y., Cao, A., Liu, Y., & Wang, H. (2011). Removal of methylene blue from aqueous solution by graphene oxide. *Journal of colloid and interface science*, 359(1), 24-29.
- Yang, S., Hai, F. I., Nghiem, L. D., Nguyen, L. N., Roddick, F., & Price, W. E. (2013). Removal of bisphenol A and diclofenac by a novel fungal membrane bioreactor operated under non-sterile conditions. *International Biodeterioration & Biodegradation*, 85, 483-490.
- Yao, Y., Miao, S., Liu, S., Ma, L. P., Sun, H., & Wang, S. (2012). Synthesis, characterization, and adsorption properties of magnetic Fe<sub>3</sub>O<sub>4</sub>@ graphene nanocomposite. *Chemical Engineering Journal*, 184, 326-332.
- Yao, Y., Xu, F., Chen, M., Xu, Z., & Zhu, Z. (2010). Adsorption behavior of methylene blue on carbon nanotubes. *Bioresource technology*, 101(9), 3040-3046.
- Yener, J., Kopac, T., Dogu, G., & Dogu, T. (2008). Dynamic analysis of sorption of Methylene Blue dye on granular and powdered activated carbon. *Chemical Engineering Journal*, 144(3), 400-406.
- Yong, Z., Fang, L., & Zhi-Hua, Z. (2011). Synthesis of heterostructured helical carbon nanotubes by iron-catalyzed ethanol decomposition. *Micron*, 42(6), 547-552.
- Yoon, Y., Ryu, J., Oh, J., Choi, B.-G., & Snyder, S. A. (2010). Occurrence of endocrine disrupting compounds, pharmaceuticals, and personal care products in the Han River (Seoul, South Korea). *Science of the Total Environment*, 408(3), 636-643.
- Yu, D., Goh, K., Wang, H., Wei, L., Jiang, W., Zhang, Q., . . . Chen, Y. (2014). Scalable synthesis of hierarchically structured carbon nanotube-graphene fibres for capacitive energy storage. *Nature nanotechnology*, 9(7), 555-562.
- Yu, F., Chen, J., Yang, M., Zhou, L., Jin, L., Su, C., . . . Yu, L. (2012). A facile one-pot method for synthesis of low-cost magnetic carbon nanotubes and their applications for dye removal. *New Journal of Chemistry*, 36(10), 1940-1943.
- Yu, F., Wu, Y., Ma, J., & Zhang, C. (2013). Adsorption of lead on multi-walled carbon nanotubes with different outer diameters and oxygen contents: Kinetics,

- isotherms and thermodynamics. *Journal of Environmental Sciences*, 25(1), 195-203.
- Yu, J.-G., Zhao, X.-H., Yang, H., Chen, X.-H., Yang, Q., Yu, L.-Y., . . . Chen, X.-Q. (2014a). Aqueous adsorption and removal of organic contaminants by carbon nanotubes. *Science of the Total Environment*, 482-483(Supplement C), 241-251.
- Yu, J.-G., Zhao, X.-H., Yang, H., Chen, X.-H., Yang, Q., Yu, L.-Y., . . . Chen, X.-Q. (2014b). Aqueous adsorption and removal of organic contaminants by carbon nanotubes. *Science of the Total Environment*, 482-483, 241-251.
- Yu, J.-G., Zhao, X.-H., Yang, H., Chen, X.-H., Yang, Q., Yu, L.-Y., . . . Chen, X.-Q. (2014c). Aqueous adsorption and removal of organic contaminants by carbon nanotubes. *Science of the Total Environment*, 482, 241-251.
- Yu, S., Wang, X., Yao, W., Wang, J., Ji, Y., Ai, Y., . . . Wang, X. (2017). Macroscopic, spectroscopic, and theoretical investigation for the interaction of phenol and naphthol on reduced graphene oxide. *Environmental science & technology*, 51(6), 3278-3286.
- Yüksel, S., Kabay, N., & Yüksel, M. (2013). Removal of bisphenol A (BPA) from water by various nanofiltration (NF) and reverse osmosis (RO) membranes. *Journal of hazardous materials*, 263, 307-310.
- Zare, K., Gupta, V. K., Moradi, O., Makhlof, A. S. H., Sillanpää, M., Nadagouda, M. N., . . . Wang, Z.-j. (2015). A comparative study on the basis of adsorption capacity between CNTs and activated carbon as adsorbents for removal of noxious synthetic dyes: a review. *Journal of Nanostructure in Chemistry*, 5(2), 227-236.
- Zare, K., Sadegh, H., Shahryari-ghoshekandi, R., Maazinejad, B., Ali, V., Tyagi, I., . . . Gupta, V. K. (2015). Enhanced removal of toxic Congo red dye using multi walled carbon nanotubes: Kinetic, equilibrium studies and its comparison with other adsorbents. *Journal of Molecular Liquids*, 212, 266-271.
- Zhang, A., & Li, Y. (2014). Removal of phenolic endocrine disrupting compounds from waste activated sludge using UV, H<sub>2</sub>O<sub>2</sub>, and UV/H<sub>2</sub>O<sub>2</sub> oxidation processes: effects of reaction conditions and sludge matrix. *Science of the Total Environment*, 493, 307-323.
- Zhang, D., Pan, B., Zhang, H., Ning, P., & Xing, B. (2010). Contribution of Different Sulfamethoxazole Species to Their Overall Adsorption on Functionalized Carbon Nanotubes. *Environmental Science & Technology*, 44(10), 3806-3811.
- Zhang, F., Lan, J., Yang, Y., Wei, T., Tan, R., & Song, W. (2013). Adsorption behavior and mechanism of methyl blue on zinc oxide nanoparticles. *Journal of Nanoparticle Research*, 15(11), 2034.
- Zhang, J., Li, X., Chen, H., Qi, M., Zhang, G., Hu, H., & Ma, X. (2017). Hydrogen production by catalytic methane decomposition: Carbon materials as catalysts or catalyst supports. *International Journal of Hydrogen Energy*, 42(31), 19755-19775.

- Zhang, J., Ping, Q., Niu, M., Shi, H., & Li, N. (2013). Kinetics and equilibrium studies from the methylene blue adsorption on diatomite treated with sodium hydroxide. *Applied Clay Science*, 83, 12-16.
- Zhang, L., Song, X., Liu, X., Yang, L., Pan, F., & Lv, J. (2011). Studies on the removal of tetracycline by multi-walled carbon nanotubes. *Chemical Engineering Journal*, 178, 26-33.
- Zhang, L., Xu, T., Liu, X., Zhang, Y., & Jin, H. (2011). Adsorption behavior of multi-walled carbon nanotubes for the removal of olaquinox from aqueous solutions. *Journal of hazardous materials*, 197, 389-396.
- Zhang, X., Huang, Y., Wang, Y., Ma, Y., Liu, Z., & Chen, Y. (2009). Synthesis and characterization of a graphene–C 60 hybrid material. *Carbon*, 47(1), 334-337.
- Zhang, X., Shen, J., Zhuo, N., Tian, Z., Xu, P., Yang, Z., & Yang, W. (2016). Interactions between Antibiotics and Graphene-Based Materials in Water: A Comparative Experimental and Theoretical Investigation. *ACS applied materials & interfaces*, 8(36), 24273-24280.
- Zhang, Y., Cheng, Y., Chen, N., Zhou, Y., Li, B., Gu, W., . . . Xian, Y. (2014). Recyclable removal of bisphenol A from aqueous solution by reduced graphene oxide–magnetic nanoparticles: Adsorption and desorption. *Journal of colloid and interface science*, 421(Supplement C), 85-92.
- Zhang, Z., Wang, W., & Wang, A. (2015). Highly effective removal of methylene blue using functionalized attapulgite via hydrothermal process. *Journal of Environmental Sciences*, 33, 106-115.
- Zhang, Z., Zhang, Z., Fernández, Y., Menéndez, J., Niu, H., Peng, J., . . . Guo, S. (2010). Adsorption isotherms and kinetics of methylene blue on a low-cost adsorbent recovered from a spent catalyst of vinyl acetate synthesis. *Applied surface science*, 256(8), 2569-2576.
- Zhao, D., Zhang, W., Chen, C., & Wang, X. (2013). Adsorption of Methyl Orange Dye Onto Multiwalled Carbon Nanotubes. *Procedia Environmental Sciences*, 18, 890-895.
- Zhao, H., Liu, X., Cao, Z., Zhan, Y., Shi, X., Yang, Y., . . . Xu, J. (2016). Adsorption behavior and mechanism of chloramphenicols, sulfonamides, and non-antibiotic pharmaceuticals on multi-walled carbon nanotubes. *Journal of hazardous materials*, 310(Supplement C), 235-245.
- Zhao, J., Buldum, A., Han, J., & Lu, J. P. (2002). Gas molecule adsorption in carbon nanotubes and nanotube bundles. *Nanotechnology*, 13(2), 195.
- Zhao, J., Lu, J. P., Han, J., & Yang, C.-K. (2003). Noncovalent functionalization of carbon nanotubes by aromatic organic molecules. *Applied physics letters*, 82(21), 3746-3748.
- Zhao, M., & Liu, P. (2008). Adsorption behavior of methylene blue on halloysite nanotubes. *Microporous and Mesoporous Materials*, 112(1), 419-424.



- Zhao, X., Zhang, L., Murali, S., Stoller, M. D., Zhang, Q., Zhu, Y., & Ruoff, R. S. (2012). Incorporation of manganese dioxide within ultraporous activated graphene for high-performance electrochemical capacitors. *ACS nano*, 6(6), 5404-5412.
- Zhao, Z., Fu, D., & Zhang, B. (2016). Novel molecularly imprinted polymer prepared by palygorskite as support for selective adsorption of bisphenol A in aqueous solution. *Desalination and Water Treatment*, 57(27), 12433-12442.
- Zheng, S., Sun, Z., Park, Y., Ayoko, G. A., & Frost, R. L. (2013). Removal of bisphenol A from wastewater by Ca-montmorillonite modified with selected surfactants. *Chemical Engineering Journal*, 234, 416-422.
- Zhou, L., Ji, L., Ma, P.-C., Shao, Y., Zhang, H., Gao, W., & Li, Y. (2014a). Development of carbon nanotubes/CoFe<sub>2</sub>O<sub>4</sub> magnetic hybrid material for removal of tetrabromobisphenol A and Pb(II). *Journal of hazardous materials*, 265, 104-114.
- Zhou, L., Ji, L., Ma, P.-C., Shao, Y., Zhang, H., Gao, W., & Li, Y. (2014b). Development of carbon nanotubes/CoFe<sub>2</sub>O<sub>4</sub> magnetic hybrid material for removal of tetrabromobisphenol A and Pb (II). *Journal of hazardous materials*, 265, 104-114.
- Zhou, Q., Wang, Y., Xiao, J., & Fan, H. (2016). Adsorption and removal of bisphenol A,  $\alpha$ -naphthol and  $\beta$ -naphthol from aqueous solution by Fe<sub>3</sub>O<sub>4</sub>@ polyaniline core-shell nanomaterials. *Synthetic Metals*, 212, 113-122.
- Zhou, Y., Chen, L., Lu, P., Tang, X., & Lu, J. (2011). Removal of bisphenol A from aqueous solution using modified fibric peat as a novel biosorbent. *Separation and Purification Technology*, 81(2), 184-190.
- Zhou, Y., Lu, P., & Lu, J. (2012). Application of natural biosorbent and modified peat for bisphenol a removal from aqueous solutions. *Carbohydrate Polymers*, 88(2), 502-508.
- Zhou, Z.-W., Liu, Y.-T., Xie, X.-M., & Ye, X.-Y. (2016). Constructing novel Si@SnO<sub>2</sub> core-shell heterostructures by facile self-assembly of SnO<sub>2</sub> nanowires on silicon hollow nanospheres for large, reversible lithium storage. *ACS applied materials & interfaces*, 8(11), 7092-7100.
- Zhu, D., & Pignatello, J. J. (2005). Characterization of aromatic compound sorptive interactions with black carbon (charcoal) assisted by graphite as a model. *Environmental science & technology*, 39(7), 2033-2041.
- Zhu, X., Zhu, L., Chen, Y., & Tian, S. (2009). Acute toxicities of six manufactured nanomaterial suspensions to *Daphnia magna*. *Journal of Nanoparticle Research*, 11(1), 67-75.
- Ziebro, J., Łukasiewicz, I., Borowiak-Palen, E., & Michalkiewicz, B. (2010). Low temperature growth of carbon nanotubes from methane catalytic decomposition over nickel supported on a zeolite. *Nanotechnology*, 21(14), 145308.

Zielińska, M., Bułkowska, K., Cydzik-Kwiatkowska, A., Bernat, K., & Wojnowska-Baryła, I. (2016). Removal of bisphenol A (BPA) from biologically treated wastewater by microfiltration and nanofiltration. *International Journal of Environmental Science and Technology*, 13(9), 2239-2248.

Zohre, S., Ataallah, S. G., & Mehdi, A. (2010). Experimental study of methylene blue adsorption from aqueous solutions onto carbon nano tubes. *International Journal of Water Resources and Environmental Engineering*, 2(2), 016-028.

University of Malaya

## LIST OF PUBLICATIONS

- 1- **Alayan, H.M**; AlSaadi, M.A.; Abo-Hamad, A.; AlOmar, M.K.; Aljumaily, M.M; Das, R.; Hashim, M.A, Hybridizing carbon nanomaterial with powder activated carbon for an efficient removal of Bisphenol A from water: The optimum growth and adsorption conditions. *Desalination and Water Treatment Journal*. 2017 (95),128-143.
- 2- **Alayan, H.M**; AlSaadi, M.A.; Das, R.; Abo-Hamad; A., AlOmar, M.K; Hashim, M.A, The formation of hybrid carbon nanomaterial by chemical vapor deposition: An efficient adsorbent for enhanced removal of methylene blue from aqueous solution. *Water Science and Technology Journal*. 2018, 77 (6), 1714-1723.
- 3- **Alayan, H.M**; AlSaadi, M.A.; AlOmar, M.K.; Hashim, M.A, Growth and optimization of carbon nanotubes in powder activated carbon for an efficient removal of methylene blue from aqueous solution. *Environmental Technology Journal*. 2018, (38).

### Conference Papers (Presenter)

- **Alayan, H.M**, AlSaadi, M.A., & Hashim, M. A. (2015). Study the activity of platinum and palladium zeolite supported catalysts for hydrocarbon reactions. *Utility Reaction and Environmental Research-PURE2015*.